EFFECTS OF PURE AND IMPURE CARBON DIOXIDE (CO_2) ON SOIL CHEMISTRY

By

YANG WEI, BSc. MSc.

Thesis submitted to the University of Nottingham

for the degree of Doctor of Philosophy

July 2013

ABSTRACT

A cleaner use of fossil fuels supported by Carbon Capture and Storage (CCS) techniques is considered to be one of the main short-term strategies for addressing the global climate change problem. However, potential CO_2 or CO_2/SO_2 seepage during some of the phases of a CCS project not only reduces its performing efficiency, but also impacts the local environment, which could have further impacts on human health. It is therefore essential to assess the potential risks and provide evidence that the impacts are well understood. Moreover, studying the effects of CO_2 leakage is useful for identifying monitoring parameters if the leakage does happen, leading to the development of new approaches in detecting CO_2 leaks. Accordingly, this research is carried out to assess the relevant impacts on the local environment of CO_2 leakage, focusing on the environmental impacts caused by CO_2 seepage associated with various soil types, mostly on the soil geochemical changes, which is currently lacked.

As a cost effective approach, this research was carried out with two types of well controlled laboratory experiments: Stage I- Closed reactor experiments and Stage II- A flow through column system (designed by the author). As a supplementary study to the research of the ASGARD site, Stage I experiments were carried out with soil samples collected from the ASGARD site and gave directions for Stage II column system design. Stage II experiments were carried out with two contrasting mono-mineral sediments considering sensitivity to CO_2 gas, Trucal 5 and Trucal 6 (limestone sand of different particle size) and silica sand.

Certain limitations of this research have to be considered. Firstly, highly idealised samples were used in the experiments instead of true soils and there was no heterogeneity in the samples used, which is not representative of the full complexity of a natural system. Secondly, the scale limitation of the laboratory work would lead to a higher gas/mineral ratio compared with field conditions. Therefore, results from the laboratory work cannot simply represent all the soils in the field, except the specific soil related problem and the results are better to be used to demonstrate the conditions where the soils/sediments are surrounded by high levels of CO_2, such as the ones nearby a leaking injection well or along a fracture/fault. Nevertheless, this study is believed to provide a step towards understanding the potential impacts of CO_2 seepage in soil, and potentially to be useful as a mean of identifying indicators of related problems when applying to the full-scale design, leading to the development of new approaches in detecting CO_2 leaks.

Throughout the experiments, the experimental apparatus (the continuous column system) newly designed by the author was run successfully, providing an alternative way in respect to the majority of soil-column studies for assessing issues of CO_2 seepage. The main impact of CO_2 emissions on soil properties is to drop the pH which triggers metals mobilisation from soils (all within safety limits to plant growth). The change of pH associated with both limestone and silica sand indicates that pH is an excellent parameter to indicate the CO_2 intrusion into sediments once the background is set. The response of calcium (Ca) to CO_2 flux highlights that carbonate minerals are sensitive to CO_2 increase and could possibly be used as a parameter to monitor CO_2 leakage once the baseline for the pre-injection concentration is set.

ACKNOWLEDGEMENTS

I appreciate all the support from many people during this research. Firstly, I want to thank my supervisor and co-supervisors, Professor Paul Nathanail, Professor Mercedes Maroto-Valer, Professor Mike Steven and Dr. Giorgio Caramanna, for bringing me into this research field and for being sufficiently confident and supportive in me. Also, thanks to my internal and external examiners, Professor Sarah Metcalfe and Dr Diganta B Das, for providing useful comments during the viva and the following modification on the thesis. Thanks to Dr. Das for providing equipments in Loughborough University for me to test the sediments permeability used in the research, and thanks to Mr. Luqman Abidoye and Mr. Ronald Wairagu for helping me with the experiments.

Thanks to the Engineering and Physical Sciences Research Council (EPSRC) via Centre for Innovation in Carbon Capture and Storage (CICCS) (EPSRC, EP/F012098/1) and the International Office at the University of Nottingham for providing the financial support and scholarships.

Thanks to the support of all my friends and technicians in the School of Geography and the Department of Chemical and Environmental Engineering.

Last but not least, thanks to my farther (Mr. Wei Cheng Cai), my mother (Mrs. Yang Ying), my brother (Mr. Wei Zheng Jie) and my husband (Dr. Tianjian Zuo) for their unwavering support and belief in my ability and for their endless love and encouragement helping me go through all the difficulties. Without it, the completion of this work would never have become a reality.

This thesis is dedicated to

my family and Dr. Tianjian Zuo

TABLE OF CONTENTS

LIST OF FIGURES

LIST OF TABLES

ABBREVIATIONS

Al	Aluminium
Ar	Argon
ASGARD	Artificial Soil Gassing and Response Detection
BAL	Balanced Gas
B.E.T	Brunauer-Emmett-Teller
BGS	British Geological Survey
BSE	Back Scattered Electron
Ca	Calcium
$CaCO_3$	Calcium Carbonate
CC	Carbonate Content
CCS	Carbon Capture and Storage
Cd	Cadmium
CEC	Cation Exchange Capacity
CO_2	Carbon Dioxide
Cr	Chromium
Cu	Copper
DMAA	Dimethyl Arsenic Acid
DOC	Dissolved Organic Carbon
DOM	Dissolved Prganic Matter
DTPA	Diethylene Triamine Pentaacetic Acid
DW	Dry Weight
EDTA	Diammonium Ethyldiaminetetraacetic Acid
EDX	Energy Dispersive X-ray Analysis
EOR	Enhanced Oil Recovery
Fe	Iron
H_2CO_3	Carbonic Acid

He	Helium
HF	Hydrofluoric Acid
ICP/MS	Inductively Coupled Plasma Mass Spectrometry
IR	Infrared
K	Potassium
L-L	Luer-Lock
LOI	Loss on Ignition
MC	Soil Moisture Content
Mg	Magnesium
MMAA	Monomethyl Arsenic Acid
Mn	Manganese
N	Nitrogen
Ni	Nickel
OC	Organic Content
O_2	Oxygen
P	Phosphorus
PA	Phenolphthalein Alkalinity
pCO_2	CO_2 Partial Pressure
R&D	Research and Development
RF	Radio Frequency
SEM/EDX	Scanning Electron Microscope/Energy Dispersive X-ray spectroscopy
SO_2	Sulphur Dioxide
SPT	Standard Temperature and Pressure
TA	Total Alkalinity
XRD	X-ray Diffraction
ZERT	Zero Emission Research and Technology Centre
Zn	Zinc

Chapter 1 Introduction

1.1 Carbon Capture and Storage (CCS)

Since Arrhenius (1896) proposed the concept that high concentrations of atmospheric CO_2 caused anthropic global warming, research was carried out to validate the hypothesis (Pearson and Palmer, 2000; Petit et al., 1999; Zachos et al., 2001). It is now widely accepted and recognised that increased CO_2 concentration in the atmosphere is likely to be the reason for global climate change and the rise in average global temperature over the last century (Harvey, 2007; Hofmann et al., 2009).

Global warming causes direct and indirect problems worldwide. For example, it increases ice and snow melting, especially at the Earth's poles, and further increases sea levels (Jones, 1994). It could also pose further risks to human health by either increasing the prevalence of diseases (e.g. malaria and diarrheal disease), worsening malnutrition especially in poor countries, or enhancing bacterial growth in food causing concerns over food security (Green et al., 2011; St. Louis and Hess, 2008). Besides, a higher level of atmospheric CO_2 concentration is likely to lead to ocean acidification (Wernberg et al., 2011), and it may influence crop yields and cause a reduction in protein concentration in food (Taub et al., 2008; Tubiello et al., 2007).

Fossil fuels (coal, natural gas and oil) are responsible for about 85% of the anthropogenic CO_2 emission produced annually (Sims et al., 2007). According to world energy outlook by International Energy Agency (IEA) (IEA, 2008), fossil fuels are the dominant energy sources in the world economy and they are expected to continue to contribute about 80% of

total energy supply at 2030. A cleaner use of fossil fuels supplemented by CCS techniques is considered to be one of the main short-term strategies for addressing the global warming problems and is expected to make a key contribution to the mitigation of global anthropogenic CO_2 emissions (Benson et al., 2003; Pacala and Socolow, 2004; Pires et al., 2011; Van der Zwaan and Smekens, 2009). Fig. 1.1 illustrates a schematic diagram of possible CCS systems, which includes carbon capture, compression, transportation and storage (IPCC, 2005b).

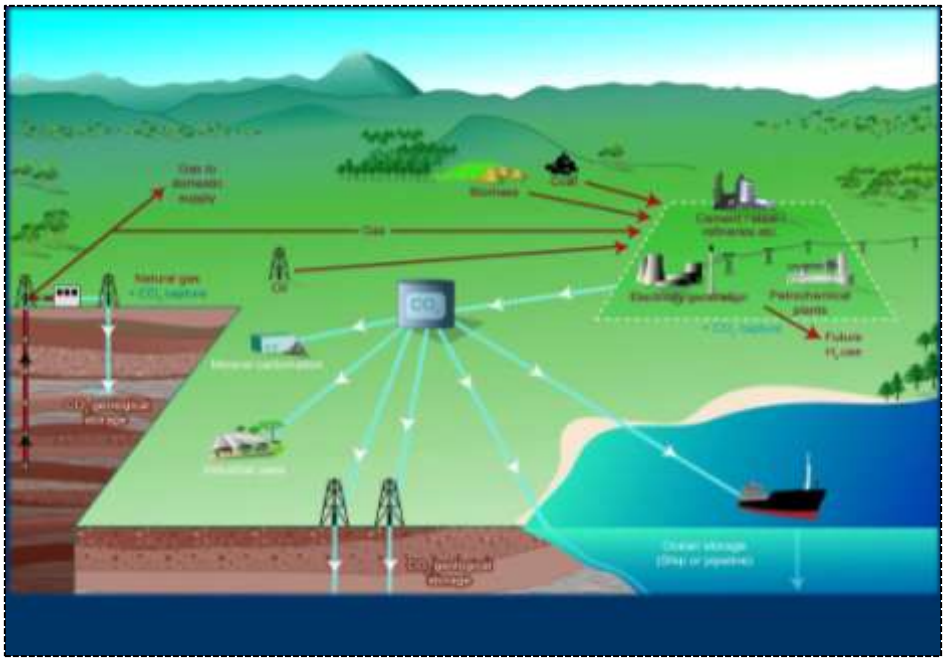

Fig. 1.1 Schematic diagram of possible CCS systems (modified from (IPCC, 2005b)).

From an economic and policy making perspective, if stored CO_2 gradually leaked back to the atmosphere, depending on different CO_2 leakage rates, CO_2 geological storage may not be an effective climate change reduction option (Van der Zwaan and Smekens, 2009). Some studies were carried out to assess the acceptable CO_2 leakage rate to make CCS an effective abatement option. The common conclusions are that, with a 550 ppmv atmospheric CO_2 concentration target by 2100, a leakage rate of less than

0.1% per year is acceptable for CCS to be deployed on a large scale, while a leakage rate of 0.5% renders storage unattractive and 1% CO_2 leakage per year is too high for making CCS an effective option (Ha-Duong and Keith, 2003; Kannan, 2009; Van der Zwaan and Smekens, 2009). The detailed discussions on the economic issues of CO_2 leakage from CCS scheme are not analysed here, as this goes beyond the scope of the thesis, but it's available in the above references.

Potential CO_2 seepage during some of the phases of a CCS project not only reduces its performance efficiency, but also impacts the local environment, which could have further impacts on human health. In order to progress to a large scale application, it is essential to examine all the potential risks and provide evidence that the potential impacts are well understood. Moreover, studying the effects on the local environments of CO_2 leakage is useful for identifying monitoring parameters if the leakage does happen. Accordingly, the impacts on the local environment of CO_2 leakage interest this research the most and are its main focus.

1.2 Potential leakage across the CCS chain

The potential CO_2 leakage pathways across the CCS chain are mainly associated with the carbon transportation and storage process (Damen et al., 2003; Gale and Davison, 2004; Steeneveldt et al., 2006), which will be described in detail in the following sections.

Pipeline transportation is the preferred method to transport CO_2 (IPCC, 2005a). A major hazard related to CO_2 transportation is pipeline failure. Based on the experience with natural gas and CO_2 gas transportation, there were 10 incidents of pipeline failure recorded in the USA during 1990 to 2001 without any injuries or fatalities (Gale and Davison, 2004). The

failure rates for CO_2 pipelines are considered between 0.7 and 6.1 x 10^{-4} yr^{-1} km^{-1} (0.007-0.0061% per year per km) (Damen et al., 2003; Gale and Davison, 2004; Koornneef et al., 2012). Though the likelihood of such failure is relatively small, pipeline breaches have occurred during the last few years as recorded by Damen et al. (2003) and Gale and Davison (2004). The failure could be a puncture or a rupture primarily caused by third party interference, acidic gas corrosion, construction or material faults such as welding and other operator errors, which cause potential CO_2 leakage (Gale and Davison, 2004; Koornneef et al., 2009). Considering the low failure rate as mentioned above, the leakage problem during pipeline transportation will not be the main focus of this research. But the related research regarding CO_2 release and dispersion models and its possible impacts on the local area are reviewed by Koornneef et al. (2012).

The last step associated with CCS chain is to pump the captured CO_2 into a medium which it will be stored in and isolated from the biosphere. The main options for carbon storage are: deep underground geological storage and ocean storage (Benson and Surles, 2006; IPCC, 2005a; Maroto-Valer et al., 2005). As a safer and more mature technique, CO_2 geological storage is currently considered as an earlier ready and more acceptable option for practical implementation of CO_2 storage demonstrated worldwide (Celia et al., 2005; Van der Zwaan aand Smekens, 2009; Wilson and Gerard, 2007). Three main industrial-scale storage projects are currently in operation, the Sleipner project in an offshore saline formation in Norway; the Weyburn enhanced oil recovery (EOR) project in Canada, and the Salah project in a gas field in Algeria. For all these three projects, there are roughly 3–4 million tonnes per year of CO_2 captured and stored in deep geological formations (Benson and Surles, 2006; Torp and Gale,

2002). The CO_2 geological storage process is therefore the main focus of this research.

Several potential pathways could lead to CO_2 leakage from a geological storage reservoir. Often investigated pathways (Fig. 1.2) include diffuse leakage through caprock formations, concentrated leakage through natural or induced faults and fractures, and leakage through poorly plugged old abandoned wells nearby (Celia et al., 2005; Damen et al., 2003; Oldenburg and Lewicki, 2005). Among all these pathways, injection wells and abandoned wells are considered as the most probable migration pathways for CO_2 storage projects (Oldenburg et al., 2009).

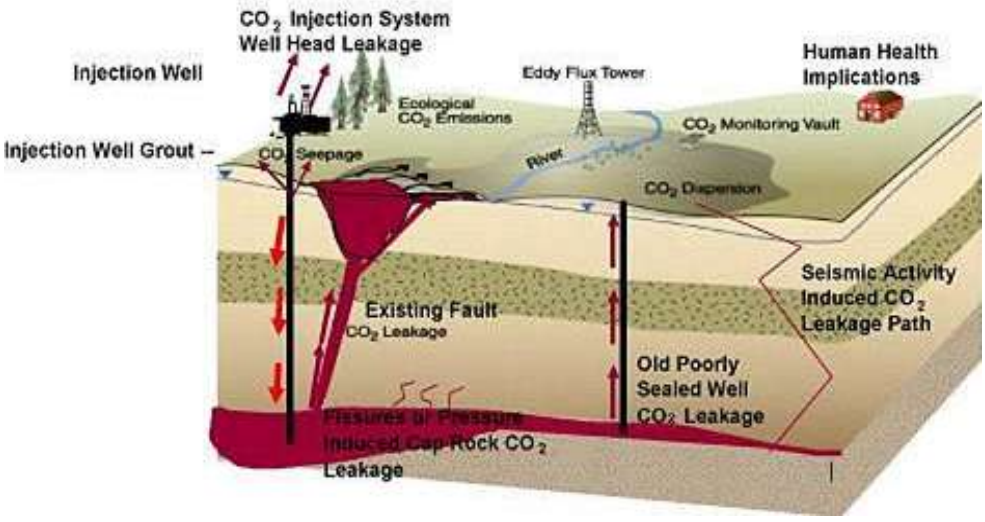

Fig. 1.2 The potential CO_2 leakage pathways from a geological storage reservoir to the site surface (modified from Dooley et al. (2010)).

According to Ide et al. (2006), orphan wells are those wells that are unowned and inactive, while abandon wells are normally termed as properly abandoned wells under the existing regulations but with no monitoring by the local governments. There is little information about the state of old wells (either orphan wells or abandoned wells) nearby CO_2 storage site, and those significant numbers of wells normally lack of

monitoring (Celia et al., 2005; Ide et al., 2006; Nogues et al., 2012). For example, there are currently around 135,000 orphan wells in Texas, USA with no monitoring (Ide et al., 2006). Therefore, the possibility that the stored CO_2 could leak to the nearby biosphere via these kinds of old wells nearby storage sites cannot be ruled out (Koornneef et al., 2012).

Fig. 1.3 shows the potential leakage pathways along an existing well. If the existing well is poorly sealed or failed in casing, the CO_2 could leak by passing through a corroded casing wall (Fig. 1.3 (c-e)), moving upward alongside the casing (Fig. 1.3 (a, b) and (f)) or travelling through the adjacent formations to the surface (Celia et al., 2005).

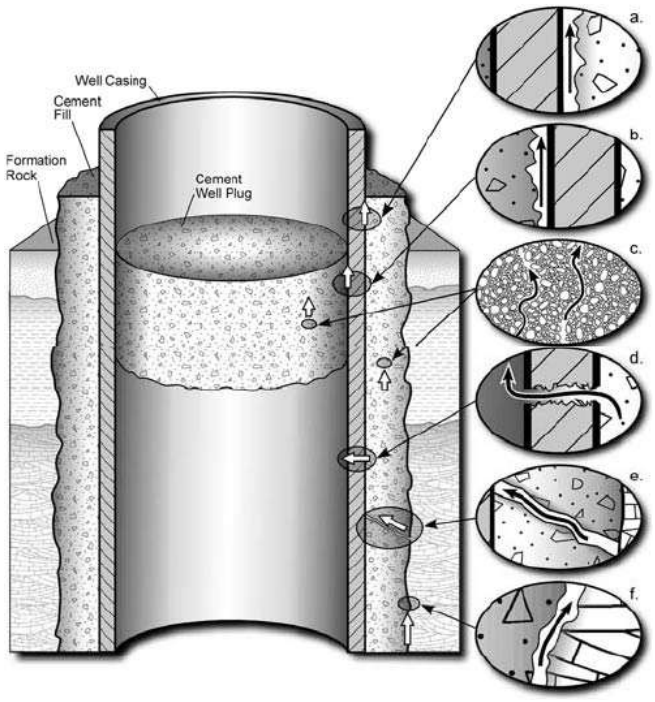

Fig. 1.3 Potential leakage pathways along an existing well: between cement and casing (paths a and b), through the cement (c), through the casing (d), through fractures (e), and between cement and formation (f) (Celia et al., 2005).

When the released CO_2 leaked to the surface, it could be present as a large gas plume over a big area (e.g. leaked through an existing fault or cracking areas around the storage site) or a small release (e.g. leaked

through a corroded casing wall or adjacent formations of an abandon well or an old well). Therefore, the potential impacts on the local area of both high concentrations of CO_2 gas and low release of CO_2 are studied in this research to simulate these two conditions. A detailed experimental design is presented in Chapter 3.

1.3 Previous research and knowledge gaps on impacts on the local environment of CO_2 leakage

The most studied areas related to local effects due to CO_2 leakage are the impacts on human health, animals and ecosystems. The effect of CO_2 exposure on human health and animals is in general well known (Damen et al., 2003; Koornneef et al., 2012; Roberts et al., 2011). Hepple (2005) provided a detailed review of human health effects after exposure to high concentrations of CO_2 and reviewed regulations protecting workers and public. It noted that no adverse effects for humans were observed at or below 1% v/v CO_2 (Hepple, 2005). Bachu (2008) stated that CO_2 could be dangerous to human health when its concentration increased to more than 0.5-1.5% v/v. More than 3% v/v CO_2 in a close environment would affect brain and cause consciousness to human (Roberts et al., 2011). High level of CO_2, for example 20-30% v/v, will cause death to humans and oxygen depended animals (Benson et al., 2003; Damen et al., 2003). For example, a natural disaster of a sudden release of 0.24 Mt CO_2 in volcanic areas Lake Nyos (Cameroon) caused the deaths of at least 1,700 people and thousands of animals on the evening of 21 August 1986 (Damen et al., 2003; Freeth and Rex, 2000). A detailed description of this site and the observed effects on the local environments by the release of CO_2 are presented in section 2.3.1.

There is limited information on impacts on ecosystems after exposure to high concentrations of CO_2 compared with effects on human health and animals (Damen et al., 2003; Hepple, 2005; Stenhouse et al., 2009).

Damen et al. (2003) are among the early researchers to discuss the safety issues related to a CCS storage project. Further research were carried out to examine the effects of CO_2 leakage on ecosystems either by laboratory experiments (Ardelan et al., 2009; Little and Jackson, 2010; Lu et al., 2010), natural analogue studies (Beaubien et al., 2008; McGinnis et al., 2011) or field-scale investigations (Kharaka et al., 2010). A soil acidification scenario caused by long-term climate change was also carried out to address impacts on ecosystems of elevated CO_2 concentration (Blake et al., 1999; Mayer, 1998). A detailed literature review is presented in Chapter 2.

Throughout the above mentioned research, it was noticed that CO_2 leakage would likely reduce groundwater pH and cause significant deterioration in the quality of potable groundwater by altering groundwater chemistry and cause changes of groundwater taste, colour or smell (Jaffe et al., 2003; Stenhouse et al., 2009). In addition, the acid water might cause increases in the concentration of trace elements in the soil solution, which will potentially increase the hardness of water as well as increase the concentration of toxic metals, such as sulphate and chloride (Jaffe et al., 2003; Stenhouse et al., 2009; Wilson et al., 2007). Rapid and systematic changes in ground water chemistry were reported by Kharaka et al. (2010) in a field study with CO_2 injected into the field on purpose; the pH decreased from 7.0 to 5.6, alkalinity increased from 400 to 1,330 mg L^{-1} as $CaCO_3$, and electrical conductance increased from 600 to 1,800 μS/cm. Increases in the concentration of alkali and alkaline

metals and increases in the concentration of certain ions, such as B, Ba, Ca, Cd, Co, Fe, K, Mg, Mn, Si, Sr and Zn were also reported (Aiuppa et al., 2005; Little and Jackson, 2010; Lu et al., 2010; McGrath et al., 2007).

CO_2 leakage rising to soils may change subsurface microbial populations either by favouring species or restricting them, depending on microbial species and site characteristics (Jossi et al., 2006; Kruger et al., 2009; Tian et al., 2001). For example, anaerobic conditions favour some microorganisms, such as methane-producing archaea or sulphate-reducing bacteria (Kruger et al., 2009); it may also cause significant inhibition for other aerobic microorganisms and such inhibition is observed for spores of *Monilinia fructicola* (Tian et al., 2001). Other research shows that the microorganisms appear to adapt to the elevated CO_2 condition by species substitution or adaptation shifting towards anaerobic and acidotolerant to acidophilic species (Kruger et al., 2011).

However, it has been noticed that the overall tendency in surface and subsurface soil chemistry changes with CO_2 leakage is not very clear, either to a chronic, high level exposure or to a short-term, small continuous release of CO_2 (Koornneef et al., 2012; Kruger et al., 2009; Stenhouse et al., 2009). Besides, the instantaneous response of sediments to the CO_2 release is unclear, as well as the recovery once CO_2 leakage stops. Soils, as part of any regional ecosystem, serve as the root layer for the majority of plants and also filter much of the water into streams, lakes and groundwater. The changes on soil chemistry could therefore have direct and indirect effects on other parts ecosystem and could further pose risks to human health (Ardelan and Steinnes, 2010; Bachu, 2008; Garfield, 1985; Gerlach et al., 2001). Moreover, as the last boundary for stored CO_2 leaked back to atmosphere, impacts on soil chemistry changes could be an

indicator for developing monitoring techniques to detect CO_2 leakage early and inform the design of the remediation approaches once the leakage is observed. It is therefore important to study the impacts on surface and subsurface soil chemistry changes by potential CO_2 leakage and it is the main focus of this research.

Variations in the initial physical and chemical properties of soils at any particular site would lead to their different responses to CO_2 leakage (Zheng et al., 2012). It is therefore necessary to address the soil response to CO_2 with different soil properties. Calcite dissolution is sensitive to CO_2 flux and could be the primary process buffering pH (Romanak et al., 2012; Zheng et al., 2012). Even for bedrock dominated by quartzofeldspathic gneiss and granite with only ~1% carbonate in the watershed, the dissolution of minerals mainly come from the weathering of carbonate minerals contained (Blum et al., 1998). Also, some areas are dominated by limestone sand and experiments with limestone sediments are representative of such landhood, for example, the beach sand on the coast of Cyprus and beach sand on the White Park Bay beach in Northern Ireland (Sandatlas, 2012). In contrast, silicate minerals react slowly with CO_2 and the leaked CO_2 may hold limited impacts on silicate minerals (Wilson et al., 2007). Limited work has been done on direct comparison of these two sediments. Therefore, limestone sand and silica sand (two end members) are both used in this research to understand the soil response to CO_2 flux with different soil properties. As particle size and moisture content are considered to be important factors to influence the response (Rowell, 1994a; Shih et al., 2000; Xu et al., 2005; Zhang et al., 2007), it is also necessary to examine the soil response associated with different particle size and moisture content. Therefore, a set of soil/sediment samples with different particle size and moisture content are prepared and

used in the experiments. The detailed information of the prepared samples is presented in section 3.1.1.3 and 3.2.3.

Moreover, most research to date has focused on the impacts of pure CO_2 on the environment. However, at the Zama oil field in Alberta, Canada, there is an ongoing EOR project co-injecting CO_2 with around 30% hydrogen sulfide (H_2S) (Smith et al., 2009). The gas could be further oxidised to SO_2, which will escape and be trapped in the topsoil or release to the atmosphere and may have a more serious influence on living plants than CO_2 alone (Lee et al., 1997; Lee et al., 2002; Yanagi et al., 1995). In addition, according to different types of capture techniques, even after purification during the carbon capture process, the captured CO_2 flue gas may still contain up to 7% vol. H_2O, 0.9% vol. N_2 and 0-1.5% vol. SO_2 (Benson, 2005b; Bouillon et al., 2009; Li et al., 2009; Pipitone and Bolland, 2009a, 2009b; Radosz et al., 2008). For both reasons, it is necessary to assess the potential risks caused by CO_2 leakage with SO_2 impurities. Depending on different types of power plant and capture techniques, the impurities in CO_2 captured stream from flue gas may still contain up to 1% SO_2. This research undertakes the assessment with 1% SO_2 concentration (section 3.1.2) to assess the effects with impure gas under the worst scenario.

This study is designed to better understand the relevant impacts on soil chemistry changes caused by CO_2 seepage to fill the knowledge gaps described above. A detailed literature review, which is the main motivation of the proposed aim and objectives of this research, is presented in Chapter 2. Accordingly, the following aim and objectives of this research were set.

1.4 Aim of this research and structure of this thesis

The aim of this research is to investigate the surface and subsurface soil chemistry changes caused by CO_2 seepage using well-controlled two stage laboratory experiments.

The following objectives were set to accomplish the overall aim:

1). Investigate soil responses to chronic, high level exposure of CO_2/SO_2, particularly changes in soil mineralogy, pH and the phytoavailability of elements;
2). Investigate soil responses to a short-term, small continuous release of CO_2, focusing on the changes in pH and ion concentration;
3). Assess the correlation between sediment properties and their response to CO_2 release, variations in sediments chemical composition (carbonate vs silica), particle size as well as different moisture content of sediments; and
4). Examine the recovery effects of soils after CO_2 exposure stops.

To achieve these aim and objectives, two different sets of experiments were carried out: Stage I- Closed experimental system and Stage II- A flow through column system (see methodologies for both stages in Chapter 3). Stage I composed laboratory based experiments to simulate the soil response to long term, high level exposure to CO_2/SO_2 (objective 1 as above) and to inform the design of the Stage II experiments. Stage II experiments were designed to achieve objectives 2-4 listed above.

During Stage I, to simulate long term exposure to a high level of CO_2/SO_2 gas, a set of soils (section 3.1.1) were run with high pressure/high temperature closed reactors (section 3.1.2). A detailed rationale and description of the experimental design is presented in section 3.1. Because

the author had access to a nearby field study site (section 3.1.1), which has similar research aims to this research, the soils for the Stage I experiments were collected from the site and the analysed aspects (section 3.1.3) were compared with the results from the field study and others (Chapter 4). Besides, the research in the stage I experiments can be used as a supplementary work to the field study. During stage I experiments, all the prepared set of soil samples were supposed to run with both CO_2 and CO_2/SO_2 mixture gas. However, during the Stage I experiments, there was only one CO_2/SO_2 mixture gas reactor and it was broken after one set of runs. Therefore, only one set of experiments with CO_2/SO_2 gas (section 3.1.2.2) was run. The results and discussion of the Stage I experiments are presented in Chapter 4. Throughout the Stage I experiment, it was observed that metal concentrations would likely change after the CO_2 or CO_2/SO_2 incubation and became the main focus in this research examined in both stage experiments.

In Stage II, a flow through column system was designed by the author (section 3.2). The column experiment is designed to simulate laboratory scale seepage of CO_2/SO_2 through sediments and water to investigate the real time responses of soil to a release of CO_2. Stage II experiments were designed to achieve objectives 2-4 listed above. The detailed description and basis of the experiments design is presented in section 3.2. The column system was pre-tested and checked several times before the real experiments to make sure there was no gas leak during the experiments and the column system functioned well. The detailed testing process is not presented in this thesis. During Stage II experiments, a set of runs on different sediments (section 3.2.3), varying in particle size and chemistry composition, were carried out under different conditions (different moisture content) (section 3.2.4). Results from both columns were

compared before, during and after the experiments and the analysed aspects (section 3.2.5) are compared with current research (see Chapter 5). During the Stage I experiments, the tested soils were collected from a field, which contained organic content and other factors that would influence the results slightly (Nikolaidis et al., 1994; Sass and Rai, 1987; Wu et al., 2010) and cause difficulties in understanding the geochemical reactions by CO_2 only. Different from Stage I, in order to better identify the main geochemical reactions with the system, the samples used in Stage II experiments are mono-mineral sediments instead of a real soil. As described above, limestone sand and silica sand (two end members) (section 3.2.3) are both used in this research to understand the soil response to CO_2 flux with different soil properties. Therefore, unlike Stage I experiments, for the chosen sediment samples in Stage II with known characterisation, XRD and particle size distribution analysis etc. were not carried out on the samples in the Stage II experiments (section 3.2.5.1). Moreover, the column experiments were designed for both CO_2 and CO_2/SO_2 mixture. As it was a newly designed column, for safety reasons, pure CO_2 gas was first used in the experiments instead of the impure CO_2/SO_2 gas. During Stage II, the experiments were run successfully with the pure CO_2 gas. However, within the constraint of the research time, no more impure CO_2/SO_2 gas was run in this research. These are considered as future work (Chapter 7).

The results and discussion of Stage II flow through column system experiments are presented in Chapter 5, followed by results interpretation in Chapter 6 to examine the correlation between sediment properties and their response to the CO_2 release. Finally, Chapter 7 summarises the main findings from this research as well as proposing further work.

Chapter 2 Literature Review

2.1 Introduction

Damen et al. (2003) are among the early researchers to discuss the safety issues related to CCS storage projects. They provided a good review of the risks associated with CO_2 geological storage, the mechanisms behind CO_2 leakage, and the local impacts of CO_2 leakage. They pointed out the gaps in knowledge of the impacts of CO_2 on well performance and cap rock integrity, and suggested that the risks caused by CO_2 leakage were less well understood. Further projects and experimental work were suggested to assess the potential effects on the local environment and ecology by potential CO_2 leakage.

There is limited information on impacts on ecosystems after exposure to high concentrations of CO_2 compared with effects on human health and animals (Damen et al., 2003; Hepple, 2005; Stenhouse et al., 2009). For consequences of CO_2 leakage on the environment, it is suggested that high levels of soil CO_2 are likely to affect the pH of soil water and have adverse impacts on the chemistry of nutrients, redox-sensitive elements (e.g. Fe, Mn and Co), and trace metals (e.g. Al, Ni and Pb). High levels of soil CO_2 may eventually influence or cause death of vegetables because of suppressed respiration in the root zone or enhanced harmful high levels of heavy metals (Ardelan and Steinnes, 2010; Bachu, 2008; Gerlach et al., 2001). Detailed description of these studies addressing the impacts on the local environment of elevated CO_2 is reviewed in section 2.3.

This chapter covers impacts on local environments by potential CO_2 leakage, focusing on impacts on soil chemistry. The following chapter

includes reviews of potential impacts of CO_2 leakage on soil chemistry (section 2.2) in terms of changes in soil pH (section 2.2.1), metal and metalloid changes (section 2.2.2), nutrient changes (section 2.2.3), potential mineralogy and oxide changes (section 2.2.4), as well as previous and ongoing research on the effects of elevated CO_2 on the local environment (section 2.3).

2.2 Potential CO_2 leakage impacts on soil chemistry

Potential CO_2 leakage impacts on soil chemistry are summarised in the following sections in terms of changes in pH of soil pore water (section 2.2.1), metal and metalloid concentration (section 2.2.2), and mineralogy and oxide (section 2.2.4).

2.2.1 Changes in soil pH and the acid rain problem

The pH of a soil solution can be defined as $-\log[H^+]$, where H^+ is the hydrogen ions dissociated from soil pore water as follows (Little and Jackson, 2010; Rowell, 1994a),

$$H_2O \leftrightarrow H^+ + OH^- \tag{2.1}$$

Soil pore water absorbs CO_2 to form carbonic acid, H_2CO_3, a weak acid, which will partially dissociate to release H^+, HCO_3^- and CO_3^{2-}:

$$CO_2 + H_2O \leftrightarrow H_2CO_3 \tag{2.2}$$

$$H_2CO_3 \leftrightarrow HCO_3^- + H^+ \tag{2.3}$$

$$HCO_3^- \leftrightarrow CO_3^{2-} + H^+ \tag{2.4}$$

CO_2 saturated water at atmospheric conditions has a pH value of 5.6 (Garfield, 1985). Most soils have pH values ranging from 4 to 8 (Frederick and Thompson, 1993). An input of acid (such as HNO_3 or H_2SO_4) or base (e.g. NaOH) can change soil pH by changing the concentration of the H^+ in soil solution. A strong acid gives a higher concentration of H^+ and lowers soil pH more than a weak acid (Rowell, 1994a). Acid rain was one of the problems causing the changes in the soil pH.

Chemist Robert Angus Smith first coined the term acid rain in 1872 when he described the changing chemistry of rain in the industrial city of Manchester, England. Later, when scientists realised that snow, sleet, dew, mist, fog and wind could also carry significant amount of acid, which would influence soil pH, the term acid deposition was suggested (Garfield, 1985; USEPA, 2012). For the sake of simplicity, scientists still use the term 'acid rain' to represent the general problems. Until the 1970s, acid rain was considered as a serious environmental problem and the increase in acidity of some soils, lakes and streams was observed widely (Mol et al., 2003; USEPA, 2012). Emissions of SO_x, NH_3 and NO_x are the main contributors to acidic deposition, which are typically emitted from fossil-fuel power stations, mobile sources, industrial sources, power plants, and forming sulphuric and nitric acid (Rice and Herman, 2012). Among all these acidic gas emissions, sulphates typically account for 60%, nitrates for 30%, and chlorides for 10% of the acidity of acid rain (Garfield, 1985).

In 1980, under the direction of the National Acidic Precipitation Assessment Program (NAPAP), an Acid Deposition Act which was passed by the U.S. Congress established a 10-year research program looking at the entire problem. During 1970s and 1990s, large amounts of studies were focused on acid rain issues worldwide, including the effects on soil

chemistry, freshwater and terrestrial ecosystem, vegetations species, forest yields, historical buildings and building materials, as well as potential control programme (Cogbill and Likens, 1974; Falkengren-Grerup et al., 1987; Likens and Bormann, 1974; Skiba, 1989; Tamm and Hallbäcken, 1988; USEPA, 2012). Intensive research provided convincing evidence that acid deposition plays important roles in the acidification of some soils, leading to a large decrease in soil pH. For example, it was observed that acid deposition in Scotland had caused acidification of peats and the soil pH in some peats in Scotland was decreased to less than 2.80 in the 1980s (Skiba, 1989). A decrease of 0.5-1.0 units in soil pH were also reported by Falkengren-Grerup et al. (1987) for various forest and heathland sites in south Sweden back to the 1980s. The research on the effects on soil chemistry by soil acidification was normally carried out in terms of stimulated acid deposition experiments or field experiments and observations (Bergkvist, 1987; Bini and Bresolin, 1998; Crowder, 1991; Falkengren-Grerup et al., 1987; Falkengren-Grerup and Eriksson, 1990; Henriksen and Wright, 1977; Mannings and Smith, 1996; Skiba, 1989; Stevens et al., 2009). It was observed that the acid deposition increased leaching of metals (for example, Na, K, Mg, Ca, Fe, Mn, Al, Cu, Zn, Cd, Pb, Cr and Ni) from the organic layer of soil or underlying soil mineral layers by exchanging with H^+ and pH was an important factor controlling metal mobilisation patterns from soils (Bergkvist, 1987; Crowder, 1991; Falkengren-Grerup et al., 1987; Falkengren-Grerup and Eriksson, 1990; Skiba, 1989; Tyler and McBride, 1982). Detailed metal and metalloid concentration changes with pH are presented in section 2.2.2.

Governments from different countries attempted to regulate these acid emissions to reduce the adverse effects of acid rain. In 1970, the Clean Air Act was passed by Congress in the USA followed by passing of

amendments in 1990. The amendments of 1990 targeted to reduce the annual SO_2 emissions by 10 million tons below 1980 levels of about 18.9 million tons (Rice and Herman, 2012; USEPA, 1990). In 1995, the Acid Rain Program (ARP) was set in the United States to meet the demand reduction of NO_x and SO_x emissions from the Clean Air Act (USEPA, 1995). The ARP program not only caps the target SO_x and NO_x emission of the power industry, but creates an incentive program for trading the emissions, especially SO_x emission in particular. Nitrogen-oxide reduction was achieved through performance standards set by EPA (USEPA, 1990). The regulations lead to an obvious decline of SO_2 emissions, which resulted in observed improvements in surface-water quality across the USA, Canada and European (Rice and Herman, 2012; Skjelkvale et al., 2001). Though the NO_x emissions sometimes increased again in several European Countries due to increase of vehicular transportation (Vestreng et al., 2009), a general small decrease or more or less constant trend in NOx emission was found in European countries and in the USA since 1990 (Rice and Herman, 2012).

Similar to the acid rain problem, it is highly possible that additional CO_2 concentration in soil would decrease the pH by providing H^+ and acidify the soil solution. A study was carried out at the Rothamsted Experimental Station, UK, to assess the pH changes accompanying atmospheric deposition of CO_2. The pH of surface soil (0-23 cm) decreased by approximately 2.5 units from the time of the first soil sample collection in 1883, and the drop was purely based on atmospheric CO_2 deposition over 100 years (Blake et al., 1999). For a natural analogue in Latera, Italy (section 2.3.1), a decrease in pH was also observed around the centre of the vent with different decreasing patterns towards the CO_2 venting centre, an almost anoxic area due to the high concentration and high flow of CO_2

(Beaubien et al., 2008). For the research in the ASGARD field, CO_2 gassing lowered the soil pH in comparison with the controlled plots (Patil et al., 2010), and a decrease in pH was observed in soil Horizon A with a 0.5 pH decline (West et al., 2009). More detail of the ASGARD field and pH change patterns in the site is presented in section 2.3.2.

The chemical impacts of acidification in soil in a given situation involve not only the amount of acid present but the kind of acid present, which could have a different effect on certain chemical reactions taking place in the soil zone and in the water draining the soil (Johnson et al., 1984). Though there are some similarities between the acid rain problem and the elevated CO_2 existence in soils (e.g. decrease in soil pH and increase in several cation concentration), the effects on soil chemistry changes due to elevated CO_2 cannot be represented simply by the acid rain problem because of the different kinds of acid. As presented above, though the acid rain problem had been researched worldwide since 1970, the overall tendency in soil pH and surface and subsurface soil chemistry changes with elevated CO_2 is not very clear, which is the problem when stored CO_2 leaks back to the local environment from the storage site. This is one of the gaps this research tries to fill in.

Though there was research carried out to assess the effects in soil pH by elevated CO_2 (as mentioned above), the measured pH in previous research was mostly related to the pH of soil pore water after a long time of acidification. The instantaneous response of soils in pH to additional CO_2 flux is not clear, which is important for developing CO_2 leakage monitoring techniques and explaining further ion concentration changes. Besides, the pH drop mentioned above varies from one study to another, and the difference may be caused by different initial soil properties and initial pH in

soil pore water. It is therefore important to investigate the response of soil in pH associated with different soil types. This research is carried out to fill in these gaps.

2.2.2 Metal and metalloid changes

The mobilisation of some metals following CO_2 intruding may pose higher risks to plants and human health. Changes in metal concentration in the aqueous phase due to elevated CO_2 are always a major concern when considering CO_2 leakage occurrence in soil or groundwater, which therefore has been studied frequently (Ardelan et al., 2009; Beaubien et al., 2008; Kharaka et al., 2006). The ten most investigated metals are presented in the following sections listed in alphabetical order. For each section, the research reviews the origin of each metal or metalloid in soil, the solid phases controlling each metal/metalloid, the existence of metal/metalloid species in soil associated with various pH levels, the toxicity of each metal/metalloid, the mechanism of the toxicity to plants and living organisms, and the acceptable limits to plant growth or human health. Additionally, in each section, the observed changes of metal/metalloid with CO_2 appearance in previous studies are presented, as well as metal/metalloid concentrations changes along with soil pH

2.2.2.1 Aluminium (Al)

Aluminium (Al) is a common metal in the environment which normally exists in silicate minerals such as micas ($(K,H_3O)(Al,Mg,Fe)_2(Si,Al)_4O_{10}[(OH)_2,(H_2O)]$), feldspar (orthoclase, $KAlSi_3O_8$) and in clay (such as kaolinite, $Al_2Si_2O_5(OH)_4$). Al is a major toxin

to plant growth and crop production along with acid land (Hesse, 1971a; Kochian, 1995). The potential solid phases that control the solubility of Al in soil water are mainly gibbsite ($Al(OH)_3$), jurbanite ($AlSO_4(OH)\cdot 5H_2O$) and alunite ($(KAl_3SO_4)_2(OH)_6$) (Berg and Banwart, 2000). When pH decreases in soil solution, soil minerals start to weather and neutralise some of the acidity in soil.

The species of Al formed in soils depends on pH levels as summarised in Table 2.1. With mildly acidic or neutral pH in soil (between pH 6.5 to 7.4), the dominant phase for Al is in the form of aluminium silicates or oxides, such as $Al(OH)_3$ and $Al(OH)_4^-$ (gibbsite), which are water insoluble and do not adversely affect plant growth. Higher pH of soil pore water contains more $Al(OH)_4^-$ in soil solution (Delhaize and Ryan, 1995; Kochian, 1995; Wren and Stephenson, 1991). Between pH 4.0 and 6.5, there exists more than one Al phase, including $Al(OH)^{2+}$ and $Al(OH)_2^+$, which are toxic phases to plants. Within the pH range of 4.0 and 6.5, $Al(OH)_3$ and $Al(OH)_4^-$ may also appear (Hesse, 1971a; Wren and Stephenson, 1991). When pH is lower than 5.0, an increase in the rate of Al released from silicate lattices, clay minerals and organic forms is expected (Blake et al., 1999). As pH drops below 4.2 into the Al buffer range (pH 4.2-3.0), Al is progressively weathered from interlayer and trivalent Al^{3+} is released into solution from SiO-Al groups and Al (hydro)oxides. Al^{3+} then becomes the dominant ion in the solution, which is a harmful phase for plant growth (Blake et al., 1999).

Table 2.1 Al species at different pH (Delhaize and Ryan, 1995; Kochian, 1995; Wren and Stephenson, 1991).

pH	*ALUMINIUM SPECIES*	*TOXICITY*
6.5<pH<7.4	$Al(OH)_3$, $Al(OH)_4^-$	Insoluble
4.0<pH<6.5	$Al(OH)^{2+}$, $Al(OH)_2^+$ dominate	Soluble and toxic
	$Al(OH)_3$ and $Al(OH)_4^-$ may appear	Insoluble
3.0<pH<4.2	Al^{3+}	Soluble and toxic

The speciation of Al in soil solution is important because it affects the toxicity of Al to plants and living organisms. It is agreed that free Al^{3+}, $Al(OH)_2^+$, and $Al(OH)^{2+}$ are the most toxic species (Kubova et al., 2005). The toxicity of Al increases along with a decrease in pH value. However, the toxicity of different Al species varies among plant species and some may be more sensitive to one Al phase than the other. For example, Al^{3+} is the most toxic phase to wheat roots, while dicotyledons are more sensitive to $Al(OH)^{2+}$ or $Al(OH)_2^+$ than Al^{3+} (Kochian, 1995).

The main toxicities of a high concentration of exchangeable Al are: inhibiting the uptake of nutrients in soil solution, interfering with sugar phosphorylations inside the living cell, and inhibiting root growth (Kochian, 1995; Russell, 1973). For example, a higher concentration of Al, 200 μmol L^{-1}, will inhibit plants' uptake of several nutrients, such as Mg^{2+}, Ca^{2+} as well as phosphate translocation (De Wit et al., 2001; Gessa et al., 2005; Lin, 2010). Numbers of studies suggest that rapid inhibition of root growth is the first and main symptom of Al toxicity and the root apex is the primary place of Al-induced root growth inhibition, which has become a widely accepted symbol of plants stress by Al (Delhaize and Ryan, 1995; Kochian, 1995). Higher Al concentrations have direct effects on plant metabolism by reducing the capacity for phosphorus translocation and affecting the plant's ability to take up water by shortening and thickening plant roots, and also causing injuries in plant leaves (Hesse, 1971a; Pereira et al., 2010; Poschenrieder et al., 2008; Rowell, 1994a; Zhang et al., 2010). There are many hypotheses for the mechanism of Al toxicity, such as Al interaction within the root cell wall, Al disruption of the plasma membrane, a fast inhibition of cell elongation and root cell division, and interaction with the cytoskeleton and calmodulin (Kochian, 1995; Poschenrieder et al., 2008). There is little evidence supporting any of

these hypotheses (Kochian, 1995; Poschenrieder et al., 2008). Al resistance of different plant species varies due to their different Al tolerance, which may range from 1 μg cm^{-3} to about 40 μg cm^{-3} and normally Al concentrations higher than 40 μg cm^{-3} in soil solution will restrict most plants' growth (Hesse, 1971a; Poschenrieder et al., 2008). No significant harm will be caused to plant growth if the concentration of exchangeable-Al is less than 1 μg cm^{-3} (Hesse, 1971a; Poschenrieder et al., 2008).

Previous soil acidification research shows that Al in plants is negatively correlated with soil pH in the field and increasing acidification increases the amount of aluminium in plants and soil solution (Bergkvist, 1987; Crowder, 1991; Falkengren-Grerup et al., 1987). A soil column laboratory study established that decreasing soil pH to less than 4.0 would largely increase the leaching rate for Al (Fuller et al., 1976). At Rothamsted Experimental Station in the UK (Blake et al., 1999), it was observed that exchangeable Al species in the soil surface layer (0-23 cm depth) increased by approximately 100 times between 1904 and 1991 (4 to 410 mg kg^{-1}) when pH dropped from 5.3-5.5 to 3.6-3.8. In a controlled chamber experiment investigating effects of experimental CO_2 leakage on sediments, an increase in dissolved fractions of Al in the CO_2 seepage chamber was 5.1 times higher than the control system, and Al was considered to be one of the most effective mobilised metals in the research (Ardelan et al., 2009). Berg and Banwart (2000) observed that anorthite ($CaAl_2Si_2O_8$) weathering was accelerated in the presence of CO_2, especially for neutral and near-basic pH soil. They suggested that this may be caused by "carbonation weathering" processes, a reaction between the adsorption of carbonate ion and Al complex compounds (Berg and Banwart, 2000). Lu et al. (2010) observed that the concentration of Al increased

rapidly at the start of CO_2 injection and became steady before the end of the experiments.

2.2.2.2 Arsenic (As)

Arsenic (As) is naturally contained within rocks, sediments or soils, partly as a constituent of sulphide minerals or complex sulphides of metal cations, and is partly retained by soils and sediments in occluded or adsorbed forms, such as hydrous Al and Fe oxides. Generally, the mean As concentrations in igneous rocks are within a range of 1.5 to 3.0 mg kg^{-1}, while it is within a range of 1.7 to 400 mg kg^{-1} in sedimentary rocks (Smith et al., 1998). Normally background concentration of As in soils does not exceed 15 mg kg^{-1} with various concentrations in different soil types (Smith et al., 1998). Numerous anthropogenic processes could lead to elevated levels of arsenic in the soil environment, for example agriculture, mining and mineral processing operations (Al-Abed et al., 2007; Smedley and Kinniburgh, 2002; Smith et al., 1998). Common minerals in soils containing As are ferric arsenate ($FeAsO_4$), arsenopyrite (FeAsS), mispickel (FeSAs), orpiment (As_2S_3), realgar (AsS), $Ca_3(AsO_4)_2$, $Mn_3(AsO_4)_2$ or a $Pb_3(AsO_4)_2$ phase (Masscheleyn et al., 1991; Page, 1982a). Some of the minerals dissolve with water and form soluble As. For example, $FeAsO_4$ mineral dissolves to iron hydroxide and soluble arsenate (Masscheleyn et al., 1991). In addition, As may be adsorbed on clay colloids or bound to organic matter and form water-soluble compounds with Al, Fe, Ca, and Mg in the soil matrix (Schmoger et al., 2000).

$$FeAsO_4 \cdot 2H_2O + H_2O \rightarrow H_2AsO_4^- + Fe(OH)_3 + H^+ \quad (2.5)$$

Normally, natural As in uncontaminated soil ranges from 0.2 to 40 μg g^{-1}, and can exist as -3, -5, +3, and +5 valence states in nature as organic or inorganic compounds (Page, 1982a). The water soluble form of As is more phototoxic than firmly bound forms. Inorganic arsenic (for example arsenite (As_2O_3, AsO_3^{3-}), arsenic oxide (As_2O_5), and arsenate (AsO_4^{3-})) is more toxic than organic arsenic (such as monomethyl arsenic acid (MMAA) and dimethyl arsenic acid (DMAA)) (Masscheleyn et al., 1991; Patra et al., 2004). In addition, arsenite, As(III) is more phototoxic than arsenate, As(V), and they are both considered to be toxic states of As (Masscheleyn et al., 1991; Patra et al., 2004).

Different soil redox potential (Eh) and soil pH has effects on the As species, which further influence the toxicity. For pH ranging from 4-8, the species within the soil solution could be a combination of H_3AsO_3, H_2AsO_4, $HAsO_2^-$ (Carbonell-Barrachina et al., 2000; Masscheleyn et al., 1991). Fig. 2.1 shows the dominant As species along with different Eh and pH in soil.

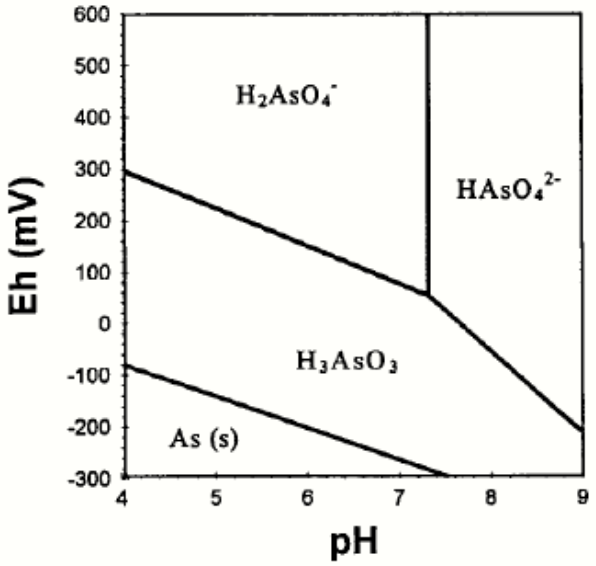

Fig. 2.1 As species associated with various Eh and pH (Carbonell-Barrachina et al., 2000).

The arsenic toxicity is considered as inhibiting enzyme activity of plants, interfering with sulfhydryl groups in the cells of most plants, and decreasing the mitotic index as well as chromosomal aberrations (Patra et al., 2004; Schmoger et al., 2000). The symptoms of arsenic toxicity can be a decrease in plant growth and crop yield, damage to leaf tips and leaf margins as well as a decrease in photosynthetic capacity (Barrachina et al., 1995; Marin et al., 1993). Tolerance of As varies among different plants and there is no consensus on safety As tolerance limits for plants. However, damage to root membranes was observed when exposed to 10 mg L^{-1} As (Barrachina et al., 1995). Merry et al. (1986) carried out a glasshouse experiment to study the uptake of As by plants with different types of soils, and they found that with soil-As concentrations between 26 and 260 mg kg^{-1}, none of the examined plants were grown. For human health, 1.0 mg kg^{-1} (dry weight) is suggested to be the acceptable limits (National Food Authority, 1993).

Previous research shows that the concentration and species of water soluble As is pH dependent (Al-Abed et al., 2007; Carbonell-Barrachina et al., 2000; Frost and Griffin, 1977; Pierce and Moore, 1980; Smith et al., 1998). For example, Carbonell-Barrachina et al. (2000) carried out a laboratory experiment examining As speciation and solubility in sewage sludge suspensions in relation to pH and Eh. They found out that the soluble As was at maximum levels at a neutral pH value and the concentration would decrease with acidic or alkaline condition. Under neutral pH condition, As biomethylation formation will be promoted, which would produce organic As compounds with a much lower toxicity than their inorganic species (Carbonell-Barrachina et al., 2000). Al-Abed et al. (2007) also observed a strong dependence of pH on As leaching in a batch experiment with As leaching followed a "V" shaped pattern with higher

leaching in both acidic and alkaline pH condition. Under acidic pH, mineral dissolution resulted in higher As concentration, while under alkaline pH, desorption of arsenic took place resulting in high As concentration. It was observed that maximum As solubilisation occurred at pH 11, and the release of As was related to the dissolution of Fe in the low pH region (Al-Abed et al., 2007). An increase in trace element As was noticed in a natural analogue due to CO_2 gas venting (Beaubien et al., 2008). The As concentration in the sediment water phase showed an rapid increase with the intrusion of CO_2 in a batch reaction experiment, and it then declined towards the end of the experiment (Lu et al., 2010). Lu et al. (2010) suggested that As would pose limited risks to water quality compared with other metals (e.g. Mn, Ba, Zn).

2.2.2.3 Cadmium (Cd)

Cadmium (Cd) normally exists in mining areas and appears at low concentrations in natural soils, depending on and largely influenced by the amount of Cd in the parent rock. The average cadmium concentration in soils derived from igneous rocks is reported to be within the range of 0.10–0.30 ppm, while soils derived from sedimentary rocks contain slightly higher Cd concentrations, 0.30–11 ppm Cd (Bradl, 2004).

Cd is detected as a toxic ionic form of Cd^{2+}. High concentrations of Cd may affect crop yield and quality and are particularly harmful to human health (Yang et al., 2006b). The concentration is accumulated by many vegetables (leafy and root) and fruits, and it can affect human health when ingestion and inhalation occurs via food, drinking water and soil/dust (Prasad, 1995; Yang et al., 2006b). Cd in soil solution is taken up by

plants not only through roots but also by root systems. When exposed to high Cd salt solution, inhibition in cell and plant growth can be seen due to Cd toxicity (Laspina et al., 2005). Other effects include strong influence on metabolic activities of crop plants (Jia et al., 2010; Prasad, 1995). Growth inhibition mechanisms due to high concentration of toxic Cd could be explained as: changes in plant water and ion metabolism; reduced water and nutrient uptake ability; reduction of enzyme activity in plants; photosynthesis inhibition by closing stomata of plants; free radical formation ($O_2^{\cdot -}$, H_2O_2 and $OH^{\cdot}$); and also severe damage to cell organelles, which further hinder plants growth (Jia et al., 2010; Laspina et al., 2005; Prasad, 1995).

The bioavailability of Cd could be influenced by many factors, e.g. pH, organic matter content, cation exchange capacity as well as specific surface areas (de Matos et al., 2011; Tyler and McBride, 1982). For example, when a soil solution contains high concentrations of H^+ and Ca^{2+}, the bioavailability and toxicity of Cd will be reduced (Wren and Stephenson, 1991). Cd^{2+} prefers to combine with colloidal and particulate size (1-12 μm) fraction and adsorb on particle surfaces. Similar situations occur when high dissolved organic matter (DOM) is present. Cd combines with and is bound to DOM (Prasad, 1995; Wren and Stephenson, 1991). In addition, Cd toxicity could be reduced by the occurrence of antioxidant properties of Zn^{2+} by regulating membrane transporter-mediated Cd uptake, alleviating Cd-induced oxidative stress and influencing the free radical species and antioxidants formation caused by Cd occurrence (Aravind and Prasad, 2005). Fig. 2.2 shows the effects on plants caused by high Cd^{2+} and rehabilitation on plants associated with Zn^{2+}.

Fig. 2.2 Different metal treatments on C. demersum (Aravind and Prasad, 2005).

Note: A) control plants without any treatments; B) with Cd-10μM; C) with Cd-10μM+Zn-10μM; D) Cd-10μM+Zn-50μM; E) Cd-10μM+Zn-100μM; F) Cd-10μM+Zn-200μM

With respect to safety levels in humans, 1 μg kg^{-1} body weight is the daily tolerable intake (Yang et al., 2006b). The safety level for plant growth was tested through experiments with tomato and maize. Yildiz (2005) agreed with previous research and suggested that increased Cd dose (up to 10 mg L^{-1}) in nutrient culture would cause large yield reduction, for example 75 % for beans, 65 % for sugar beet, and 40 % for maize.

Changes in Cd concentration were observed in previous research. Cd was suggested to be the most sensitive element to soil acidity at Rothamsted Experimental Station, UK. However, Ross (1994) reviewed the processes of mobility of toxic metals in acidified soils and noted that Cd would be mobilised after Al, Mn and Zn. In a laboratory column system, de Matos et al. (2001) measured the heavy metal movement associated with selected Brazilian soils of various chemical and mineralogical soil characteristics, and suggested that the mobility of Cd is higher than Cu and Pb and lower than Zn. Blake and Goulding (2002) observed that the effective mobilisation of Cdas 'available' heavy metal was at pH 6.0-5.5, and suggested that exchangeable Cd was the highest at pH 4 and was up to

four times greater at pH 4 than other pH values. In addition, when soil pH was at 4.0, 60-90% total soil Cd was leached, but absorbed onto ion exchange surfaces and/or complexed with soil organic matter, which leads to a decrease in NH_4OAc-exchangeable Cd and increase as 'available' metal content as EDTA extractable Cd (Blake and Goulding, 2002). Higher concentrations of Cd in sediments and ground water were also observed in other soil acidification scenarios (Ardelan et al., 2009; Mayer, 1998). For a controlled soil chamber with CO_2 injection from one side, Cd increased near CO_2 injection sites, while the authors concluded that Cd was not the most effective mobilised metal compared to Pb and Al (Ardelan et al., 2009). Those observed different effects on Cd concentration by CO_2 leakage may be caused by different initial soil properties. In addition, high DOM, Ca^{2+} and H^+ may cause a reduction of the bioavailability of Cd^{2+}. It is therefore necessary to investigate the changes in ion concentration due to CO_2 intrusion associated with different soil types.

2.2.2.4 Chromium (Cr)

Chromium (Cr) is considered as one of the most abundant elements in Earth's crust with an average concentration of 100 ppm and exists in solid phase, such as chromite and Cr-substituted goethite (Becquer et al., 2003). Normally, the Cr concentrations in soil are between 1 and 3000 mg/kg (NRC, 1974). It is found that Cr is relatively high in the more magnesian rocks, and the content of Cr decreases when rocks become more silicic (Simon and Rollinson, 1976).

Naturally, Cr exits and stabilises in either the trivalent (Cr(III)) or the hexavalent (Cr(VI)) oxidation states, which mainly depends on pH and redox conditions (Zeng et al., 2008). Generally, Cr(III) is less soluble and

mobile, and much less toxic than the Cr(VI) form (Mattuck and Nikolaidis, 1996; Nikolaidis et al., 1994). In natural systems, Cr(lll) may exist as insoluble chromium hydroxide ($Cr(OH)_3$), or may form low-solubility complexes with other ligands, while Cr(VI) normally presents as either the chromate ion (CrO_4^{2-}) or monohydrogen chromate ion ($HCrO_4$). Cr(VI) may be adopted to soil particle surface, and reduced by adsorption onto organic matter and coating onto iron oxide mineral surface (Nikolaidis et al., 1994; Sass and Rai, 1987).

High level of Cr(VI) is toxic to plants and eventually harms human health. Different studies were carried out to address the toxicity of Cr to plant growth. Turner and Rust (1971) observed that 0.5 mg L^{-1} of Cr decreased the yield of soybeans and influenced other macro- and micro- elements, such as P and Fe. Other research observed that Cr at 0.75 mmol L^{-1} (equivalents to 13.5 mg L^{-1}) caused death of treated embryos (Calevro et al., 1999), and Cr was considered toxic to most higher plants at 100 $\mu M \cdot kg^{-1}$ dry weight by Davies et al. (2002).

The increase in Cr concentration with the introduction of CO_2 was observed in most research. For example towards the CO_2 venting centre of a Mediterranean pasture of Latera Italy, an increase in Cr was observed by Beaubien et al. (2008). Cr concentration increased quickly with the intrusion of CO_2 in a batch reaction experiment (Lu et al., 2010); and there was considerable increase in Cr concentration of sediment samples pore water after flowing CO_2 gas into the chamber system (Ardelan et al., 2009). However, the Cr adsorption process also took place towards the end of the CO_2 injection in some research (Ardelan et al., 2009; Lu et al., 2010), which reduced the concentration of Cr and mitigated the hazardous effects of Cr metal mobilisation.

2.2.2.5 Copper (Cu)

Copper (Cu) is a micronutrient for plant growth and naturally exists in different compounds (Barber, 1995; Wu et al., 2010). The primary Cu ore minerals are chalcopyrite ($CuFeS_2$), chalcocite (Cu_2S), bornite (Cu_5FeS_4) and djurleite ($Cu_{31}S_{16}$). Minerals in the oxidized zones containing Cu are malachite ($Cu_2CO_3(OH)_2$), azurite ($Cu_3(CO_3)_2(OH)_2$), chyrsocolla $(Cu,Al)_2H_2Si_2O_5(OH)_4 \cdot nH_2O$, cuprite ($Cu_2O$), tenorite (CuO), native copper (Cu) and brochantite ($Cu_4SO_4(OH)_6$). Most Cu in soils exists as an unavailable form to plants (Barber, 1995; Wu et al., 2010).

The availability of Cu to vegetation is influenced by soil properties, such as pH, dissolved organic carbon (DOC), total nitrogen, available phosphorous, available potassium content, calcium concentrations, and cation exchange capacity (Römkens et al., 1999; Wu et al., 2010). The total Cu concentration increases when soil organic matter increases (Wu et al., 2010). Elevated DOC levels cause a reduction in free ionic Cu^{2+} activity as the following complexation between Cu^{2+} and DOC taking place (Römkens et al., 1999):

$$Cu^{2+} + H_X HUM \leftrightarrow CuH_{(X-N)}HUM + nH^+ \quad (2.6)$$

Cu deficiency is a problem for plant growth, which can be accentuated by high nitrogen availability (Marschner, 1995). The critical deficiency level of copper in plants is suggested to be within 1-5 μg g^{-1} dry weight (Marschner, 1995). Excessive Cu is also harmful to plant growth and its toxicity is related to the amount of free Cu^{2+} available to plants. The toxicity of excessive Cu influences root tip cell division, root elongation, and also the entire root architecture, which causes stress in plant root and

further influences plant growth (Madejón et al., 2009). The mechanism behind it is uncertain, but it may relate to the induced lipid peroxidation and membrane damage due to excessive Cu (Madejón et al., 2009). The mechanism may also include damage in oxidation and modification of cellular amino acids and proteins caused by mediate free radical formation in isolated chloroplasts and intact roots (Boojar and Goodarzi, 2007; Fang and Kao, 2000). In addition, a high concentration of Cu^{2+} will inhibit Fe^{2+} uptake by plants (Madejón et al., 2009). The critical toxicity level of copper is suggested to be above 250 μg L^{-1} (Marschner, 1995).

Higher concentration of Cu in sediments and ground water was observed in soil acidification scenarios (Mayer, 1998). Compared with Zn and Cd, Cu is more adsorbed in soils and shows less mobility than others in a laboratory column system carried out by de Matos et al. (2001). A significant increase in Cu in a controlled soil chamber near the CO_2 injection area was also observed by Ardelan et al. (2009). Harter (1983) found that with pH value above 6.0 Cu would form Cu hydrolysis, $CuOH^+$, which was the reason to soil Cu retention. King et al. (1992) observed that dissolved Cu remained similar and did not show obvious trends in lake water even pH down to 4.7

2.2.2.6 Iron (Fe)

Iron (Fe), the fourth most abundant element in the Earth's crust, has important roles in biogeochemical redox reactions in marine and freshwater environments. Naturally, Fe exists in soils as iron oxides, such as goethite (FeO(OH)), hematite (Fe_2O_3) and magnetite (Fe_3O_4), or forms as other compounds such as limonite (FeO(OH).n(H_2O)) or siderite

($FeCO_3$). Fe(II) compounds are called ferrous, and Fe(III) compounds ferric (Barber, 1995; Fortin and Langley, 2005).

In aerobic soils, Fe exists as Fe(III), Fe^{3+}, and is required for plant growth; while for soils under anaerobic conditions, such as with elevated CO_2 appearance in soil or lower pH of soil pore water, Fe^{3+} is reduced to Fe^{2+}, which is toxic to plant growth if excessive Fe^{2+} is absorbed by roots (Ammari and Mengel, 2006; Majerus et al., 2007).

Fe deficiency is normally accompanied by yellow leaves due to low levels of chlorophyll, the first sign of Fe deficiency, and appears on the younger upper leaves. Fe deficiency mainly associated with high pH in soil, as well as high available P, Mn and Zn appearance in soil (Ammari and Mengel, 2006). The critical deficiency level for Fe in leaves is in the range of 50-150 mg kg^{-1}. Excessive Fe could also be a problem for plant growth. Concentrations of Fe above 500 μg g^{-1} dry weight are generally considered to be the critical toxicity content, but very much dependent on other factors, such as other nutrients supplement (Fang and Kao, 2000; Marschner, 1995).

When pH decreased to 5.6, dissolved Fe was observed in the lake water at the Rothamsted Experimental Station, and dissolved Fe levels were markedly elevated at pH levels of 5.1 and 4.7 (Blake et al., 1999). A large increase in the dissolved concentration of Fe was also observed by Kharaka et al. (2009), which could be the result of dissolution of siderite. However, in the natural analogue in Italy (Beaubien et al., 2008), with a decline in Fe_2O_3, no obvious changes and clear trends were shown in exchangeable-Fe.

2.2.2.7 Manganese (Mn)

Manganese (Mn) is a common metal found in the Earth's crust and its occurrence in soil is related to the parent material. Mn normally acts as an essential micronutrient to plant growth (Paschke et al., 2005). However, Mn toxicity is considered to be the most important factor limiting plant productivity in acid soils after Al (Li et al., 2010). The main ores of Mn production are the oxides, such as pyrolusite (MnO_2) and hausmannite (Mn_3O_4), and minerals, for example pyrochroite ($Mn(OH)_2$), manganite (MnO(OH)) and Romanèchite ($(Ba,H_2O)_2(Mn^{+4},Mn^{+3})_5O_{10}$) (Hem, 1978). Mn ores may accumulate in metamorphic rocks or exist as sedimentary deposits. When the pH of the soil solution is between 4 and 7, Mn compounds start to weather and release toxic Mn^{2+}. When pH is <4, the Mn is leached away. For pH is >7, most of the Mn species is sparklingly insoluble, which normally results in Mn deficiency for plants (Huang and Quist, 1983). The following reactions illustrate naturally occurring deposits of Mn oxide in aqueous systems, which are normally associated with other elements, such as Fe and Pb (Hem, 1978; Huang and Quist, 1983; Nogales et al., 1997).

$$4MnOOH + 4H^+ \leftrightarrow 2MnO_2 + 2Mn^{2+} + 4H_2O \quad (2.7)$$

$$MnO_2 + 4H^+ \leftrightarrow 2Mn^{2+} + 2H_2O \quad (2.8)$$

$$MnO_2 + 4H^+ + 2Fe^{2+} \leftrightarrow Mn^{2+} + 2Fe^{3+} + 2H_2O \quad (2.9)$$

$$3MnO_2 + 6H^+ + 2Fe \leftrightarrow 3Mn^{2+} + Fe_2O_3 + 3H_2O \quad (2.10)$$

$$Mn_3O_4 + 8H^+ \leftrightarrow 3Mn^{2+} + 4H_2O \quad (2.11)$$

Mn is normally taken up by plants as a reduced bivalent form (Mn^{2+}) and the availability of Mn^{2+} in soil is influenced by pH and organic matter

(Huang and Quist, 1983; Marschner, 1995). The concentration of Mn^{2+} increases in acid soils or anaerobic conditions; while, with high pH and a high amount of organic matter content in soil, Mn deficiency occurs (Huang and Quist, 1983; Marschner, 1995). High concentrations of Mn^{2+} in soil solution inhibit plant growth by inducing nutrient deficiencies, such as Mg^{2+}, Ca^{2+} and Zn^{2+} (Marschner, 1995; Nogales et al., 1997). High concentrations of Mn^{2+} would also influence nutrient uptake by plants via inhabitation of root hair production and reducing stomata dimensions resulting in brown speckles on mature leaves (Li et al., 2010; Lidon, 2002). The threshold of toxic Mn^{2+} to plants varies due to the different tolerance of plants to toxic metals. Previous research shows that slender wheatgrass and common wheat are more sensitive to Mn compared to other grass species (Paschke et al., 2005). It is suggested that 248 mg L^{-1} and 1,000 mg L^{-1} Mn^{2+} in plant shoots could cause inhibition and significant reduction of slender wheatgrass and common wheat, while other plants could survive at a high level of Mn, 6,000 mg L^{-1} (Paschke et al., 2005). Based on estimated concentrations (707 to >6,000 mg L^{-1}) of metals that reduce plant shoot biomass by 50% after 60 days, 200 mg L^{-1} Mn^{2+} in soil solution is considered to be the safe level for plant growth (Paschke et al., 2005). Mn^{2+} concentration higher than 1,000 mg L^{-1} is regarded to be a harmful level, while 7 mg L^{-1} is considered as the basic nutrient requirement for plant growth (Paschke et al., 2005).

Effective mobilisation of Mn as an 'available' heavy metal occurred at pH 6.0-5.5 and it showed a similar trend to Al mobilisation (Blake et al., 1999; Blake and Goulding, 2002). In addition, a steady but variable increase of Mn was observed as pH decreased from 7 to 4, while a consistent decrease of Mn was observed when pH was below 4 (Blake and Goulding, 2002). It was also observed great losses (50-80%) of Mn concentrations

in south Swedish soils between 1949 and 1985 due to atmospheric acid deposition with pH decreases of 0.5-1.0 units to pH 4.0 (Falkengren-Grerup et al., 1987). King et al. (1992) observed Mn started to increase when lake water pH decreased to 5.6, and as pH decreased to 4.7 Mn was steadily increased. Other research showed that oxides in soils (Mn_3O_4) reduced with elevated CO_2 appearance in soil, and Mn was considered to be sensitive to soil acidity (Blake et al., 1999; Beaubien et al., 2008). The concentration of Mn showed a rapid increase at the start of CO_2 injection in a batch experiment, and became steady before the end of each experiment (Lu et al., 2010).

2.2.2.8 Nickel (Ni)

Nickel (Ni) is one of the micronutrients for plant growth. The primary minerals existing naturally are pentlandite ($(Fe,Ni)_9S_8$), and a weathering product, garnierite (a mixture of népouite ($Ni_3(Si_2O_5)(OH)_4$), pecoraite and willemseite ($(Ni,Mg)_3Si_4O_{10}(OH)_2$)). Ni is normally chemically bound with Fe and Co. In the biological system, the preferable oxidation state is Ni (II) (Marschner, 1995).

There is limited evidence of Ni deficiency data, and Ni toxicity is the major concern for crop growth. It was suggested that the critical toxicity of Ni to plants varies between species. For wheat, the critical toxicity levels are within 63 to 112 μg g^{-1}; while for more sensitive species root inhibition could happen even the Ni concentration is below 5 μM, especially when Ca^{2+} concentration is low (Marschner, 1995). Normally, 10 μg g^{-1} and 50 μg g^{-1} are considered to be the toxic Ni levels for sensitive and moderately tolerant species (Marschner, 1995). However, no harm may be observed to some plants even exposing to 50 μg g^{-1} Ni (Nogales et al., 1997).

Previous research showed some cations (e.g., Ca^{2+} and H^{+}) could influence Ni uptake by plants and reduce the toxicity to plant growth (Nogales et al., 1997; Wu and Hendershot, 2010). When pH decreases, the available Ni increases along with the toxicity to plants growth, which can be explained as Ni compounds dissolve at lower soil pH and is accessible for plant uptake (Nogales et al., 1997; Wu and Hendershot, 2010).

A controlled soil chamber with CO_2 injection from one side showed that available Ni increased significantly near CO_2 injection area and dissolved concentration of Ni was 4.5 times higher than that in a no CO_2 injection column (Ardelan et al., 2009). A decreasing trend in Ni towards the CO_2 vent centre was observed at the natural analogue site in Latera, Italy (Beaubien et al., 2008). Blake et al. (1999) suggested that effective mobilisation of Ni occurred at pH 5.5-5.0.

2.2.2.9 Lead (Pb)

Pb normally exists naturally in a small amount in soils as the sulphide mineral galena (PbS), carbonate cerussite ($PbCO_3$) and as sulphate anglesite ($PbSO_4$) (Hesse, 1971b). It is reported that the average Pb concentration in the lithosphere is 16 ppm and 15-25 ppm in soils (Page, 1982b). Generally, Pb is stable and sparklingly insoluble in the soil environment. Most of the Pb^{2+} precipitated or bound to the soil surfaces in insoluble form, which cannot be taken up by and is not toxic to plants (Yang et al., 2006a). Some factors can influence the Pb^{2+} desorption process in soils and can increase its solubility in soil solutions, such as H^{+}, Ca^{2+} and Zn^{2+} (Nogales et al., 1997; Sarkar et al., 2008; Yang et al., 2006a). Fig. 2.3 shows the relationship between pH and Pb^{2+} desorbability,

where the decrease in pH value clearly increases Pb^{2+} desorbability and a large amount of Pb mobilisation occurs when pH goes down to pH 4.0 (Yang et al., 2006a); while the effects are insignificant within the range of pH 5.0 to near neutral, which is also observed by Sarkar et al. (2008).

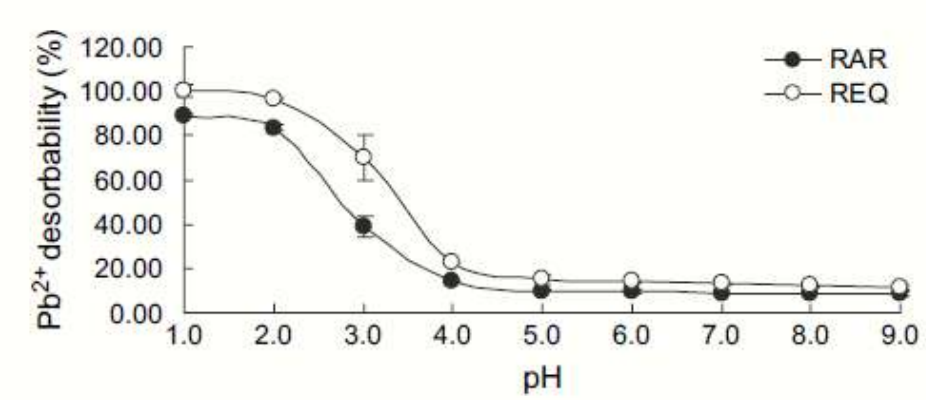

Fig. 2.3 Pb desorption as a function of pH (Yang et al., 2006a). Note: RAR and REQ represent different types of soils. RAR is ¼ red soil developed on Arenaceous rock (clayey, mixed siliceous thermic typic Dystrochrept), while REQ is a ¼ red soil developed on Quaternary red earths (clayey, kaolinitic thermic plinthite Aquult).

Apart from pH, organic acids and the occurrence of Cu^{2+} and Zn^{2+} also influence the desorption behaviour of Pb^{2+} in soils (Yang et al., 2006a). Higher concentrations of organic acid, Cu^{2+} and Zn^{2+}, enhance Pb^{2+} desorption and further increase the Pb^{2+} concentration in soil solution. It was also suggested that high concentrations of Pb would in return increase Zn^{2+}, Cu^{2+} uptake by plants (Nogales et al., 1997).

Once absorbed by plants, Pb can be accumulated through root to root nodules, stem, leaves and seeds; and higher Pb concentration in soil solution results in higher concentration in plants (Patra et al., 2004). The majority of Pb stays around root cap or cap surfaces, in cell walls of rhizodermal and cortical cells instead of translocation to shoot (Patra et al., 2004). Toxic effects of Pb on plants include diminishing DNA synthesis for

root meristem cells, and causing significant induction of micronucleus in root tip cells. High concentration of Pb shortens the length of roots and shoots (Patra et al., 2004; Xiong, 1998).

For human health, the maximum acceptable concentration in drinking water was 0.01 mg L^{-1} or 4.8×10^{-8} mol L^{-1} (Stenhouse et al., 2009). For plants, Pb tolerance and accumulation in shoots and roots varies between crop species and between soil types. Differences in soil properties could influence the uptake of ions by plants. For example, for pakchoi, celery, and hot pepper, the critical Pb concentrations at 10% yield reduction were 24.71, 28.25, and 0.567 mg kg^{-1} respectively, and it is lower in inceptisol soils and slightly higher in alluvial soils (Hong et al., 2008). There is no consensus about Pb threshold for plant growth, while less than 0.1 mg kg^{-1} would not cause any damage to plant growth and human health (Hong et al., 2008).

Previous research showed that acid deposition highly mobilised Pb concentration in both soil solution and ground water, and plant Pb is negatively correlated with pH, but only within a narrow range (±4.5-6) (Crowder, 1991; Galloway et al., 1982; Mayer, 1998). In addition, at Rothamsted Experimental Station, UK, Blake and Goulding (2002) suggested that effective mobilisation of Pb as an 'available' heavy metal occurred while pH<4.5. For a controlled soil chamber with CO_2 injection from one side, Pb increased significantly near the CO_2 injection area and it was considered to be one of the most effectively mobilised metals (Ardelan et al., 2009). Trace element Pb concentration did not show a regular trend towards the gas venting point in a Mediterranean pasture natural analogue in Latera, Italy (Beaubien et al., 2008).

2.2.2.10 Zinc (Zn)

Zinc (Zn), one of the essential micronutrients in soil, has been extensively studied. The primary Zn minerals exist in various carbonate and silicates minerals, for example smithsonite ($ZnCO_3$), hydrozincite ($2ZnCO_3 \cdot 3Zn(OH)_2$), zincite (ZnO), willemite (Zn_2SiO_4), hemimorphite ($Zn_4Si_2O_7(OH)_2 \cdot H_2O$), and Zn-containing magnetite ($[Fe,Zn]Fe_2O_4$) (Catlett et al., 2002; Chen et al., 2009; Qin et al., 2007). The solubility of Zn and the mechanism behind that may vary along with different soil properties, such as pH, organic matter content, and clay content (Catlett et al., 2002). Previous research showed that adsorption and precipitation controls Zn solubility with low and high pH respectively (Catlett et al., 2002). At pH>7.9, precipitation controls Zn solubility and precipitation of willenite (Zn_2SiO_4) is likely to occur; while at pH from neutral to alkaline, specific adsorption of a hydrolysed form of $Zn(OH)^+$ is likely to occur and it is the dominant phase for providing soluble Zn (Catlett et al., 2002; Gupta et al., 1987; Marschner, 1995). At low pH, Zn mineral weathering process can be illustrated as the following reaction (Catlett et al., 2002). The product of this reaction, a divalent cation (Zn^{2+}), may adsorb on organic matter at low pH environment and can be taken up by plants (Catlett et al., 2002; Marschner, 1995).

$$Zn_2SiO_4 + 4H^+ \rightarrow 2Zn^{2+} + Si(OH)_4 \quad (2.12)$$

$$Zn_4Si_2O_7(OH)_2 \cdot H_2O + 4H^+ \rightarrow 4Zn^{2+} + 2Si(OH)_4 + 2H_2O \quad (2.13)$$

Zn deficiency often occurs at high pH by adsorption of Zn to clay or $CaCO_3$. For example, if soil has a high HCO_3^- concentration, Zn uptake and translocation to plants is inhibited (Aravind and Prasad, 2005; Marschner,

1995). However, excessive Zn in soil could also be toxic to plants, and it could cause deficiency in micronutrient uptake of Mn^{2+}, Cu^{2+}, Fe^{2+} and Mg^{2+} when these ions appear at low levels in soil solution (Aravind and Prasad, 2005; Marschner, 1995). Toxicity levels for Zn vary between species and the level is between 6 mg L^{-1} for sensitive plants, sugar beet, to 55 mg L^{-1} for petunias based on occurrence chlorosis (Bucher and Schenk, 2000).

Higher concentration of Zn in sediments and ground water was observed in various soil acidification scenarios (Falkengren-Grerup et al., 1987; Mannings and Smith, 1996; Mayer, 1998). For example a significant leaching of Zn took place during the period 1949-1985 in most of the forest sites studied by Falkengren-Grerup et al., (1987). In a laboratory column system, by measuring the heavy metals movement associated with selected Brazilian soils of various chemical and mineralogical soil characteristics, it was suggested that the mobility of Zn is higher than other metals, e.g. Cd, Cu, Pb (de Matos et al., 2001). In a natural analogue at Latera, Italy, a decreasing trend in Zn towards the CO_2 venting centre was observed by Beaubien et al., (2008). King et al. (1992) observed that Zn mobilisation occurred at pH 5.1 and 4.7. Blake and Goulding (2002) suggested that effective Zn mobilisation occurred at pH 5.5-5.0 and the change in Zn concentration had a similar behaviour to Cd but with more variability.

2.2.3 Nutrient changes

When CO_2/SO_2 exists in soil, weak acid H_2CO_3 or strong acid H_2SO_4 are formed and the concentration of Ca and Mg etc. in soil solution is changed

subsequently, which would further influence plant growth. It is therefore important to assess the nutrients changes due to elevate CO_2 intrusion.

2.2.3.1 Calcium (Ca)

Calcium (Ca) is one of the macronutrients in soil and an essential element for plant growth. Naturally, Ca exists in minerals as calcite ($CaCO_3$), dolomite ($CaMg(CO)_3$), hornblende ($Ca(Fe,Mg)_2Si_4O_{12}$) and apatite ($Ca_5(PO_4)_3(F,Cl,OH)$) (Edwards et al., 2005; Tan, 2009). Chemically, those primary minerals are sparklingly insoluble and unavailable to plants. However, the minerals can be weathered, and release Ca to soluble ions in soil solution. For example, for a carbonation process, with the appearance of H_2O and CO_2, insoluble $CaCO_3$ can be changed to soluble weak acid calcium bicarbonate ($Ca(HCO_3)_2$) (Tan, 2009) as follow,

$$CaCO_3 + H_2O + CO_2 \rightarrow Ca(HCO_3)_2 \quad (2.14)$$

Insoluble *Soluble*

The dissolution of dolomite limestone also happens when CO_2 exists in soil water and can be explained as follows,

$$CaMg(CO_3)_2 + 2H_2CO_3 \rightarrow Ca^{2+} + Mg^{2+} + 4HCO_3^- \quad (2.15)$$

The following reaction may also take place in the soil environment,

$$Ca^{2+} + CO_2 \rightarrow CaCO_3 \quad (2.16)$$

As an essential element in soil for plant growth, Ca is rarely deficient in soil. However, with lower pH, higher levels of other mobilised metals (such as Mg and Al) compete with Ca for plant uptake and could cause Ca deficiency for plant growth (Rowell, 1994a). Back to 1970s, it was

documented that Ca^{2+} was leached by acidic atmospheric deposition from different types of soils in southern Norway and southern Sweden (Jönsson et al., 2003; Rice and Herman, 2012). It was also observed elsewhere that the loss of large amounts of Ca^{2+} from the field was accelerated due to acidic atmospheric deposition, in some cases up to 50% (Johnson et al., 1994; Likens et al., 1996; Miller and Watmough, 2009; Parnell Jr and Burke, 1990). The Ca concentrations in the collection reservoirs increased up to one order of magnitude (Berthe et al., 2011). It was also suggested that the increased CO_2 partial pressure increased the solubility of $CaCO_3$ (Clow and Mast, 2010; Karberg et al., 2005; Pokrovsky et al., 2005; Sposito, 1994).

2.2.3.2 Potassium (K)

Potassium (K) is a macronutrient and essential to plant growth as one of the three principle fertilizer elements. The primary minerals are orthoclase ($KAlSi_3O_8$), muscovite ($H_2KAl_2Si_3O_{12}$), albite ($NaAlSi_3O_8$), sylvite (KCl) and langbeinite ($K_2Mg_2(SO_4)_3$) (Tan, 2009). When excessive water or H^+ appears in soil, hydrolysis process occurs and primary minerals start to weather as follows,

$$KAlSi_3O_8 + H^+ \rightarrow HAlSi_3O_8 + K^+ \quad (2.17)$$

$$KAlSi_3O_8 + H_2O \rightarrow HAlSi_3O_8 + KOH \quad (2.18)$$

$$2KAlSi_3O_8 + 3H_2O \rightarrow H_4Al_2Si_2O_9 + KOH + 4SiO_2 \quad (2.19)$$

During the above processes, K^+ is released from minerals and becomes bio-available to plants. Lu et al. (2010) observed that K increased rapidly with the injection of CO_2 and stabilised at the end of the experiment.

2.2.3.3 Magnesium (Mg)

Magnesium (Mg) acts as a macronutrient and is essential to plant growth. It is normally absorbed through cation exchange by growing plants. Naturally, Mg exists in many minerals, such as dolomite ($CaMg(CO_3)_2$), serpentine ($(Mg,Fe)_3Si_2O_5(OH)_4$, brucite ($Mg(OH)_2$), carnallite ($KMgCl_3 \cdot 6(H_2O)$), magnesite ($MgCO_3$) and olivine ($(Mg,Fe)_2SiO_4$) (Barber, 1995).

According to previous research, the available exchangeable-Mg reduced under lower pH conditions leading to Mg deficiencies (Coyne and Thompson, 2006; Parnell Jr and Burke, 1990; Rowell, 1994a). Reduction in Mg concentrations related to acid deposition was also observed in southern Sweden between 1988 and 1999 (Jönsson et al., 2003). Mg deficiency can also be caused by high levels of other cations occurrence in soil, such as K^+, Ca^{2+}, Mn^{2+} and H^+ (Marschner, 1995). Berthe et al. (2011) observed that Mg concentrations in the water collection of reservoirs increased up to one order of magnitude, which may be due to dissolution of some carbonate minerals.

2.2.4 Potential mineralogy and oxide changes

Mineralogy change is likely to happen as the soil weathering process occurs when soil is exposed to elevated CO_2. As stated above, when CO_2 appears in soil, weak acid H_2CO_3 will form and release H^+. A hydrolysis process is therefore expected to happen when soil minerals merge into water and H^+. For example, K-feldspar and orthoclase, is likely to weather and form clay, and albite can also be weathered and release Na^+ into soil solution (Ludwig et al., 1999; Mortatti and Probst, 2003; Tan, 2009).

The weathering process can be summarised as follows (Ludwig et al., 1999; Mortatti and Probst, 2003; Tan, 2009),

$$KAlSi_3O_8 + H^+ \rightarrow HAlSi_3O_8 + K^+ \quad (2.20)$$

orthoclase *clay*

$$NaAlSi_3O_8 + 2H^+ \rightarrow HAlSi_3O_8 + Na^+ \quad (2.21)$$

albite *clay*

$$2NaAlSi_3O_8 + 2CO_2 + 11H_2O \rightarrow Al_2Si_2O_5(OH)_4 + 2HCO_3^- + 2Na^+ + 4H_4SiO_4 \quad (2.22)$$

$$Mg_2SiO_4 + 4CO_2 + 4H_2O \rightarrow 2Mg^{2+} + 4HCO_3^- + H_4SiO_4 \quad (2.23)$$

$$3KAlSi_3O_8 + 2H^+ + 12H_2O \rightarrow KAl_3Si_3O_{10}(OH)_2 + 6H_4SiO_4 + 2K^+ \quad (2.24)$$

orthoclase *illite*

$$2KAlSi_3O_8 + 2CO_2 + 6H_2O \rightarrow Al_2Si_4O_{10}(OH)_2 + 2HCO_3^- + 2H_4SiO_4 + 2K^+ \quad (2.25)$$

K-feldspar *montmorillonite*

$$CaAl_2Si_2O_8 + 2CO_2 + 3H_2O \rightarrow Al_2Si_2O_5(OH)_4 + 2HCO_3^- + 2Ca^{2+} \quad (2.26)$$

Ca-plagioclase *kaolinite*

With H^+ occurrence, illite can be converted to smectite along with K^+ releasing, and albite can be converted to kaolinite with Na releasing to soil solution as follows (Clow and Mast, 2010; Tan, 2009):

$$illteillite \leftrightarrow smectite + K^+ \quad (2.27)$$

$$albite + 5.5H_2O + CO_2 \rightarrow HCO_3^- + Na^+ + 2H_4SiO_4 + 0.5\ Kaolinite \quad (2.28)$$

$$calcite + H_2O + CO_2 \rightarrow 2HCO_3^- + Ca^{2+} \quad (2.29)$$

$$CaSiO_3 + CO_2 \rightarrow SiO_2 + CaCO_3 \quad (2.30)$$

Previous research showed that noticeable but insignificant changes in mineralogy phase were observed, such as K-feldspar, quartz, and 'mica', with an increase in K-feldspar and quartz minerals and a decrease in albite and augite towards the CO_2 venting point (Beaubien et al., 2008; Billett et al., 1990; Blake et al., 1999, 2000; Goulding et al., 1998; West et al., 2009). For example, in the Mediterranean pasture in Latera, Italy, K-feldspar increased from about 21% to 29% by weight towards the CO_2 venting point, while albite decreased from about 9% to 4% by weight (Beaubien et al., 2008). Similarly, a reduction in oxides like CaO, MgO, Fe_2O_3, and Mn_3O_4 was observed in the experiments of CO_2 intrusion in soil (Beaubien et al., 2008; Billett et al., 1990; Blake et al., 2000; Goulding et al., 1998; West et al., 2009).

2.3 Previous and ongoing research on effects of elevated CO_2 on the local environment

To date, the main approaches for assessing the effects of elevated CO_2 on the local environment were natural and industrial analogues, field-scale evaluations, laboratory studies, and modelling work (Gaus, 2010). Each of them has their own advantages and disadvantages as described in the following sections. This review focuses on previous and ongoing research of natural and industrial analogues (section 2.3.1), field-scale evaluations (section 2.3.2) and laboratory studies (section 2.3.3) on the effects of elevated CO_2 on the local environment. The main findings of those studies are presented in each section.

2.3.1 Natural and industrial analogues of effects of elevated CO_2 on the local environment

A natural analogue is a natural phenomenon or process that is similar and comparable to a technological process, from which we can learn and understand physical/chemical occurrences to reduce unknowns and uncertainties when it comes to a real application. Recently, natural analogues have been widely used to examine CO_2 leakage from CCS projects and to assess the potential environmental consequences due to elevated CO_2. Most studied natural resources of CO_2 emission (as below) are from volcanic and tectonically active areas (Holloway et al., 2005).

One of the most studied natural analogues is Mammoth Mountain, California in USA. Mammoth Mountain is a seismically active, dacitic cumulovolcano located on the south-western edge of Long Valley caldera, eastern California. There are continuous activities recorded associated with Mammoth Mountain since 1797, such as swarms of small earthquakes and very-long period of earthquakes (Hill and Prejean, 2005). These activities caused CO_2 diffusion and accumulation in soils and snow through faults and fractures, which eventually lead to tree-kills and caused ski patroller fatalities (Farrar et al., 1995; Lewicki et al., 2007b). Different studies were carried out in the Mammoth Mountain area, focusing on emitting gas degassing process, soil gas concentration in relation to volcanic activity, impacts on plant growth in this area, as well as volcanic gas hazard assessments (Cook et al., 2001; Gerlach et al., 2001; Rogie et al., 2001). It was reported that soil CO_2 concentrations were commonly >30% v/v and fluxes measured nearby was commonly >500 g m^{-2} d^{-1}, with background CO_2 concentrations and fluxes outside of the tree-kill area usually <1% v/v and 25 g m^{-2} d^{-1}, respectively. For some areas, the CO_2

soil concentration can go up to 90% v/v (Farrar et al., 1995; Lewicki et al., 2007a). The formation of tree-kill areas was observed on the southeast flank of Mammoth Mountain, California because of the CO_2 emission, and natural collapse pits were developed on the northwest shore of Horseshoe Lake as the lake level declines contain high CO_2 concentration (Lewicki et al., 2007a). Fig. 2.4 shows the location and area of the Mammoth Mountain (a & b) and a picture of the killed trees (c).

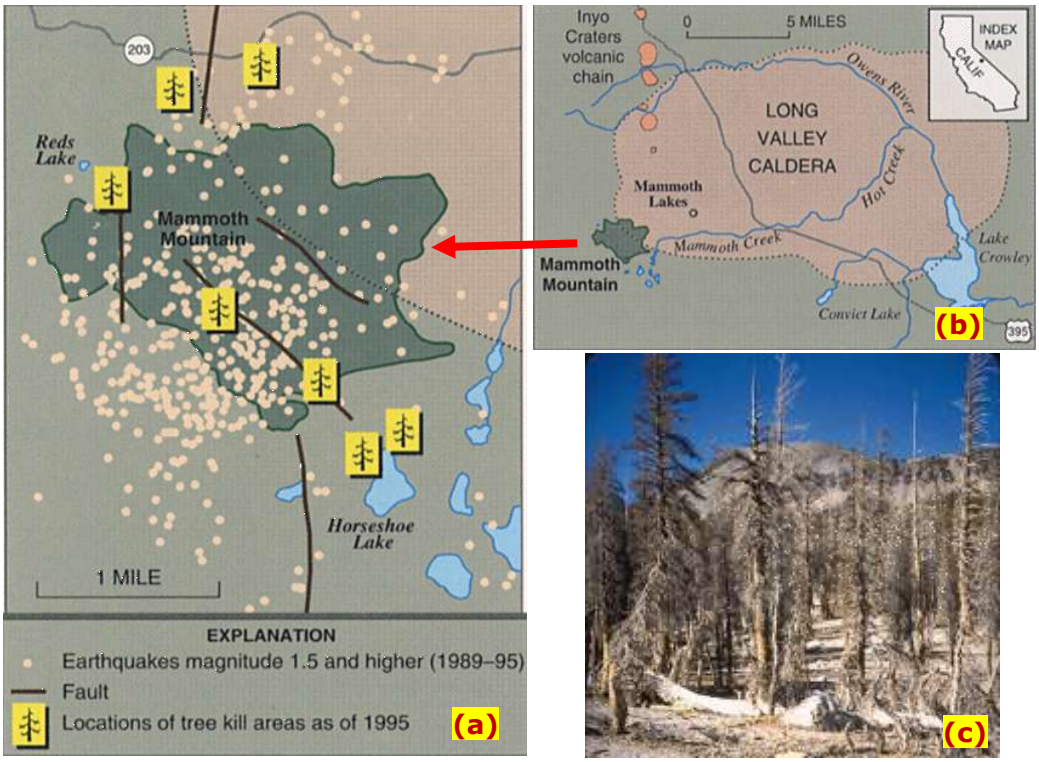

Fig. 2.4 Location and areas (a & b) of dead and dying trees (c) at Mammoth Mountain volcano in eastern California with more than 100 acres (modified from Sorey et al. (1996)).

Another frequently studied area is the Latera caldera located in west-central Italy, where CO_2 migrates upward along some major fault zones and emerges at the surface in the Latera caldera. Studies were carried out in this area to investigate the soil CO_2 concentration (Astorri et al., 2002; Lewicki et al., 2007a), and the impacts on the shallow ecosystem and soil chemistry (Annuziatellis et al., 2005; Beaubien et al., 2008). Astorri et al.

(2002) reported that the soil CO_2 gas concentration could go up to 97% v/v, with an average background value of 4.7% v/v. Vegetation was observed stressed or killed in the area (Annuziatellis et al., 2005). To better understand the potential impacts on such an event, detailed geochemical and biological research was carried out on shallow soil samples (0-20 cm depth) during two different seasons by Beaubien et al. (2008). In this research, three zones were observed and divided from the vent centre: 6m wide centre of the vent (vent zone), 6m-30m halo surrounding the core (transition zone) and 30m-50m halo surrounding the vent centre (background zone). The research showed that a significant impact is only observed in the vent zone, where CO_2 flux rates exceed 2000-3000 g m^{-2} d^{-1} and pH is low (minimum 3.5). The soil gas in the vent zone consists of CO_2 (>95% v/v) along with other trace reduced gases (CH_4, H_2S, and H_2), and a gradual decrease in CO_2 concentration and CO_2 flux is observed in the transit zone. In the vent zone, a sharp decrease in albite content (decrease to 4% from 9%) was observed compared with the background zone, along with an increase in K-felspar (increased from 5% to 11% by weight), which was due to long term dissolution of albite and precipitation of K-feldspar by leaked CO_2. Also, a slight increase in some trace elements was observed, e.g. As (increase from 10ppm to 17ppm). Not too much information on soil chemistry changes was presented in this research. Results indicate that, even at high-flux site, the effects of the gas vent are spatially limited to the vented zone and that the ecosystem appears to have adapted to the different conditions through species substitution or adaptation (Beaubien et al., 2008). Apart from the above two, other natural analogues are also well-studied, such as Lake Nyos in Cameroon, Mt. Gambier in Australia (Giggenbach et al., 1991), the Aeolian Islands, Southern Tyrrhenian Sea in the Mediterranean area in Italy (Espa

et al., 2010), the Laacher See in Germany (Kruger et al., 2009), and the French carbo-gaseous province in France (Benson, 2005a).

Moreover, two cases have been studied as industrial analogues regarding well failure: Crystal Geyser near Green River, Utah, US and Sheep Mountain Drill Well, Colorado, US (Holloway et al., 2007; Wilson et al., 2007). The failures occurred either through the injection well or the abandoned well, where a large amount of CO_2 was stored in a dry reservoir nearby. A detailed summary on selected natural and industrial analogues is listed in Table 2.2.

Natural and industrial analogues have their own advantages to assess impacts on the local environment of CO_2 leakage. The main advantages can be summarised as follows (Benson, 2005a; Gaus, 2010; Lewicki et al., 2007a): (1) they normally exist naturally over a long time (geological time) and are ideal to simulate long term impacts on the local environment of CO_2 leakage; (2) they normally occur at large scales and close to the environmental conditions of a site above a CO_2 storage site, which are ideal to mimic a real CO_2 leakage scenario; (3) direct observations are possible. However, it holds certain disadvantages for assessing the impacts. For example (Spangler et al., 2010): (1) there are too many complexities at a natural site (e.g. soil property and gas composition) and therefore it is difficult to interpret the results. For example, the flux vented from natural analogues may contain impurities other than CO_2, e.g. H_2S and CH_4 (Beaubien et al., 2008), and it is difficult to observe the effects caused by the leaked CO_2 alone; (2) These sites have a long-established flux and well established flow paths, and in which the minerals and rocks are already reacted and equilibrated with CO_2. These make it difficult to observe the short term reactions that could result from accidental leakage

of CO_2 and also hard to define detection limits when comes to developing near surface monitoring technologies; (3) as its long established condition, it is not easy to study the vegetation stress and recovery rates after excess CO_2 exposure at the natural analogue sites. All the above disadvantages make natural analogues an imperfect analogue for short term reaction with accidental leakage of CO_2.

Table 2.2 A summary of natural and industrial leakage of CO_2.

SITE AND MAIN COMPOSITION OF GASEOUS EMISSION FROM SITE	***OBSERVED CONSEQUENCES OF LEAKAGE IN THE DEGASSING AREA***	***REFERENCES***
Natural analogues		
1. Mammoth Mountain, CA, USA (37.63°N, 119.03°W) CO_2, magmatic helium (He)	a). pH was lowered by 0.5 from 5.6. b). Soil moisture and surface area increased compared with a control soil nearby. c). The concentrations of Si, Al, Mn and Fe were higher. d). Trees were killed nearby the emission point. e). Natural collapse pits was developed.	(Farrar et al., 1995; Lewicki et al., 2007a; Stephens and Hering, 2002)
2. Solfatara, Italy (40.83°N, 14.15°E) CO_2, He, CH_4, H_2	a). High contents of HCO_3^-, Ca^{2+}, and Mg^{2+} were observed in the collected water sample. b). Fumaroles, mud pools and boiling pools were formed.	(Lewicki et al., 2007a, Voltattorni et al., 2009)
3. Albani Hills, Italy (41.75°N, 12.75°E) CO_2, sulphur-rich gases and HCl	a). Groundwater collected from wells and springs in the region was high in HCO_3^-, Ca^{2+} and Mg^{2+}.	(Voltattorni et al., 2009)
5. Latera Caldera, Italy (42.60°N, 11.93°E) 80% CO_2 and 20% H_2S, CH_4 and H_2	a). An increase was observed in K-feldspar, quartz, and 'mica', trace elements (e.g. As and Cr), CEC and TOC. b). A decrease was observed in pH of soil pore water, minerals like augite, albite, and cristobalite, oxides like CaO, MgO, Fe_2O_3, and Mn_3O_4, minor elements like Ba (and Rb, Sr) and trace elements like Co (and Ni, Cu, Zn, V). c). Vegetation was stressed or killed in the degassing area.	(Annuziatellis et al., 2005; Beaubien et al., 2008; Stevens et al., 2001)
6. San Vittorino, Italy (41.66°N, 14.10°E) CO_2 (36-85 %), CH_4 (150-2100 mg L^{-1}), He (6-400 mg L^{-1}), N_2 (7-60 %) and O_2 (0.5-2 %)	a). Total hardness, conductivity and Total Dissolved Solids (TDS) of the water sample at the site increased. b). Levels of K, Mg, Ni, Mn, Al, Zr, Pd and Rb and Sr in the water samples increased.	(Beaubien et al., 2005; Lewicki et al., 2007a)

7. Panarea Island (Aeolian Islands, southern Italy) (38.64°N, 15.07°E) CO_2 (varies from 83.64 to 98.43% v/v) mixed with CH_4 (around 10 ppm), N_2 (around 0.4% v/v), He (around 11 ppm), H_2 (around 1100 ppm), H_2S (around 2.2% v/v)	a). Seawater pH was lowered locally down to 5.0 from 8.0 because of the submarine gas emissions. b). Eh decreased from +80 mV to -200 mV. c). A strong modification of the marine ecosystem was formed.	(Voltattorni et al., 2006; Voltattorni et al., 2009)
8. Laacher See, Germany (50.42°N, 7.27°E) CO_2, ^4He, O_2, CH_4, ^{222}Rn	a). pH decreased significantly from surface (pH 6.0) to below 10 cm in the area of highest CO_2 seepage (pH <5.0). b). The ecosystem adapted to elevated CO_2 concentration conditions, e.g. species showed a shift towards anaerobic and acidotolerant to acidophilic species.	(Gal et al., 2011; Giggenbach et al., 1991; Kruger et al., 2011)
9. Lake Nyos and Lake Monoun, Cameroon (6.44°N, 10.30°E) CO_2, He	a). 1,700 people and thousands of animals died because of the sudden release of CO_2. b). pH decreased highly with depth (from pH 8.0 at surface to pH 5.4 at a depth of 45 m where the upper chemocline is present). c). The lake water was dominated by high concentration of Ca^{2+}, Mg^{2+}, Fe^{2+}, HCO_3^-, and some chemical concentrations increased with depth of Lakes Nyos and Monoun, for example Na, K, Mg, Ca and Fe.	(Giggenbach, 1990; Giggenbach et al., 1991; Kusakabe et al., 2000; Lewicki et al., 2007a)
Industrial analogues		
1. Sheep Mountain, Colorado, USA (39.05°N, 107.12°W) about 97% v/v CO_2	N/A	(Lewicki et al., 2007a)
2. Crystal Geyser near Green River, Utah, US (38.99°N, 110.15°W) CO_2, H_2O, N_2	a). The results showed that the CO_2 levels on site were below safety limits to humans, which would not cause acute human health effects.	(Holloway et al., 2007; Wilkinson et al., 2008; Wilson et al., 2007)

2.3.2 Field-scale evaluations of effects of elevated CO_2 on the local environment

The field-scale evaluation approach normally involves injecting CO_2 into a designed site at different depths to investigate effects on the local environment of elevated CO_2.

Two important field-scale evaluations described below are currently being carried out to assess the potential effects on environmental aspects caused by CO_2 leakage: the Artificial Soil Gassing and Response Detection (ASGARD) field and the Zero Emission Research and Technology Centre (ZERT) field.

The ASGARD field is an artificial soil gassing facility located at the Sutton Bonington Campus, the University of Nottingham; it is designed to observe and monitor the effects of different adjustable CO_2 concentrations on various crops and plants, soil microbes and invertebrates, and soil geochemistry. The field was formerly used for livestock grazing. It is an open field and divided into several plots with or without CO_2 gas injection. Monitoring was carried out to observe and compare any changes among those plots in the field (Patil et al., 2010). Different experiments were carried out at the ASGARD field (Cunningham, 2010; Ekene, 2011; Patil et al., 2010; West et al., 2009). Over 19 weeks CO_2 injection at a rate of 3 L min^{-1} lowered the soil pH in comparison with the controlled plots (Patil et al., 2010), and the biggest decrease in pH was observed in soil Horizon A with a 0.5 pH decline compared with the preinjection pH, which was in the range of 6.0 to 6.2 (West et al., 2009). Even with a low injection rate as above, injected CO_2 displaced soil O_2 quickly and CO_2 increased to >75% v/v for some areas (Patil et al., 2010). At a very high CO_2 level (>75% v/v), the leaves of plants turned to yellow or brown growth and the growth of plants was inhibited. No significant variations in mineralogy were observed with depth at a gassed plot, and no obvious changes of mineralogy were observed between gassed and ungassed plots. However, not too many studies have been done on the soil chemistry changes of CO_2 injection in the ASGARD field. Recently, some tests were carried out at the ASGARD field by Mr. James Cunningham, an undergraduate student

in the department of Environmental Science at the University of Nottingham, to assess the effect on the recovery of plants and soils of the below ground CO_2 emission (Cunningham, 2010). Before the test, gassing occurred for a period of 42 days in June 2010 and the test was carried out one year after the CO_2 gas injection stopped, measuring the soil and plants in 8 gassed and ungassed plots to observe the effects in the soil and vegetation after the one year buffering. It was observed that the effects on the soils and plants of gassing were still present even after one year buffering with a certain recovery. Phosphorus, nitrogen deficiency and enhanced Al^{3+} were observed by visual signs on the vegetation on the gassed site. It was also observed that Ca concentrations decreased in all sampled soil at gassed plot over the injection period with the largest decrease around the injection point (West et al., 2009).

The ZERT field is located at an agriculture field at the western edge of the Montana State University (MSU)-Bozeman campus in Bozeman, Montana, USA; it is a research collaboration focusing on understanding the basic science of underground (geologic) CO_2 storage and developing technologies to ensure the safety and reliability of CO_2 geological storage. The main research goals were to develop measurement techniques to verify storage sites and to investigate leakage from the storage process. It was also designed to develop computer modelling suites to predict the underground behaviour of CO_2, and to develop mitigation techniques for CO_2 leakage. During the shallow CO_2 field injection at the ZERT site, an increase in the aqueous concentration of major and trace elements (e.g. As, Ca, Cr, Co, Cu and Pb) in groundwater was observed, and it was suggested that calcite dissolution could be the primary process buffering pH and releasing Ca^{2+} in groundwater (Strazisar et al., 2009; Zheng et al., 2012). According to Zheng et al. (2012), the release most of major cations

and trace metals could be explained by Ca^{2+}-driven exchange reactions and the increase in total Fe concentration can be explained as the dissolution of reactive Fe minerals (such as fougerite). Lakkaraju et al. (2010) observed stress in vegetation (Dandelion (*T. officinale*) plants) associated with high level of soil CO_2 concentration (>20% vol.), which was detectable by visible symptoms (purple discoloration and chlorosis) and changes in spectral reflectance. This stress and the induced response (a decrease in chlorophyll concentration) could be detected and related to the changes in the spectral reflectance of vegetation. It was therefore suggested that application of hyperspectral remote sensing could potentially be used to monitor CO_2 leakage from a geological CO_2 sequestration site (Lakkaraju et al., 2010).

Compared with natural analogues and laboratory experiments, field-scale experiments have their advantages. For example, certain conditions can be controlled (e.g. injection gas and initial soil properties), and vegetables can be planted in the field, which are ideal to assess the impacts on targeted species under certain experimental conditions (Lakkaraju et al., 2010; Patil et al., 2010). As an open field, field-scale evaluations have fewer limitations compared with laboratory studies (e.g. boundary effects), and field-scale experiments are normally scaled enough to be able to be used to develop monitoring techniques (Spangler et al., 2010). However, a field site is less easy to be controlled compared with laboratory work. Once experiments were carried out in the field site, it took times for the weathered soils to recover for the next set of experiment.

2.3.3 Laboratory studies of effects of elevated CO_2 on soil

In order to study the environmental effects of increased levels of CO_2 on soil, laboratory scale experiments were developed using vessels filled with soils and exposing the soils to different concentrations of CO_2.

A laboratory batch experiment and column system experiments are normally used to represent the typical examples of such a system (Wang et al., 2009). Batch experiments are carried out by adding a certain amount of targeted soil into water with a certain solid/liquid ratio. In this case, a laboratory-batch experiment (Little and Jackson, 2010; Lu et al., 2010) usually involves releasing CO_2 into a pre-equilibrated water-sediment environment, and then sampling from the system to assess potential influences by elevated CO_2. Lu et al. (2010) performed a laboratory-batch experiment to explore the impacts on the groundwater quality of a range of representative aquifers samples by the leaked CO_2. The samples were all quartz dominant aquifer rock samples with small amount of K-feldspar, carbonate minerals, illite/smectite, and kaolinite. The results from these experiments recognised two types of cations according to their concentration changes during the CO_2 injection. Type I cations, including Ca, Mg, Si, K, Sr, Mn, Ba, Co, B and Zn, increased rapidly at the start of CO_2 flux and reached stable concentrations before the end of the experiment. Type II cations, including Fe, Al, Mo, U, V, As, Cr, Cs, Rb, Ni and Cu, increased at the beginning of CO_2 injection but decreased to less than pre-injection concentration, indicating adsorption/desorption happened during the experiments. The research also suggested that dissolution of dolomite and calcite was the main cause for the increase in cation concentrations, and suggested that carbonate minerals were the dominant contributor of changes in groundwater quality.

Similar studies were carried out by other researchers to assess the impacts on ground water (Little and Jackson, 2010; McGrath et al., 2007; Smyth et al., 2009). Increases in certain trace metals were observed in these studies, for example an increase in cadmium concentrations in a batch experiment (McGrath et al., 2007), and an increase in concentrations of Ba, Ca, Fe, Mn and Sr in laboratory batch experiments with various aquifer materials exposed to CO_2 (Smyth et al., 2009).

On the other hand, column system experiments, known as accumulation chamber methods, have been used widely for many purposes as they can be easily controlled and used to simulate complex environments. The column experiments involve packing the relevant targeted soils into columns and monitoring the changes in soils with elevated CO_2 appearance. Some of the applications are shown in Table 2.3. Due to the various applications, the column system is therefore ideal to be used as a simplified and well-controlled system to assess the consequences of CO_2 seepage in soils. There are some experiments using a column system to assess impacts on solubility and transport of trace metals by CO_2 seepage in sediments (Ardelan et al., 2009; Berthe et al., 2011). By comparing with a control column experiment, Ardelan et al. (2009) investigated the behaviour of seven metals (Al, Cr, Ni, Pb, Cd, Cu, and Zn) in membrane filtered seawater samples with CO_2 injection. They observed that the increase in dissolved fractions of Al, Cr, Ni, Cu, Zn, Cd and Pb was respectively 5.1, 3.8, 4.5, 3.2, 1.4, 2.3 and 1.3 times higher than that in the control.

Table 2.3 Main applications of column experiments.

NO.	APPLICATIONS	REFERENCES
1	To investigate soil CO_2 flux measurements interval in different soils that vary in physical properties	(Butnor et al., 2005; Camarda et al., 2009; Nay et al., 1994; Widen and Lindroth, 2003)
2	To trace solute, contaminant components transportation and heavy metal accumulation in column system experiments	(Binley et al., 1996; Ermakov et al., 2007; Mirbagheri, 2004; Xu et al., 2006)
3	To examine in both horizontal and vertical column experiments the dense gas diffusion associated with different volcanic ash soils	(Hamamoto et al., 2008)
4	To investigate the solute transportation in both small (30cm long) and large columns (6m long column)	(Wierenga and Van Genuchten, 1989)
5	To investigate soil leaching process to see the effects on soil solution and soil drainage chemistry changes by variable sulphate loads	(Egiarte et al., 2006; Hodson and Langan, 1999; Wierenga and Van Genuchten, 1989;)

Comparing with natural analogue and field-scale experiments, it is well known that laboratory experiments have limitations (presented as section 2.3.4), for example, samples used in laboratory studies may not properly represent field conditions (Zheng et al., 2012), and there might be unwanted oxidation during the experiment (Little and Jackson, 2010) which might reduce the effect of CO_2 on the reaction of some redox sensitive elements. However, this type of experiment is very useful for providing insight into the potential impact of CO_2 (Zheng et al., 2012). Also, laboratory study is easy to control and is a useful tool to investigate soil response to elevated CO_2 under various conditions. For example, it is easy to modify parameters to investigate the relevant effects, such as injection gas concentration, soil/sediment properties (e.g. moisture content, particle size, and organic content) (Ardelan et al., 2009; Ardelan and Steinnes, 2010; Lu et al., 2010). The results are also helpful towards understanding water-sediment-gas interaction under elevated CO_2 and recognising indicators to early detect CO_2 leakage for developing CO_2

leakage monitoring techniques. Due to the advantages of laboratory experiments, both a laboratory batch experiment and a flow through column system are utilised in this project to investigate the effects on soil chemistry of elevated CO_2. A detailed description of methodologies of both systems is given in Chapter 3. Results from this research are compared with the ASGARD field and those from natural/industrial analogues to better understand the effects on soils (Chapter 4, 5 & 6).

2.3.4 Laboratory versus field studies

As mentioned in section 2.3.3, laboratory study is a cost-effective approach to achieve the research objectives (section 1.4) and it is therefore chosen to be used in this research. However, it must be recognised that the laboratory experiments have their limitations compared with larger field scale experiments; they cannot represent completely the full complexity of a natural system (Stephens, 2002). It is important to understand the differences between laboratory-scale results and larger-scale situations, such as the ones of a real leaking scenario. The aim of this section is to explain how to utilize the results of the laboratory studies and to what extent they are representative of real-scenarios.

Soil/sediment samples used in the laboratory experiments are different from the ones of field studies. Usually, laboratory studies are carried out with pure materials (single sediment mineral) (Chou et al., 1989), prepared soils/sediments (Stephens, 2002) or whole soils/sediment cores collected in the field (Little and Jackson, 2010; Lu et al., 2010). In this research, the experiments used prepared homogeneous soil samples collected from the ASGARD field (section 3.1.1) and well sorted mono-

mineral pure sediments (section 3.2.2). However, the natural soil composition includes elements such as gas, water, organic matter and microbes which, for the typology of samples used, not present in the experimental samples. Moreover the undisturbed soil retains its structure which is inevitably lost in the sediments used in the laboratory experiments (Nikolaidis et al., 1994; Rowell, 1994b; Sass and Rai, 1987; Wu et al., 2010). Such differences could lead to discrepancies between laboratory results and field studies, mostly in terms of different mineral weathering rates and gas-soil interaction (Gal et al., 2012; Stephens, 2002; van Grinsven and van Riemsdijk, 1992; Velbel, 1993). In contrast to what happens in the samples used for the laboratory incubation experiments, which are sieved and homogenised, chemical reactions in the natural soil are characterized by lesser reactivity. The gas transport within the pore space, in the natural soil, is controlled by preferential flow paths and permeability barriers, e.g. in clay soils (Abichou et al., 2011) both of which are not present in small-scale samples.

Weathering rates in the laboratory experiments with pure minerals and for some soil samples are normally several orders of magnitude higher than rates estimated from field studies (Stephens, 2002; van Grinsven and van Riemsdijk, 1992; Velbel, 1993). It was suggested by Stephens (2002) that the difference could be partially related to the different uncertainties in surface area measurement in the laboratory compared with the ones of field studies. Overestimation of active soil surface area in contact with percolating water in the field could lead to underestimation of weathering rates. Moreover, the common methods of determining the surface area, the Brunauer-Emmett-Teller (B.E.T) method, using N_2 adsorption and the geometric approximation method, normally give diverse values, which could cause the discrepancy of the calculated weathering rates between

laboratory and field samples (Stephens, 2002). Furthermore, the already-weathered soil minerals in the field could cause minerals to be less reactive than the unreacted minerals used in laboratory experiments leading to the lower weathering rates measured in the field (Velbel, 1993). Stephens (2002) also suggested that the lower field weathering rates may also reflect the influence of hydrological conditions, which cause a shift from surface-controlled dissolution under laboratory conditions to transport-controlled dissolution in the field. All these reasons lead to the observed higher weathering rates in laboratory studies compared with field studies. van Grinsven and van Riemsdijk (1992) also observed that discrepancies between weathering rates existed among various laboratory methods. For example, batch experiments give higher weathering rates compared with column experiments; this may be due to the mechanical abrasion of the mineral particles in batch experiments.

In addition, unlike the well prepared soil/sediments used in the laboratory reactors, soil heterogeneity and stratification phenomena exist in the field, which play an important role in gas channel development (Semer et al., 1998). The flow patterns are controlled by many factors, such as soil stratigraphy, soil lenses, and soil properties (e.g. porosity, permeability, organic matter and water content) (Gidda et al., 2006; Ji et al., 1993; Johnson et al. 1993; Semer et al., 1998). When the gas passes through layers of low permeability, which are usually composed of fine sediments, it is forced to spread horizontally to bypass the hydraulic barrier (Ji et al., 1993). It was also noted that turbulent flow, with the generation of bubbles, normally developed when the gas flowed through coarser-grained sediments (4 mm in diameter), while linear flow normally formed when the gas was moving through the finer-grained material (0.75 mm in diameter) (Ji et al., 1993; Marulanda et al., 2000). Throughout

experiments performed with different-sized beads, simulating different soil grain size and low permeability, it was observed by Ji et al., (1993) that the heterogeneity of actual field soils may hinder the development of a symmetrical air distribution pattern leading to the development of asymmetrical air flow. CO_2 leakage along discrete sections relies on the nature of the media and the permeability of discontinuities, which would further influence the impacts on different soils/sediments of the leaked CO_2 (Gal et al., 2012; Ji et al., 1993). Therefore, results from the laboratory work cannot be applied to all the possible soils; nevertheless the information obtained using specific samples allows for reliable/credible identification of the main consequences of CO_2 seepage.

There is a scale factor between laboratory and field studies to be considered in interpreting the results, the ratio between CO_2 supply and soil/sediments volume being smaller in a field study than in the laboratory experiments (Lu et al., 2010). It was observed in the ASGARD field that the released CO_2 was diffused laterally beneath the surface into neighbouring areas instead of being trapped within the leaked area, the diffused gas spreading over a large area (Patil et al., 2010). It was predicted by Patil (2012) that if CO_2 leaks from geological storage sites located >800m deep via fractures/faults in the caprock, the gas would firstly diffuse upwards spreading in a funnel-like shape generating a large footprint at the soil surface therefore involving a very large volume of soil. However, in laboratory experiments, the injected CO_2 gas would be trapped inside the boundaries of the reactor and the ratio of CO_2/soil would be much higher than in the field; this explains the higher dissolution rates and stronger weathering observed in the laboratory experiments (see above). The reactors used in the laboratory experiments were totally filled by 100% CO_2 after a certain time (Chapter 4 and 5). However, the

observed soil CO_2 concentration in natural seeps varies from 30%- 95% as presented in section 2.3.1, depending on the background CO_2 levels, soil properties and CO_2 leaking rate. The results from this research should be considered representative of the impact on soils/sediments of high levels of CO_2, such as the ones nearby a leaking injection well or along a fracture/fault.

In summary, differences exist between small scale laboratory experiments and large field scale experiments as described above, which lead to difficulties in linking the different scales and in the prediction of long-term effects based on small scale tests only (Johnson et al., 1997). The results of the laboratory experiments can reasonably describe the main effects of CO_2 leakages over sediments and soil when a specific composition is considered. Even if a generalisation of these results to any kind of soil composition would not be realistic, the outcomes give a good general idea of the potential consequences of CO_2 leakage, and on the main parameters, such as pH, which should be monitored for the prompt detection of anomalous levels of CO_2 in the surface soil. Based on the observed high weathering rates under high CO_2 concentration in the laboratory experiments, the results are more representative of field conditions where soils/sediments of similar composition are affected by high levels of CO_2 (Lu et al., 2010). The main contribution of this laboratory study is providing an alternative approach (Chapter 3) to supply chemical data helping the understanding of the geochemical process involved in the CO_2-soil system. This research is also aimed at identifying the best geochemical indicators for early detection of CO_2 leakage in real-scenarios as monitoring tools of potential CO_2 leakage from geological storage areas.

2.4 Summary

This chapter reviews previous and ongoing research on potential CO_2 leakage impacts on local environments, focusing on impacts on soil chemistry. The impacts are mainly related to changes in the pH of soil pore water, metal and metalloid changes (Al, Cd, Cr, Pb, As, Mn, Fe, Cu, Ni, Zn, Mg, Ca and K), and potential mineralogy and oxide changes due to lower pH.

As explained in section 2.2.1, since 1970, the effects on soil chemistry by acid rain have been widely studied worldwide (Cogbill and Likens, 1974; Falkengren-Grerup et al., 1987; Likens and Bormann, 1974; Skiba, 1989; Tamm and Hallbäcken, 1988; USEPA, 2012). These studies provide useful information understanding the potential impacts on soil chemistry with low soil pH. However, the chemical impacts of acidification in soil in a given situation involve not only the amount of acid present but the kind of acid present, which could have a different effect on certain chemical reactions taking place in the soil zone and in the water draining the soil (Johnson et al., 1984). Therefore, the effects on soil chemistry changes due to elevated CO_2 cannot be represented simply by the acid rain problem because of different kinds of acid. This research is carried out to assess the overall tendency in soil pH and surface and subsurface soil chemistry changes with elevated CO_2, which is currently unclear.

Previous research related to the effects in soil chemistry by elevated CO_2 was mostly related to the changes after a long time of acidification instead of the instantaneous response to additional CO_2 flux. However, the instantaneous response is important for developing CO_2 leakage monitoring techniques and explaining further ion concentration changes. It is necessary to assess the instantaneous response, and Stage II

experiments are carried out to provide the real time response in soil chemistry due to leaked CO_2.

Besides, the results from previous research vary among different investigations. This may be caused by the differences in the initial physical and chemical properties of soils at a particular site, which lead to the different responses to CO_2 leakage (Zheng et al., 2012). To the author's knowledge, there is no research carried out to compare directly the impacts on soil chemistry due to leaked CO_2 associated with different soil types. This research is carried out to fill in this gap. As explained in section 1.3, calcite dissolution is sensitive to CO_2 flux and could be the primary process buffering pH (Romanak et al., 2012; Zheng et al., 2012). Even for silicate sediments, the dissolution of minerals may come from carbonate content in the watershed (Blum et al., 1998). Besides, as particle size is considered to be an important factor to influence the response (Shih et al., 2000; Zhang et al., 2007), it is necessary to examine the soils' response in association with different particle sizes. To simplify the experimental conditions and better understand the reasons behind the results, limestone sand and silica sand with different particle size are therefore chosen to be used in the Stage II experiment (Chapter 3) in this research.

Natural and industrial analogues, field scale evaluations, laboratory experiments as well as modelling are the main methodologies used in the past years to examine the impacts. As described in section 2.3.3, small scale laboratory experiment is the most cost-effective way for improving understanding of the related problem. Based on the advantages of laboratory experiments, this study is carried out using well-controlled laboratory experiments to help understanding the effects on soil chemistry

by leaked CO_2. Both batch experiment systems and a flow through column system are used as the main research method in this research. It is necessary to note that differences exist between small scale laboratory experiments and large field scale experiments, which lead to difficulties in linking different scales and in prediction of long-term performance based on small scale tests (Johnson et al., 1997). Based on the higher weathering rates and higher CO_2 concentration in the laboratory experiments, the results from this research are better to be used to represent the long term impacts on the specific related soils and to demonstrate the conditions where the soils/sediments are surrounded by high levels of CO_2, such as the ones nearby a leaking injection well or along a fracture/fault (Lu et al., 2010). It is hard to link quantitatively between laboratory works and field works. The results of this research are comparable with specific soil related problems or soil under similar conditions in the field. The contribution of this laboratory study is mainly providing an alternative approach to supply chemical data helping understanding geochemical process involved in the system in related to various soil types; also, potentially identify better geochemical direct/indirect indicators for early detection of CO_2 leakage in the field, which could serve as monitoring tools of CO_2 leakage into surface when applying to the full-scale design.

This research is carried out on the above aspects to fill in the gaps and better understand the relevant impacts on soil chemistry caused by CO_2 seepage. The detailed research methodologies are described in Chapter 3.

Chapter 3 Methodologies

As described in Chapter 2, both a laboratory-batch experiment (Stage I) and a flow through column system (Stage II) were utilised in this research. This chapter focuses on giving a detailed description of the methodologies in terms of Stage I (section 3.1) and Stage II (section 3.2) experiments. In each stage, sampling process, laboratory work design and analytical methods are described. The design of the flow through column system in the Stage II experiments has been published in Caramanna et al. (2012).

3.1 Stage I - Closed reactor experiments

Stage I consists of a series of lab-based experiments using a high temperature/high pressure rig to simulate the soil's response to long term exposure to CO_2/SO_2 seepage. Moreover, the results from Stage I informed the design of the Stage II experiments, a flow through column system experiment.

During Stage I, three replicates of each soil sample were run using a high pressure/high temperature batch vessel. Samples were collected before and at the end of the incubation and analysed in order to identify the main differences due to the CO_2 incubation. The experimental conditions and procedure are explained in detail in the following sections.

3.1.1 Soil sampling

3.1.1.1 Sampling site description

As stated in section 2.3.2, the ASGARD field (18 m×16 m) (Fig. 3.1) is an artificial soil gassing facility located in a field of permanent pasture at the University of Nottingham's Sutton Bonington Campus (52.8° N, 1.2° W). It was sprayed off, ploughed and re-seeded with the present grass, remaining as a grassland for over 10 years. Since 2004, it has been used to inject CO_2 gas into the field and several studies were carried out in this unique field to study the effects on plants, soil microbes and soil properties by elevated soil CO_2 concentration (Patil et al., 2010; Smith et al., 2005; West et al., 2009).

As a complement to the ASGARD field work, the Stage I laboratory study was carried out using samples from the ASGARD field. The detailed sampling process is presented in section 3.1.1.2 The reasons for taking samples from the ASGARD field re that: 1) as a part of the ASGARD project, the author has access to the field and it's practical to collect soils from the field considering its location; 2) the results from this experimental work can be combined with previous studies carried out in the ASGARD field (Chapter 4) to better understand the impacts on the local environment by the CO_2 leakage; and 3) the results from this research can be compared with other studies (Cunningham, 2010; Ekene, 2011; Patil et al., 2010; Smith et al., 2005; West et al., 2009) carried out on the soil chemistry changes in the ASGARD field and provide useful information to relate findings here with a larger field work.

A detailed description of the geology of the ASGARD site is presented in the following sections.

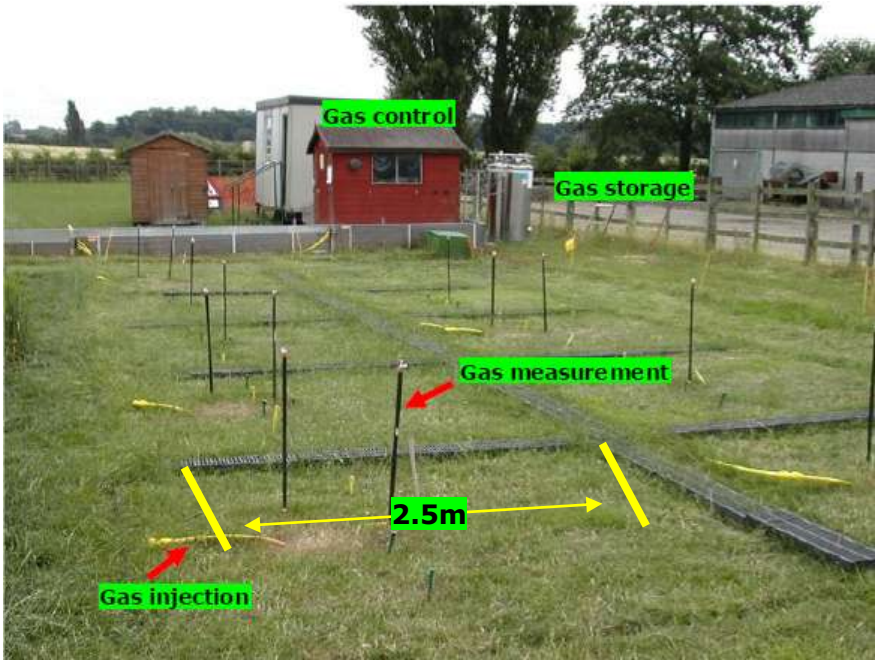

Fig. 3.1 The ASGARD field in Sutton Bonington, the University of Nottingham.

The ASGARD site is characterised by a 'head' deposit with up to 1.5 m thick which overlies mudstone deposits of the Mercia Mudstone Group (Ford, 2006; Smith et al., 2007). The topsoil ranges from 0.2-0.4 m depth underlain with deposits of gravel, sand and clay to a depth of 1-1.2 m. Locally the superficial deposits are characterised by river terraces rich in sand and gravel, surrounded by sheets of the lithologically variable 'head'. Lithologically, the 'head' is characterised by moderately well-consolidated sand with abundant rounded polymict gravel derived from Triassic sandstones and pebble-beds. These sand and gravel deposits are broken down and highly degraded. The resulting 'head' deposits incorporate various amount of red clay from the Mercia Mudstone Group with a wide range of grain sizes, degrees of sorting and levels of consolidation.

A consistent thickness of approximately 0.3 m of dark brown sandy topsoil with a reasonably sharp base with the undifferentiated 'head' is

interpreted to be present over much of the site (Smith et al., 2007). The undifferentiated 'head' varies considerably in thickness ranging from 0 m in the west of the site to approximately 0.3 m in the east. This unit is typically composed of red-brown slightly clayey, gravelly silty sand. A relatively persistent horizon of gravelly 'head', typically 0.15 m thick, occurs in the west and north of the site at a regular depth of 0.3 to 0.6 m beneath the ground surface. This unit is typically associated with the base of the overlying undifferentiated head, and is characterised by abundant medium to coarse gravelly sand.

Sandy head occurs in the central and northern part of the site and is characterised by comparatively well sorted red-brown or light red sand and silty sand with occasional fine to medium gravel. Clayey head is present across much of the site, occurring at a relatively low level in the succession. This unit is characterised by red-brown silty, clayey sand with occasional gravel. Locally, thin red clay laminae (up to 2 cm thick) are present. The increased clay content associated with this unit may be due to the relative proximity to rockhead. This unit varies dramatically in thickness, ranging from over 1 m in the south-west of the site, to less than 0.2 m in the north of the site.

The site was chosen to set up the ASGARD facility because of its reasonable uniformity of soil type down to a depth of 1 meter, which was established from the geological map and by coring (Smith et al., 2007). The field was divided into 12 experimental plots, each 2.5 x 2.5 m, to be compared with six untreated reference plots (Smith et al., 2005). Fig. 3.2 shows the experimental layout of the ASGARD facility. The gas flow is supplied by CO_2 cylinders in liquid phase, individually regulated by mass

flow controllers and the gas is injected to 60 cm underneath the ground surface (Patil et al., 2010).

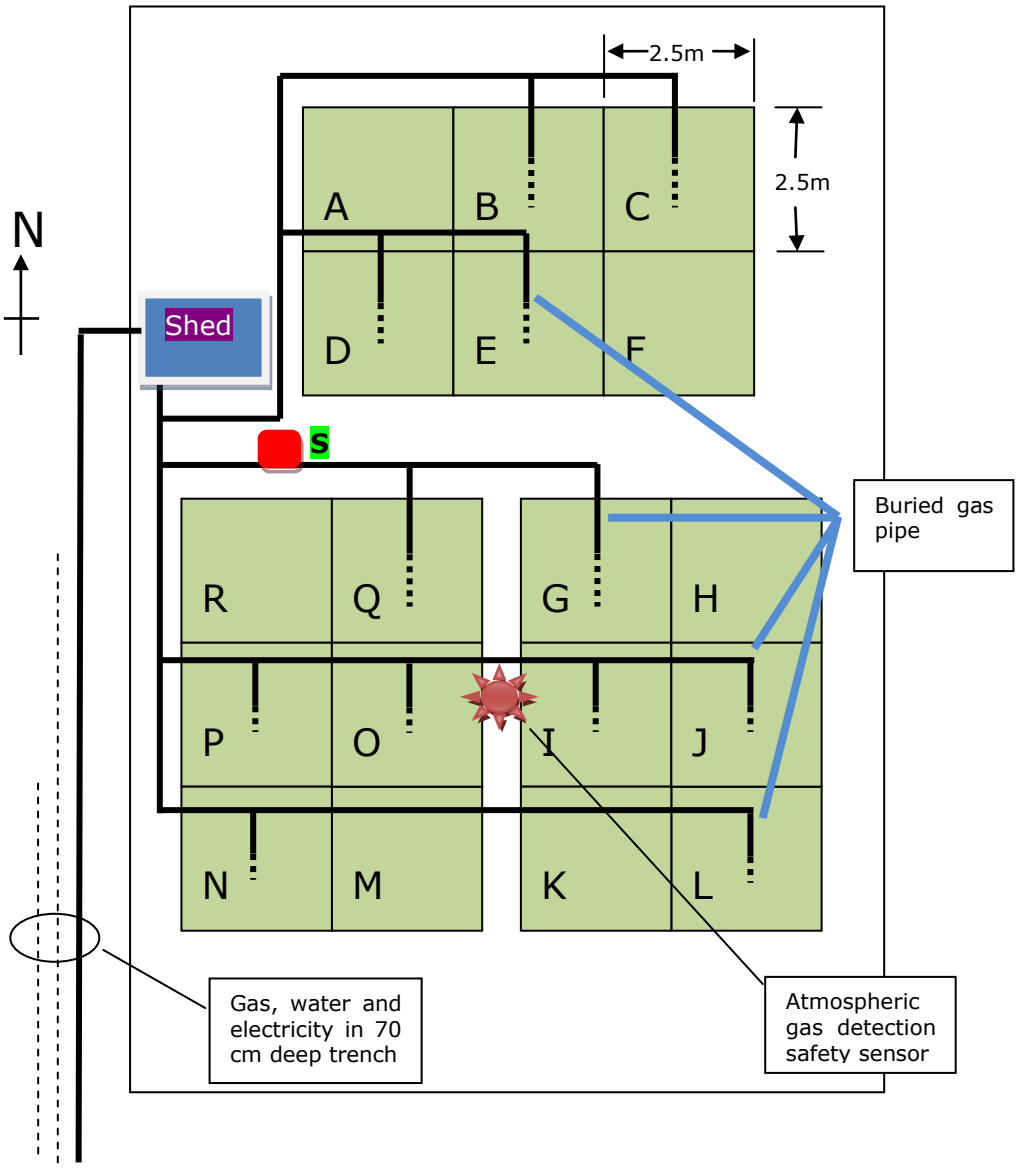

Fig. 3.2 Experimental layout of the ASGARD facility with 12 experimental gassed plots and six control ungassed plots (modified from Smith et al. (2005)). Plots A–F were planted with grass, plots G–L with bean and plots M–R with winter wheat.

Note: Red square labelled with 'S' is the sampling point where soil sample collected for this research, which is described in section 3.1.1.2.

3.1.1.2 Soil sample collection

In order to examine the effects on soil chemistry of CO_2 leakage under various laboratory conditions (section 3.1.2), ungassed soils instead of the gassed soils in the ASGARD field were collected for the Stage I experiments. The reasons for not sampling the soils of the gassed areas are that: 1) sampling soils from the gassed areas may change the physical properties of the gassed plot, for example permeability of the soil, and further influence the ongoing experiments in the field; 2) soils of the gassed plots may have already weathered and adapted to the high CO_2 concentration condition, which will leave the soils less sensitive to CO_2 injection in the laboratory study and less to be observed. Therefore, the soil sample for Stage I experiments were collected from untreated area at the ASGARD field and the results were compared with the results of previous research (Chapter 4).

As explained in section 3.1.1.1, the ASGARD field site is reasonably uniformed down to a depth of 1 meter (Smith et al., 2007) and many studies were carried out to compare between the gassed and ungassed plots. With the assumption that the artificial site contains reasonable undifferentiated top soil across the site, soils from one spot of untreated area (point S in Fig. 3.2) were collected. Also, considering the aim of this research, the soil sampling process was aimed at collecting top soil from the site, which was within roughly the first 30 cm of the ASGARD site. To sample the targeted soil in the field, firstly, all the grass above the soil surface was removed. Then, the soil immediately beneath the grass was removed and placed alongside the sampling spot during the sampling process. The targeted soil samples were subsequently dug by a spade from site (8 cm-22 cm in depth within about a 20 cm square). The

collected soil (roughly 13 kg) was then stored in a clean bucket covered by a foil to avoid any contamination during the sampling process. The removed soils were then placed back to the spot after sample collection, together with the plants and grass removed before. A label including relevant information such as sample depth, collection date and name of operator, was placed on the surface of the buckets. All the samples were safely stored in a cold store for the following experiments.

3.1.1.3 Soil sample preparation

Soils consist of the mass of weathered rock and loose material lying upon solid rock underneath. All the mineral and naturally occurring organic material within soils is a 2 mm or less in particle size. They are normally used to distinguish between soils and gravels, and where the main chemical reactions take place when exposing to CO_2 gas (Barth et al., 1989). Therefore, the minerals and organic matter that were less than 2 mm in diameter were extracted from the collected soils as a universal procedure used in other laboratory experiments (Irha et al., 2009). Two sets of samples (unground soils and ground soils) were prepared using these particles. The ground samples were prepared in order to have more homogenous soils and to assess the difference in soil responses to CO_2 release due to different soil particle sizes. A detailed description of these two samples preparation is presented in the following sections.

Unground soils

- The collected soils were firstly oven-dried at 40 °C for seven days. 40 °C is considered an appropriate temperature to dry soil samples properly without destroying their structure and texture (Rowell, 1994b). During the process, larger lumps were broken up by hand to avoid soil aggregates.
- The dried sample was then sieved through a 2,000 μm sieve to remove large roots and rock fragments, vegetable matter and other particles larger than 2,000 μm in size. The > 2,000 μm fractions were weighed and the values were recorded (see section 4.1).
- The soil samples were then well mixed by a riffle splitter (Fig. 3.3). During the splitting process, the soil sample was poured into the feed hopper of a Jones-type riffle splitter on top (see description in the figure), and then a small release gate drops the sample into two receiving bins. The reason for choosing riffle splitting to mix the samples is that riffle splitting methods performed the best mixing results with approximately 99% confidence level with less than 2% biases compared with other four commonly used mixing methods, e.g. paper cone riffle splitting, fractional shovelling, coning and quartering, and grab sampling (Gerlach et al., 2002). The detailed information is available in the research carried out by Gerlach et al. (2002).
- Finally the well mixed samples were stored in clean plastic zip-lock bags and labelled as "oven-dried unground soils".

After the mixing, five 0.5 g samples were randomly subsampled from the well-mixed oven-dried unground soils to test how uniformly the samples have been prepared by examining particle-size distribution, loss on

ignition organic matter, and pH (Schumacher et al., 1990). The detailed methods for examining particle size analysing, loss on ignition organic matter and pH are described in sections 3.1.3.1 and 3.1.3.2. The standard deviation of those random five subsamples was calculated based on measured particle size distribution, loss on ignition organic matter and pH (Appendix 1). The calculated standard deviation was much higher than their intralaboratory precisions and indicated that all the samples were well mixed. For example, standard deviations for total sand (63-2000 μm), silt (3.9-63 μm), and clay (0-3.9 μm) contents are 0.62 wt%, 1.36 wt%, and 1.98 wt%, respectively. The results met the intralaboratory precision goals set for the Mid-Appalachian soil survey of 3.0 wt% standard deviations for sand and silt; 2.0 wt% standard deviations for clay (Schumacher et al., 1990).

Fig. 3.3 Riffle splitter apparatus, which consists of a feed hopper of a Jones-type riffle splitter on top and a small release gate under. The split soils drop through the riffles into two receiving bins.

Soil moisture content (MC) may influence the absorption of CO_2/SO_2 (Rowell, 1994a; Xu et al., 2005). In order to assess how moisture interferes with the exposure to CO_2 leakage, samples with different MCs

were prepared. Based on the measured natural soil MC in the ASGARD field (about 17% MC), a subsample of 100 g was taken and different amounts of Mill-Q water was added to the soil and well mixed by a glass rod to simulate various MC.

- 0 g - oven-dried ground soil
- 20 g - near field MC
- 30 g - moderate MC
- 40 g - nearly saturated soil

The samples were labelled as: oven-dried unground soil, 20% MC unground soil, 30% MC unground soil and 40% MC unground soil, respectively, and later were used for the experiments with two reactors (see section 3.1.2.1).

Ground soils

Another set of soils were prepared as ground soils in order to have more homogenous soils and assess the difference in soil responses to CO_2 release due to different soil particle sizes. All the samples for the preparation process described below were obtained from the oven-dried unground soils prepared as described above.

- The sample was firstly collected from oven-dried unground soils and filled in a glass bottle to up to 2/3 of its maximum volume.
- The soil was next poured in a silica core container and the container was then sealed well and placed inside a mill machine (see Fig. 3.4).
- The grinding time was set to be 3 min.

- Once the grinding stopped, the silicate container was taken out from the grinding machine and the ground soils were poured out of the container and stored in a zip-lock bag.

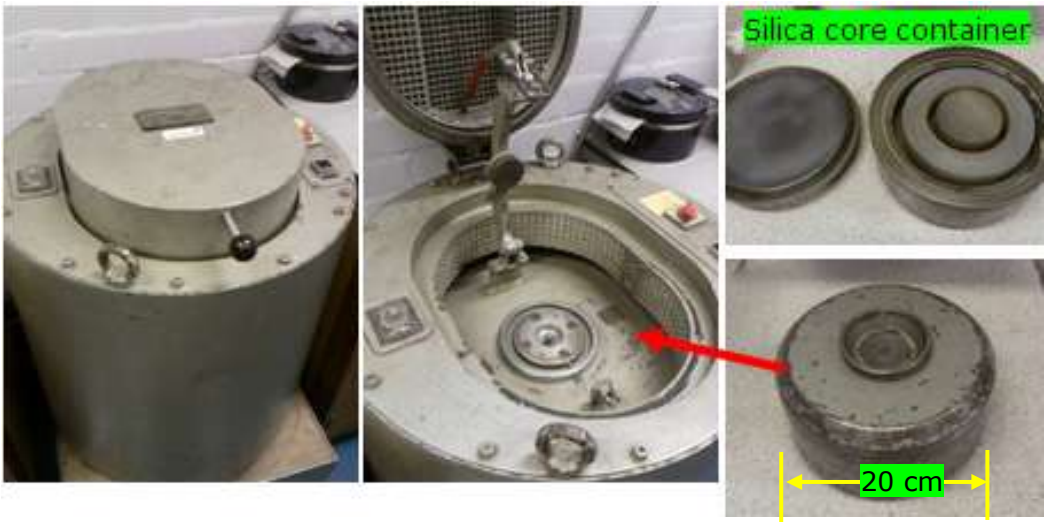

Fig. 3.4 Grinding mill.

After the grinding process, all the soils were mixed using a raffle splitter again. Then, using the same process as applied to the unground soils (section 3.1.1.3), a subsample of 100 g was taken from the main sample and saturated with various weights of Mill-Q water: 0 g, 20 g, 30 g, and 40 g. The soils were labelled as: oven-dried ground soil, 20% MC ground soil, 30% MC ground soil and 40% MC ground soil, respectively, and later were used for the experiments (see section 3.1.2.1).

3.1.1.4 Soil sample numbering

All the soil samples run in Stage I experiments are listed and numbered as Table 3.1. Samples S15-S17 were tested using with the Parr reactor model

4840; while, the rest were run with the Parr reactor model 4843. See section 3.1.2.1 for the detailed description of both reactors.

Table 3.1 Soil sample numbering in Stage I experiments.

No.	***DESCRIPTION***		
S1	Unground	oven-dried	No incubation
S2	Unground	oven-dried	Incubated with 100% CO_2
S3	Unground	oven-dried	Incubated with 100% CO_2
S4	Unground	oven-dried	Incubated with 100% CO_2
S5	Unground	20% MC wet	Incubated with 100% CO_2
S6	Unground	20% MC wet	Incubated with 100% CO_2
S7	Unground	20% MC wet	Incubated with 100% CO_2
S8	Unground	40% MC wet	Incubated with 100% CO_2
S9	Unground	40% MC wet	Incubated with 100% CO_2
S10	Unground	40% MC wet	Incubated with 100% CO_2
S11	Ground	oven-dried	No incubation
S12	Ground	oven-dried	Incubated with 100% CO_2
S13	Ground	oven-dried	Incubated with 100% CO_2
S14	Ground	oven-dried	Incubated with 100% CO_2
S15	Ground	oven-dried	Incubated with 99% CO_2 + 1% SO_2
S16	Ground	oven-dried	Incubated with 99% CO_2 + 1% SO_2
S17	Ground	oven-dried	Incubated with 99% CO_2 + 1% SO_2
S18	Ground	20% MC wet	No incubation
S19	Ground	20% MC wet	Incubated with 100% CO_2
S20	Ground	20% MC wet	Incubated with 100% CO_2
S21	Ground	20% MC wet	Incubated with 100% CO_2
S22	Ground	30% MC wet	No incubation
S23	Ground	30% MC wet	Incubated with 100% CO_2
S24	Ground	30% MC wet	Incubated with 100% CO_2
S25	Ground	30% MC wet	Incubated with 100% CO_2

3.1.2 Laboratory work design and investigation process

3.1.2.1 High Pressure/ High Temperature Reactor

To speed up the experimental process, two reactors were used for the incubation experiments. The prepared soil samples were placed into high pressure/high temperature reactors (described below), and then a

controlled flow of CO_2/SO_2 was injected into each reactor, either 100% v/v CO_2 or CO_2/SO_2=99/1 vol. (as explained in section 1.3).

Parr reactor model 4840

For the CO_2/SO_2 mixture gas incubation, a high pressure/high temperature reactor (Parr reactor model 4840) was used. Fig. 3.5 and Fig. 3.6 show the schematic of the experimental set-up and the laboratory rig. During the gas injection process, the volume of the injected CO_2 and SO_2 gas was controlled by a mass flowmeter and injected into the reactor separately from the CO_2 and SO_2 gas cylinder to obtain the targeted mixture concentration. The total amount of the injected gas can be calculated based on the flow gas rate and injecting time.

The whole process was monitored by an adjacent computer. To meet the target pressure, a CO_2 pump was used to raise the pressure from the value at the outlet of the regulator (5 bar) to the operational value of 25 bar. Calibration was carried out by trying different injection times of CO_2 and SO_2 gas to verify the time needed to reach the target pressure. Once the gas injecting time is set, based on the injection rate for CO_2, 10 L/min and SO_2, 1.5 L/min by mass flow controller, the amount of gas can be calculated by the following equation,

$$V = T * R \tag{3.1}$$

where *V* is volume of gas, *T* is injection time and *R* is injection flowrate for the CO_2 and SO_2 gas.

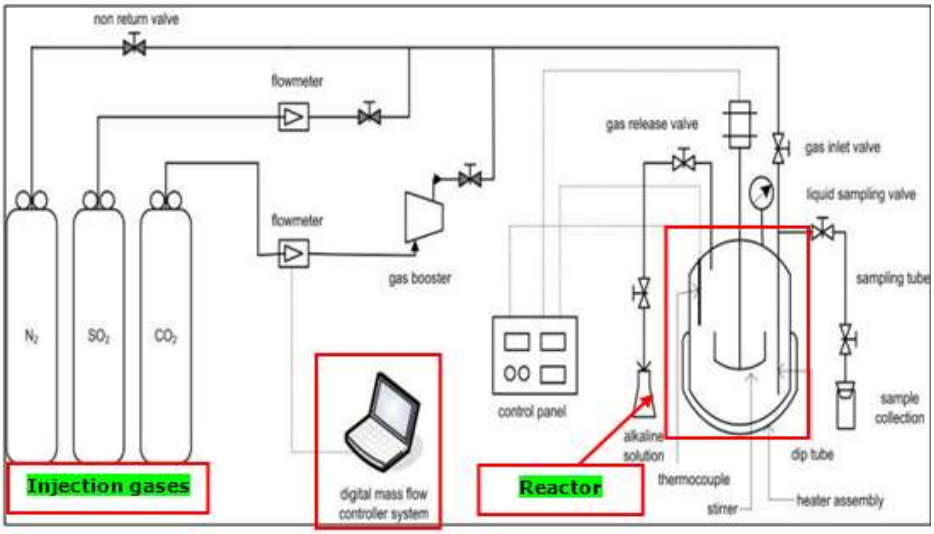

Fig. 3.5 Schematic of the experimental set-up (modified from Garcia (2010)).

Note: The CO_2 and SO_2 gas was controlled by the digital mass flow controller system and was injected into the reactor separately from the CO_2 and SO_2 cylinder. N_2 gas was used to flush the tubes and reactors at the beginning or at the end of the experiment to clean the system. The residual CO_2/SO_2 gas was released through an alkaline solution to atmosphere at the end of the run.

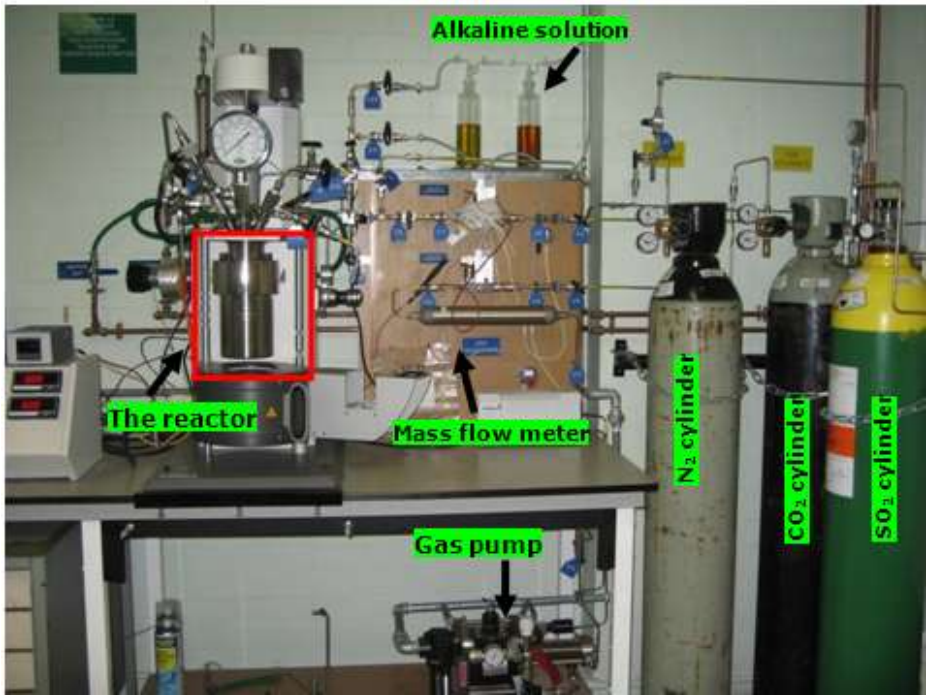

Fig. 3.6 High pressure-high temperature experimental (Parr reactor model 4840) set-up.

Parr reactor model 4843

For the 100% CO_2 incubation, a high pressure/ high temperature Parr reactor model 4843 (Fig. 3.7) was used. The prepared soil sample was introduced into the vessel and afterwards CO_2 was injected up to the required pressure (see 3.1.2.2 for the incubation conditions).

Fig. 3.7 High pressure-high temperature experimental (Parr reactor model 4843) set-up in the laboratory.

For the experiments with those two models, the diameter of the reactor is the same, the soils inside two columns were the same, and the incubation conditions were the same for both reactors as seen in section 3.1.2.2. Though the volume of the reactor of Parr reactor model 4843 (300 mL) is different from that of Parr reactor model 4840 (600 mL), under the higher pressure and temperature inside the reactor, the soils inside those two reactors were all saturated with the injected CO_2/SO_2 gas (as shown in Chapter 4). The difference in the gas volumes is not a limiting factor to the reactions. Therefore, the results from both reactors are comparable and the differences of the impacts on soil chemistry could be related to the additional SO_2 added, which will be shown in Chapter 4.

3.1.2.2 Incubation conditions

Previous research showed that increased CO_2 partial pressure (pCO_2) and temperature applied on soil enhanced CO_2 consumption during mineral weathering process (Clow and Mast, 2010; Karberg et al., 2005; Pokrovsky et al., 2005; Sposito, 1994). In order to speed up the experimental process, the reaction temperature and pressure was raised during the experiments as follows. With the purpose of avoiding any CO_2 phase changes during the experiments, it is necessary to consider the critical point for CO_2 gas based on the CO_2 gas phase diagram (Fig. 3.8). Liquid CO_2 only forms at pressure above 5.11 atm and the critical temperature and pressure are 31.1 °C and 72.8 atm, respectively.

As stated before, different controlled ratios of mixture gas were used in the incubation at this stage: 100% CO_2, and CO_2/SO_2=99/1. Due to the presence of SO_2 in the gas mixture (CO_2/SO_2), the possibility of small changes in the CO_2 phase diagram should be considered, but the details of such changes are not certain (Sass et al., 2005; Seevam et al., 2007; Toftegaard et al., 2010). Therefore, temperature and pressure were needed to set at values far enough away from the phase-changing limits to avoid any changes. Moreover, as the experiments are intended to mimic the ambient environment, the temperature was maintained within the ambient range. Overall, the following reaction conditions were selected to run the experiments, 25 bar and 25 °C.

To examine the soil response to elevated CO_2, the soil needs to be incubated in the CO_2 gas long enough to obtain the impacts. However, the experiment for each cannot be too long considering the constraint of the length for this research. To set a reasonable incubation length, several

trial incubations with 25 bar and 25 °C were carried out. It was seen that after three days, no obvious pressure difference was observed for the following incubation, and clear impacts were obtained in the changes in the ion concentration of extracted soil solution (Chapter 4). Three days incubation was therefore selected in this research, with 25 bar and 25 °C as stated above. During the process, the CO_2 and CO_2/SO_2 were injected as a gas phase.

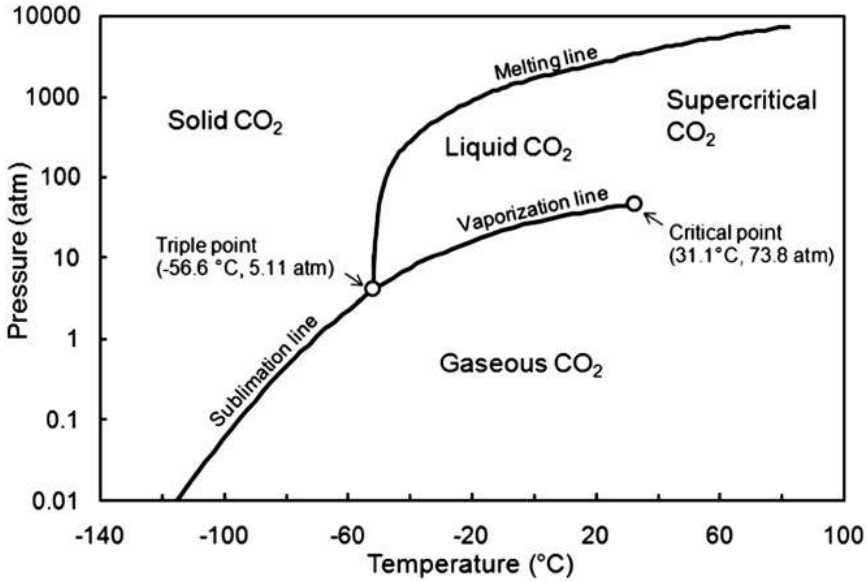

Fig. 3.8 Phase diagram for CO_2 (Toftegaard et al., 2010).

3.1.3 Analytical methods

3.1.3.1 Soil characterisation

X-ray Diffraction (XRD)

As explained in section 2.2.4, mineralogy is likely to change when soil is exposed to elevated CO_2. XRD was used to identify the crystalline elements in the soil, therefore defining the mineralogical composition of the samples used in this research and also comparing the changes in the mineralogical composition before and after the gas incubation.

Each pure mineral or a crystalline compound has a specific X-ray diffraction pattern dependant on its atomic structure. The XRD method is usually used to identify the unknown phases that are contained within a sample. This is achieved by analysing solid and powdered samples and matching the results, which are represented by a series of peaks on a graph generated by the X-ray scatter at different angles, against the ones from a database of 70,000 or more recorded phases (Klute, 1990). The errors in accuracy are low and within 3 wt. % deviation from actual values at the 95% confidence level (Hillier, 2000; Srodon et al., 2001). As the high accuracy of XRD analysis, the methods have been previously widely used to observe the mineralogy changes in soils after exposing to CO_2 (Annuziatellis et al., 2005; Beaubien et al., 2008; Stephens and Hering, 2002).

The principle for the XRD is as follows as described by Pecharsky and Zavalij (2009) and Waseda et al. (2011). The sample is placed in the Goniometer and bombarded with X-rays generated from a copper or cobalt tube. The rays diffracted by the sample are collected by a detector and the information is sent to a computer where it is converted to d-values of specific intensities by using of the Bragg equation. This information can then be shown graphically in the form of a diffraction pattern or 'diffractogram'. The diffractogram from the unknown sample can then be matched against the database using the PC-Identify software.

The HILTONBROOKS X-ray powder diffraction with 35 position sample holder was used in this observation. The HILTONBROOKS X-ray powder diffraction consists of: Hiltonbrooks 3kW generator model DG3 *(operated at 40kV, 20mA)*, Hiltonbrooks detector control module, Hiltonbrooks step motor drive module, Philips PW 1050 goniometer and proportional detector,

Seifert copper long fine focus X-ray tube *(Cu radiation at 1.5406 Angstroms)*, and Sietronics curved graphite monochromator *(improves peak intensity)*. A nickel filter is used to absorb Cu K_β radiation. Sietronics 'siehilt' automation software or Hiltonbrooks HBX data collection software *(Hiltonbrooks HBX is used by default)* and diffraction Technology 'traces v.3' scan processing software were applied in the equipment.

For this technique, the XRD specimens should be flat, densely packed, very fine-grained powders. The soil samples for the XRD analysis were prepared as follows (Davis et al., 1998):

- Approximately 0.5 g air-dried soil sample was placed into an agate mortar and carefully ground by a pestle to make it a fine powder (<45 μm particle size) (Fig. 3.9 (a-b)).
- A flat piece of clean glass was taped over the upper surface of an aluminium cavity holder, so as to cover the rectangular window. Then, the prepared fine powder was filled into the cavity holder and applied to overfill the cavity (Fig. 3.9 (c)).
- A gently press was then applied over the taped glass on the powder to make it flat, which left a flat, densely packed cavity.
- Then, the sample was powdered and packed into an aluminium holder ready for the XRD analysis (Fig. 3.9 (d)).

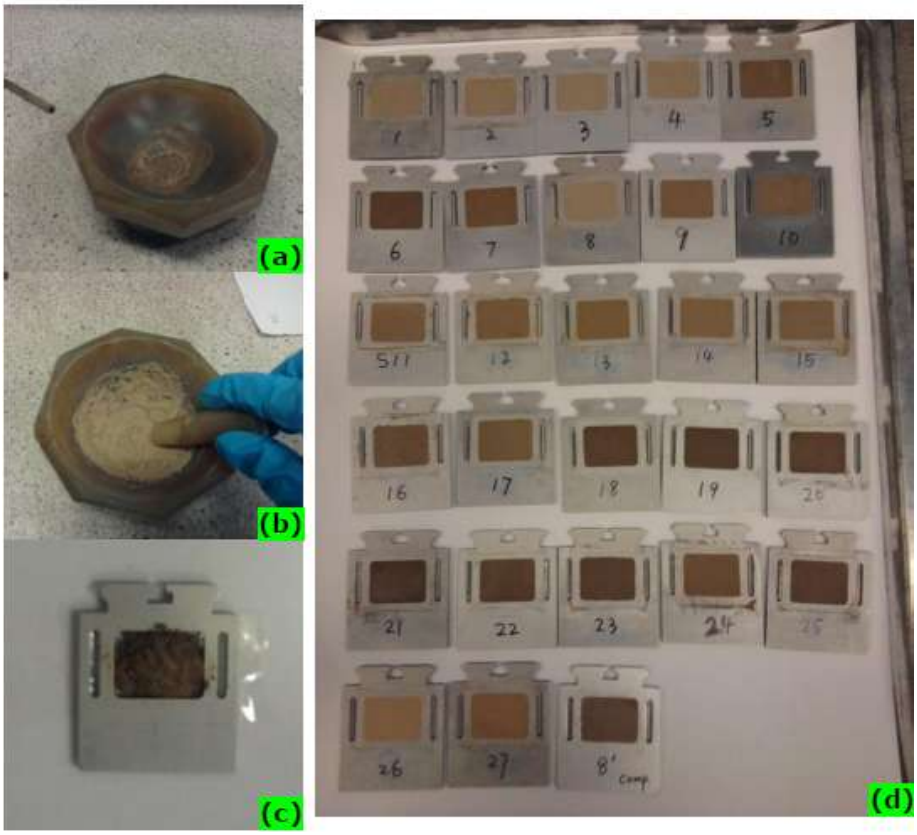

Fig. 3.9 Sample preparing for XRD analysis, where (d) shows the samples ready for XRD examination.

Scanning Electron Microscope/Energy Dispersive X-ray spectroscopy (SEM/EDX)

The available reacted surface would influence the reaction rate and amount of toxic and nutrient elements released from the soil sample. It is therefore important to determine the morphology of the soil sample, and this can be achieved by SEM/EDX in this research. In addition, SEM/EDX was chosen to investigate any surface changes after the CO_2 incubation. The methods have been previously widely used to observe the surface changes of samples (Madland et al., 2006; Noiriel et al., 2004).

All the samples were prepared prior to the SEM/EDX analysis as follows.

- Firstly, the samples were oven dried at 40 ^{o}C for four hours.
- Then, about 0.5 g of the dried samples was collected and sprinkled on top of a pin type aluminium stub with a double sided carbon sticky tab on it. A bellow was used to blow off the loose material on the tab to leave a single layer of sample for the better analysis.
- Later, the samples were stored in a weighing bottle with desiccators inside for better drying.
- Then, the samples were ready for the SEM analysing (Fig. 3.10).

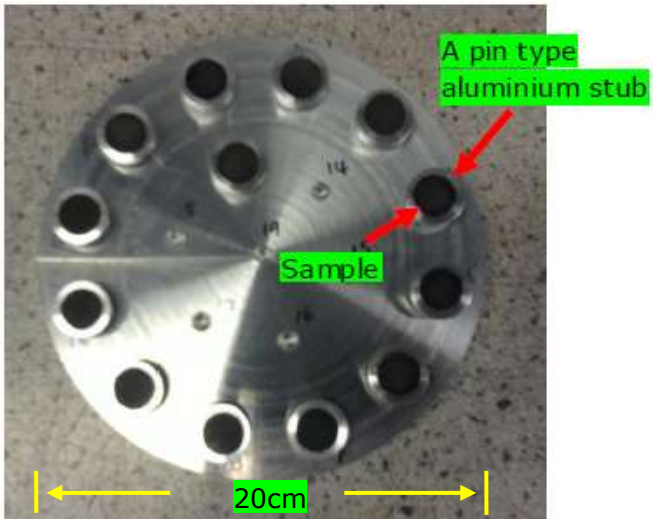

Fig. 3.10 Prepared samples ready for SEM imaging.

Once the samples were ready for the SEM/EDX examination, a Quanta 600 by FEI Company was used for the analysis and back scattered electron (BSE) detector was used for capturing the images. During the process, 25 kV high energy electron beam was generated by the tungsten hairpin filament. The electrons were accelerated and focused into a narrow beam, passing through the BSE detector and scanned onto the samples. The high energy beam interacted with nuclei and was eventually backscattered as a lower energy signal detected by the BSE detector. BSE mode gave a mean atomic number difference information/contrast. Therefore, elements lower in the periodic table showed darker than elements higher in the periodic

table, which helped with visual information of elemental differences. During the process, the low vacuum mode was used for the observation. Elemental analysis was carried out by Genesis Spectrum Version 5.21 software by EDAX Company. Energy Dispersive X-ray analysis (EDX) techniques were used in the software for elemental quantification.

Particle size distribution

In order to characterise the soils, samples were classified and defined by a Coulter Laser Scattering analyser employing Fraunhofer diffraction (LS 200, Variable-Speed Fluid Module Plus (VSM+)) (Fig. 3.11). The instrument is capable of measuring particle diameter ranging from 0.375 to 2000 μm and typically has better than 1% reproducibility of data (Beckman Coulter, Inc., no date).

The soil samples were prepared prior to the analysis as follows:

- The sample (0.5 g each) was firstly placed into a centrifuge tube.
- 10 ml peroxide (H_2O_2) was added in the centrifuge tube and left to dissolve soil organic matter overnight.
- The tube was then heated in a water bath for another 60 minutes.
- Distilled water was added into the tube up to 25 mL. The tube was then centrifuged at 3500 rpm for five minutes. The upper solution within the tube was disposed and replaced by 25 mL distilled water, and then the tube was centrifuged again. The centrifuge process was repeated three times.
- 25 ml 25% sodium hexametaphosphate ($(NaPO_3)_6$, Calgon) was added into the tube containing soils, and shaken manually for a minute.

- Finally the tube was placed in an ultrasonic bath for a minimum of 30 minutes.

The solution was then ready to be placed in the particle size distribution analyser as shown in Fig. 3.11. A simplified diagram was shown in Fig. 3.12 to explain how the equipment works. The principle can be summarised as follows. According to Beuselinck et al. (1998) and Keck and Muller (2008), firstly, a laser beam was generated by a laser source listed on the left of Fig. 3.12. Converged by an optical lens, the laser beam passed through an upward moving suspension. Then, the diffracted light was collected by Fourier lens and focused onto a ring detector, by which the intensities and the distance of the rings were measured. Based on the principle that particles of a given size diffract light through a given angle and the angle increased with decreasing particle size, the particle size can be calculated by a computer (software).

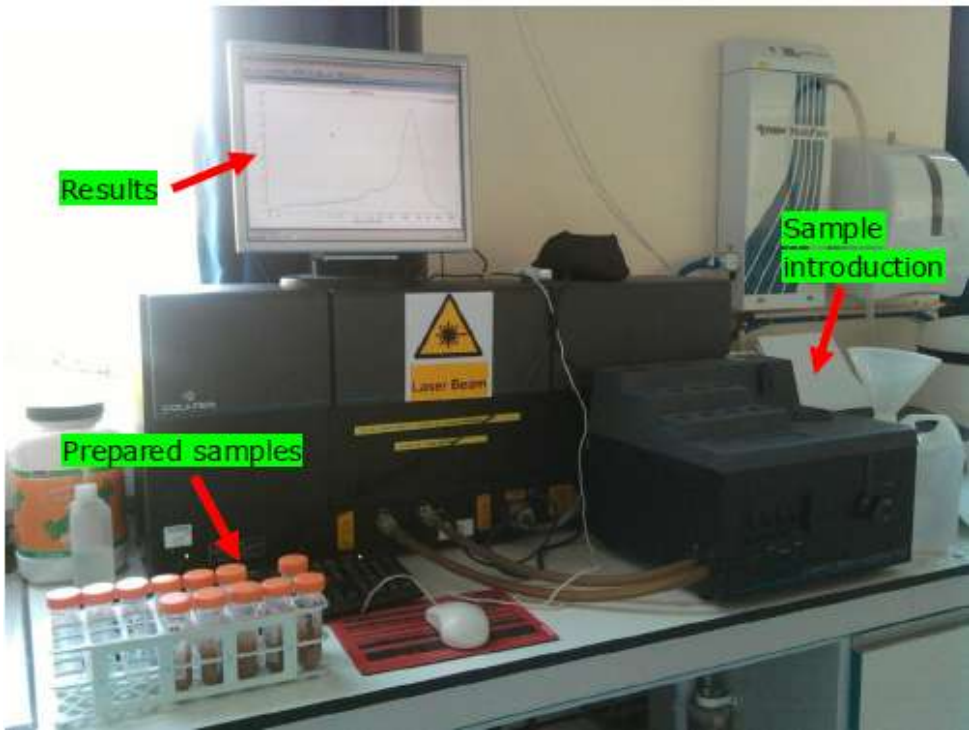

Fig. 3.11 Particle size distribution analyser (Model LS 200).

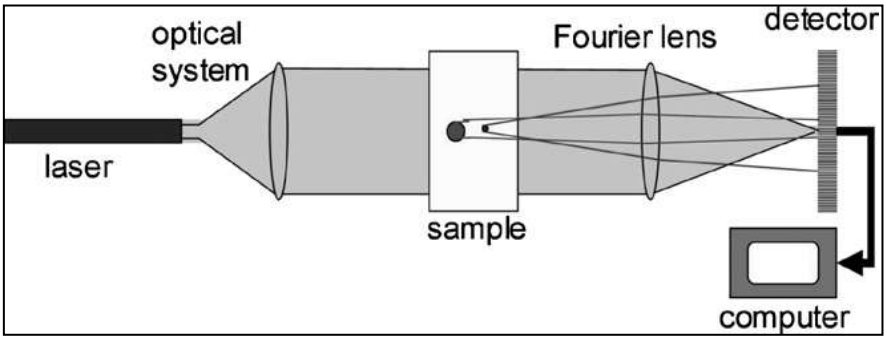

Fig. 3.12 Simplified setup of a laser diffractometer from Keck and Muller (2008). The graph listed from left to right are: light source (laser beam) to illuminate the particles, optical system to converge the laser beam, sample cell containing particles, Fourier lens to collect the diffracted light, ring detector, PC (software) to calculate the particle size.

Soil Moisture Content (MC), Organic Content (OC) and Carbonate Content (CC)

MC, OC and CC are other key parameters to be measured in order to better describe the soil characteristics.

To measure soil MC, the sample was first placed in a crucible and heated in an oven (model Sanyo Gallenkamp OMT) at 105 ^{o}C for 24 hrs. Soil MC was calculated by the weight loss during the process by the following equation (Heiri et al., 2001),

$$MC = \frac{W_2 - W_1}{W} \% \quad (3.2)$$

where, W_2 is the weight of the crucible with sample after the 105 ^{o}C oven heating, W_1 is the weight of the crucible with sample before oven drying and W is the weight of the collected soil (all in g).

Samples were further heated by the oven to 550 ℃ for 24 hrs and soil OC, LOI_{550} (loss on ignition), was calculated by the weight loss during this process (Heiri et al., 2001) by the following equation,

$$LOI_{550} = \left(\frac{DW_{105} - DW_{550}}{DW_{105}}\right) * 100 \quad (3.3)$$

where, LOI_{550} represents *LOI* at 550 ℃ (as a percentage), DW_{105} represents the dry weight of the sample before combustion and DW_{550} is the dry weight of the sample after heating to 550 ℃ (both in g).

Continue heating to 950 ℃ for 2 hrs (no more than 4 hours), the soil CC, LOI_{950} (loss on ignition), was calculate using the following equation,

$$LOI_{950} = \left(\frac{DW_{550} - DW_{950}}{DW_{105}}\right) * 100 \quad (3.4)$$

where, LOI_{950} represents *LOI* at 950 ℃ (as a percentage), DW_{105} represents the dry weight of the sample before combustion, DW_{550} is the dry weight of the sample after heating to 550 ℃, and DW_{950} is the dry weight of the sample after heating to 950 ℃ (all in g).

3.1.3.2 Soil pH

Before and after the reactor incubation, the pH of soil pore water was determined by pH electrodes to assess the level of acidification caused by the incubation of CO_2/SO_2 gas.

Soil pH was measured by using a soil test kit from Palintest Ltd., and the pH was measured in aqueous solution (at a 1:2 (w/w) soil-to-water ratio) following an equilibration, which is a standard commonly used method

(Stephens, 2002). During the testing process, two levels of 2 mL scoops of soil were collected and placed in a sample container, mixed with up to 10 mL deionised water (Palintest, 2012). Then the container was capped and shaken gently for one minute, and the pH was read by a Denver's Portable pH meter (model accumet portable AP10) (Fig. 3.13). The accuracy for pH measurement is ±0.01, while the accuracy for measuring temperature is ±0.4^{o}C.

Before each measurement of soil pH, the pH meter was calibrated by using of three standard calibration solutions purchased from Hanna Instrument Ltd.. These three standard calibration solutions are pH 4.01 buffer solution (HI-7004), pH 7.01 buffer solution (HI-7007), pH 9.18 buffer solution (HI-7009). These three points was automatically compared with the memorised buffer values of the portable meter during the pH calibration. After each measurement, the pH probe was moist by a storage solution for electrodes (HI-70300 purchased from Hanna Instrument Ltd.) to minimize clogging. A detailed procedure of the calibration process is listed in the instruction manual of each calibration solution in the website of Hanna Instrument Ltd..

Fig. 3.13 A Denver's Portable pH meter (model accumet portable AP10).

3.1.3.3 Exchangeable metals in soil solution

Soil solution extraction

There are three main metal contents within a soil solution: total metal content, 'available' metal content and exchangeable metals. Total metal content can be determined by digesting soil with aqua-regia solution or hydrofluoric acid (HF) (Ščančar et al., 2000). 'Available' metal content which is available for plant uptake normally is extracted by diammonium ethyldiaminetetraacetic acid (EDTA) or diethylene triamine pentaacetic acid (DTPA). Exchangeable metals cations, which are bioavailable metals to plants are usually adsorbed on soil charged surface and can be extracted by ion exchange, such as $CaCl_2$, NH_4OAc or NH_4NO_3 (Blake and Goulding, 2002; Feng et al., 2005; Pueyo et al., 2004).

In order to determine any changes in ion concentrations caused by carbonic acid (H_2CO_3) which could further harm plants, the "exchangeable" fraction of metals in pore water was assessed. The soil solution was extracted by a weak salt 0.01 M $CaCl_2$ extraction solution, which is a suitable method for performing a harmonisation process, giving an appropriate extraction capacity, and also a simple matrix for metal determination (Irha et al., 2009; Novozamsky et al., 1993; Pueyo et al., 2004; Stephens and Hering, 2004; van Gestel, 2008). The detailed procedure on adjusted $CaCl_2$-extraction method is described as follows,

- 5.0 g soil was weighed and placed into a centrifuge tube.
- 25 mL 0.01 M $CaCl_2$ was added into the centrifuge tube and the tube was shaken overnight by a machine.

- The solution was centrifuged at 3700 rev/min for 10 minutes and filtered into a test tube.
- 100 μL 50% Nitric Acid was added into each solution at the end to prevent oxidation of ions and stabilise the metal concentrations.

Then the solution was ready for Inductively Coupled Plasma Mass Spectrometry (ICP/MS) analysis.

ICP/MS analysis

ICP/MS is an atomic emission technique and one of the main instrumental techniques used for the analysis of cations and some anions. It is a multi-element technique, applicable to over 70 elements with detection limits typically in the ppb range. The main components of an ICP/MS are a sample introduction system, ICP torch, Lens, quadrupole, vacuum system, detector, and data handling and system controller (Fig. 3.14).

The principle for the ICP/MS is as follows (Rehkämper et al., 2007). First, for the sample introduction system, the solutions (can also be solids and gas) are vaporized by a nebulizer. During the process, sample aerosol is produced from sample solutions through a spray chamber and then fine aerosol droplets are transported into plasma. Once the sample passes through the nebulizer, the aerosol moves into the ICP torch body and become singly charged atoms. The ICP, produced by passing initially ionized Argon (Ar) gas into a quartz torch, is located inside a coupling Cu coil connected to a radio frequency (RF) generator inside. When the RF generator provides up to 3 kW power to heat the argon gas, it will produce an argon plasma "flame" located at the torch and make a high-energy

argon plasma, which consists of electrons and positively charged argon ions. Therefore, when aerosol samples travel through the plasma, they absorb more energy from the plasma, lose electrons and then form as single charged ions. Then, ions produced from the plasma will pass through the interface process between plasma and MS components, which include apertures, photon stop, and lens. During the process, the charged ions from plasma will cool to room temperature and change to high vacuum, which provides an environment for ions to move freely in MS components without collisions with air molecules. Subsequently, after the interface, the ion beam enters the quadrupole mass analyser. In the quadrupole, due to different mass-to-charge ration of different elements, the ions are separated and each element will produce its unique mass spectrum, which will be collected by detector and analysed by a data handling system.

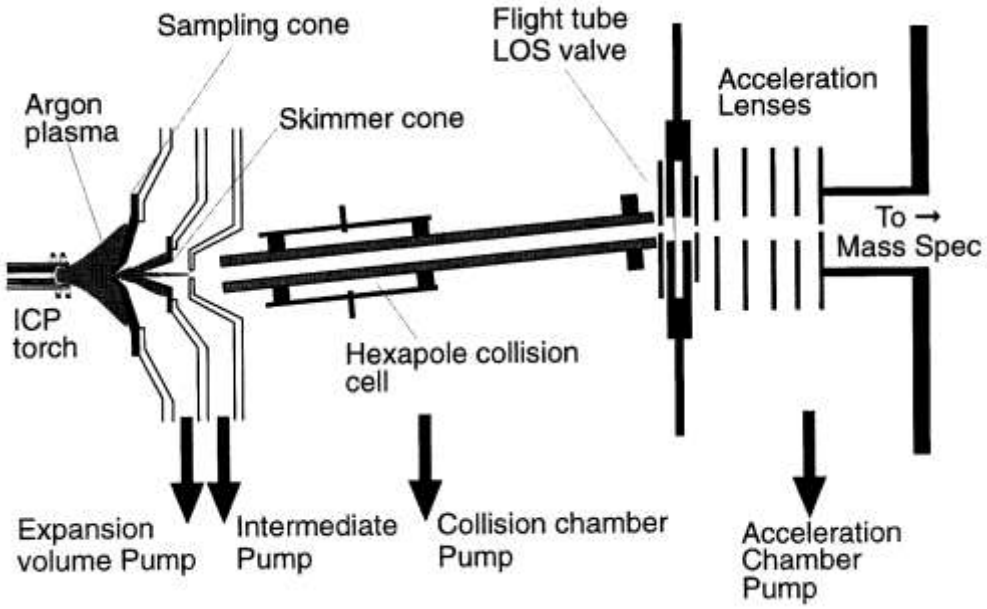

Fig. 3.14 Schematic diagram of the plasma interface and the hexapole collision cell of the Micromass IsoProbe (Rehkämper et al., 2007).

In this research, the multi-element analysis of diluted digestions was undertaken by ICP/MS (Thermo-Fisher Scientific X-Series^{II} as Fig. 3.15) employing a 'hexapole collision cell' (7 % hydrogen in helium) to remove polyatomic interferences. Samples were introduced from an autosampler (Cetac ASX-520 with 4x60-place sample racks) through a concentric glass venturi nebuliser (Thermo-Fisher Scientific; 1 mL min^{-1}). Internal standards were introduced to the sample stream via a T-piece and included Sc (100 µg L^{-1}), Rh (20 µg L^{-1}), Ge (20 µg L^{-1}) and Ir (10 µg L^{-1}) in 2% trace analysis grade (Fisher Scientific, TAG) HNO_3. External multi-element calibration standards (Claritas-PPT grade CLMS-2 from *Certiprep/Fisher*) included Al, As, Ba, Bi, Cd, Co, Cr, Cs, Cu, Fe, Mn, Mo, Ni, Pb, Rb, Se, Sr, U, V, and Zn, all in the range 0 – 100 µg L^{-1} (0, 20, 40, 100 µg L^{-1}) (NIST, 2009). A bespoke external multi-element calibration solution (PlasmaCAL, SCP Science) was used to create Ca, Mg, Na and K standards in the range 0-30 mg L^{-1}. Sample processing was undertaken using Plasmalab software (version 2.5.4; Thermo-Fisher Scientific) set to employ separate calibration blocks and internal cross-calibration where required.

Fig. 3.15 Inductively coupled plasma mass spectrometer (ICP/MS); model XSeries^{II} produced by Thermo-Fisher, Bremen, Germany.

The ICP/MS analysis can provide highly accurate data of heavy metal concentrations, and it was found that some heavy metals can be measured accurately with a precision of less than ± 0.03‰ (95% confidence interval), for example Fe and Pb (Dauphas et al., 2009; Rehkämper et al., 2007). The detection limits for ICP/MS for most ions general range from 0.1 to 10 ppt, and it can be higher for some ions. For example, the detection limits of Zn and Fe are a few tens of ppt for most occasions and range from a few tenth ppt to 200 ppt for Al (Ho et al., 2010). Appendix 2 includes results of a recent run of water samples (around 06/2012) which shows typical certified reference comparisons and also the LOD for selected elements, which was expressed as 3 x the standard deviation of 10 blank samples. As a high efficiency, highly accurate technique with low detection limits, multi elemental capacity and

wide linear range, ICP/MS has been widely used for heavy metal concentration determination in previous research (Ardelan et al., 2009; Blake et al., 1999; Blake and Goulding, 2002; Sahan et al., 2007).

Calculation

The concentration values for ICP/MS are mg L^{-1}. All elemental concentrations were then converted to mg kg^{-1} dw as follows,

$$C_{\text{soil}} = \frac{(C_{\text{soil}} - C_{\text{blank}}) \times Vol}{W_{\text{soil}}} \quad (3.5)$$

where C_{soil} is the elemental concentration (mg kg^{-1}) in the soil; C_{soil} and C_{blank} are the concentrations (μg L^{-1}) in the soil and blank digests, corrected for dilution, *Vol* is the digest volume (25 mL) and W_{soil} is the dry weight (dw) of digested soil (mg).

3.2 Stage II – Flow through column system experiments

3.2.1 Aim of the flow through column system

Results from closed reactor experiments showed changes in pH of soil pore water, metal concentrations, and nutrient concentrations (see Chapter 4), which gives guidance for further research. However, as described in section 3.1.2, the closed reactor experiments were using high pressure and high temperature, which might not reflect the real response in the field to the CO_2 leakage under ambient conditions. Moreover, the results can only show the soil end response to CO_2/SO_2 gas and not any intermediate stage of the reactions. In order to mimic a more realistic environment and examine the real time soil response to CO_2/SO_2 release,

a flow through column system was designed by the author and used in the Stage II experiments as presented in section 3.2.4.

The main structure of the system is represented by a vertical Plexiglas column, which was filled with pre-mixed sediments of different compositions and moisture content (Section 3.2.3). This flow through column system was set to achieve the objectives 2-4 listed in section 1.4.

3.2.2 Laboratory work design and experimental process

3.2.2.1 Layout of the laboratory rig

Two identical columns were set up next to each other as shown in Fig. 3.16 in the lab. The tubing of the rig is made of ¼ inch hoses with two manual valves controlling the injection of the gas into the rig through the base of the columns. The left column (N_2 column) is connected with the N_2 cylinder and it is utilised as a control column to be compared with the right one (CO_2 column), which is connected with the CO_2/SO_2 gas cylinder. During the experiments, N_2 and CO_2/SO_2 gases were injected into each column at the same time. A separated line was also added to connect the CO_2 column and the N_2 cylinder at the bottom of the system, to flush and clean the CO_2 column with N_2 at the end of each experiment.

A picture of the flow through column system in the laboratory is shown as Fig. 3.17. During the experiment, it was noticed that the inlet pressure was not measureable based on the column design, which is a limitation of the column system design. If the permeability of the packed sediments is desirable, it is better to include a pressure gauge (same as pressure meter in Fig. 3.16) in the inlet line to measure the inlet pressure and to further calculate physical properties of the packed sediments.

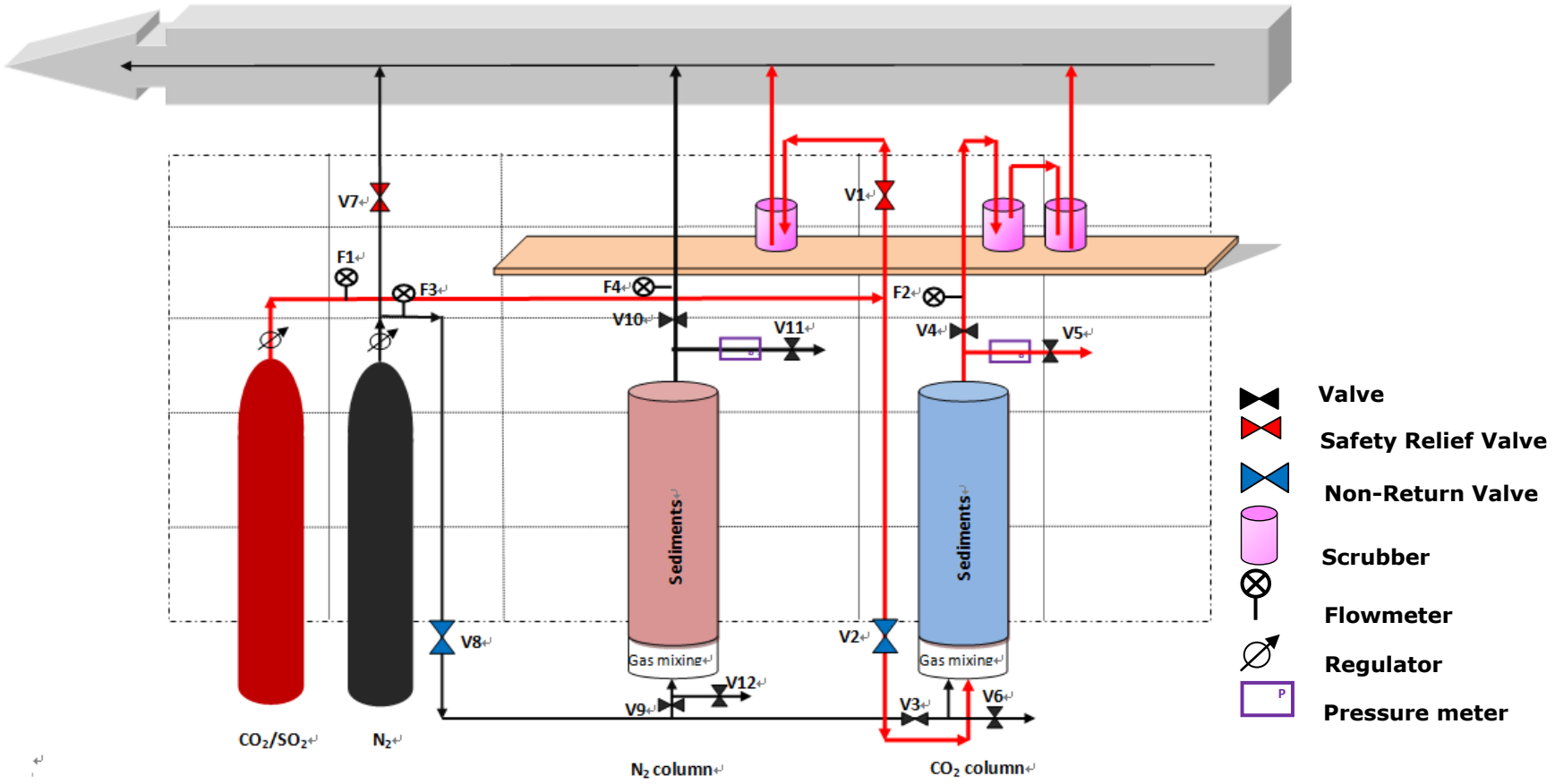

Fig. 3.16 Flow through columns laboratory setting and layout.

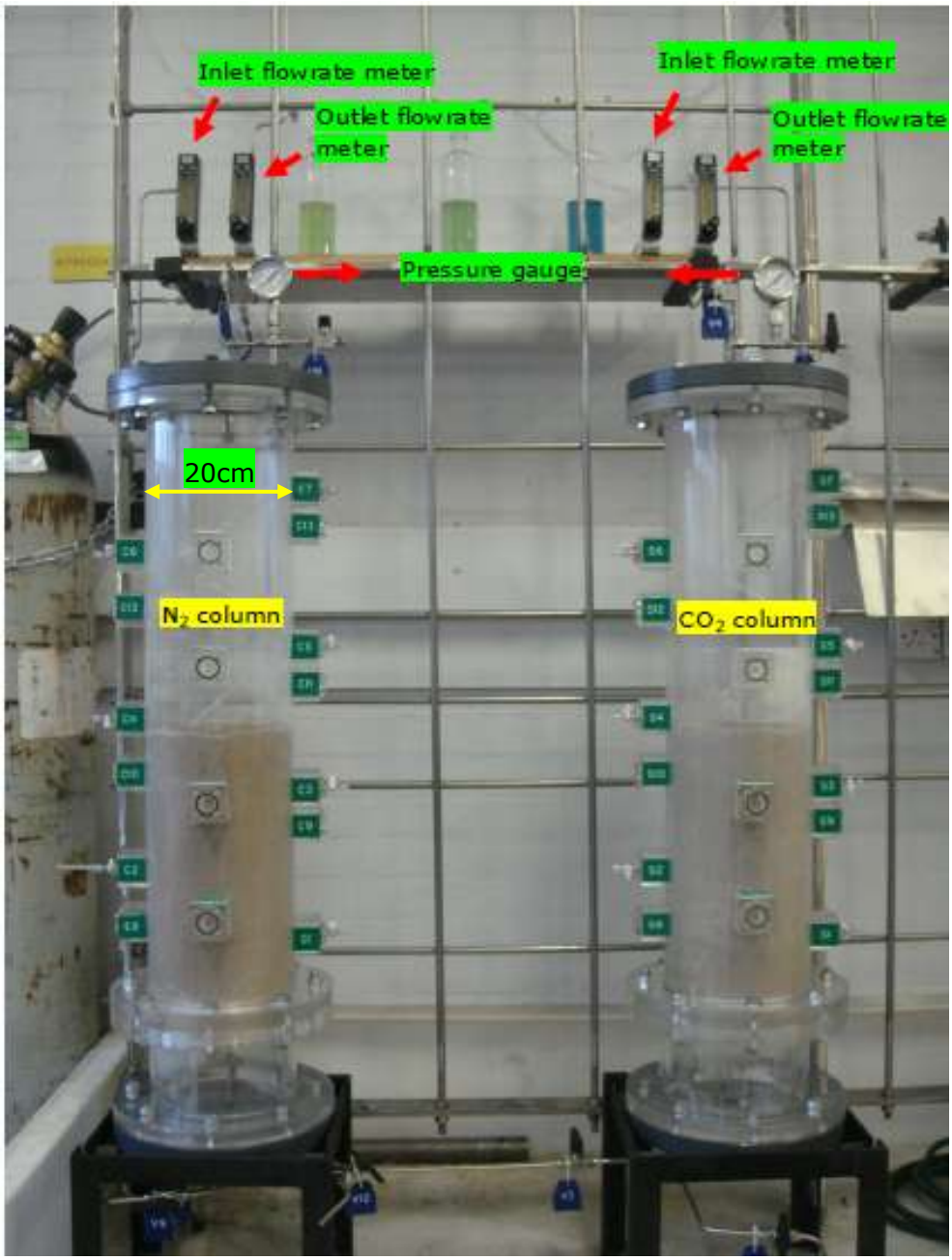

Fig. 3.17 Flow through columns system in the lab.

3.2.2.2 The flow through column set-up

The basic design for each column is shown in Fig. 3.18. The core of the rig is a vertical transparent Perspex cylinder approximately 1 m in length and

20 cm in diameter sealed by two bolted removable lids, C. It is composed of a lower section, a gas mixing chamber (canister), and an upper section (column) that can be filled with pre-mixed sediments. The lower section and the upper column section are linked together by a bolted watertight flange. The mixing chamber is used to allow a homogeneous mixing of the gas before it flows through the sediments. A perforated septum, G as shown in Fig. 3.18, is introduced between the column and the canister to separate sediments and gas, and to allow a more even flow of the gas through the sediments, if compared with a punctual injection orifice. The rig is designed to operate mostly at atmospheric pressure, but it can be pressurized up to 3.0 bar. A pressure gauge, P, is placed into the head-space of each column in order to read the internal pressure and to avoid any over-pressure build up in the headspace, which could exceed the rig specifications causing mechanical damage and further safety issues. For the same reason a safety relief valve (I), is introduced alongside the injection line. In case of any blockage along the line, or in the gas injecting and venting points, the safety relief valve will open once a blow-up pressure of 4 bar is reached, thus venting the injection gas through the red line shown in Fig. 3.18. A non–return valve is fitted along the line between the canister injection manual valve and the flow meter; this valve aims to prevent water back-flow from the rig toward the flow meter and regulator. Avoiding water in the gas line is of particular importance when using CO_2/SO_2 because it can easily react with moisture generating H_2CO_3/H_2SO_4 with corrosive effects on the metal.

Before running the experiment, the column was filled with pre-mixed sediments. Different moisture levels in sediments can be achieved by injecting various amount of water through water injecting and discharging

points, H. Excess water can be discharged by using port H before injecting the gas into the columns. A more detailed description of sediments and sediments packing methods will be described in section 3.2.3.

Lutron Professional Soil Moisture Meter - PMS-714 was purchased from Lurtron Electronic Enterprise co., Ltd. to measure moisture content of the packed sediments under unsaturated conditions. The meter was designed to use its 2 pins electrode to measure the principal conductive ability of the species, then converted to the reading of % "Moisture content" of soil sample. However, the sediments used in Stage II experiments have a really low electrical conductivity (~ 0 S/m), which lead to an unreliable reading in the moisture content. It is therefore not ideal to use the moisture meter to measure the moisture content of the packed sample in this case. However, for future work, if samples with a readable electrical conductivity were used in the experiment, soil moisture meter could be directly used to measure the moisture content. During the experiments in the Stage II, it was also realised that it might be better to have a water meter near V6 and V12 in Fig. 3.16 to measure the volume of water injected into the system, which is considered as a limitation of the design in this thesis.

During the experiments the gas, provided by a cylinder, was continuously injected from the bottom of the column into the mixing chamber. The gas flowed through the sediments and the valve A into wash bottles filled with a NaOH solution “scrubber” S before being vented in the atmosphere for safety purpose. During the process, the inlet and outlet flow rate of gas was controlled and measured by a manual flow meter, M, to obtain the desired flow rate. The head space is connected with a sampling point B allowing the analysis of the gas composition during the experiments. Along

the 1 m column, there are several ports (S1-S13 in Fig. 3.18) for inserting sensors at different levels for measuring the pH. Once the experiment starts, all sampling ports, B, C, D, E and F will be closed. Considering the bottom lid, C, as base line, the distance of each element to C was measured as listed in Fig. 3.18.

A Cole Parmer float-sphere flowmeter, M, regulates the flow in a range from 55 to 489 mL min^{-1} for CO_2 and from 42 to 530 mL min^{-1} for N_2 at Standard Temperature and Pressure (SPT). These ranges were chosen because they are consistent, at the scale of the laboratory rig, with what is observed in real CO_2 seepage scenarios (Aliani et al., 2010; Rogie et al., 2001). At the beginning of each run, the inlet flowrate was set at 300 mL/min with the outlet valve completely open in order to avoid any pressure building-up. During the experiment, inlet rates for both columns were recorded and shown in Chapter 5.

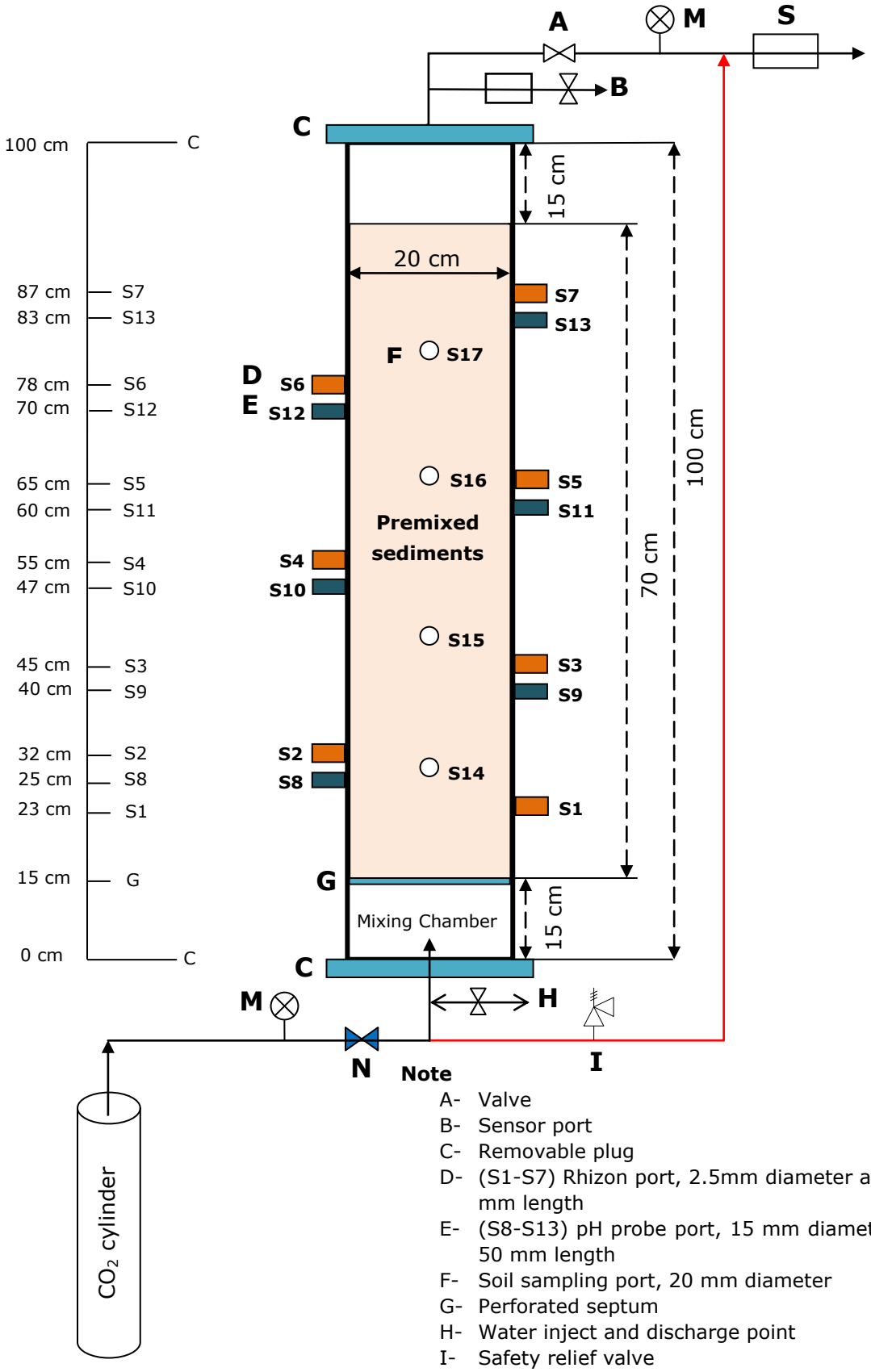

Note

A- Valve
B- Sensor port
C- Removable plug
D- (S1-S7) Rhizon port, 2.5mm diameter and 100 mm length
E- (S8-S13) pH probe port, 15 mm diameter and 50 mm length
F- Soil sampling port, 20 mm diameter
G- Perforated septum
H- Water inject and discharge point
I- Safety relief valve
P- Pressure meter
M- Flow meter
N- Non-return valve
S- Scrubber

Fig. 3.18 Rig dimension for a single column.

3.2.3 Sediments characterisation and packing

In order to better identify the main geochemical reactions of the system, mono-mineral sediments were selected to be used in the experiments instead of a real soil. Otherwise, more complex composition, such as the presence of different minerals, different granulometry of the sediment and eventually organic matter, would have generated a far too complex environment to be studied at this stage. Two different sets of sediments were selected: granulated limestone and silica sand. Limestone sand, being composed by calcium carbonates mainly, is more reactive when exposed to CO_2 release; silica sand, being composed mainly of silica dioxide, which is basically inert to many chemicals, shows far less interaction with the vented CO_2. Two different sizes for the limestone sand, named Limestone sand Trucal 5 and Limestone sand Trucal 6, were chosen to examine the influence of the particle size on the chemical reaction with CO_2. To pack sediments into each column identically, a standard procedure was developed. The detailed process for sediment packing is listed in Appendix 3. Details of these samples can be found in the following sections.

3.2.3.1 Limestone sand Trucal 5

The sediment sample used for the experiments, commercially named Trucal 5, is high purity Limestone granules and grits supplied by Tarmac - Buxton Lime and Cement. Trucal 5 is made of a range of closely graded materials that are dried, crushed and screened several times. They are quarried from Ballidon Quarry, near Ashbourne, Derbyshire. The typical particle size analysis is listed in Table 3.2. This kind of material was selected for its very well controlled particle size and composition. The

average bulk density is 1,480 Kg m^{-3}. The composition of Trucal 5 is mainly calcium carbonate ($CaCO_3$ >98%) sand with small quantities of impurities as oxides of magnesium, silica and trace elements (Table 3.2). The solubility of Trucal 5 in water is approximately 100 mg L^{-1} at 20°C. All the information in Table 3.2 is provided by Tarmac Ltd.

Table 3.2 Typical particle size distributions and chemical analysis of limestone sand Trucal 5.

PHYSICAL PROPERTY		
Grading		100% passing 850 µm
		60% min passing 600 µm
		4% max passing 300 µm
		2% passing 250 µm
Uncompacted Bulk Density (kg/cm^3)		1,480
CHEMICAL ANALYSIS		
Magnesium	(MgO) (%)	0.3
Aluminium	(Al_2O_3) (%)	0.06
Iron	(Fe_2O_3) (%)	0.05
Silica	(SiO_2) (%)	0.25
Lead	(Pb) (ppm)	1
Cadmium	(Cd) (ppm)	0.9
Arsenic	(As) (ppm)	<1
Mercury	(Hg) (ppm)	<0.1

3.2.3.2 Limestone sand Trucal 6

Trucal 6 is a high purity fine granular Limestone sand of 2.5 mm nominal size with an off-white colour; its average bulk density is 1,480 Kg m^{-3}. The sand sample is packed as 25 kg per bag. Limestone sand Trucal 6 is similar to Trucal 5 except particle size distribution (Table 3.3). See Table 3.2 for its chemical composition.

Table 3.3 Particle size distributions for limestone sand Trucal 6.

PARTICLE SIZE DISTRIBUTIONS							
Sieve aperture	2.0 mm	1.4 mm	1.18 mm	1.00 mm	850 µm	600 µm	300 µm
% Passing	100	73	49	34	19	1	1

3.2.3.3 Silica sand (BS EN 1097-8 AAV)

The silica sand used in this experiment was purchased from David Ball Group plc named as BS EN 1097-8 AAV test sand. The sand is washed, dried and graded Leighton Buzzard silica sand from Bedfordshire with grain shape from sub angular to rounded. The main particle size is between 850 μm and 300 μm, which are similar to the ones of Limestone Trucal 5 sand. The composition of this silica sand is mainly silica (SiO_2, about 99.72%) with small quantities of impurities as oxides of aluminum, iron, magnesium and other trace elements. More physical and chemical properties of the sample are presented in Table 3.4. All the information is from product data sheet provided by David Ball Group plc.

Table 3.4 Physical and chemical properties of BS EN 1097-8 AAV test silica sand.

PHYSICAL PROPERTY		
Grading		100% passing 850 μm 75% min passing 600 μm 25% max passing 425 μm 0% passing 300 μm
Colour		White
Specific Gravity		2.65
Uncompacted Bulk Density (kg/cm^3)		1,560
CHEMICAL ANALYSIS		
Silica	SiO_2 (%)	99.72
Aluminium	Al_2O_3 (%)	0.07
Titania	TiO_2 (%)	0.011
Iron	Fe_2O_3 (%)	0.048
Magnesium	MgO (%)	0.02
Calcium	CaO (%)	<0.01
Sodium	Na_2O (%)	0.04
Potassium	K_2O (%)	0.02
Phosphate	P_2O_5 (%)	0.01
Manganese	MnO_2 (%)	<0.005
Chromium	Cr_2O_3 (%)	0.0003

3.2.4 Experimental conditions for each run

During the Stage II experiments, eight runs with different sediments (Trucal 5, Trucal 6 and silica sand) under different conditions were carried out as listed in Table 3.5. The Stage I experiment results (Wei et al., 2011) showed that greater moisture in soils results in higher CO_2 uptake during the incubation leading to higher dissolution rates. Following these indications, wet sediments were used in the stage II experiments as this would probably enhance and speed up the response of limestone sand to CO_2 release. All sediments used in the experiments were either in flooded or in unsaturated conditions. The flooded conditions are used to simulate near-saturation field water contents, which are common conditions in Northern Europea in winter and under which condition the pollutants inside could be transported through water movement (McGechan and Lewis, 2002). The unsaturated conditions were used to simulate other unsaturated conditions in the field. The amount of water injected into each run was recorded before each run as indicated in Table 3.5. When SO_2 contacts with water, it will form strong acid, H_2SO_4, which is more corrosive compare with H_2CO_3. At the beginning of the Stage II experiments, considering safety issues, 100% CO_2 was used first instead of the CO_2/SO_2 mixture gas.

For unsaturated conditions, after packing the sediments inside the columns, tap water was injected from the bottom of the columns into the sediments through the injection points, V6 and V12 (Fig. 3.16). The water level was set at about 10 cm above the sediments and left inside each column for 24 hrs; excess water was then drained through V6 and V12. For flooded conditions, tap water was injected into each column through

the same injection points V6 and V12. The amount of water and the level of water inside the columns were recorded as indicated in Table 3.5. No water was released leaving the sediments in flooded conditions.

Run 1 was a trial run to test the performance of the columns. Because it was not certain whether the injected gas would effectively go through the sediments, only a small amount of sediment (18 kg Trucal 5) was used to run the initial experiments. The initial run showed that the columns worked as planned and therefore, 25 kg of each sample was used for each run. Runs 2 and 4 were duplicates of Runs 1 and 3, respectively, with the results showing good consistency (Chapter 5). Therefore, it was decided to not carry out replicates for silica sand and Trucal 6 sediments. As Runs 1-4 showed consistent results from the N_2 column and no obvious changes during each run (see section 5.1). The chemical composition of Trucal 5 and Trucal 6 is similar; so no big difference is expected from the N_2 column between Trucal 6 and Trucal 5. No appreciable effects were expected when exposing the silica sand to N_2 (Blum et al., 1998; Romanak et al., 2012; Zheng et al., 2012). Therefore, the CO_2 column was only used for runs using Trucal 6 sample and silica sand.

All the experiments were carried out under ambient temperature and pressure lasting from May 2011 to December 2011. The temperature was within the range of 13-20 ^{o}C and was recorded while taking measurements of other parameters during the experiments. N_2 and CO_2 were injected into the columns simultaneously with an initial inlet pressure of 2.0 bar. The inlet flow rate was around 300 ml min^{-1} for both columns with the outlet flow meter completely open in order to avoid over-pressurisation.

Table 3.5 Labelling of runs in Stage II-Flow through column experiments.

No.	***DESCRIPTION***						
	Sediments name	Measured weight of sediments (kg)	Measured height of sediments (m)	Calculated sediments density* (kg/m^3)	Measured water level above the injection point (m)	Sediments conditions	Injected gas
Run 1	Trucal 5 (limestone sand)	18	0.38	1,509	N/A	Unsaturated	100% CO_2
	Trucal 5 (limestone sand)	18	0.38	1,509	N/A	Unsaturated	100% N_2
Run 2	Trucal 5 (limestone sand)	25	0.55	1,448	N/A	Unsaturated	100% CO_2
	Trucal 5 (limestone sand)	25	0.55	1,448	N/A	Unsaturated	100% N_2
Run 3	Trucal 5 (limestone sand)	25	0.55	1,448	0.72	Flooded	100% CO_2
	Trucal 5 (limestone sand)	25	0.55	1,448	0.72	Flooded	100% N_2
Run 4	Trucal 5 (limestone sand)	25	0.54	1,471	0.77	Flooded	100% CO_2
	Trucal 5 (limestone sand)	25	0.54	1,471	0.77	Flooded	100% N_2
Run 5	Trucal 6 (limestone sand)	25	0.55	1,448	N/A	Unsaturated	100% CO_2
Run 6	Trucal 6 (limestone sand)	25	0.55	1,448	0.79	Flooded	100% CO_2
Run 7	BS EN 1097-8 AAV test sand (silica sand)	25	0.48	1,659	N/A	Unsaturated	100% CO_2
Run 8	BS EN 1097-8 AAV test sand (silica sand)	25	0.48	1,659	0.75	Flooded	100% CO_2

Note: *The sediments density was calculated based on the measured height, weight of the sediments inside each column and the dimensions of each column. The measured water level was relative to the injection point labelled in Fig. 3.16.

3.2.5 Measuring aspects and analytical methods

3.2.5.1 Sediments characterisation

SEM/EDX examination

As in Stage I, SEM/EDX techniques were used for the determination of the morphology of sediment samples in Stage II experiments.

During the SEM/EDX examination of the oven dry only samples described below, it was noted that there were small particles attached to the surface of bigger particles of sediments, and it sometimes influenced the observation of the surface changes of the bigger particles. Therefore, apart from the standard sediment preparation (as oven dry only sample described below), an ultrasonic bath was also used during the preparation of the samples to remove the attached smaller particles and to better separate and observe the big ones. Therefore, two different sets of samples were prepared during the experiments, 'oven dry only samples', and 'ultrasonic bath + oven dry sample'. For 'oven dry only samples' preparation, the procedure is the same as the sample preparation described in section 3.1.3.1 (for details see the relevant steps in the section). For the 'ultrasonic bath + oven dry sample' preparation, before following the procedure of preparing the oven dry samples (section 3.1.3.1), an ultrasonic bath was used to vibrate the collected sediments, and the sample was washed with de-ionised water three times.

To have a better resolution of the images by the SEM/EDX, high vacuum mode was used in Stage II examination (Belz and Auchterlonie, 1995; Robinson and Nickel, 1983). Accordingly, after the sample preparation, all the samples were sent to the gold coating process to have a thin layer of gold on top of the samples to make the sample to be conductive.

Otherwise, when using high vacuum mode by SEM/EDX, there will be charging effects (Belz and Auchterlonie, 1995).

The gold coating process was carried out by a POLARON, SEM/EDX coating unit PS3 with argon gas. During the process, all the samples were placed into the gold coating chamber for 50 seconds of the sputtering process. Overall, 150 Å thickness of gold was placed on the surface of each sample. Fig. 3.19 shows prepared samples after the gold coating process. The samples were then ready for the SEM/EDX examination as described in section 3.1.3.1.

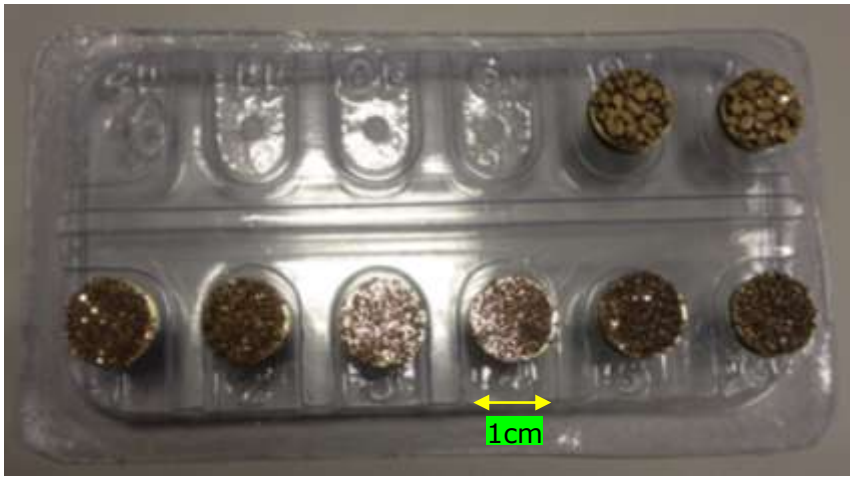

Fig. 3.19 Gold coated samples ready for the SEM/EDX observation.

Porosity determination

Porosity is the fraction of the volume of voids over the total volume of a soil. Normally it is expressed as follows,

$$\phi = \frac{V_V}{V_T} \tag{3.6}$$

where, ϕ represents porosity, V_v and V_T stands for the measured voids and the total volume of the media.

The sample with a higher porosity will typically have more open areas for the flow of fluid, which make fluid flow through easier (Fetter, 1994). Literature related to soil colloid-facilitate contaminants transportation was reviewed by McGechan and Lewis (2002). They concluded that, if a particle has a dimension similar to or much smaller than the pore size of the media, it will be potentially impeded when moving through the soil (porous media) by means of straining or filtration. In order to understand the fluid behaviour well and make better applications of the results from this research, it is therefore important to measure the porosity of the sediments used in this research.

A basic volumetric method as described by Kamann et al. (2007) was used to measure the porosity of the samples as follows. Firstly, a certain volume of sediments, V_T, was added to a graduated cylinder. During the process, the bulk density of the sediments inside the cylinder was kept the same as the one used in the Stage II experiments. Then, water was slowly added to the sediments within the graduated cylinder by using of a burette until the added water just reached the surface level of the sediments. During the process, to avoid air bubbles trapped in the sediments, the burette was hung close to the wall of the cylinder and the waterdrop was then allowed to flow down one side of the glass to the sediments reaching the bottom of the graduated cylinder. In this case, the air trapped inside would be forced out in the pore spaces above. The volume of water used to saturate the sediments was read by the burette and recorded as V_V, which was considered as the volume of void space within the sediments. The porosity of sediments, ϕ, was then calculated by using of equation (3.6). For each sediment sample, the above procedure was repeated three times, during which 5 ml, 10 ml and 15 ml was used separately as the volume of sediments, V_T. The porosity of each sediment sample was

presented as 'average of three repeats±3σ''. Based on the above measurement, the porosity of Trucal 5 and Trucal 6 used in Stage II experiment were measured and they were 39.2%±0.0312 and 40.1%±0.0233 respectively.

The porosity and intrinsic permeability (see below) measurement was run to supply extra information of the used sediments. At the time of running the experiments, no silica sand (BS EN 1097-8 AAV) was left for the porosity and permeability test. Fortunately, similar silica sand (DA 14/25 (50%)) was previously tested for the porosity and intrinsic permeability at Loughborough University using the same method and equipment. The particle size of DA 14/25 (50%) are mainly between 701 to 1000 μm with an average pore size of 780 μm, which is similar to the BS EN 1097-8 AAV silica sand with the particle size ranging from 300 to 850 μm with an average pore size of about 600 μm (Table 3.4). The data of the DA 14/25 (50%) was therefore used to stand for the porosity and permeability of the BS EN 1097-8 AAV test sand. DA 14/25 (50%) is a mixture of 50% w/w Leighton Buzzard DA 14/25 and 50% w/w Leighton Buzzard DA30, which are silica sand samples from "mineral marketing's limited, Cheshire, UK". Leighton Buzzard DA 14/25 has a particle size ranging from 600 to 1200 μm, and Leighton Buzzard DA 30 has a particle size ranging from 150 to 700 μm. The detailed information of DA 14/25 and DA 30 is presented by Das and Mirzaei (2013). The porosity of DA 14/25 (50%) is 37.5%.

Intrinsic permeability determination

Permeability is defined by measuring the pressure difference ΔP between the sample inlet and outlet. According to Darcy's law, the permeability of

the sample, k, can be expressed by (Noiriel et al., 2009; Wong et al., 1984):

$$k = -\mu \times L \times Q/(S \times \Delta P) \quad (3.7)$$

where, μ is the dynamic viscosity of the fluid (kg m^{-1} s^{-1}), L is the length of the sample in the flow direction (m), Q the volumetric flow rate (m^3 s^{-1}), S is the area of the sample (m^2). The unit of permeability values is presented in Darcy units (1 D≈0.987×10^{-12} m^2).

The fluid flow processes in porous media are determined by various factors (e.g., pressure, gravitational and viscous forces, temperature, medium permeability and heterogeneity) (Das et al., 2006; Das and Mirzaei, 2013); porosity property alone could not define fluid behaviour through porous media. For example, if rocks contain high porosity but lack of interconnect voids (e.g. vesicular basalt) or the pores inside are so small that fluid has difficulty to flow through (e.g. clay and shale), the fluid flow would also be affected (Fetter, 1994). Intrinsic permeability is an important physical property of a sediment sample showing its ability of holding and transmitting fluid between voids inside the sediment (Fetter, 1994). It is therefore also important to measure the intrinsic permeability of the sediment samples to explain the fluid flow and mass transport behaviour through the sediments samples.

The intrinsic permeability was determined by a standard constant-head method in accordance with clause 5 of BS 1377-5:1990 (BSI, 1990; Das and Mirzaei, 2013). The degree of permeability was determined by applying a hydraulic pressure gradient in a sample under saturated conditions and measuring the consequent rate of flow. The experiment was carried out at Civil Engineering Department, Loughborough University by a constant head permeameter with manometers (Fig. 3.20). The rig

mainly consists of a constant head permeameter cell, a vertical adjustable reservoir tank capable of maintaining a constant-head supply of water to the permeameter cell, a graduated cylinder holding the constant discharged water, a pair of manometer and a balance measuring the weight of discharged water. Please refer to BS 1377-5:1990 (BSI, 1990) for the detailed description of the methods. The test sediments were packed by using of the method 5.4.2 b in clause 5 of BS 1377-5:1990 'placing under water' (BSI, 1990) to avoid air trapped in the sediments. During the process, the tested sediments were packed the same density as the one used in the Stage II experiments (as listed in Table 3.5).

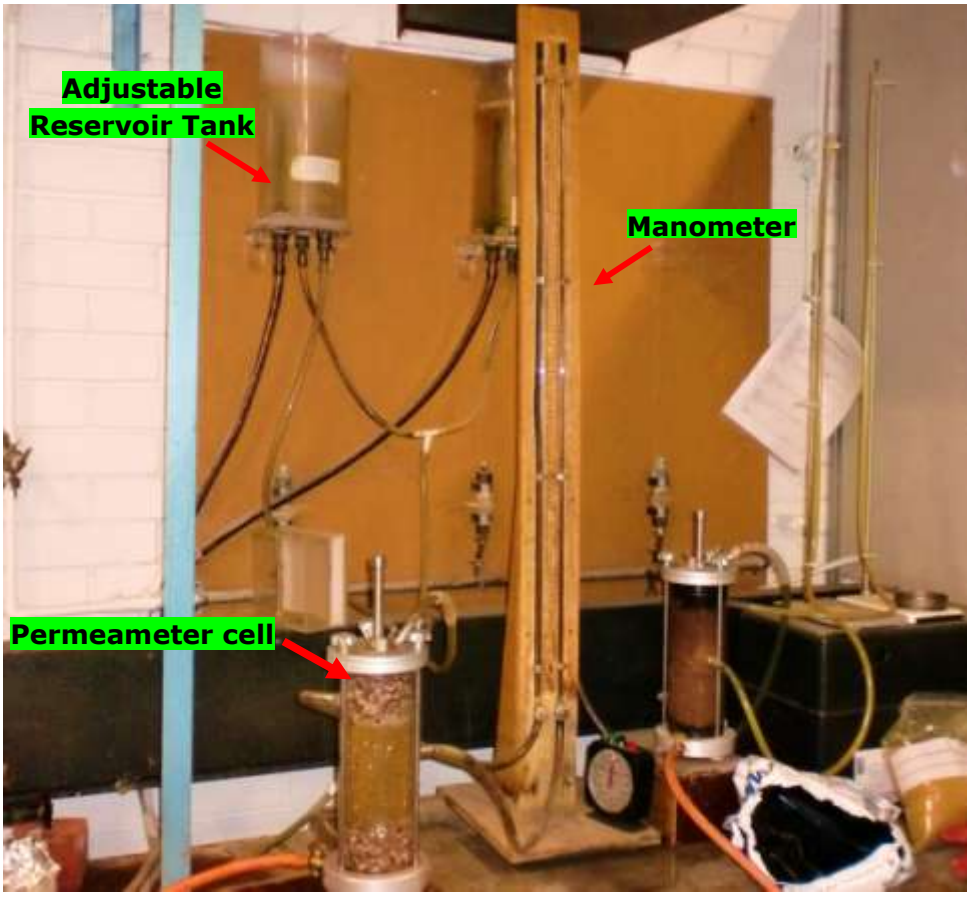

Fig. 3.20 The constant-head permeability cell set up at Civil Engineering Department, Loughborough University (provided by Mr. Luqman Abidoye and Mr Ronald Wairagu)

In the case of single-phase flow in porous media, based on Darcy's law (Darcy, 1856; Das and Mirzaei, 2013) and equations from clause 5 of BS 1377-5:1990 (BSI, 1990), the intrinsic permeability of a porous media is expressed as follows,

$$k_i = \left(\frac{Q}{t}\right) \cdot \left(\frac{y}{h}\right) \cdot \left(\frac{R_t}{A}\right) \cdot \left(\frac{\mu}{\rho g}\right) \tag{3.8}$$

where, k_i (in m^2) is the intrinsic permeability of the tested sand, Q (in m^3) is the volume of water collected from the outlet reservoir during each time period t (in s), y (in mm) is the difference between the corresponding gland points, h (in mm) is the difference between the two manometer levels, R_t is the temperature correction factor for the viscosity of water to standardize the permeability to 20 °C, A (m^2) is the area of cross section of the sample, μ (in kg/(m·s)) is the dynamic viscosity of the fluid (here is water), g (in m/s^2) is the acceleration due to gravity, and ρ (in kg/m^3) is the density of the fluid (here is water).

During the experiments, the above procedure was repeated three times for each sediment sample. The intrinsic permeability of each sediment sample was presented as 'average of three repeats±3σ'. Based on the above calculation, it was found that the intrinsic permeability of Trucal 5 and Trucal 6 was $1.67\pm0.84\times10^{-10}$ m^2 and $4.67\pm1.77\times10^{-10}$ m^2. See Appendix 4 for the general information of the rig and the collected data from the experiment. As with the porosity determination (described above), the permeability of silica sand (BS EN 1097-8 AAV) is presented by the permeability of DA 14/25 (50%) sand, which is 4.16×10^{-11} m^2.

3.2.5.2 Gas concentration

Before being vented outside the columns through the discharge system, the gas accumulated in the headspace of each column above the sediments. A secondary outlet was used to collect samples of gas from this headspace (point B in Fig. 3.18), which was located downstream from the pressure control gauge and it was controlled by a manual valve. The same line was also used to connect an infrared gas analyser (GA2000 from Geotech, Warwickshire) as shown in Fig. 3.21. The analyser extracts a sample at flowrate of 350-400 mL min^{-1} and gives concentrations in % (vol) of CO_2, oxygen (O_2) and the balanced gas (BAL) simultaneously.

The GA2000 Analyser operates on the principle of infrared (IR) absorption for the CO_2 and the CO_2 is read by a dual wavelength infrared cell with a reference channel. When a gas sample is pumped into the CO_2 measurement cell, the radiation from a broad band IR source is passed through the CO_2 gas onto a detector. The detector selects only the wavelengths that are absorbed by CO_2. Meanwhile, a separate reference beam is used to compensate for any instrument drift.

O_2 is read by an internal electrochemical cell. The electrochemical oxygen sensors comprise an anode, a semi-solid electrolyte and an air cathode. When O_2 enters the sensor and comes into contact with the cathode, it is immediately reduced to OH^-. The OH^- ions then migrate through the electrolyte to the lead anode. The lead anode is then oxidised to lead oxide by the OH^- ions. During the above process, electrons are released and a current is generated which can be measured by the instrument. This current is proportional to the O_2 (vol) % which leads to an accurate measurement of O_2. Table 3.6 shows the range and typical accuracy of the measured gas.

Table 3.6 Measuring range and typical accuracy of the measured gas by GA2000 infrared gas analyser.

Range	CH_4	0 - 70% to specification, 0-100% reading			
	CO_2	0 - 40% to specification, 0-100% reading			
	O_2	0 - 25%			
Typical accuracy	**Gas**	**0-5% vol**	**5-15% vol**	**15%-Full Scale**	**Full Scale**
	CH_4	±0.5% (vol)	±1.0% (vol)	±3.0% (vol)	70%
	CO_2	±0.5% (vol)	±1.0% (vol)	±3.0% (vol)	60%
	O_2	±1.0% (vol)	±1.0% (vol)	±1.0% (vol)	25%

Fig. 3.21 The CO_2 gas analyser, a GA2000 infrared gas analyser, and the connecting point.

3.2.5.3 pH and alkalinity measurement

Along the wall of the column, ports S8-S13 (see Fig. 3.18) allow the insertion of pH electrodes at different heights inside the sediments (Fig. 3.22). A Hanna-HI-98140N pH/C portable meter with plastic body pH electrode was used for measuring the pH values in the interstitial water. The accuracy of the pH measurement at 20°C is ±0.01 pH. The electrode was inserted and the port was sealed before adding water to the rig to avoid water spilling out. The insertion of pH electrodes directly in the sediments was mainly used in unsaturated conditions where there was

limited water to be collected from the column. The direct reading with the interstitial water was preferred during the flooded runs as described below. The pH electrode was calibrated before each set of measurement and calibrated again at the end of each run. For details of the calibration procedure see the relevant steps in section 3.1.3.2.

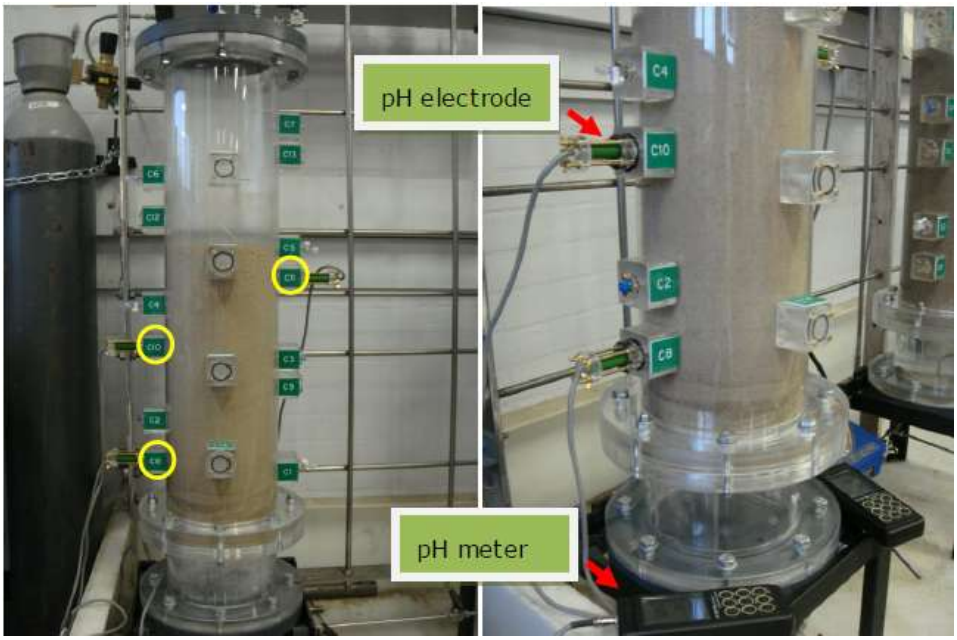

Fig. 3.22 Insertion of pH electrodes in the column system to measure the pH.

Another way to measure the pH of the system was to collect the interstitial water from the specified sampling ports (see below for details of the water sampling procedure) and measure its pH by the Hanna – HI-98140N pH/C portable meter. The accuracy of the pH measurement at 20^{o}C is ±0.01 pH. This method was mainly used in runs with flooded conditions where there was enough water to be sampled. An advantage of such a method is that it is possible to correlate the pH with the alkalinity and the ion concentration of water sampled from the same port.

To collect the pore water, Rhizon samplers were inserted inside the

columns through the S1-S7 ports. The standard Rhizon sampler consists of a 10 cm porous polymer tube connected to a 10 cm PVC tube and a Luer-Lock (L-L) male connector. The pore diameter of the porous polymer tube is 0.1 μm. It is generally possible to use vacuumed tubes or syringes to collect the water connecting them to the Rhizon by a "luer-lock" valve, which prevents the water to leak once the syringe is detached. In this research, a syringe was used combined with Rhizon sampler to collect pore water for the analysis (see Fig. 3.23). One of the advantages of Rhizon samplers is that they have a small dead-space and that the collected water does not need further filtration. Moreover the Rhizon samplers are a reliable way of collecting interstitial water with very limited disturbance (Dickens et al., 2007; Seeberg-Elverfeldt et al., 2005).

Fig. 3.23 Soil pore water collection from the column system by Rhizon sampler and syringes.

Alkalinity basically measures the concentrations of HCO_3^-, CO_3^{2-} and OH^-, and it is expressed as an equivalent concentration of $CaCO_3$. Additional CO_2 will change the alkalinity in sediments and soil (Lerman and Stumm, 1989; Wojtowicz, 2001) and it is necessary to measure it in this research. A HI 3811 alkalinity test kit from Hanna Instruments Ltd. was used to

measure the water alkalinity; the values are expressed as Phenolphthalein Alkalinity (PA) and Total Alkalinity (TA). The detailed determination of PA and TA is listed in the manual of the HI 3811 test kit as in Appendix 5. CO_3^{2-} and HCO_3^- concentration is calculated from PA and TA values according to a standard method recommended by American Public Health Association (Kemp, 1971) as in Table 3.7.

Table 3.7 Alkalinity determination by titration.

Results of Titration	***Hydroxide Alkalinity***	***Carbonate Alkalinity***	***Bicarbonate Alkalinity***
PA=0	0	0	TA
PA=TA/2	0	TA	0
PA=TA	TA	0	0
PA<TA/2	0	2PA	TA-2PA
PA>TA/2	2PA-TA	2(TA-PA)	0

3.2.5.4 Exchangeable metals concentration in sediment solution

ICP/MS analysis

As explained before, one of the advantages of the Rhizon samplers is that they have a small dead-space and that the collected water does not need further filtration. Therefore, the water can be used directly for ICP/MS analysis. However, in case a Rhizon sampler was left inside the column too long and not working properly, the solution collected from columns was further filtered with a Tissue Culture Filtropur S 0.2 µm. Fig. 3.24 shows the main process for collecting pore water.

After the pore water was collected from the columns with the Rhizon sampler, the solution was filtered. 100 µL 50% nitric acid was added into each solution at the end to stabilise the metal concentrations. Later, the solution was stored in polyethylene tubes with caps in a fridge ready for the ICP/MS test.

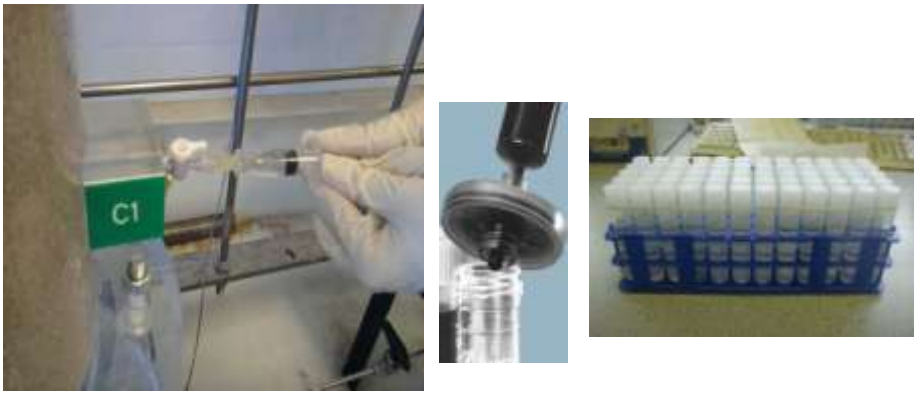

Fig. 3.24 Sample collecting process from the column system for ICP/MS analysis.

3.2.5.5 Sediment sampling

A simple corer was designed and used to collect the sediments along the diameter of the columns at the end of each run as Fig. 3.25. It is made of a stainless-steel tube with a sharp edge at one extremity and a handle at the other. The sampler can be inserted through the four frontal ports (S14-17 in Fig. 3.18) and the sharp edge can be pushed inside the sediments to collect a core of 1.5 cm diameter and 40 cm length. The sample was analysed later by SEM/EDX to observe any surface changes after CO_2 flowed through.

Fig. 3.25 The soil core (1.5 cm in diameter and 40 cm length) collected from the column system at the end of each run.

Chapter 4 Closed Reactor Experiments: Results and Discussion

As described in section 3.1, the collected soils were incubated in reactors to investigate the impacts on soils of the CO_2/SO_2 incubation. This chapter focuses on presenting results from Stage I- closed reactor experiment, including soil characterisation in section 4.1, pressure record in the reactors in section 4.2, soil pH changes in section 4.3 and metal concentration changes in section 4.4 before and after the CO_2/SO_2 gas incubation. By analysing and comparing the results, impacts on soils by the CO_2/SO_2 gas from Stage I are concluded. Parts of the results have been published in Wei et al. (2011) and have been cited by Harvey et al. (2013), Patil (2012) and Zhou et al., (2013).

4.1 Soil characterisation

4.1.1 Soil Profile

As described in section 3.1.3.1, the soil MC and the particle size distribution were assessed for the original soil from the ASGARD field, the unground oven-dried soil sample (S1) and ground oven-dried soil samples (S11) as described in Table 3.1. During the examination, each measurement was carried out on five replicates and the results below are shown as 'mean value of the five repeats±3σ'.

The MC of the original soil from the ASGARD field is 15.56%±0.00. The MC of S1 and S11 are similar and they are 0.94%±0.01. The original soil from the ASGARD field contains approximately 20% dw particles larger than 2,000 μm. The remaining 80% of the sieved soil was analysed to

obtain its particle size distribution as presented in Table 4.1. The particle size distribution of S1 and S11 was also measured and presented in Table 4.1. The results confirm that the ground soil contains more fine particles compared with the unground soil.

Table 4.1 Particle size distributions for the original sample from the ASGARD field and the prepared oven-dried unground and ground soil (S1 and S11).

ANALYSED SAMPLES		***PARTICLE SIZE DISTRIBUTION (%±3σ)***		
		Clay (0-3.9 μm)	Silt (3.9-63 μm)	Sand (63-2000 μm)
The original soil		8.9%±0.01	22.9%±0.03	68.2%±0.04
Oven-dried	S1	8.1%±0.01	21.1%±0.03	70.8%±0.04
	S11	13%±0.03	36%±0.05	51%±0.07

4.1.2 Soil OC and CC

Soil OC and CC were determined for all unground soils with or without CO_2 incubation, S1-S10 (Table 4.2). Each of the values listed in the table was presented as a mean value of five replicates±3σ.

The results show that there are no big differences among the original sample, S1, and other incubated samples, S2-S10, and no trends were observed based on the results. This could be due to the very low amount of organic and carbonate content present in the original soil, which leads to very minor changes within the soil samples as presented in Table 4.2.

Table 4.2 OC and CC for samples S1-S10.

No.	***OC(%±3σ)***	***CC(%±3σ)***
S1	0.53%±0.00	0.11%±0.00
S2	0.60%±0.00	0.11%±0.00
S3	0.82%±0.00	0.13%±0.00
S4	0.70%±0.00	0.13%±0.00
S5	0.61%±0.00	0.13%±0.00
S6	0.55%±0.00	0.11%±0.00
S7	0.62%±0.00	0.20%±0.00
S8	0.91%±0.00	0.12%±0.00
S9	1.08%±0.00	0.17%±0.00
S10	0.94%±0.00	0.19%±0.00

The soil OC and CC were also measured for sample S1 and S11, which are similar and around 0.53% and 0.11%.

4.1.3 Soil mineralogy

4.1.3.1 Soil S1 - Oven-dried unground soil with no incubation

Fig. 4.1 shows the XRD result for sample S1, unground soil with no incubation. All the high peaks in Fig. 4.1 represent quartz (SiO_2), which is over 90% of the soil. In addition, there are small peaks at 27.5° and 27.9° 2θ degree, which may correspond with feldspar anorthoclase ($(Na,K)AlSi_3O_8$). Additionally, there are peaks at 23.5° and 27.9°, which are related to albite ($NaAlSi_3O_8$). Moreover, there are peaks associated with dolomite ($CaMg(CO_3)_2$), as well as clays, such as kaolinite ($Al_2Si_2O_5(OH)_4$) (12.3°), illite/mica ($(K,H_3O)(Al,Mg,Fe)_2(Si,Al)_4O_{10}[(OH)_2,(H_2O)]$) (8.9° and 17.7°) and montmorillonite ($(Na,Ca)_{0.33}(Al,Mg)_2(Si_4O_{10})(OH)_2{\cdot}nH_2O$) (5°-7.5°), while the amounts of feldspar and clays are small.

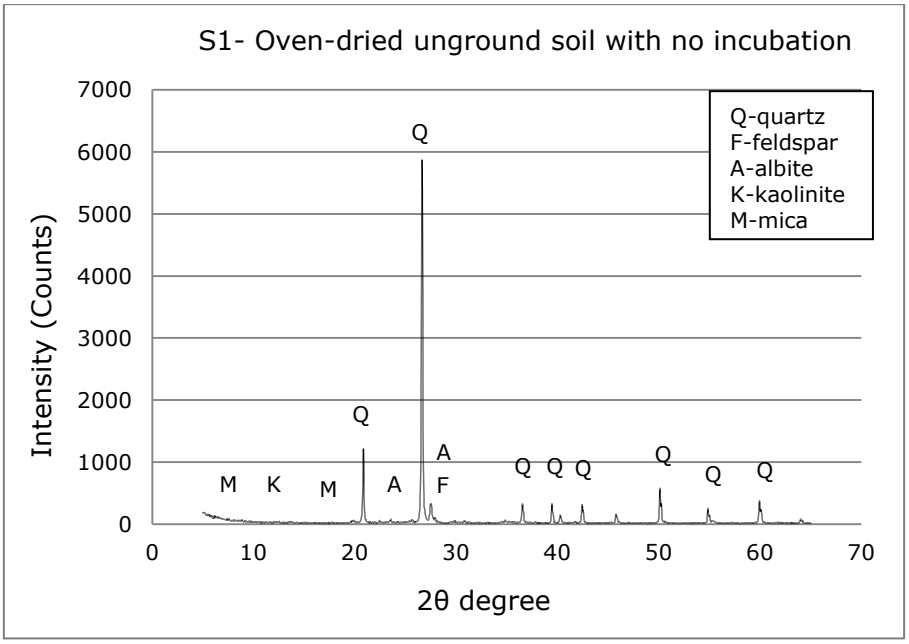

Fig. 4.1 XRD results for sample S1.

4.1.3.2 Ground and unground soil

Fig. 4.2 shows the mineralogical composition of both oven-dried unground (S1) and ground soil (S11) sample by shifting S11 up 500 counts. The two XRD patterns correspond well with each other, suggesting that for the soil in this research the three minutes mill grinding did not cause significant changes of the crystalline phase.

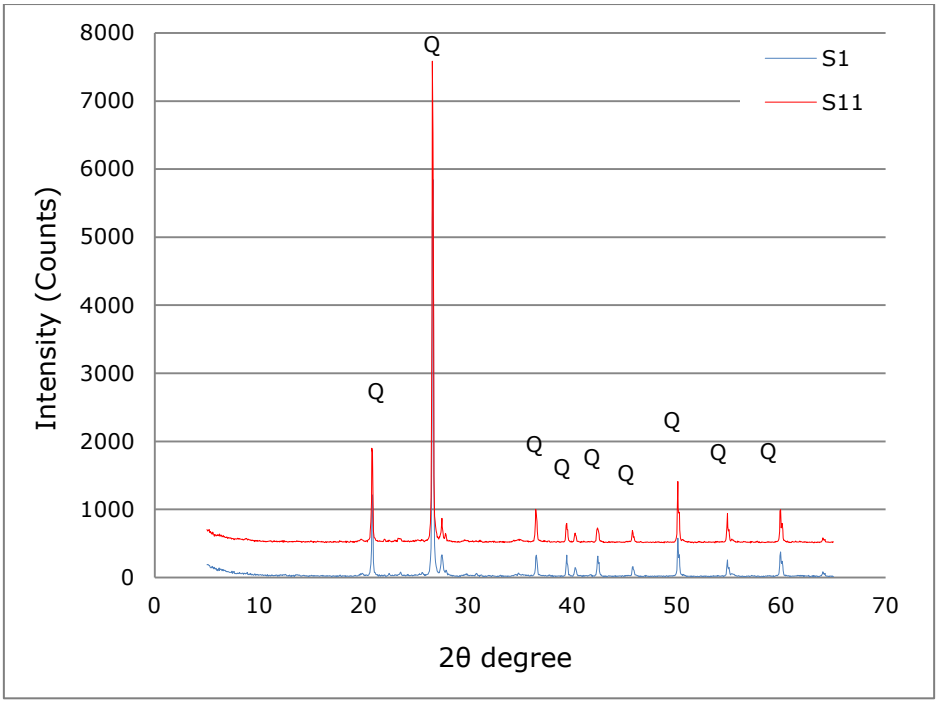

Fig. 4.2 XRD results for both ground (S1) and unground soil (S11) with no incubation. (Q stands for quartz)

Fig. 4.3 shows images of particles for ground and unground soils, S1 and S11. The figure shows that after the grinding process, the particle size was reduced for S11 and broken down to more fine particles as presented in Table 4.1. Due to the breakdown of big particles in S11, after the incubation, noticeable but small differences in ion concentrations in the soil solution may be observed in S11 compared to S1. The results are analysed and presented in section 4.4.3.

It is also noticed that fine particles are separated from bigger particles. For S1, the soil contains particles larger than 400 μm, and the bigger particles, quartz, are partly covered by clay or feldspar on the surface, while bigger particles (around 100 μm) in S11 have a more flat surface.

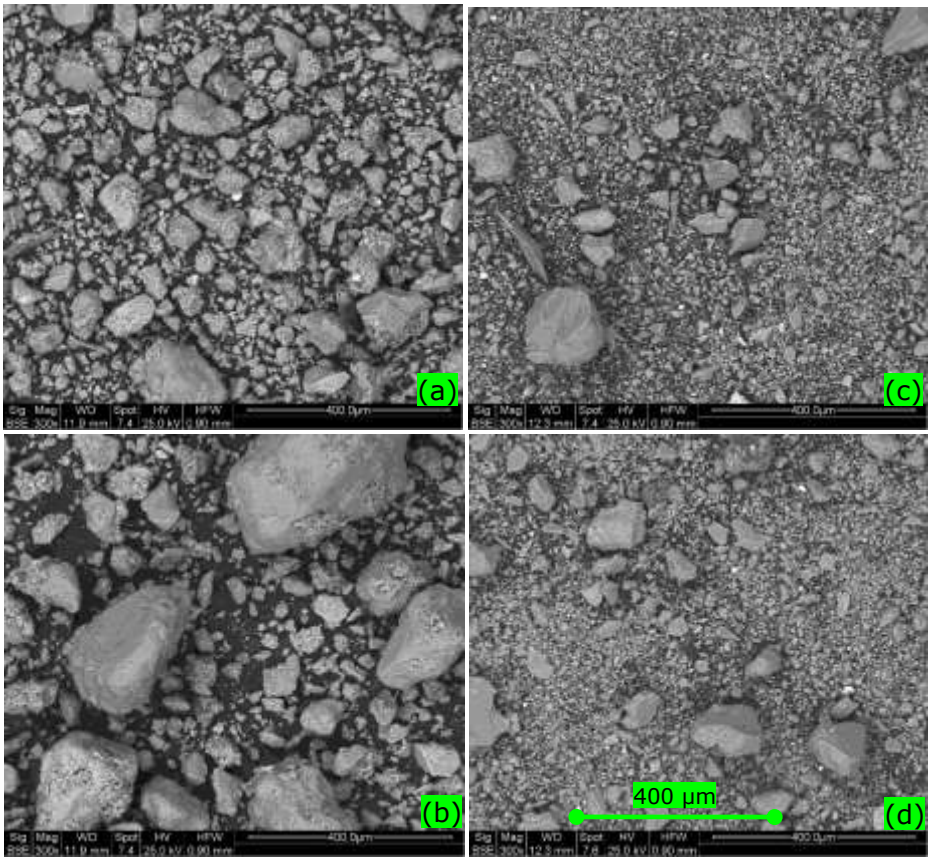

Fig. 4.3 SEM images for ground and unground soil S1 (a, b) and S11 (c, d).

4.1.3.3 Incubated and non-incubated unground soil

XRD analysis was also carried out to ascertain mineralogy changes of both incubated and non-incubated soil samples associated with different water content. The XRD results show good consistency within the replicated samples, S2-S4, S5-S7 and S8-S10. Only the representative XRD results for each group are chosen and presented in Fig. 4.4, which are S1, S2, S5,

and S8 as described in Table 3.1. To compare among samples, S2, S5 and S8 are shifted up for 500, 1,000 and 1,500 counts respectively.

Fig. 4.4 shows that the XRD patterns for S1, S2, S5 and S8 sample are very similar indicating that there are no significant differences in soil mineralogy composition among CO_2 incubated and non-incubated soils. Similar results are also observed on ground samples S11-S25. This can be explained as the main phase quartz present in soils is not expected to change with CO_2 incubation. Similar results were observed in the ASGARD field by West et al. (2009) showing no significant alteration of the mineralogical assemblages from gassed and non-gassed plots. However, this does not rule out minor changes that may be gone undetected with this technique, as XRD has difficulties to detect the presence of crystalline phase at concentrations below 3 wt %-5 wt %. Further investigation of the ion concentration in soil solution by ICP/MS is required to assess the impacts on soils, and the results are described in section 4.4.

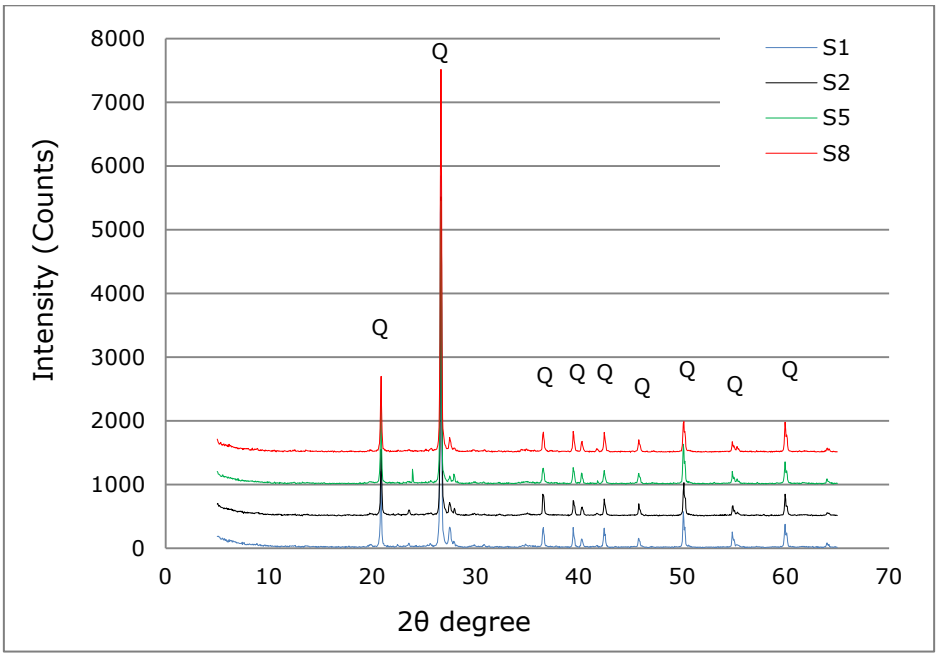

Fig. 4.4 XRD results for non-incubated soil, S1, and incubated soil, S2, S5 and S8. (Q stands for quartz)

4.2 Pressure changes during incubation

As described in section 3.1.2.2, the initial pressure for all the incubation studies was set at 363 psi. The pressure changes during incubation were recorded for sample S1-S25 as described in Table 3.1 and presented in the following sections.

4.2.1 Pure CO_2 investigation

Before the incubation process, the soils were pre-heated overnight to 25^{o}C. The CO_2 gas was then injected into the reactor and the pressure was recorded. During the incubation process, the temperature was kept to be around 25^{o}C.

It was noticed that there was a slow leakage of the CO_2 gas from the reactor during the incubation process. To assess the leakage, two blank samples were run on two separate days before and after all the incubation studies. These two blank runs shown in Fig. 4.5 were run with a five months interval. The latter blank run (07/2010) shows slightly smaller leaks than the former one (02/2010), and there is no significant difference between these two runs comparing with the CO_2 adsorption rate (see below). By fitting linear trendlines for both runs with an intercept at 363 (the initial pressure), equations are shown for both runs in Fig. 4.5. The decreasing rate in the pressure is around 0.02 for both runs indicating the leakage is about 0.02 psi for every minute.

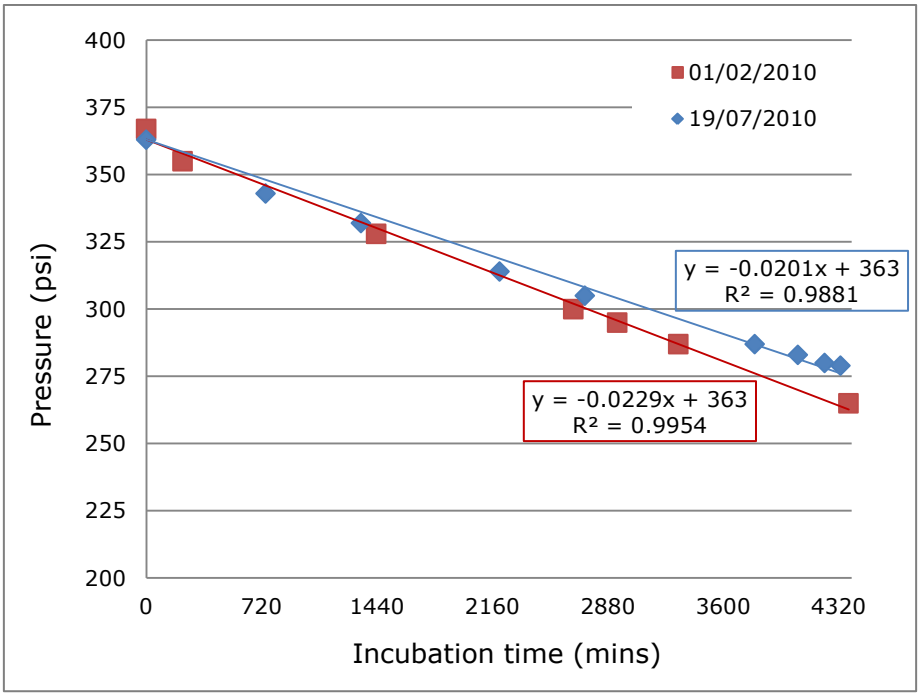

Fig. 4.5 Pressure variation with time for the two blank runs.

To compensate for the leakage, the pressure changes observed during the incubation process were compared with the blank sample. The pressure drop during each run is presented in Fig. 4.6. In the figure, 'oven-dried' represents the pressure changes of sample S2-S4, '20% MC' represents for the pressure changes of sample S5-S7, and '40% MC' stands for the pressure changes of sample S8-S10. Linear trendlines are fitted with the data in the graph with the R-squared values shown besides them.

By comparing with the blank runs, a higher pressure drop is observed for the incubated samples, indicating CO_2 was taken up by soil over the time of incubation, with a greater pressure drop occurring for the samples with the highest moisture content (S8, S9 and S10). For the oven-dried sample, S2-S4, there are more variations in pressure during the incubation process. More consistent pressure recording is observed in the soil samples with the highest moisture content, 40% MC. Fig. 4.6 shows that the pressure

drop rate decreases with time, which implies that the uptake of the CO_2 slows down as the incubation goes on. The absorption of CO_2 may occur either by reacting with pore water in the soil or through filling in voids between soil particles. The greater pressure drop with wet soil can be explained as more CO_2 is absorbed by the pore water within soils to form H_2CO_3 in the soil solution. Similar trends are observed for ground-soil samples S11-S25.

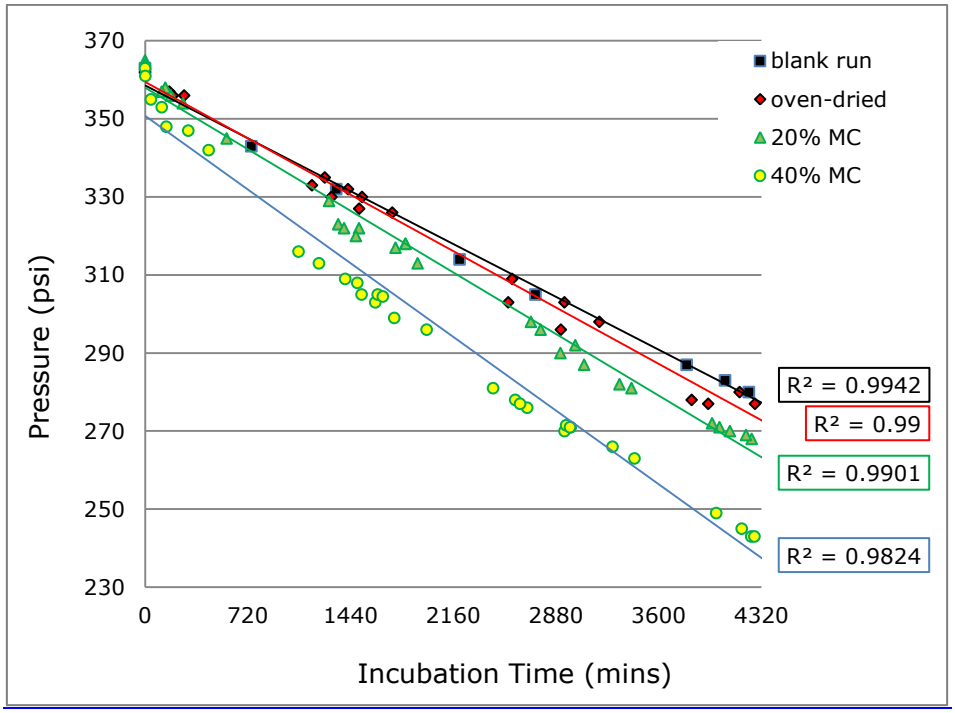

Fig. 4.6 Pressure changes for a blank run and the CO_2 incubated runs. The results for the oven-dried soil, 20% MC and 40% MC are a combination of results of S2-S4, S5-S7, and S8-S10, respectively.

Fig. 4.7 shows the relationship between the soil MC and the average pressure drop (End Pdiff) after three days incubation. The Pdiff is calculated based on the pressure drop with oven-dried sample (S2-S4), 20% MC sample (S5-S7), and 40% MC sample (S8-S10) compared with the pressure drop of the blank run. Error bars are added in the figure to show

the maximum and minimum pressure drop within that group. For oven-dried sample, the End Pdiff is 11.0 psi; for 20% MC sample, the End Pdiff is 20.7 psi; and with 40% MC sample, the End Pdiff is 43.7 psi. This indicates that with increasing MC, the pressure drop was higher and more CO_2 was absorbed. A non-linear relation between soil MC and pressure drop rate was observed. The non-linear relationship may be explained as the higher water content increased the reaction rate between CO_2 and the soil weathering process. However, with three sets of data, it is hard to predict the relationship between pressure drop and MC. More runs are required.

Similar trends of pressure changes are obtained for the ground soils, S12-S14, and S19-S21 and S23-S25 with higher pressure drop for higher MC soil samples, S23-S25.

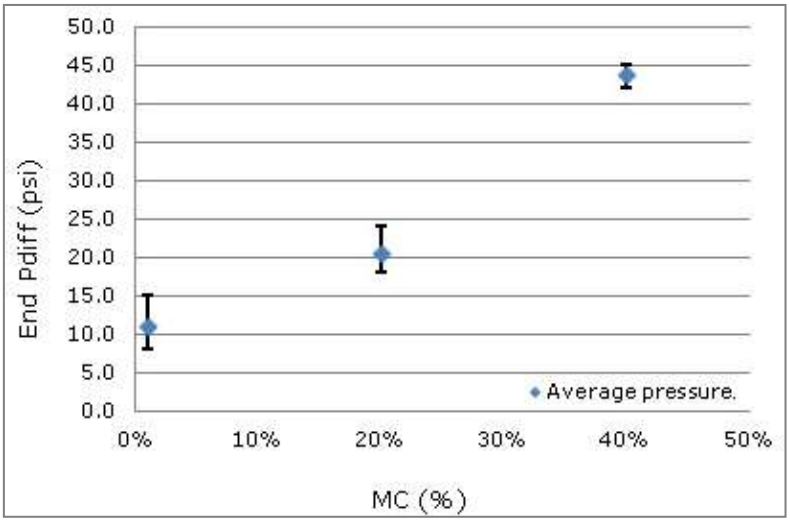

Fig. 4.7 Pressure changes against soil MC.

4.2.2 CO_2/SO_2 (99:1) incubation studies

One set of experiments was run with CO_2/SO_2 gas mixture using a Parr reactor model 4840 at 25^oC, 25 bars for three days. All three incubations

were carried out with oven-dried ground soils (S15, S16 and S17 in Table 3.1). The pressure variation was automatically recorded by the computer as described in section 3.1.2.2 and the data are shown in Fig. 4.8. A CO_2 pump was used for the gas injection process to meet the target pressure, and the starting pressure may not be exactly 25 bars due to a few second operation delays during the CO_2 injection process. Unlike the previous set of experiments using the Parr reactor model 4843, no leakage was observed for these studies.

A high peak in the pressure values of S16 is shown in Fig. 4.8. The fluctuation is due to temperature changes during the incubation process, as the temperature control was mistakenly shut down and the temperature dropped down to around 16^{o}C. When the temperature control system was restarted the next day, the temperature increased suddenly to 47^{o}C and then decreased and stabilised around 25^{o}C. The temperature changes caused the fluctuation in the pressure recording process.

For the three samples with up to 1% MC, the pressure dropped quickly during the first six hours of the experiment, which can be explained as gas filling the soil voids within and reacting with soil pore water to form both weak and strong acid, H_2CO_3 and H_2SO_4. After this, the pressure slightly decreases and tends to stabilise slowly. At the end of three days incubation, the pressure for each study was nearly constant, which indicated the reactions equilibrate in the reactor. The total pressure drops for all these three samples are similar and the values are 2.33 bar, 2.01 bar and 1.56 bar respectively, indicating the good reproducibility of these studies. Fig. 4.8 shows that the run with a higher initial pressure also presented a higher pressure drop. This can be explained and confirms the hypothesis in section 3.1.2.2 that higher pressure would induce and

enhance reactions between soil minerals and CO_2/SO_2 gas (Clow and Mast, 2010; Karberg et al., 2005).

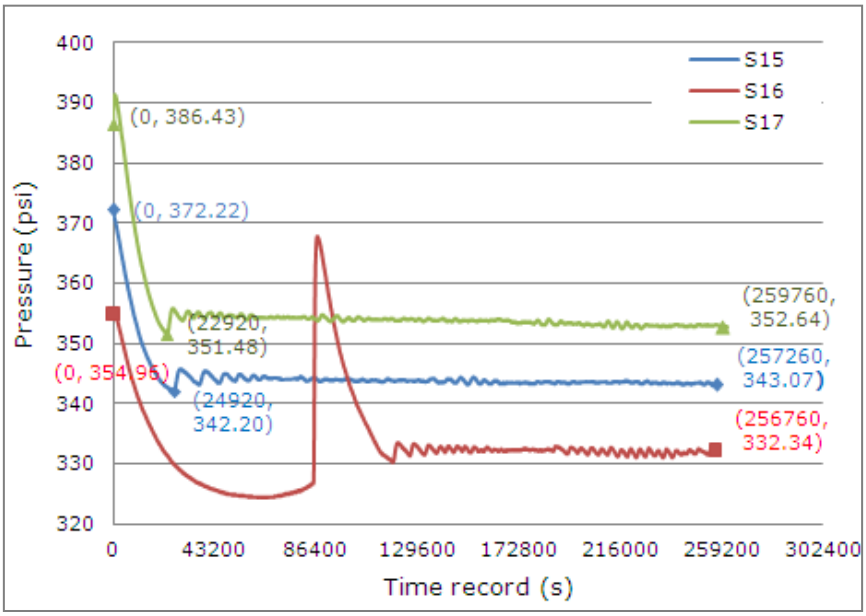

Fig. 4.8 Pressure variation with time for sample S15, S16 and S17.

4.3 pH of soil pore water

4.3.1 Pure CO_2 investigation

For all the studies carried out in this research, it was only possible to measure pH after the incubation and the values are presented in Table 4.3. For each pH value measured, three repeats were carried out and the mean value is listed in the table. Replicate measurements of the pH of the soil solution from the experiments indicate an uncertainty of reported pH (25 °C) value of ±0.01 units.

An increase in pH was observed in the incubated samples (S2-S10, S12-S14, S19-S21, and S23-S25 in Table 3.1) compared with the non-incubated sample S1 and S11, which can be explained as follow. When the

soil was incubated with CO_2 gas and the presence of moisture, CO_2 was absorbed and formed H_2CO_3. This process could reduce pH by providing H^+, which further caused the soil mineral dissolution. When the incubation stopped and the reactor was opened, the trapped CO_2 within the reactor was released quickly outside. But the soil mineral dissolution was kept on by consuming H^+ within the soil solution. As the pH was measured 3-4 days after the incubation, by then, the H^+ could be consumed by the soil mineral dissolution process and H^+ concentration within the soil solution could be reduced, compared with the original H^+ concentration. In this case, the pH will be increased slightly as shown in Table 4.3. A similar trend in the pH change was also observed in other batch experiments (Fu et al., 2009).

Table 4.3 pH values for all the CO_2 incubated samples.

Sample No.	***pH***	***Sample No.***	***pH***
S1	5.67	*S11*	5.86
S2	5.72	*S12*	5.89
S3	5.72	*S13*	5.90
S4	5.68	*S14*	5.83
S5	6.54	*S19*	6.54
S6	6.49	*S20*	6.79
S7	6.55	*S21*	6.77
S8	6.67	*S23*	6.28
S9	6.67	*S24*	6.92
S10	6.83	*S25*	6.61

4.3.2 CO_2/SO_2 (99:1) incubation studies

S15-S17 in Table 3.1 were incubated with a mixture of SO_2/CO_2=1:99. Table 4.4 lists the pH values after the CO_2/SO_2 incubation. The pH of all three soils decreased greatly to around 3.3 from 5.4 (pH of S11). When SO_2 contacts with water, the SO_2 gas forms H_2S and H_2SO_4 in a disproportionation reaction as reaction (4.1) (Palandri and Kharaka, 2005).

As the strong acid H_2SO_4 occurrence in the soil pore water, dissociation of H_2SO_4 yields H^+ further reduce the soil water pH.

$$4\,SO_2(g) + 4H_2O(l) \leftrightarrow H_2S(aq) + 3H_2SO_4(aq) \quad (4.1)$$

Table 4.4 pH values for all the CO_2/SO_2 incubated samples.

Sample No.	***pH***
S15	3.24
S16	3.39
S17	3.36

The above results show changes in the pH after the incubation with CO_2/SO_2 gas (100% CO_2 or CO_2/SO_2=99:1). Associated with the changes in the metal concentration (see results in section 4.4), it shows the occurrence of the soil mineral dissolution process. However, pH was measured 3-4 days after the incubation. The H^+ concentration could be consumed by the soil mineral dissolution process during the buffering period. The stated pH above cannot be used to reflect the soil's instantaneous response to the additional CO_2/SO_2 gas. To see the actual response of soils to the additional gas, it is necessary to measure the real time pH changes during the experiments. Further research was carried out in the Stage II experiments for this purpose. In Stage II, the pH was measured continuously while the CO_2 was injected into the experimental system, as well as the pH buffering effects after the CO_2 injection stopped (see Chapter 5).

4.4 Metal concentration

4.4.1 Pure CO_2 investigation

ICP/MS was done for the non-incubated soil, S1, and incubated soil samples, S5-S10. All the ion concentrations (mg/kg) were calculated

according to equation (3.5), by using the measured metal concentrations (mg/L). All the measurement carried out by ICP/MS was from five repetitions. Uncertainties for all elements are estimated to be within ±1%.

As described in section 2.2.2, ten metals (Al, As, Cd, Cr, Cu, Fe, Mn, Pb, Ni, and Zn) were investigated in the soil solution, as well as K and Mg ions. The metals concentration changes present different patterns. Generally, the results show an increase with incubation in several $CaCl_2$-exchangable metal concentrations in the soil solution: Al, As, Cr, Cu, Fe, K, Mg, Mn and Pb, while the metal Cd and Zn concentrations decrease slightly. Other trace elements do not show a regular trend. The average concentration of 20% MC sample (S5-S7), $C_{20\%}$, and 40% MC samples (S8-S10), $C_{40\%}$, was calculated. By comparing with the metal concentration in S1, C_{S1}, the increased rate in 20% MC sample, $I_{20\%}$, and 40% MC sample $I_{40\%}$ were determined as follows:

$$\mathrm{I}_{20\%} = \frac{\mathrm{C}_{20\%} - \mathrm{C}_{\mathrm{S1}}}{\mathrm{C}_{\mathrm{S1}}} \tag{4.2}$$

$$\mathrm{I}_{40\%} = \frac{\mathrm{C}_{40\%} - \mathrm{C}_{\mathrm{S1}}}{\mathrm{C}_{\mathrm{S1}}} \tag{4.3}$$

Apart from Cd and Zn, which show decreases in their concentration after the 100% CO_2 incubation, three types of metals were identified as presenting increasing concentration (Table 4.5). The changes in the concentration of selected metals are described in the following sections.

Table 4.5 Four different concentration increasing patterns of four different types of metals.

No.	***$I_{20\%}$***	***$I_{40\%}$/ $I_{20\%}$***	***Metals***
Type I	>50%	>2	Al, Fe, Mn
Type II	<50%	>2	As, Cr, Cu, Pb
Type III	<50%	<2	K, Mg
Type IV	$I_{20\%}$, $I_{40\%}$ <0		Cd, Zn

4.4.1.1 Type I metals

Fig. 4.9 groups the Type I metals, which experienced the largest increase in both 20% MC and 40% MC samples, as presented in Table 4.5. The average concentration of sample S1, 20% MC and 40% MC represents C_{S1}, $C_{20\%}$ and $C_{40\%}$ as described before. Error bars are added in the figure to show the minimum and maximum metal concentration within that group.

For the non-incubated soil S1, the exchangeable-Al concentration is 1.82 mg/kg. After 100% CO_2 gassing, the Al concentrations in S5-S7 increases by an average of 59%, compared to S1. Al concentrations in S8-S10 are approximately 254% higher than S1 and 123% higher than S5-S7 (Fig. 4.9 (a)). The change suggests that Al is mobilised and released from soil when CO_2 is present, with greater CO_2 uptake by pore water and more Al mobilised in moister soils. The increase in Al concentration in soil solution exposed to CO_2 has been previously reported by Ardelan et al. (2009) and Blake et al. (1999). When the CO_2 is dissolved into the pore water, H_2CO_3 is formed, and H^+ is present in the soil solution. Soil has a buffering capacity and clay minerals start to weather and neutralise the pH by releasing cations which exchange with H^+, leading to an increase in the $CaCl_2$-exchangeable concentration of Al (Delhaize and Ryan, 1995; Wren and Stephenson, 1991). In this research, the mobilised Al may mainly come from $Al(OH)_3$ complexed with organic matter as well as soil mineral, feldspar anorthoclase ($(Na,K)AlSi_3O_8$, albite ($NaAlSi_3O_8$), Anorthite($CaAl_2Si_2O_8$), which are the potential solid phases controlling the solubility of Al in soil water (Berg and Banwart, 2000).

However, even if the exchangeable-Al concentration in S8-S10 is 254% higher than the non-incubated soil sample, S1, the concentration of Al observed in this study is still lower than plant tolerance limits. As stated in

section 2.2.2.1, Al resistance of different plant species varies due to their different Al tolerance, which may range from 1 µg cm^{-3} to around 40 µg cm^{-3} (Hesse, 1971a; Poschenrieder et al., 2008). The highest concentration in soil sample is with S8-S10 and the concentration of S8-S10 is equivalent to 1.07 µg cm^{-3}, 1.05 µg cm^{-3}, and 0.72 µg cm^{-3}, respectively. The concentration is close to the minimum safety limit. In addition, the soils in this research were incubated with 100% CO_2, which will not be the case under ambient environmental conditions because CO_2 will be diluted by air in soils and will be diffused into neighbouring areas instead of trapping within the area as observed in the ASGARD field (Patil et al., 2010). In addition, in reality, the MC in soil is close to that of S5-S7 (as presented in section 4.1.1), and the average exchangeable-Al in S5-S7 is <0.5 µg cm^{-3}. Therefore, for the soil investigated here, the Al contamination is unlikely to happen in nature.

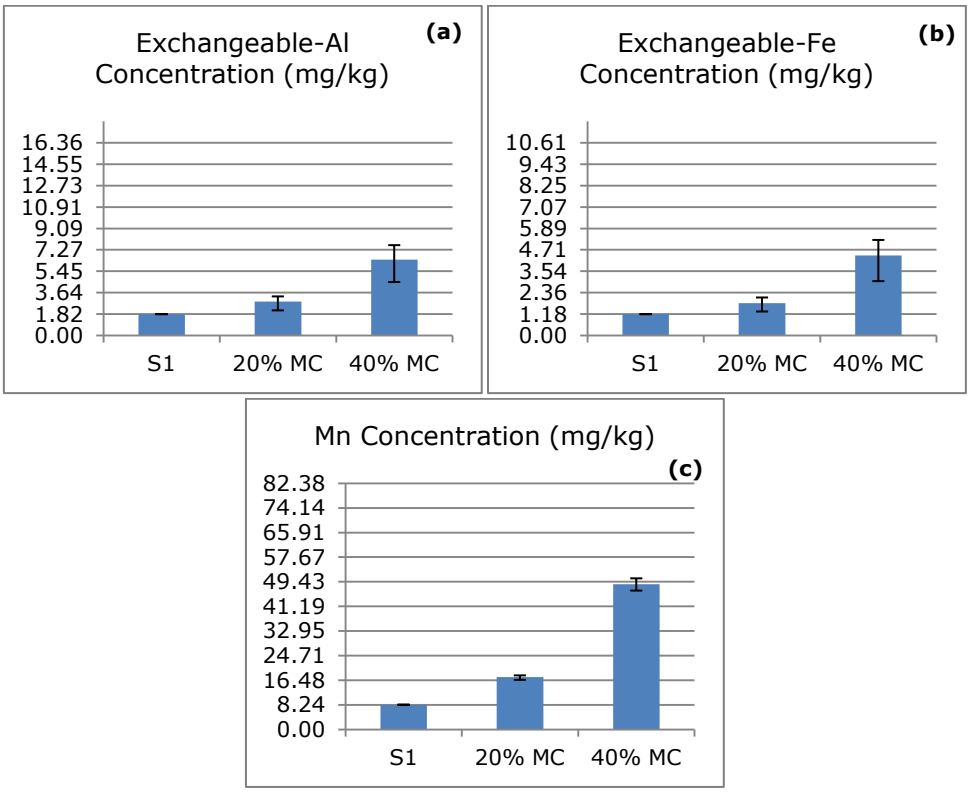

Fig. 4.9 Changes in the Type I metals concentrations after 100% CO_2 incubation.

Similar changes as for Al were observed for Fe (see Fig. 4.9 (b)) with the highest concentration in S8-S10, and the lowest concentration in S1, suggesting that these metals are slightly mobilised by the injected CO_2 gassing.

Similar but more pronounced trends can also be observed in Mn concentration changes (Fig. 4.9 (c)), which correspond with previous research suggesting that Mn is more sensitive to soil acidity (Blake and Goulding, 2002). The exchangeable-Mn concentration for S1 is 8.2381 mg/kg. This value increases by an average of 112% in S5-S7 (20% MC) compared to S1, with a pressure drop of around 1 bar; the Mn concentration in S8-S10 increases by an average of 490% compared to S1, with a pressure drop of about 2 bar. These results show that the more moisture is contained in the soil, the more CO_2 uptake during the incubation, and the more metal will be mobilised from the soil. As suggested by Hem (1978), Huang and Quist (1983) and Nogales et al. (1997), the mobilised Mn in this research could be from MnOOH, Mn_3O_4 or MnO_2 reacted with H^+. As described in section 2.2.2.7, 7 mg/L Mn^{2+} is the basic requirement for plant growth and less than 200 mg/L is considered to be safe. Average Mn concentration detected for S5-S7 and S8-S10 is 3.00 mg/L and 7.21 mg/L respectively (Fig. 4.9). Both concentrations are within the safety range to plants as described above. Similarly to Al (as stated in section 4.4.1.1), for ambient conditions (with less CO_2 concentration), the metals concentration is expected to be less than the concentrations obtained here. The results suggest that pure CO_2 won't cause harmful mobilisation of Mn for the investigated soil here.

4.4.1.2 Type II metals

A moderate increase in Type II metal concentration in the 20% MC and 40% MC samples is observed (Fig. 4.10).

For the non-incubated soil S1, the As concentration within the soil solution is 0.0091 mg/kg. After the 100% CO_2 gassing, the As concentrations in S5-S7 (20% MC) decrease by an average of 0.8% compared with S1; the As concentration in S8-S10 (40% MC) all increases by an average of 113.3% compared to S1 (Fig. 4.10 (a)). Because the As concentration in the 20% MC sample is close to the that in S1 and it is highly mobilised in the 40% MC sample, As is included as a Type II metal. A similar increasing pattern is seen in exchangeable-Cr (Fig. 4.10 (b)).

A lower increasing rate is observed in exchangeable-Cu in the soil solution (Fig. 4.10 (c)). For the non-incubated soil S1, the Cu concentration within soil solution is 0.0678 mg/kg. After the 100% CO_2 gassing, the Cu concentrations in S5-S7 (20% MC) and S8-S10 (40% MC) all increased by an average of 3.4% and 53.8%, respectively, compared to S1. A significant increase in Cu concentration in a controlled soil chamber near CO_2 injection area was also observed by Ardelan et al. (2009).

Higher increases are observed in exchangeable-Pb among Type II metals (Fig. 4.10 (d)). For the non-incubated soil S1, the Pb concentration within soil solution is 0.0058 mg/kg. After the 100% CO_2 gassing, the Pb concentrations in S5-S7 (20% MC) and S8-S10 (40% MC) all increased by an average of 8.6% and 216.6%, respectively, compared to S1. An increase in Pb concentration response to CO_2 intrusion was also observed by Mayer (1998). For a controlled soil chamber with CO_2 injection from one side, Pb increased significantly near the CO_2 injection area and was

considered to be one of the most effectively mobilised metals (Ardelan et al., 2009).

The toxicity level of each metal to plants is described in section 2.2.2. For all the listed metals in this section, the highest concentration of each metal is within safety limits to plants and far below the harmful limits to plants. For example, the tolerance of As varies between different plants and damage to root membranes was observed when exposing to 10 mg/L As (Barrachina et al., 1995). The highest concentration of As for S8, S9, S10 (40% MC samples) are 3.066 µg/L, 3.811 µg/L and 1.759 µg/L, respectively, which are much lower than the harmful level. As described in section 2.2.2.4, it is considered Cr is toxic to most plants if the concentration is higher than 5.0 µg/L (Calevro et al., 1999; Davies et al., 2002; Turner and Rust, 1971). The highest concentration of Cr for S8, S9, S10 (40% MC samples) are 1.81 µg/L, 1.91 µg/L and 1.53 µg/L, respectively, and they are less than the Cr toxic level to plants. As described in section 2.2.2.5, the critical toxicity level of copper is suggested to be above 250 µg L^{-1} (Marschner, 1995), while the highest concentration of Cu for S8, S9, and S10 are 20.46 µg/L, 18.78 µg/L and 17.09 µg/L. There is no consensus about Pb threshold for plant growth (section 2.2.2.9), while less than 0.1 mg kg^{-1} would not cause any damage to plant growth and human health (Hong et al., 2008). The highest concentration of Pb for S8, S9, and S10 are 0.0204 mg/kg, 0.0221 mg/kg, and 0.0122 mg/kg, which is within the safety limits to plant growth.

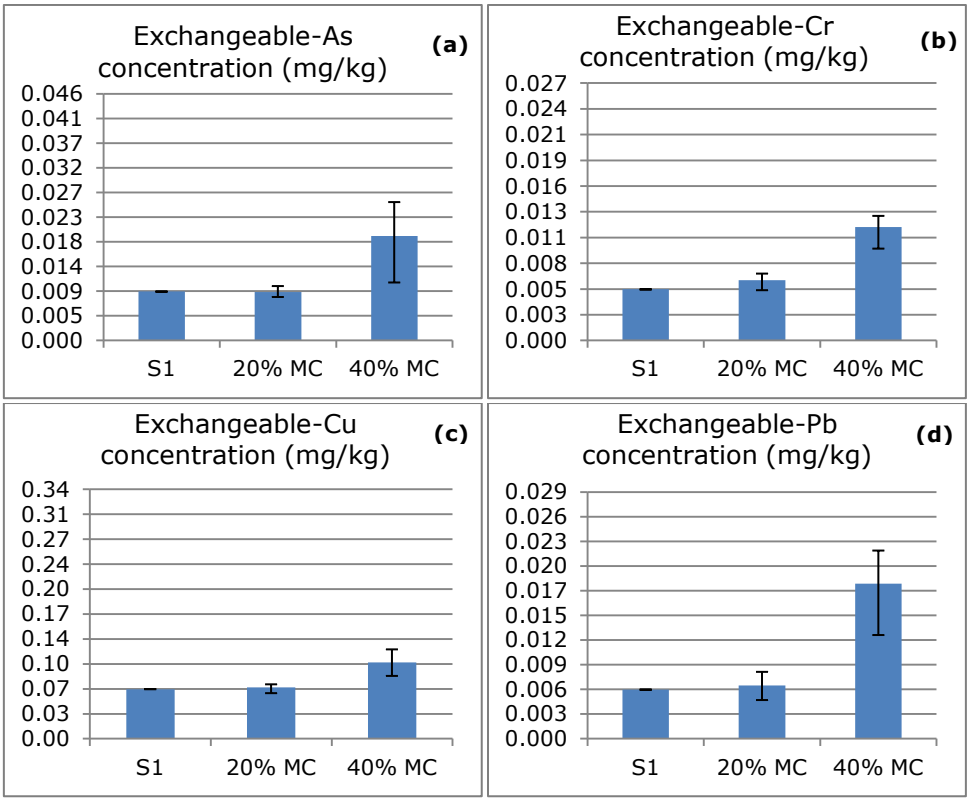

Fig. 4.10 Changes in the Type II metals concentrations after 100% CO_2 incubation.

4.4.1.3 Type III metals

The concentration of Type III metals after 100% CO_2 incubation are presented in Fig. 4.11. The concentration of the metal concentration in this group increased the least comparing with the Type I and II metals. The results of sample S1, 20% MC and 40% MC represents C_{S1}, $C_{20\%}$ and $C_{40\%}$ as described in section 4.4.1.1. Error bars are added in the figure to show the minimum and maximum values of the metal concentration within that group.

This type of metals is mobilised from soil with the CO_2 incubation but with a lower increase rate than Type I and II metals. Higher increase in the 20% MC and 40% MC are observed for K compare with Mg. For the non-incubated soil S1, the K concentration within soil solution is 39.35 mg/kg.

After the 100% CO_2 gassing, the K concentrations in S5-S7 (20% MC) and in S8-S10 (40% MC) all increases by an average of 9% and 16%, respectively, compared to S1 (Fig. 4.11 (a)).

The change in the exchangeable-Mg concentration is shown in Fig. 4.11 (b). For the non-incubated soil S1, the Mg concentration within soil solution is 145.49 mg/kg. After the 100% CO_2 gassing, the Mg concentrations in S5-S7 (20% MC) and S8-S10 (40% MC) all increased by an average of 3.1% and 4.7%, respectively, compared to S1.

The changes suggest that Mg and K are mobilised and released from soil when CO_2 is present, with greater CO_2 uptake by pore water and more Mg, K mobilisation in moister soils. Based on the XRD results, the mobilised Mg could come from dolomite ($CaMg(CO_3)_2$), as well as some clays, such as illite/mica ($(K,H_3O)(Al,Mg,Fe)_2(Si,Al)_4O_{10}[(OH)_2,(H_2O)]$) or montmorillonite ($(Na,Ca)_{0.33}(Al,Mg)_2(Si_4O_{10})(OH)_2{\cdot}nH_2O$). The mobilised K could come from feldspar anorthoclase ($(Na,K)AlSi_3O_8$). A smaller increase in the mobilisation of K was also observed by Lu et al. (2010).

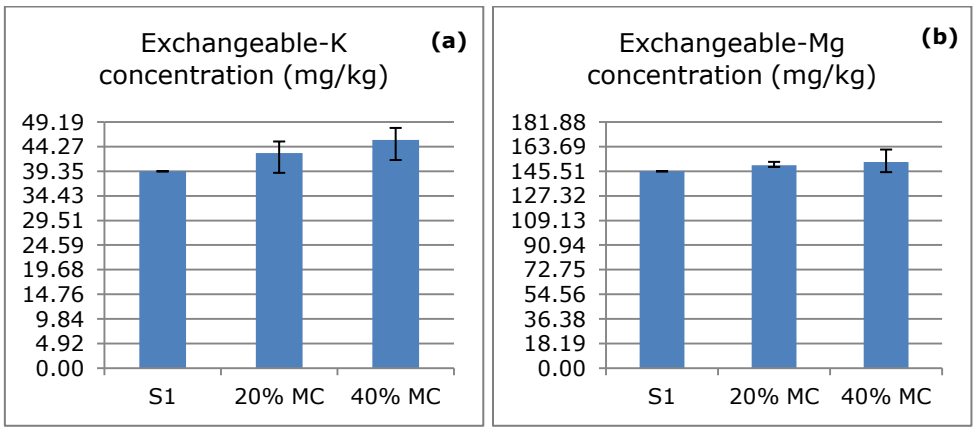

Fig. 4.11 Changes in the Type III metals concentrations after 100% CO_2 incubation.

4.4.1.4 Type IV metals

Fig. 4.12 groups the Type IV metals, which show decreases in the metal concentration in both 20% MC samples and 40% samples after 100% CO_2 incubation.

On average, the $CaCl_2$-exchangeable Cd concentration decreases slightly after exposure to the CO_2 (Fig. 4.12 (a)). The concentration of Cd in S8-S10 (40% MC) is about 18% below S1 and in S5-S7 it is about 8% (20% MC) below S1. However, these differences are insignificant and they may be within the analytical error among samples. Blake and Goulding (2002) and Wren and Stephenson (1991) noted a significant increase in Cd concentration when pH is below 5.0; when pH decreases from neutral to 5.5, it appears that the mobilised Cd is absorbed onto ion exchange surfaces and/or complex with soil organic matter. For all the soils investigated, the pH is within the range 5.5-6.8. This may explain the insignificant change in the Cd concentration. For the soil investigated here, the results show that the Cd contamination is not sensitive to the CO_2 incubation.

As described in section 2.2.2.3, Yildiz (2005) confirmed the previous research and concluded that increased Cd dose in nutrient culture up to 10 mg/L will cause large yield reduction, for example 75 % for beans, 65 % for sugar beet, and 40 % for maize. The highest concentration of Cd in S1 is 2.042 µg/L and the exchangeable-Cd concentrations in other samples are less than 2.042 µg/L (Fig. 4.12 (a)). Moreover, Jia et al. (2010) observed that elevated CO_2 concentration in soil would reduce the toxicity of Cd for plant growth on Cd contaminated soils; and high concentration of Ca^{2+}, H^+, Zn^{2+} as well as high DOM will compete with Cd^{2+} and reduce its toxicity (Aravind and Prasad, 2005; Prasad, 1995). Therefore, for the

investigated soil, compared with other metals, such as Al and Mn, Cd toxicity should not be the main concern when exposed to elevated levels of CO_2. Similar changes in the Zn concentration are observed as well in Fig. 4.12 (b).

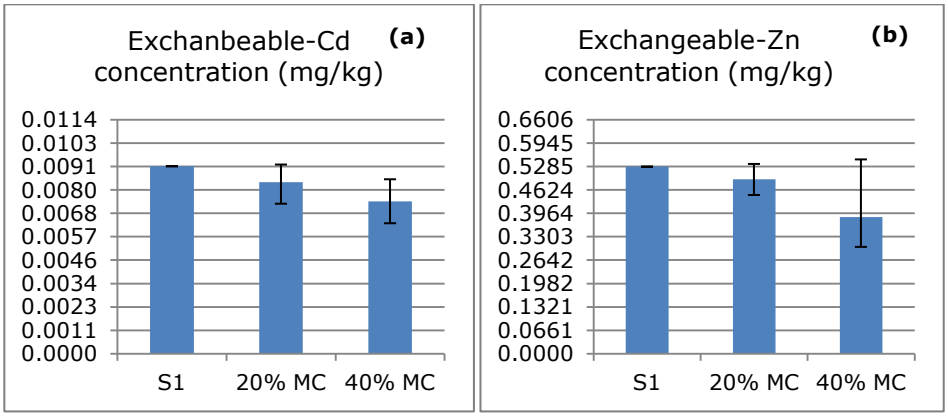

Fig. 4.12 Changes in the Type IV metals concentrations after 100% CO_2 incubation.

4.4.1.5 Summary

In conclusion, with pure CO_2 incubation on unground soils with different soil MC, the results show an increase with incubation of several $CaCl_2$-exchangable metal concentrations in soil solution: Al, As, Cr, Cu, Fe, K, Mg, Mn, and Pb, while the metal Cd and Zn concentrations decrease slightly. Other trace elements do not show a regular trend. All the changes show different patterns and can be grouped into four types. Type I metals- Al, Fe and Mn- experienced the highest mobilisation from soils, followed by Type II metals- As, Cr, Cu and Pb, while the Type III metals- K and Mg showed the least increases. A slightly decreasing trend was observed in Type IV metals- Cd and Zn.

The incubation process indicates that the more moisture within a soil sample, the higher the concentration of mobilised metal. However, even in

the highest moisture content soil, which holds the highest concentration of exchangeable mobilised metals, the metal concentration is still far below the safety limits. Considering temperature and pressure in the real environment and leaked CO_2 concentration in the field, heavy metal mobilisation to a toxic level is unlikely to happen for the investigated soils in this research.

4.4.2 CO_2/SO_2 (99:1) incubation studies

One set of experiments was run with CO_2/SO_2 gas mixture using a Parr reactor model 4840 at 25^oC, 25 bars for three days. ICP/MS analysis was carried out for the set of soil samples, S11 and S15-S17 (Table 3.1). All the measurements were carried out by ICP/MS.

Generally, the results show an increase in metal concentrations with incubation in the soil solution compared to the non-incubated sample. Following the descending order of the increasing rate, the metals are Ni, Cr, Fe, Co, Pb, Al, Zn, Cd, Mn, Cu, As, K, and Mg. The variation of selected metals concentrations is discussed in the following sections.

4.4.2.1 Exchangeable-Ni

Fig. 4.13 shows the changes in the exchangeable Ni concentration after the mixture gas incubation. Ni concentration increases the most among all the metals. The Ni concentration in the untreated sample S11 is 0.0116 mg/kg. After the CO_2/SO_2 mixture gassing, the average Ni concentrations in S15-S17 is 102.86 mg/kg, which increases nearly four orders of magnitude compared with S11. The differences in the concentration

among sample S15, S16, and S17 may be caused by minor variations among soil sample properties. However, the Ni concentrations in S15-S17 are all higher compared with the untreated sample. This change suggests that Ni is highly mobilised and released from soil when the CO_2/SO_2 is present. This high mobilisation can be explained by the strong acid, H_2SO_4, occurrence in the soil solution when the SO_2 is absorbed by the soil pore water, which causes high degree soil mineral weathering. This is applicable to all the increase of other metals as described in the following sections.

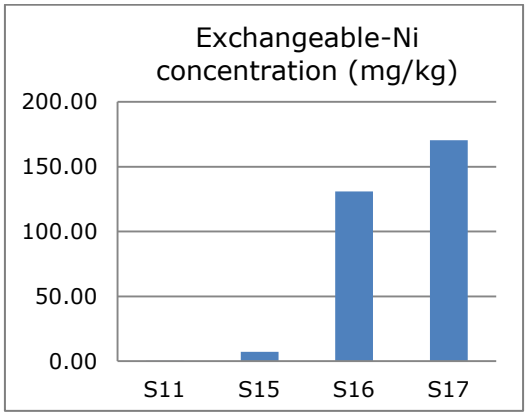

Fig. 4.13 Exchangeable-Ni concentration results for S11 and S15-S17.

The significant increase in Ni mobility has been previously reported at pH lower than 5.0-5.5 (Ardelan et al., 2009; Blake et al., 1999). It is suggested that Ni is normally chemically bound with Fe and Co (Marschner, 1995). In this research, Fe and Co are both highly mobilised and increase about two orders of magnitude compared with that of S11. The high increase in Ni, Fe and Co concentration could come from metal contained oxide or minerals within the soils.

As described in section 2.2.2.8, normally, 10 μg g^{-1} and 50 μg g^{-1} are considered to be the toxic Ni levels for sensitive and moderately tolerant

species (Marschner, 1995). However, no harm may be seen to some plants even when exposed to 50 μg g^{-1} Ni (Nogales et al., 1997). The average concentration of Ni in S15-S17 is 102.86 mg/kg, which is equivalent to 102.86 μg g^{-1}. Even with <1% MC within a soil sample, SO_2 appearance causes much higher mobilisation than pure CO_2 incubation. The mobilisation exceeds the highest Ni tolerant concentration to plants and could be harm to plant growth.

4.4.2.2 Exchangeable-Al

Fig. 4.14 shows the results of exchangeable-Al concentration for S11, and S15-S17. The concentration of Al in S11 is 1.43 mg/kg and the average concentration of Al in S15-S17 is 93.94 mg/kg. The exchangeable-Al within S15-S17 increases significantly compared to S11, indicating that more Al is mobilised from soil particles. Even with <1% MC within a soil sample, SO_2 appearance causes much higher mobilisation than pure CO_2 incubation as described in section 4.4.1. In addition, the higher mobilisation of Al by impure gas mixture corresponds with higher pressure drop in S15-S17 incubation, and suggests that 1% SO_2 is the main factor causing the changes. Higher exchangeable-Al concentration in S15 may be caused by slight differences among soil samples properties. Similar as the explanation in section 4.4.1.1, the mobilised Al may mainly comes from $Al(OH)_3$ complexed with organic matter as well as soil mineral, feldspar anorthoclase ($(Na,K)AlSi_3O_8$, albite ($NaAlSi_3O_8$), Anorthite($CaAl_2Si_2O_8$), which are the potential solid phases controlling the solubility of Al in soil water (Berg and Banwart, 2000).

As described in section 2.2.2.1, the Al concentration within S15-S17 is much higher than safety levels for plant growth, even for high Al tolerant plants, which can only tolerate around 60 mg/kg within the soil solution.

A similar trend is shown for Pb concentration in Fig. 4.17, which also exceeds the safety levels, approximately 0.5 mg/kg, for plant growth and the maximum acceptable concentration in drinking water, 0.01 mg/L (Hong et al., 2008; Stenhouse et al., 2009).

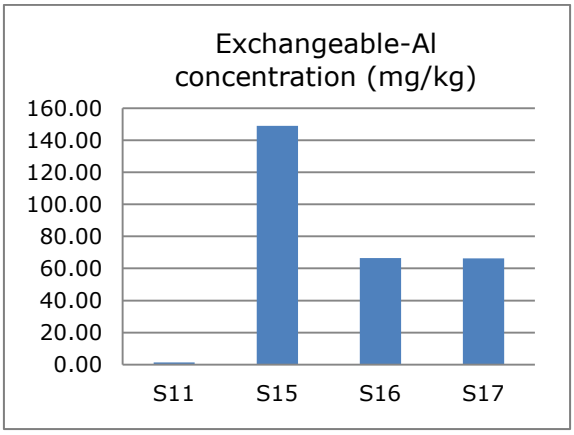

Fig. 4.14 Exchangeable-Al concentration results for S11 and S15-S17.

4.4.2.3 Exchangeable-Mn

Fig. 4.15 shows exchangeable-Mn concentration for S11, and S15-S17. Exchangeable-Mn within S15-S17 increases significantly compared with S11 indicating that more Mn is mobilised from soil particles. The concentration of Mn in S11 is 14.19 mg/kg and the average concentration of Mn in S15-S17 is 131.45 mg/kg, which shows a 10 fold increase over the original soil sample. High mobilisation of Mn has been previously reported and considered to be sensitive to soil acidity (Beaubien et al., 2008; King et al., 1992; Lu et al., 2010). The high mobilisation of Mn can

be explained as the strong acid H_2SO_4 occurrence in the soil solution when the SO_2 combines with the soil pore water. When the pH is lower than 4.0, a high degree soil mineral weathering from Mn oxides takes place as previously suggested (Huang and Quist, 1983). Similar to the explanation in section 4.4.1.1, the mobilised Mn in this research could be from MnOOH, Mn_3O_4 or MnO_2. Though Mn is highly mobilised from the soil, the Mn concentration within S15-S17 is still within safety ranges levels for plant growth as described in section 2.2.2.7.

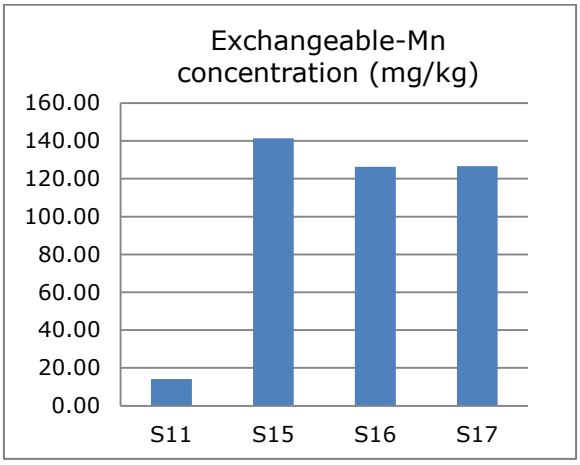

Fig. 4.15 Exchangeable-Mn concentration results for S11 and S15-S17.

4.4.2.4 Exchangeable-Cd

Fig. 4.16 shows the Cd concentration for S11 and S15-S17. Exchangeable-Cd increased 10 times compared with S11 after the incubation, which corresponds with previous work that a significant increase in Cd concentration appears when pH is below 5.0 (Blake and Goulding, 2002; Wren and Stephenson, 1991). As presented in section 2.2.2.3, 1 μg kg^{-1} body weight is the daily tolerable intake by human (Yang et al., 2006b). Yildiz (2005) agreed with previous research and suggested that increased

Cd dose (up to 10 mg L^{-1}) in nutrient culture would cause large yield reduction. The exchangeable-Cd measured here exceeds the safety levels and might cause problems to human health and plant growth.

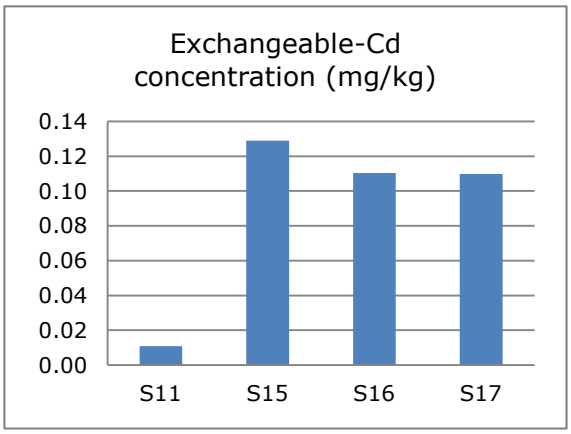

Fig. 4.16 Exchangeable-Cd concentration results for S11 and S15-S17.

4.4.2.5 Other exchangeable metals

Smaller increases in metal concentrations were observed for K, and Mg with an average increase of 63% and 57% compared with that of S11. Most of the $CaCl_2$-exchangable metals/metalloids were highly mobilised from the soil as presented in Fig. 4.17. Among all these metals/metalloids, some of them exceeded their safety limits for plant growth, e.g. Fe, Pb, Zn and Cu (section 4.4.2).

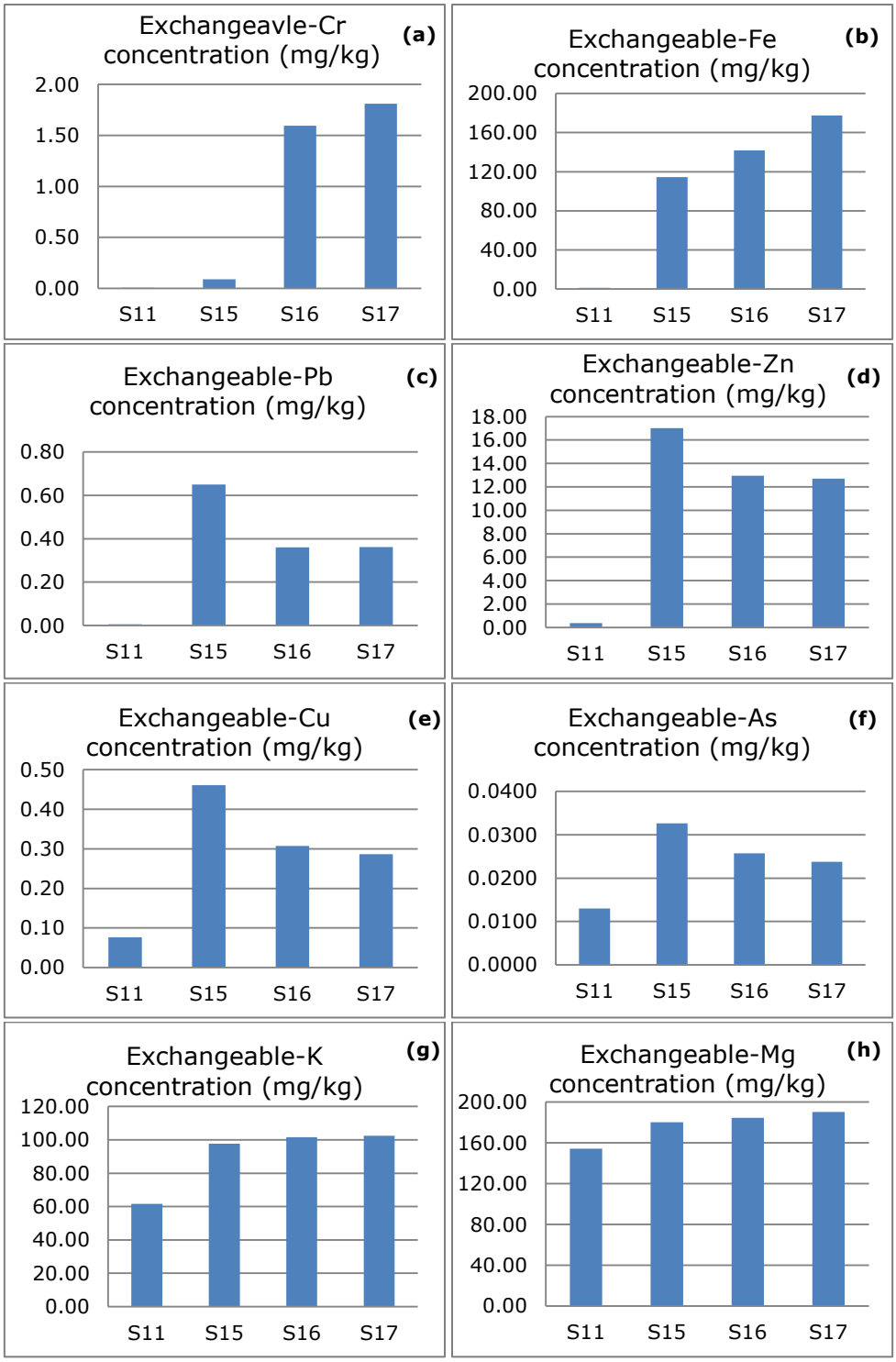

Fig. 4.17 Changes in other metal concentrations for S11 and S15-S17.

4.4.2.6 Summary

One set of experiments (three repeats) was run with CO_2/SO_2 gas mixture using a Parr reactor model 4840 at 25°C, 25 bars for three days. The incubated samples were oven-dried ground soils.

In conclusion, the results showed an increase with the incubation of most $CaCl_2$-exchangable metal concentrations in the soil solution compared with the non-incubated sample. In descending order of the increasing rate, the metals are Ni, Cr, Fe, Co, Pb, Al, Zn, Cd, Mn, Cu, As, K, and Mg. Even with <1% MC within a soil sample, SO_2 appearance caused much higher mobilisation than pure CO_2 incubation as described in section 4.4.1. The higher mobilisation of Al by impure gas mixture corresponds with higher pressure drop in S15-S17 incubation, and suggests that 1% SO_2 is the main factor causing the changes.

Some of the metals, for example $CaCl_2$-exchangeble Ni, Al, Fe, Pb, Zn and Cu are highly mobilised due to 1% SO_2 appearance and exceed their safety limits to plant growth even with 1% MC within soil samples. Based on the results shown with pure CO_2 gas incubation (section 4.4.1), under real environmental conditions, more moisture content may absorb more SO_2 and cause serious impacts on soil heavy metal mobilisation. Attention needs to be given to the heavy metal mobilisation by the impure CO_2/SO_2 gas.

4.4.3 Comparison of metal concentration changes in ground and unground soil

Previous research showed that dry grinding of soils may cause physical changes, such as breakage of the weakly bound large aggregates,

reduction in the tactoids' thickness by delamination, reduction in the plates' area, formation of colloidal matter (Hrachová et al., 2007), and cation changes in solution (Kasai et al., 1994) as well as organic matter release, which was previously adsorbed on clay surfaces or held by salt or hydrogen bonds on clay surfaces and inaccessible (Craswell and Waring, 1972). The metal concentrations of S1 and S11 are therefore compared. The results show that the grinding process increased the concentration in S11 for most of the metals. The concentration was increased in Mg, K, Ti, Mn, Co, Cu, As, Cd, Pb etc., while slightly decreased in Al, Fe, and Zn.

The changes in the metal concentration of the treated ground soils follow similar trends as that of the treated unground soils. But the metal concentration in the soil solution with ground soils is higher than that of unground soils. Table 4.6 shows the Al concentration of 20% MC wet ground samples after CO_2 incubation. The average concentration of exchangeable-Al of the ground soil is nearly two times that of the unground soil. The results indicate a higher mineral dissolution of the ground soils after the CO_2 incubation compared with the unground soil, and imply that particle size may influence the soil response. Similar results are shown in other metals and have been previously reported (Shih et al., 2000; Zhang et al., 2007). Stage II were carried out to study the differences in the impacts associated with different particle sizes.

Table 4.6 The concentrations of exchangeable-Al of sample S19-S21 after CO_2 incubation.

No.	***Al CONCENTRATION (mg/kg)***
S11	1.4313
S19	4.5819
S20	5.1319
S21	6.4388

4.5 Summary

This chapter presents results from Stage I-Closed reactor experiments and discusses them in detail. The results imply the occurrence of the soil mineral dissolution process and point out the metals that are sensitive to CO_2 and CO_2/SO_2 flux. With the CO_2/SO_2 incubation, some obvious differences in soils were observed after the incubation compared with the CO_2 incubation. For example, a higher decrease in pH of soil pore water to around pH 3.3 (section 4.3) was observed with the CO_2/SO_2 incubation, while with the CO_2 incubation the pH fluctuated within the range of 5.5 to 6.5. Besides, for the CO_2/SO_2 incubation, a higher mobilisation in some exchangeable metal concentrations (section 4.4) was observed compared with the CO_2 incubation. For example $CaCl_2$-exchangeble Ni, Al, Fe, Pb, Zn and Cu is highly mobilised due to 1% SO_2 appearance and exceeds their safety limits to plant growth even with 1% MC within soil samples. The impacts on ground and unground soils were also compared, and the results indicate that particle size may influence the soil response (section 4.4.3).

All the results from Chapter 4 provided useful information to inform the design of Stage II experiments. Further research was accordingly carried out in the Stage II experiments. The results are presented in Chapter 5.

Chapter 5 Flow Through Column System Experiments: Results and Discussion

As described in section 3.2, different runs (see Table 3.5) were carried out in Stage II-flow through column experiments to assess the real time response of various sediments following CO_2/SO_2 injection. This chapter presents and discusses results from the Stage II experiments using limestone sand Trucal 5 (section 5.1), limestone sand Trucal 6 (section 5.2) and silica sand (section 5.3). Results from all runs from Stage II experiments (see Chapter 5) are interpreted in Chapter 6 to examine the correlation between sediment properties and their response to the CO_2 release. Part of the results has been published in Caramanna et al. (2013).

5.1 Experiments on limestone sand Trucal 5

5.1.1 Flowrate change

CO_2 and N_2 were injected into the columns at the same initial inlet flowrate, 300 ml/min. Unexpected changes in the inlet and outlet flowrate of the CO_2 column were recorded during the run. The reason of these changes is beyond the scope of this study. Nevertheless the flowrate changes can play a role on the impacts on the sediments of the injected CO_2. Therefore, the values of the inlet and outlet flowrate are presented and a hypothesis of these changes is suggested as follows.

5.1.1.1 Unsaturated conditions

Run 1 and Run 2 were carried out under unsaturated conditions (see Table 3.5). For the N_2 column in both runs, the outlet flow meter indicated that the N_2 gas was flowing immediately after the beginning of the injection; this highlights a very fast movement of the gas through the sediments. After about five minutes, both the inlet and outlet flowrate were balanced and stable at around 300 ml/min.

For the CO_2 column, the same procedure as for the N_2 column was followed. The CO_2 column was connected to a scrubber with NaOH solution to absorb most of the vented CO_2. This created a back pressure measured of 0.08-0.1 bar. It was noticed that the measured gauge pressure in the CO_2 column continuously increased up to 0.08 bar during the first six minutes; thereafter, the pressure increased further up to 0.1 bar until the CO_2 injection stopped. During the first five minutes of this pressure build-up there was no outlet flow. From the sixth minute onwards, the outlet flow increased becoming equal to the inlet flow.

Fig. 5.1 shows the inlet flowrate change over time. The x-axis is logarithmic scale, and therefore the time 0 cannot be shown in the figure. The inlet flowrate for actual time 0 (initial injected flowrate) is 300ml/min. During the injection an unexpected decrease of the inlet flowrate was noticed; this decrease cannot be explained by the pressure building-up as during the first six minutes. A detailed analysis and possible explanation is presented below. To maintain the inlet flowrate around 300 ml/min during the run, same as for the N_2 column, the inlet flowrate was increased manually to 300 ml/min after 10 minutes of gas injection. As it kept decreasing, the inlet flow was manually increased several times as

indicated by the red square in Fig. 5.1. During the run the injection of the CO_2 gas was stopped at 52, 156, 1,306, 2,945, 4,329, 5,879 minutes to allow the opening of the ports to measure the pH. These stops are labelled as the green diamond points in Fig. 5.1. The gas injection lasted for about five days for Run 1.

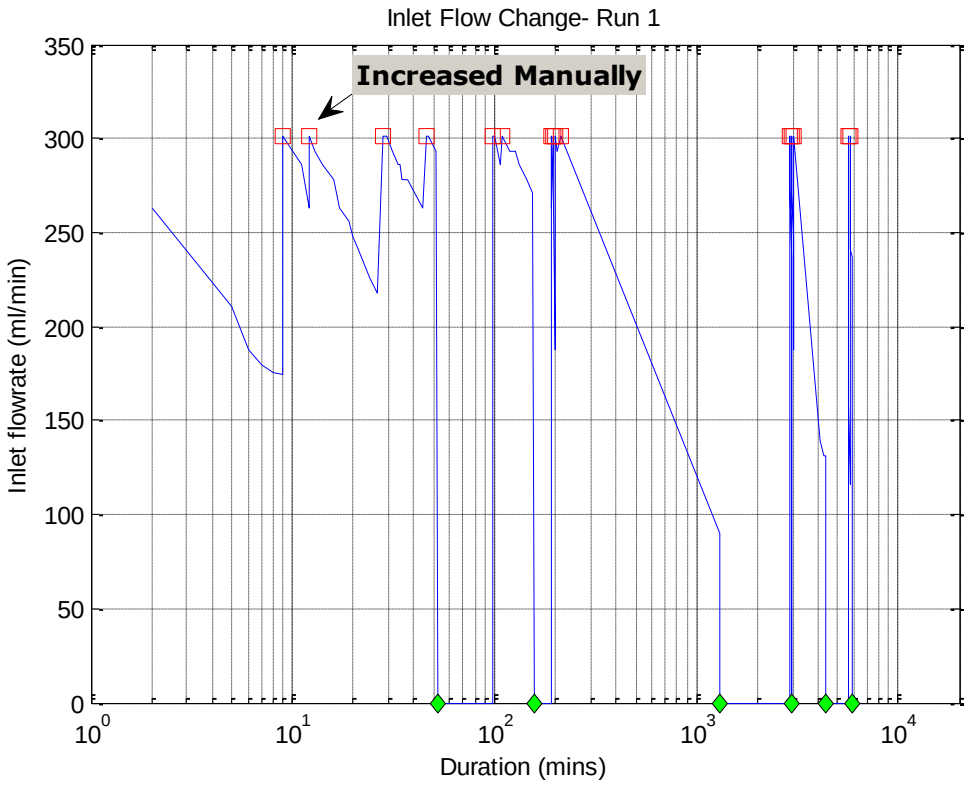

Fig. 5.1 Inlet flowrate changes over time- Run 1 (see Table 3.5). The initial inlet flowrate at time 0 is 300 ml/min, which cannot be plotted in the figure as the x-axis is logarithmic scale.

Fig. 5.2 shows the inlet flowrate change and the flowrate drop slope during the first 46 minutes. By comparing every two adjacent points in Fig. 5.2 (a), the gradient of each point was calculated and plotted in Fig. 5.2 (b). For every point the flowrate increased manually, as the time interval was close to zero, the calculated drop slope was infinite. To fit all the calculated values in one figure, the gradient at that point was given the value of its previous point as labelled with red squares in Fig. 5.2 (b).

A general increase in the flowrate drop slope was observed, with the value getting close to zero (Fig. 5.2 (b)). Similar trends were also observed after 46 minutes. This indicates that the flowrate kept decreasing during the run but at a progressively slower rate. A possible explanation for the observed continuous decrease in the inlet flowrate could be that once the CO_2 gas was injected into the CO_2 column, there was an initial dissolution of the limestone sand followed by cementation during the CO_2 injection as suggested in other research (Madland et al., 2006). This limestone dissolution/precipitation may possibly reduce the porosity and permeability of the sediments leading to the formation of a back pressure with a reduction in the volume of the injected flow. The decrease needs to be compensated for by a manual increase of the flow rate until equilibrium is reached.

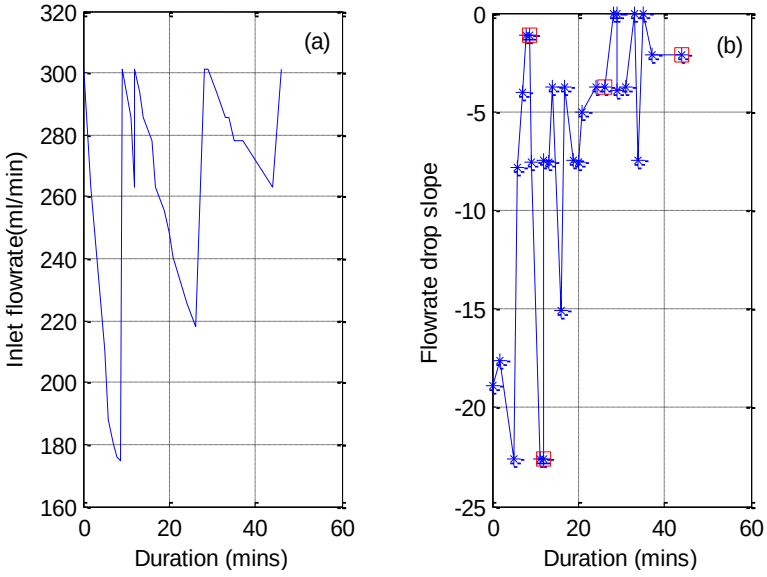

Fig. 5.2 Inlet flow changes and slope changes during 0-46 minutes of Run 1 (Table 3.5).

As a duplicate of Run 1, Run 2 was carried out. A similar trend in the inlet flowrate change was observed. A decrease in the inlet flow was also noticed, with a sharper decreasing rate at the beginning and a slower

decreasing rate towards the end of the run. These similarities between the runs highlight the consistency of the observed phenomena.

5.1.1.2 Flooded conditions

The CO_2 injection lasted for about three days for Run 3 and Run 4 (see Table 3.5) under flooded conditions. It was noticed from Run 1 and Run 2 that there would be a decrease in the inlet flow. To minimise the interference with the column system for Run 3 and Run 4, the manual increase of CO_2 inlet flowrate was kept at a minimum possible rate and frequency. Flowrate changes during Run 3 and Run 4 are presented in Fig. 5.3 and Fig. 5.4, respectively. In each figure, (a) represents the real-time changes in the inlet flowrate of each run; while (b) is the graph showing the flowrate drop slope by comparing every two adjacent points in (a) and plotting the gradient of each point at time, t. For a time, t, in (a), if the flowrate was manually increased to 300 ml/min, the drop slope at that point was given the value of its previous point, and these points were labelled in the red squares in graph (b).

When the CO_2 was injected into the system, the gas partially dissolved in the water inside the column, which could delay the pressure build-up process. Measuring the gas concentration in the head space is necessary to detect when CO_2 starts flowing through the columns; such analysis was carried out in subsequent runs and is presented in section 5.1.3.

By comparing the results from Run 3 and Run 4 with the results from Run 1 and Run 2, a similar but clearer decreasing trend in the inlet flow was observed. The flowrate drop slope increased towards zero following the CO_2 injection (Fig. 5.3 (b)), which indicated that the decrease rate was

progressively reduced during the run. Besides, Fig. 5.3 and Fig. 5.4 indicate the repeat run Run 4 matched well with Run 3, which highlights the consistency within these experiments. More results are compared in the following sections between these repeated runs.

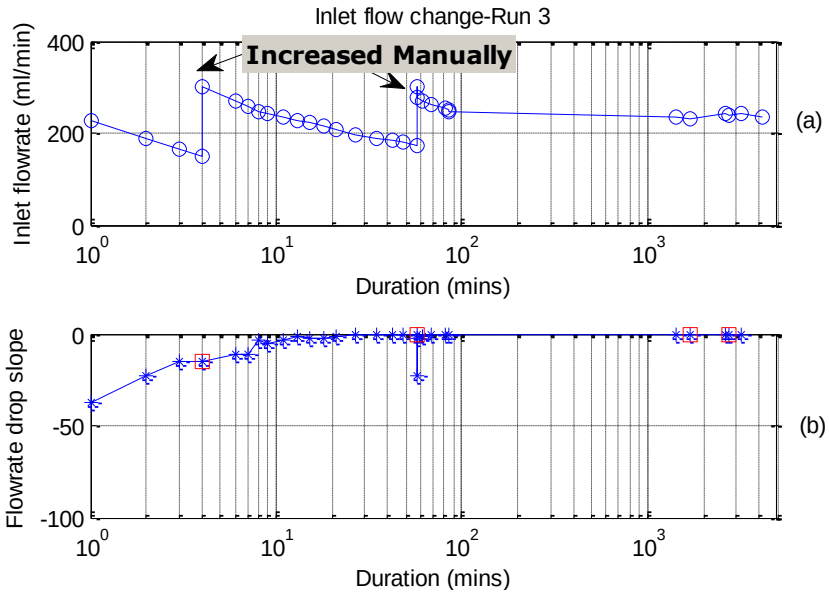

Fig. 5.3 Changes in the inlet flowrate and the flowrate drop slope for Run 3.

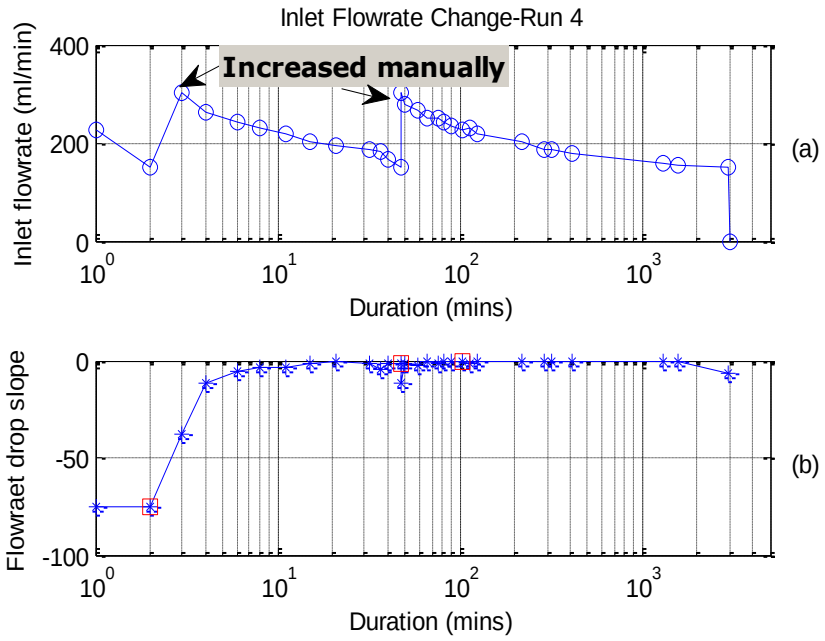

Fig. 5.4 Changes in the inlet flowrate and the flowrate drop slope for Run 4.

5.1.2 pH changes

5.1.2.1 Unsaturated conditions

Fig. 5.5 shows the changes in the pH of Run 1 during the gas injection process for the N_2 column and the CO_2 column. The pH measured ports, C8 and S8 in each column, were 25 cm away from the N_2/CO_2 injection point. Each value shown in Fig. 5.5 has a ±0.01 standard error.

For the approximate five days of gas injection, six measures were taken. At the very beginning, the pH for both the N_2 and the CO_2 column was measured as the initial pH values, which were both around 8.0. On the first day of gas injection, both the N_2 and the CO_2 injection process were stopped twice for two measurements, which were at 80 and 180 minutes elapsed time. For the rest of the run, the pH was measured daily until day five.

For the N_2 column, the pH (as N_2 column-C8 in Fig. 5.5) was between 7.69 and 8.21 following the gas injection with a seesaw pattern during the run. For the CO_2 column, the initial pH (as CO_2 column-S8 in Fig. 5.5) was 7.80, similar to the pH of the N_2 column. After about 80 minutes following the CO_2 injection, the pH decreased to 6.53. At 100 minutes, the CO_2 was injected for another 50 minutes and the pH decreased to 6.16. Soon after, the CO_2 injection was restarted again and stopped at 1,300 minutes. The pH was measured at 1,346 minutes showing a value of 6.07. The same procedure was carried out for the following CO_2 injection and the pH was measured at 2,978, 4,365 and 5,912 minutes with a value of 6.14, 6.21 and 6.10, respectively.

By comparing the results of the CO_2 column and the N_2 column, a quicker pH drop was observed in the CO_2 column solely. Considering that both

columns were under the same conditions, the quick changes in the pH values in the CO_2 column can be considered due to the effect of the CO_2 flux.

The pH was measured soon after the CO_2 injection stopped (Fig. 5.6). The figure shows a quick increase in the pH immediately after the gas injection ceased. In about 100 minutes, the pH increased about 0.3 units from 6.03 to 6.33. As there was some interference during Run 1, e.g. stop the injection and measure the pH, it was necessary to run another experiment to confirm the results.

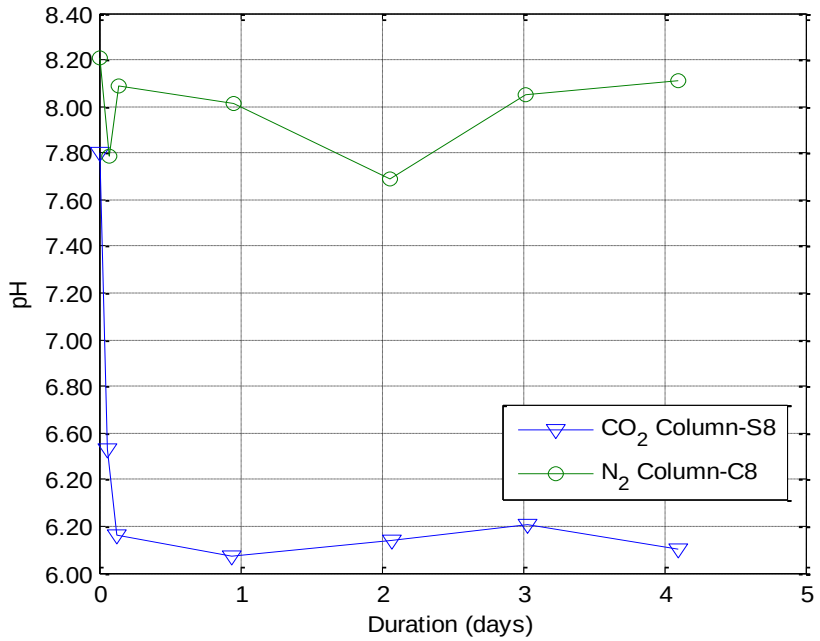

Fig. 5.5 pH changes for the N_2 column and CO_2 column of Run 1.

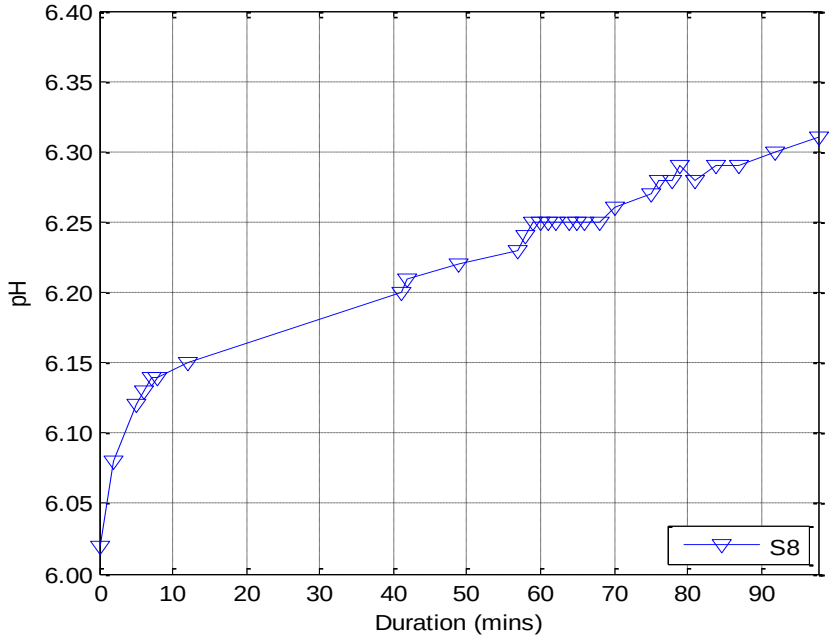

Fig. 5.6 Recovery effects for S8 for the first 100 minutes once CO_2 injection ceased.

Accordingly, Run 2 was carried out to verify the results from Run 1. To avoid any interference by opening the column, the pH meter was left and sealed inside the columns (port C8 and S8, 25 cm away from the gas injection point) to measure the pH continuously. The results from Run 1 showed a quick pH drop at the beginning of the experiment and an increase in the pH when the CO_2 injection stopped. Attention was paid for these two periods. Fig. 5.7 shows the pH changes during Run 2.

A similar result as Run 1 was obtained in Run 2. The initial pH for C8 and S8 was 7.95 and 7.90. For the N_2 column, the pH was within a range of 7.90-8.40 with a slightly increase at the beginning followed by a decrease at the end (Fig. 5.7). The small variation of the pH in the N_2 column may be due to the flow of the injected gas, causing a mechanical mixing of the smaller sediments thus enhancing the dissolution of limestone. The fluctuation in the pH and ion concentration was also observed by Lu et al. (2010) with argon (Ar) gas flushing through a water-rock system.

For the CO_2 column, a quick continuous drop in the pH from 7.90 to 6.10 was noticed at the beginning of the injection with a sharp drop after five minutes followed by a slower decrease (Fig. 5.7). After 90 minutes from the beginning of the CO_2 injection, the pH was stable around 6.10. The vertical red line in Fig. 5.7 indicates the time when the CO_2 injection stops, which is approximately three days after the starting of the CO_2 injection. The pH was measured once a day for the following five days. A quick and steady recovery in the pH was observed and the pH bounded back to basicity (around 7.58) after five days.

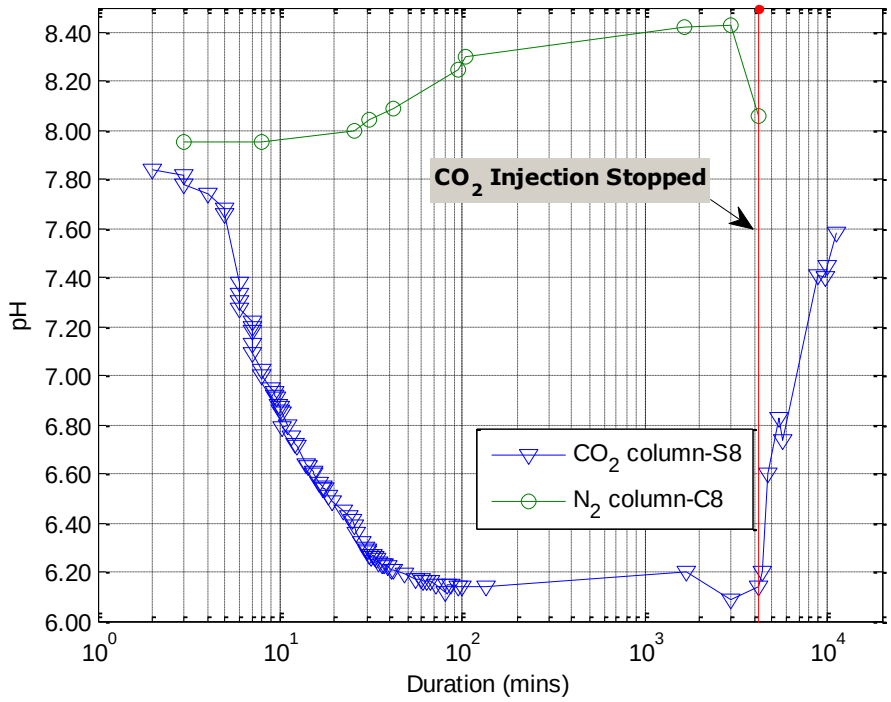

Fig. 5.7 pH changes following gas injection in N_2 and CO_2 columns of Run 2 and the buffering effects. (The x-axis is logarithmic scale)

The quick decrease in the pH at the beginning of the run, and the recovering effects once the CO_2 injection ceased can be explained and summarised considering the reactions listed below (Little and Jackson, 2010). Firstly, gas phase $CO_{2(gas)}$ dissolves into porous water and forms an

aqueous phase $CO_{2(aq)}$ (reaction (5.1)). $CO_{2(aq)}$ then reacts with H_2O and generates a weak carbonate acid, $H_2CO_{3(aq)}$, as from reaction (5.2), which eventually dissociates into CO_3^{2-} and releases H^+ (reaction (5.3) and (5.4) respectively). The noticeable but modest pH drop during the first 5-6 minutes in the CO_2 column (Fig. 5.7) may be caused mainly by reactions (5.1), (5.2) and partially by (5.3). Once the reaction (5.1) reaches its equilibrium under the experimental conditions and the $CO_{2(aq)}$ is close to its saturation value, reactions (5.3) and (5.4) become dominant forming H^+, which leads to the observed further quick drop in the pH.

$$CO_{2(gas)} \leftrightarrow CO_{2(aq)} \tag{5.1}$$

$$CO_{2(aq)} + H_2O \leftrightarrow H_2CO_{3(aq)} \tag{5.2}$$

$$H_2CO_{3(aq)}{}^{*} \leftrightarrow H^+{}_{(aq)} + HCO_3{}^-{}_{(aq)} \tag{5.3}$$

$$HCO_3{}^-{}_{(aq)} \leftrightarrow H^+{}_{(aq)} + CO_3{}^{2-}{}_{(aq)} \tag{5.4}$$

The main reactions involving the limestone sediments can be summarised as (5.5)-(5.7) (Madland et al., 2006; Pokrovsky et al., 2009). The carbonate component of the limestone sediments ($CaCO_3$) forms OH^- when in contact with water (reaction (5.5)), which neutralises H^+ through reaction (5.6). In addition, under acidic conditions, limestone sand dissolves as reaction (5.7), which further enhances the reaction (5.3) and (5.4) by consuming H^+. The equilibrium of all of these reactions contributes to the final pH value.

$$CaCO_{3(solid)} + H_2O \leftrightarrow Ca^{2+}{}_{(aq)} + HCO_3{}^-{}_{(aq)} + OH^-{}_{(aq)} \tag{5.5}$$

$$OH^- + H^+ \leftrightarrow H_2O \tag{5.6}$$

$$CaCO_{3(solid)} + 2H^+{}_{(aq)} \leftrightarrow Ca^{2+}{}_{(aq)} + H_2O_{(aq)} + CO_{2(gas)} \tag{5.7}$$

The buffering effect, due to the strong buffering ability of the limestone sand, was observed once the CO_2 injection stopped. Limestone sand consumed H^+ by either directly reacting with it or forming OH^-, which can be further consumed to react with H^+ ((5.5) and (5.6)). Once the CO_2 injection stopped, no additional CO_2 can dissolve in water, resulting in the lack of H^+ source that can be used to neutralise the OH^- generated from the solid $CaCO_3$. Moreover, under acidic conditions, carbonate would dissolve to consume H^+ (5.7). Subsequently, the reactions above lead to an increase in the pH during the buffering period.

However, even if limestone sand has strong buffering ability, the continuous injection of CO_2 would overcome this buffering capacity leading to the observed quick decrease in the pH during injection. A pH recovery toward the initial conditions was observed only after the CO_2 injection stopped.

5.1.2.2 Flooded conditions

Run 3 and Run 4 were aimed to investigate the pH changes of Trucal 5 under flooded conditions. Water samples were collected from the column for ICP/MS analysis for measuring ion concentrations. In order to correlate the pH change and the changes in ion concentrations, the same water sample was used for both pH and ion concentrations analysis. The samples were collected from S1, S3 and S5 ports at 23, 45 and 65 cm, respectively above the injection point (Fig. 3.18). With only 2 cm difference in height between S1 and S8, the results of S1 from Run 4 is used to compare with the results of S8 from Run 1 and Run 2. In Run 4, the pH changes at different heights from the injection point were also assessed (Fig. 5.8).

Similarly as for Run 1 and Run 2, all the data presented here have ±0.01 standard error.

During Run 3, because of lack of sampling experience for the run, when the water samples was collected from the CO_2 column, the author was busy with preparing the samples for the following ion concentration measurement by ICPMS, which left the author insufficient time to measure the pH of the collected samples. Later on, when pH was measured, it was realised that the obtained pH could not represent the real pH values during the CO_2 injection because the pH of the collected water was quickly buffered. Therefore, no useful data of pH was obtained for Run 3. Based on the experience with Run 3, samples were collected by more people and pH of the collected samples was immediately measured during Run 4 to observe pH changes during the CO_2 injection (Fig. 5.8).

As presented in Fig. 5.8, the initial pH for all ports of the CO_2 column and the N_2 column of Run 4 were around 7.60. The pH for the N_2 column of Run 4 was within the range of 7.40-7.66 with a seesaw trend following the N_2 injection; a similar trend was observed in the control system by Ardelan et al. (2009). A decrease in the pH was noticed for the CO_2 column (Fig. 5.8). For the pH in S1, a sharp decrease was noticed at the beginning of 10 minutes from 7.28 to 6.30 and the pH was then stable at 6.30 for another five minutes. From 15 minutes to 100 minutes, a seesaw trend in the pH was noticed from about 6.30 to about 6.70. After 100 minutes, the pH dropped again and stabilised around 6.10 at 160 minutes until the end of the CO_2 injection process (Fig. 5.8 (c)). For the pH in S3, the initial pH was 7.40 and there was no big change in the pH at the first 20 minutes. A minute later, the pH dropped with fluctuations towards 6.20 and was stable around 6.20 at the end of the CO_2 injection (Fig. 5.8 (b)). For the

pH in S5, a delay in the decrease of the pH was observed compared with that in S3. The first quick pH drop was noticed after 30 minutes and the pH continuously decreased to around 6.10 until 300 minutes. The pH stabilised around 6.10 until the end of the run (Fig. 5.8 (a)). Similar to Run 1 and Run 2, the pH for all three ports (S1, S3 and S5) was stable around 6.10 at the end of the run.

The differences in the three ports can be correlated with the different distances to the injection point. Being closer to the injection point resulted in quicker response to the CO_2 flux and quicker decrease in the pH. Similar results were observed in other research (Beaubien et al., 2008; Patil et al., 2010), showing higher pH drop near the CO_2 source point compared with adjacent areas. Despite the interference by the standard error, the fluctuation in the pH for all the three ports could be caused by the presence of larger amount of water (flooded conditions). Higher water content could influence the absorption of the injected CO_2 by sediments (Xu et al., 2005) and interfere with carbonate dissolution leading to the fluctuation in the pH.

The buffering effect was assessed for all three ports, as shown in Fig. 5.8. There were three data points less in S5 than that of S3 and S1 because there was not sufficient water left to be collected from S5. The buffering effects were observed for the following 30 days; there was a slightly increase in the pH (from 6.10 to 6.50). However, the buffering was not as obvious as Run 1 and Run 2, which may be because the water contains more dissolved CO_2 leading to more H^+ under flooded conditions than that of the unsaturated conditions, and therefore this delayed the buffering process.

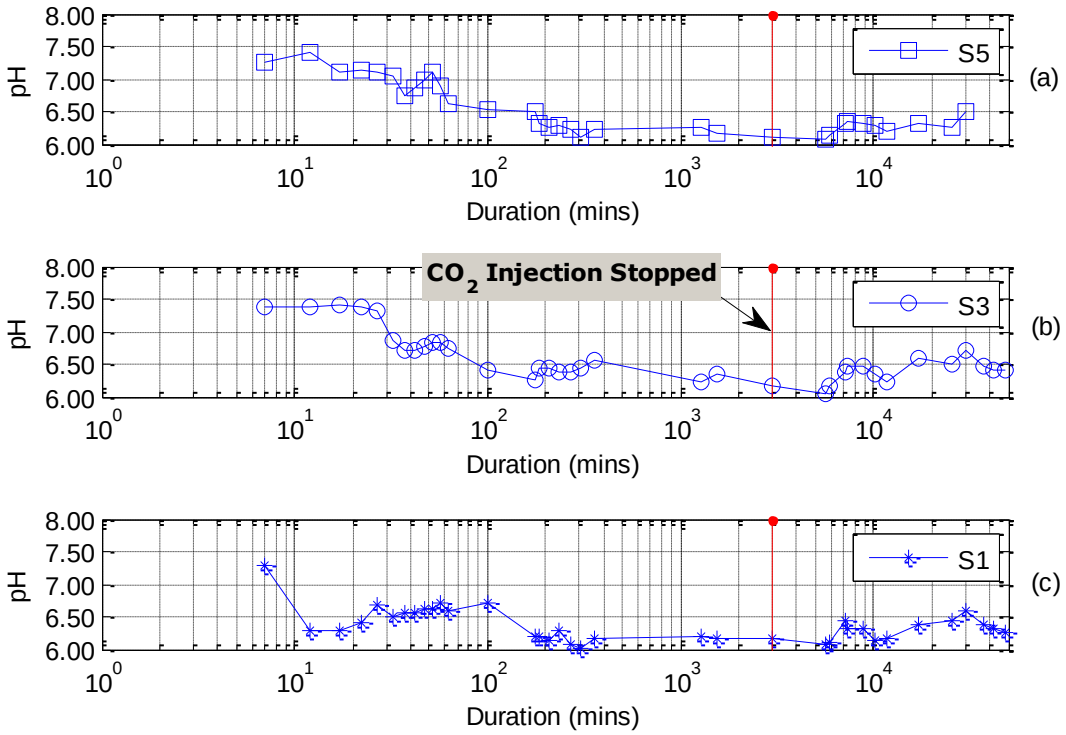

Fig. 5.8 pH changes during the CO_2 gas injection in the CO_2 column of Run 4. (The x-axis is logarithmic scale)

For sediments either under unsaturated conditions or under flooded conditions, a quick pH drop was noticed once the CO_2 was injected into the system and a buffering effect was observed only once the CO_2 injection ceased. Even if limestone sand has a strong buffering effect, the continuous injection of CO_2 would overwhelm this buffering potential leading to a quick decrease in the pH during the injection from around 8.00 to 6.10.

5.1.2.3 Comparison between repeat runs

Fig. 5.9 shows pH changes during the CO_2 gas injection of the CO_2 column of Run 1 and Run 2. During each run, pH was measured at port S8, 25 cm away from the gas injection point. The detailed measurements were

explained in section 5.2.1.1. For Run 1 and Run 2, the initial pH was around 7.80. Once CO_2 was injected into the CO_2 column, pH starts to decrease as shown in Fig. 5.9. During approximately the first 100 minutes after the CO_2 injection, pH of both runs dropped quickly from 7.80 to around 6.10 and stabilised at around 6.10 for the following gas injection period. Fig. 5.9 shows that these two runs corresponded with each other well and they are repeatable.

As explained in section 5.1.2.2, there is no useful pH value for Run 3 to be compared with Run 4. These repeats with pH changes were not compared here. More comparison between these repeat runs is presented in the following sections in terms of dome formation (section 5.1.4) and exchangeable-Ca concentration (section 5.1.5.1).

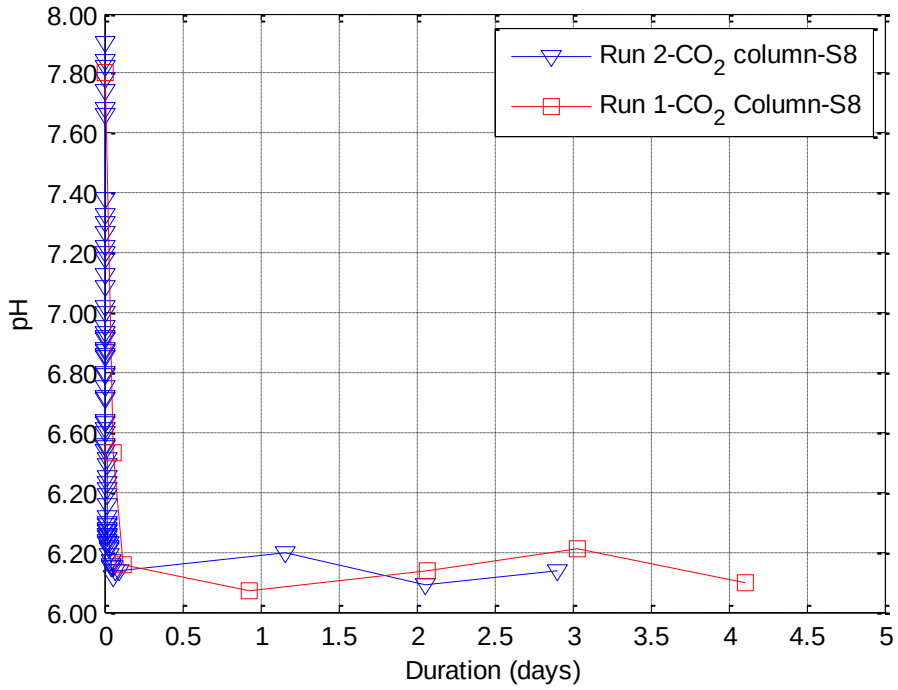

Fig. 5.9 pH changes during the CO_2 gas injection in the CO_2 column of Run 1 and Run 2. Run 2 is a repeat of Run 1, which are both with limestone Trucal 5 under unsaturated conditions.

5.1.3 Gas concentration

The gas concentration within the head space of the column was measured during Run 4 and presented in Fig. 5.10. BAL in the figure stands for the remaining gas in the head space except the CO_2 and O_2 and can be considered to be composed mostly of N_2. The accuracy of each measurement by GA 2000 is presented in Table 3.6.

Fig. 5.10 shows that CO_2 started accumulating after about 10 minutes of flowing through the sediments. Between 10-20 minutes, a quick increase in the CO_2 concentration was noticed. After 20 minutes, a steady and sharp increase of the concentration of CO_2 was observed with consequent reduction of the O_2 and the BAL gas concentration. At about 250 minutes, the concentration of CO_2 within the head space was close to 99% and stabilised afterwards. At the end of the run, the CO_2 concentration reached 99.9%, with no O_2 being detected. For the N_2 column, the injected N_2 flowed through the sediments within a few seconds and resulted in the fast increasing of the N_2 concentration in the head-space. In comparison, the delayed CO_2 flow in the CO_2 column can be explained by the dissolution of CO_2 gas in the porous water. Once the level was close to the saturation limit the CO_2 started to flow into the head space.

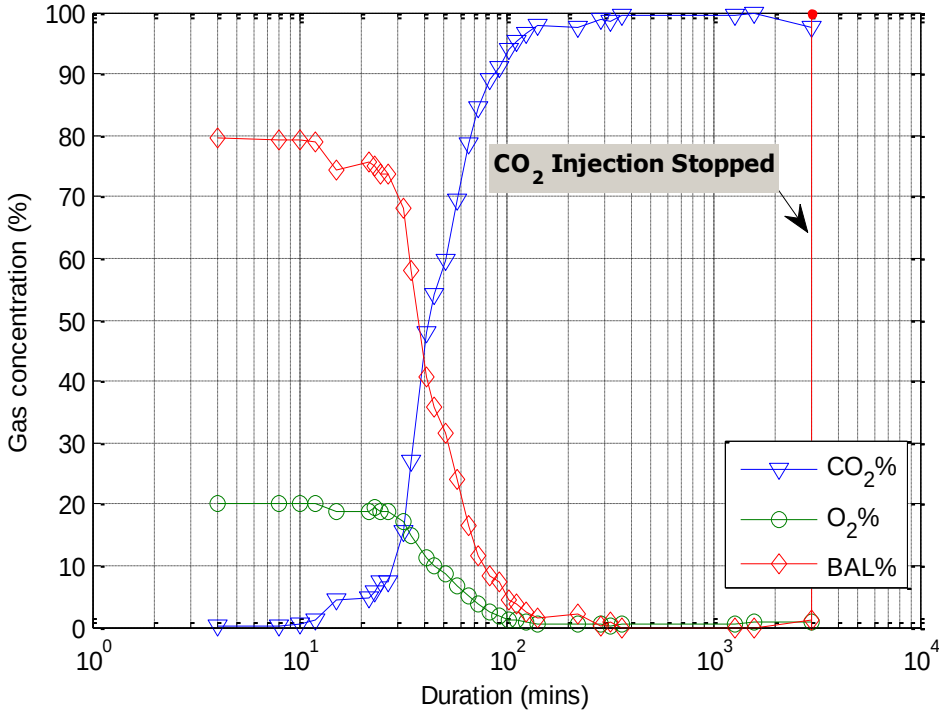

Fig. 5.10 Changes in the gas concentration inside the CO_2 column of Run 4.

5.1.4 Dome formation

A dome structure was formed following the N_2/CO_2 injection for Trucal 5 under flooded conditions (Fig. 5.11 and Fig. 5.12) for both Run 3 and Run 4. Fig. 5.11 is a top down view of the dome in the N_2 column (a) and in the CO_2 column (b) of Run 3; while Fig. 5.12 is a front view of the dome formed in the CO_2 column of Run 4. At the beginning of each run, all the sediments had a flat surface. At the end of each run, a dome was formed and the sediments inside becoming denser. For Run 3, the height of the surface level of the sediments dropped from 55 cm to 53 cm; and the highest point of the dome was about 5 cm higher than the surrounding surface for the N_2 column, while it was about 4 cm higher in the CO_2 column. For Run 4, the highest point of the dome was about 5 cm higher than the surrounding surface level in the CO_2 column. The change of the

sediment height inside the columns complies with previous suggestion (section 5.1.2) and shows that a mechanical mixing was happening in the columns while the N_2/CO_2 gas injection. During the runs, channelling of the injected CO_2 or N_2 gases was also observed.

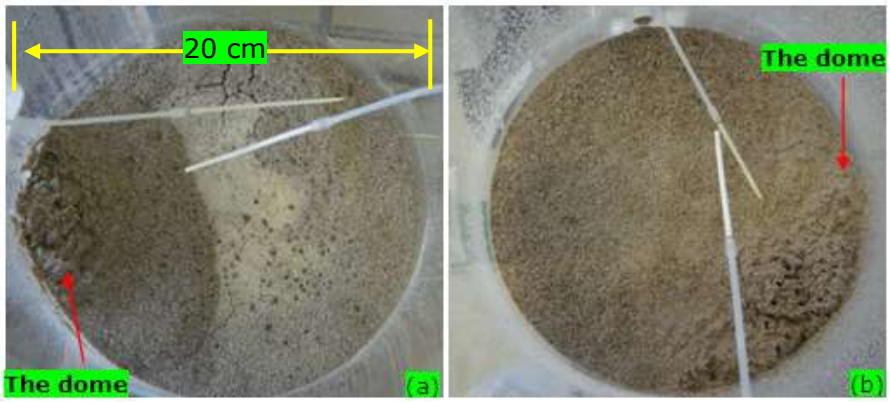

Fig. 5.11 Top down view of the dome formed in the N_2 column and CO_2 column after the gas injection. (a) is the image from the N_2 column; while (b) is the image from the CO_2 column.

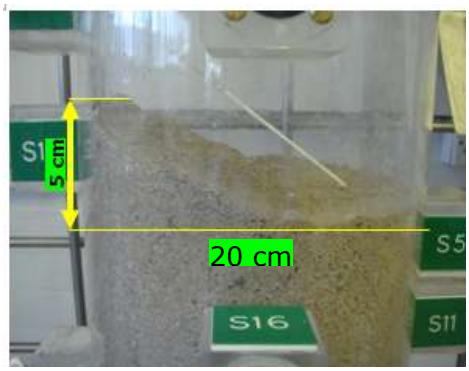

Fig. 5.12 The formed dome in the CO_2 column during Run 4.

The explanation for the above phenomenon is as follows. Within the column system under flooded conditions, the limestone sand acts as a water-saturated porous medium. When a gas is injected into the system, its free-flowing is restricted by the presence of the solid matrix. The bubbles would partially be trapped between the limestone grains, and partially flow along the less resistant pathways. The big voids between the larger particles would be the preferred flow pathways for the gas to pass

through. In addition, the trapped gases accumulated in the sediments, which would form a connected path for the gas to pass through. With a continuous upward gas flow, a preferred channeling would be formed as observed by Oldenburg and Lewicki (2005). Previous research shows that when gas invades a water-saturated, unconsolidated porous media with sufficiently small particle size (i.e. 0.1 μm), fracture-dominated invasion happens, where the gas will fracture cohesive sediments and move sediment particles out of the way (Fauria and Rempel, 2011; Jain and Juanes, 2009). Otherwise, capillary invasion takes place, where the gas normally displaces liquid to move through. In this research, the gas stream displaces the finer particles which are transported upwards along the column accumulating as a dome presented here. It is to be noted that this dome is close to the wall of the column therefore it is likely to be, at least partially, due to the boundary effect which generates low-resistance paths between the sediments and the wall itself. The phenomenon always took place around the gas release point on the surface of the sediments.

Being CO_2 an acidic gas, its mechanical effect on the formation of channels inside the sediments is enhanced by the chemical dissolution of part of the sediments. The injected CO_2 gas would react with water forming H_2CO_3 which dissolves material ahead of its front. The dissolution process reduces the resistance of the media to the gas flow and subsequently more acid would accumulate in this area, resulting in even higher dissolution. The dissolution creates interconnected channels throughout the media and forms secondary channels for the injected gas to pass through (Fredd and Fogler, 1998; Hoefner and Fogler, 1988). Due to this dissolution process, a more concentrated flux of gas in a specific area is therefore to be expected. This leads to the formation of a smaller dome as

observed in the CO_2 column comparing with the N_2 one, where such dissolution did not happen.

A higher content of water generates a less dense packing of the sediments with a generic fluidification of the system. Therefore the finest particles can be more easily displaced by the gas stream. Because of the above described effects, under the same conditions as the CO_2 column of Run 3, a bigger dome was formed during Run 4.

In a real seeping scenario a high CO_2 flux and/or very loose or liquefied sediments may be prone to the formation of domes above the leaking paths and this morphological feature could be used to detect the presence of such leakages. Such an surface uplifting phenomenon was previously observed in Colorado Plateau area of the United States by Haszeldine et al. (2005) and Pederson et al. (2002), where the surface had been uplifted by 2 km in the last 6 Ma due to natural CO_2 release.

5.1.5 Exchangeable ion concentrations in the solution

Pore water was collected from S1, S3 and S5 to measure the changes in the exchangeable ion concentrations following the N_2 and CO_2 injection. As there was insufficient water in Run 1 and Run 2 to be collected, it was possible to measure the ion concentration changes in the runs under flooded conditions only. For Run 3, the sampling frequency was not matched with the Ca^{2+} concentration change path during the CO_2 injection. The sampling missed the big Ca^{2+} changes during the run and left the Ca^{2+} changes less representative of the actual change path during Run 3. Based on the experience from Run 3, a more appropriate sampling pace was

adopted in Run 4 as shown in the following section to observe the actual Ca^{2+} change path. All the measurements were carried out by ICP/MS.

5.1.5.1 Exchangeable-Ca

Fig. 5.13 presents the Ca^{2+} concentration changes in both the N_2 column and CO_2 column. For the N_2 column, Ca^{2+} concentration of C1 and C5 was within 68.04-91.26 mg/L. For the CO_2 column, the results for S5 are incomplete because an insufficient volume of water was obtained for the ICP/MS analysis. During the two days and 100 minutes of CO_2 injection, the samples were collected at the same time for all the three ports, 0 hr, 0.5 hr, 1 hr, 3 hrs, 4 hrs, 5 hrs, 7 hrs, 21 hrs, 26 hrs, and 50 hrs following the CO_2 injection. For all the three ports, a sharp increase in Ca^{2+} concentration was noticed between the first and the eighth hours of the injection followed by a slow increase in the Ca^{2+} concentration afterwards towards the end of the run (Fig. 5.13). In the first 20 minutes, the Ca^{2+} concentration from S1 increases, meanwhile no big changes are measured from S3 and S5. In the following hour, Ca^{2+} concentration was increased in S5. This may be due to the rise in the CO_2 partial pressure within the head space, to which S5 is closer thus leading to quicker carbonate dissolution compared with S3 (Dreybrodt, 1999). The dissolution of limestone sand was clearly delayed for port S3. This highlights the expected direct correlation between the CO_2 concentration and its dissolution effects on the limestone sand, which is the source of the increased Ca^{2+} concentration (as detailed below).

After about 50 hours of gas injection, the Ca^{2+} of S1 increased from about 76 mg/L to 409 mg/L; the Ca^{2+} of S3 increased from about 74 mg/L to

398 mg/L; and the Ca^{2+} of S5 increased from about 74 mg/L to 435 mg/L. After 50 hours the gas injection was stopped and the recovering effects of Trucal 5 were assessed for the following 30 days. During the recovery period, the concentrations of Ca^{2+} for all three ports were analysed. The samples were collected once a day at the beginning and once every two days or once every five days. For all the three ports, a steady decrease in the Ca^{2+} concentration was observed for about six days after the CO_2 injection stopped with an average drop of about 50 mg/L, and the Ca^{2+} concentration was stable for the following 25 days with small fluctuations. Appendix 6 provides the detailed sampling frequency and results of Ca^{2+} concentration in both columns.

Although the sampling frequency during Run 3 did not match with the Ca^{2+} concentration changes path during the CO_2 injection, a consistent change trend of Ca^{2+} concentration was noticed between Run 3 and Run 4. These repeated runs both show a steady and slow increase rate of Ca^{2+} concentration with the first hour followed by a quick increase for the following hours until the CO_2 injection stopped. The results of exchangeable-Ca in S3 over time during Run 3 are attached as Appendix 7.

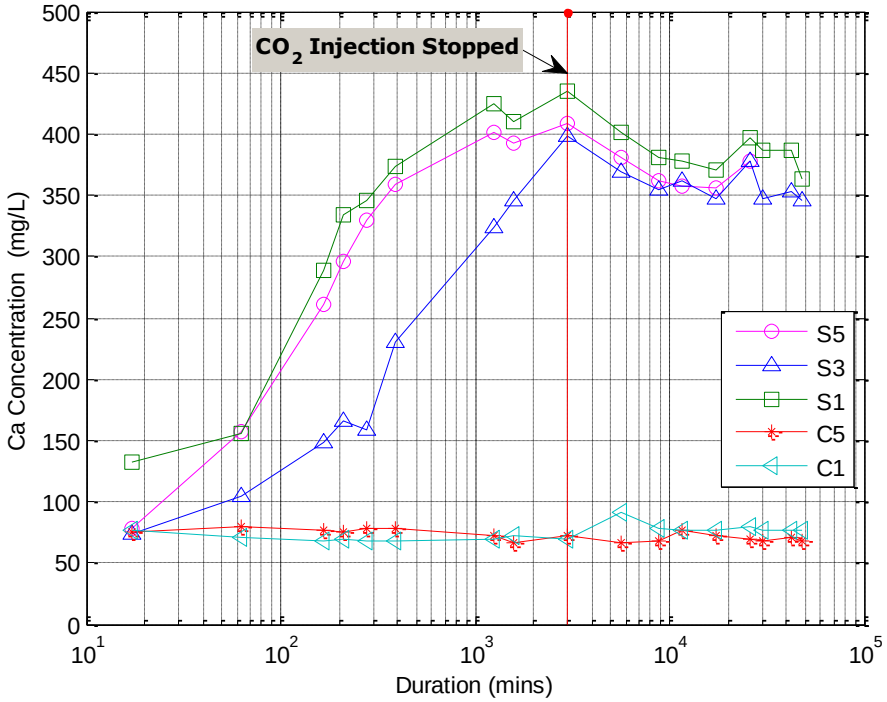

Fig. 5.13 Changes in Ca^{2+} concentration of S1, S3 and S5 following the CO_2 injection of Run 4.
Note: x-axis is logarithmic scale

The changes in the Ca^{2+} concentration can be explained as follows. When the CO_2 was injected into the system, it would firstly react with water to release H^+ (reactions (5.2)-(5.4) as described above). Later, the H^+ reacted with $CaCO_3$ to dissolve it generating the observed increase in Ca^{2+} concentration. The overall reaction between $CO_{2(aq)}$ and $CaCO_{3(solid)}$ is described in reaction (5.8). Under acidic conditions, both calcium dissolution and precipitation would take place. The precipitation of Ca^{2+} removed the Ca^{2+} from the equilibrium solution and further enhanced the limestone sand dissolution, resulting in a further rapid increase in Ca^{2+} concentration as shown in Fig. 5.13 (Madland et al., 2006).

$$CaCO_{3(solid)} + CO_{2(aq)} + H_2O \leftrightarrow Ca^{2+} + 2HCO_3{}^-{}_{(aq)} \quad (5.8)$$

When the CO_2 injection stopped, the solution was oversaturated in Ca^{2+}. Along with the observed pressure drop in the head space, the precipitation of Ca^{2+} occurs as previously observed by Chen et al. (2004), Short et al. (2005) and Wojtowicz (2001).The oversaturated Ca^{2+} reacted with CO_3^{2-} to form solid $CaCO_3$ as in reaction (5.9), which in turn to the decrease in Ca^{2+} concentration. Once the reactions reach the equilibrium between limestone dissolution/precipitation, the Ca^{2+} concentration is stable and no further decrease in the concentration was observed afterwards (Fig. 5.13).

$$Ca^{2+} + {CO_3}^{2-}{}_{(aq)} \leftrightarrow {CaCO_3}_{(solid)} \quad (5.9)$$

5.1.5.2 Other ion concentration

Changes in other ion concentrations were also measured. The sample collection started before the CO_2 injection, and was collected following the 2,982 minutes (~2 days) CO_2 injection as well as during the buffering period.

A clear trend was observed for Mg^{2+} concentration, as presented in Fig. 5.14. The initial Mg^{2+} concentration for all three ports was similar and around 18 mg/L. During the CO_2 injection an increase in Mg^{2+} concentration from 18 mg/L to 21 mg/L was observed. During the buffering period, the dissolution of Mg continued. Fig. 5.14 shows similar trends in all the three ports, with the first increase in S1 corresponding with the starting of the CO_2 injection. The recorded values are similar for all the three ports during the CO_2 injection. At the end of the injection, Mg^{2+} concentration in S1, S3 and S5 increased by an average of 19%, compared to the original conditions. After the buffering period, Mg^{2+} in S1,

S3 and S5 increased further by an average of 49%, compared to the original conditions.

The observed dissolution of Mg was due to the increased concentration of H^+, which was also observed by other research (Berthe et al., 2011; Parnell Jr and Burke, 1990). The further increase in Mg^{2+} concentration during the buffering period correlated with the increase in the pH once the CO_2 injection was stopped (Golubev et al., 2005; Pokrovsky et al., 2009) as presented in Fig. 5.8.

Different changes in concentration were observed for other trace elements (Fig. 5.15). In general, ionic concentrations reached the highest levels towards the end of the CO_2 injection. Al concentrations in S1, S3 and S5 increased by an average of 18% compared to the original conditions. Fe concentration increased by an average of 119%. Cd concentration increased by an average of 22%. As concentration increased by an average of 98%. The detection limits for ICP/MS for most ions general ranges from 0.1 to 10 ppt, and it can be higher for some ions. For example, the detection limits of Zn and Fe are a few tens of ppt for most occasions and ranges from a few tenth ppt to 200 ppt for Al (Ho et al., 2010). The concentrations of these trace elements were in μg/L and they were higher than the detection limits of ICP/MS as stated above. However, the low concentrations could influence the accuracy of the results and lead to the unclear trend in the ion concentration after CO_2 intrusion.

The concentration of each element is below safety limits for biological impact, as described in section 2.2.2. For example, as stated in section 2.2.2.2, the tolerance of As varies between different plants and damage to root membranes was observed when exposing to 10 mg L^{-1} As (Barrachina

et al., 1995). The highest concentration of As for S1 is 0.80 μg L^{-1}, which is much lower than the harmful level. Similarly, as stated in section 2.2.2.1, the highest concentration of Al for S1 is 2.92 μg L^{-1} (equivalent to 2.92×10^{-3} μg cm^{-3}), which is far less than the Al biological toxic limit (1 μg cm^{-3} to 40 μg cm^{-3} (Hesse, 1971a; Poschenrieder et al., 2008). As describe in section 2.2.2.2, Yildiz (2005) confirmed the previous research and concluded that increased Cd dose in nutrient culture up to 10 mg/L will causes large yield reduction, for example 75 % for bean, 65 % for sugar beet, and 40 % for maize. The highest concentration of Cd in S1 is 0.06 μg/L, which is much less than the biological toxic limit. As described in section 2.2.2.6, the critical deficiency level for Fe in leaves is in the range of 50-150 mg kg^{-1}. Concentrations of Fe above 500 μg g^{-1} dry weight are generally considered to be the critical toxicity content, but very much dependent on other factors, such as other nutrients supplement (Fang and Kao, 2000; Marschner, 1995). The highest concentration of Fe of S1 is less than 4 μg L^{-1}, which is far below safety limits for biological impacts for plants.

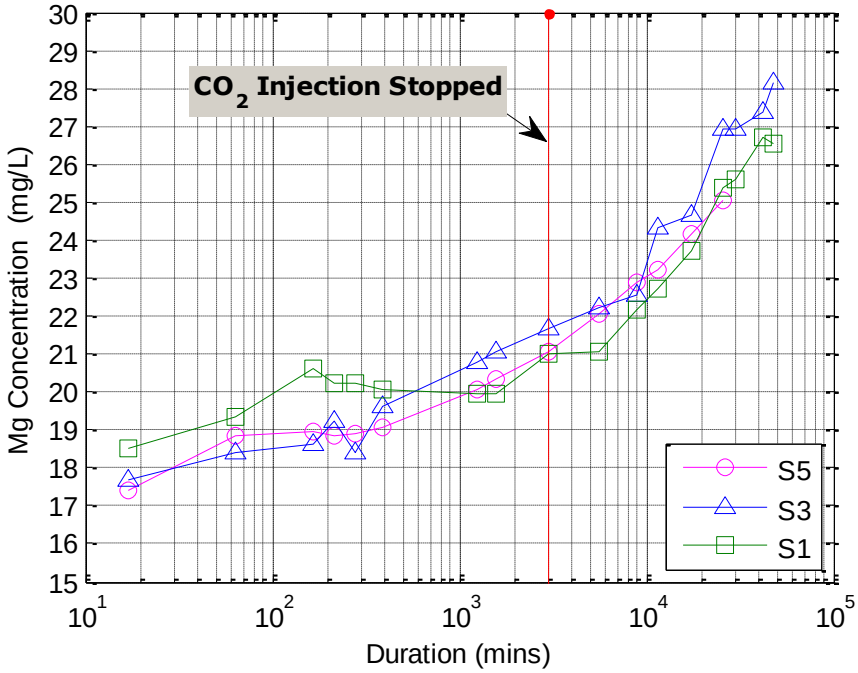

Fig. 5.14 Changes in Mg^{2+} concentration in S1, S3 and S5 following the CO_2 injection of Run 4.

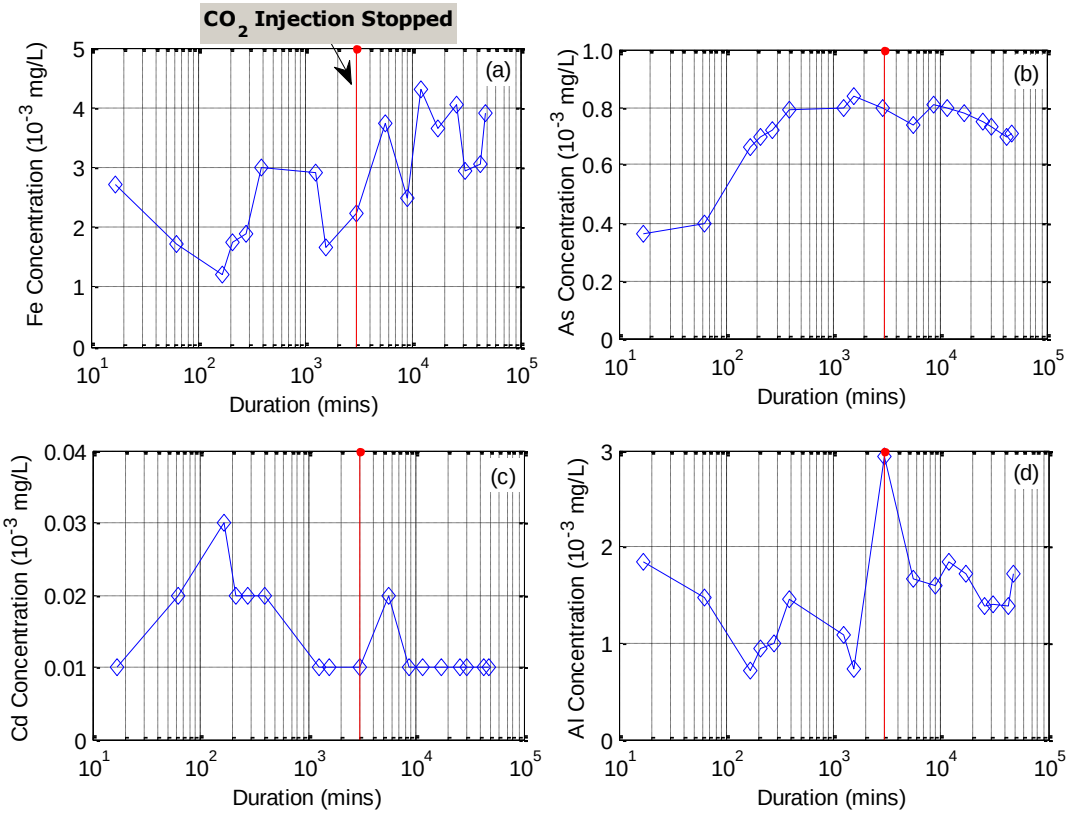

Fig. 5.15 Changes in concentration of Fe, As, Cd, Al of S1 following the CO_2 injection of Run 4.

5.1.6 Changes in alkalinity

The alkalinity was also measured in Run 4, as described in section 3.2.5.3. The carbonate concentration was close to zero throughout the experiment. The alkalinity is therefore presented here as bicarbonate concentration, (mg/L as $CaCO_3$ equivalent).

The alkalinity of S1 increased from about 216 mg/L to up to 1,482 mg/L, following the CO_2 injection (Fig. 5.16). The bicarbonate concentration increased sharply from 216 mg/L to 470 mg/L during the first five minutes, after it was within a range of 387-486 mg/L for the following 1.5 hours with moderate oscillation in the values. Another sharp increase took place after 100 minutes towards the end of the CO_2 injection. The vertical line in Fig. 5.16 indicates the point where the CO_2 injection stopped (two days and 100 minutes after the CO_2 injection) and presents the highest alkalinity value of 1,482 mg/L. Within the following first six days after the CO_2 injection stopped, the alkalinity decreased to its lowest point, 1,020 mg/L. The alkalinity fluctuated during the following buffering period within a range of 1,025-1,095 mg/L. The highest alkalinity concentration was correlated with the peak CO_2 concentrations in the column (Fig. 5.16). The increase in soil alkalinity was typically associated with increased levels of CO_2 (Andrews, 2001; Ardelan et al., 2009; Macpherson et al., 2008; Raymond and Cole, 2003).

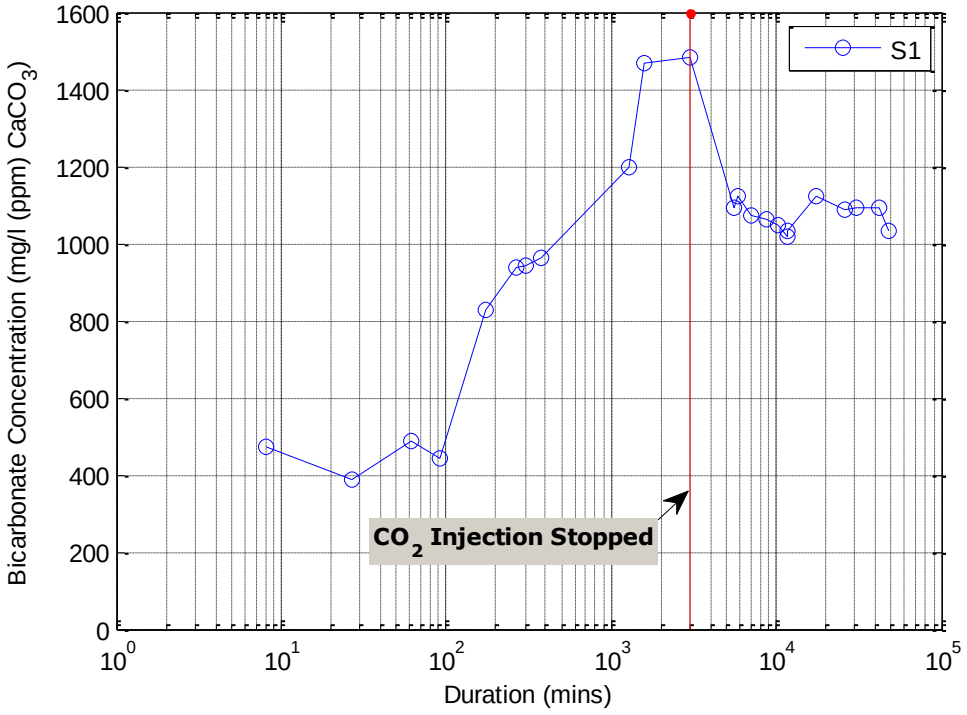

Fig. 5.16 Alkalinity changes of S1 in the CO_2 column of Run 4.

The change in the alkalinity can be explained as follows. As described in section 5.1.2, when the CO_2 was firstly injected into the system, the injected CO_2 reacted with water to form bicarbonate and carbonate and this lead to the quick increase in the bicarbonate concentration for the first 10 minutes. In the meanwhile, with the CO_2 injection, the H^+ within the solution was increased by reactions (5.1)-(5.4). With high concentrations of H^+, HCO_3^- and CO_3^{2-}, the reactions (5.3) and (5.4) also reversed back to form bicarbonate and $H_2CO_3^*$. Due to these reactions and the equilibrium between the water and solid limestone sand, the bicarbonate concentration in the water phase increased even higher after 100 minutes of CO_2 injection (Fig. 5.16).

Once the CO_2 injection stopped, a quick drop from 0.1 bar to ambient pressure was observed inside the column. The pressure change lead to

calcite precipitation as described in section 5.1.5, which was associated with the alkalinity decrease (Dreybrodt, 1999; Short et al., 2005). Besides, the quick pressure drop could lead to CO_2 degassing as described by Chen et al. (2004). The reactions (5.10) and (5.11) compensate for the quick decrease in CO_2 gas concentration. Overall, the equilibrium of these reactions lead to the decrease in the bicarbonate concentration once the CO_2 injection stopped. As the reactions are reversible there is a dynamic balancing dissolution/precipitation of limestone and therefore, the concentration of bicarbonates fluctuates during the run as in Fig. 5.16.

$$H_2CO_{3(aq)} \leftrightarrow CO_{2(gas)} + H_2O \tag{5.10}$$

$$H^+_{(aq)} + HCO_3{}^-_{(aq)} \leftrightarrow CO_{2(gas)} + H_2O \tag{5.11}$$

5.1.7 Changes in particle surface of sediments

In order to observe the surface changes after the CO_2 injection, SEM analysis was carried out for different runs on sediment samples. Table 5.1 lists the detailed description of the investigated samples. The S1-S5 and US1-US5 represent oven-dried sample only and ultrasonic bath oven-dried sample, respectively, as described in section 3.2.5.5.

Table 5.1 Description of samples for SEM imaging.

NO.	***RUN***	***DESCRIPTION***
S1	N/A	Original Trucal 5
S2	Run 1	Trucal 5+N_2 flow (Unsaturated conditions) from port C14 (Fig. 3.18)
S3	Run 1	Trucal 5+CO_2 flow (Unsaturated conditions) from port S14 (Fig. 3.18)
S4	Run 4	Trucal 5+CO_2 flow (Flooded conditions) from port S14 (Fig. 3.18)
S5	Run 4	Trucal 5+CO_2 flow (Flooded conditions) (Dome sample)
US1	N/A	Original Trucal 5
US2	Run 1	Trucal 5+N_2 flow (Unsaturated conditions) from port C14 (Fig. 3.18)
US3	Run 1	Trucal 5+CO_2 flow (Unsaturated conditions) from port S14 (Fig. 3.18)
US4	Run 4	Trucal 5+CO_2 flow (Flooded conditions) from port S14 (Fig. 3.18)
US5	Run 4	Trucal 5+CO_2 flow (Flooded conditions) (Dome sample)

Fig. 5.17 presents the SEM results for S1-S5. After observing the whole sample, a representative image of the sample was chosen and presented with 3000 times magnification. All the images were labelled with the corresponding sample number. The scale listed in all images is 20.0 μm. All the bigger pits of each image were measured and the dimensions are listed in the Figure. The biggest pit on the surface of the sample, S1, is about 6 μm in length, and there are only two of them. The pits in the sample S2 are bigger if compared with the ones in S1, the biggest pit being about 10 μm in length. The two biggest pits in the image for S3 are about 8 and 9 μm in length. The image for S4 shows more corroded and larger pits (10 and 16 μm in length) compared with S1. In the image of S5 more pits are identified; the largest of them are about 11 and 14 μm in length.

Compared with the original sample, bigger and more corroded pits are clearly visible in samples S2-S5. The increase of such erosion features in

S2 can be explained as the enhancing of the dissolution of the limestone sand due to acidified water by the dissolved CO_2 inside the column. In S3, no obvious corrosion pits can be seen on its surface. This could be caused by the much lower water content of the sediments in this point with subsequent reduced chemical reactivity. Bigger differences are shown in S4 and S5, either as an increase of the size of bigger pits or as an increase of the amount of pits on the surface. This can be due to the presence of more pore water as indicated by other research (Madland et al., 2006; Noiriel et al., 2004). These observations support one of the conclusions in the Stage I that the higher volume the pore water, the more the CO_2 will be absorbed leading to higher carbonate dissolution.

Similar and even clearer changes in the surface of sample are seen after the ultrasonic bath and oven dry process. The removal of the smaller particles from the surface of the bigger ones allowed a better imaging of the changes in the surface area after the CO_2 injection. Consistent results with S1-S5 were obtained from the US1-5, with more and larger pits shown with Trucal 5 sand after exposing to CO_2 under flooded conditions.

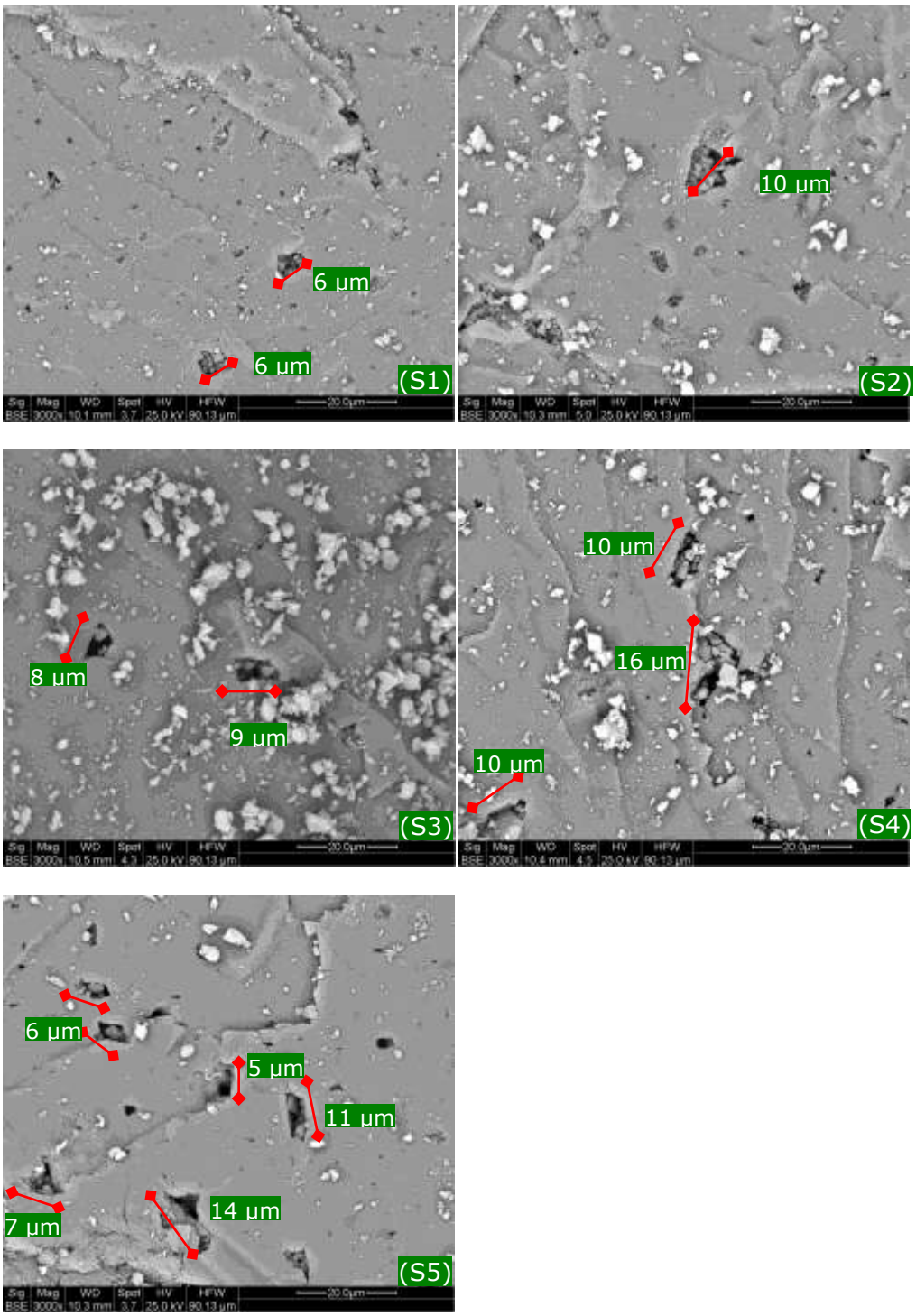

Fig. 5.17 SEM results for sample S1-S5.

5.1.8 Summary

Fig. 5.18 summarises the main parameters measured during Run 4, with Trucal 5 limestone sand under flooded conditions and CO_2 injected continuously. Due to the constant injection of CO_2 into the system (see flowrate change in Fig. 5.18 (a)), a change in the CO_2 concentration within the head space was recorded as shown in Fig. 5.18 (b). Fig. 5.18 (b) shows that CO_2 was detected after eight minutes of flowing through the sediments, and later the CO_2 concentration increased slowly for the following 20 minutes followed by a sharp increase towards the end of the injection. The CO_2 concentration reached its peak value after about 300 minutes. As stated in section 5.1, compared with the N_2 column, the injected CO_2 was detected in the head –space of the column about six minutes later than N_2. This delay can be explained by the dissolution of CO_2 in the porous water which slows its speed through the sediments. Fig. 5.18 (c) summarises the pH changes of S1 during the gas injection. A quick decrease in pH was noticed at the beginning of the injection. Within the first 12 minutes, the pH decreased from 7.57 to 6.30. This drop in pH can be explained by the reaction of the injected CO_2 with water forming H_2CO_3, which further released H^+. This is also supported by the observed changes in the CO_2 head-space concentration. A further decrease in the pH was observed during the injection and the pH dropped to around 6.10 (Fig. 5.18 (c)). The decrease in the pH resulted in the dissolution of limestone sand and the increasing in Ca^{2+} concentration (Fig. 5.18 (d)). A detailed description and explanation of the reactions are given in section 5.1.

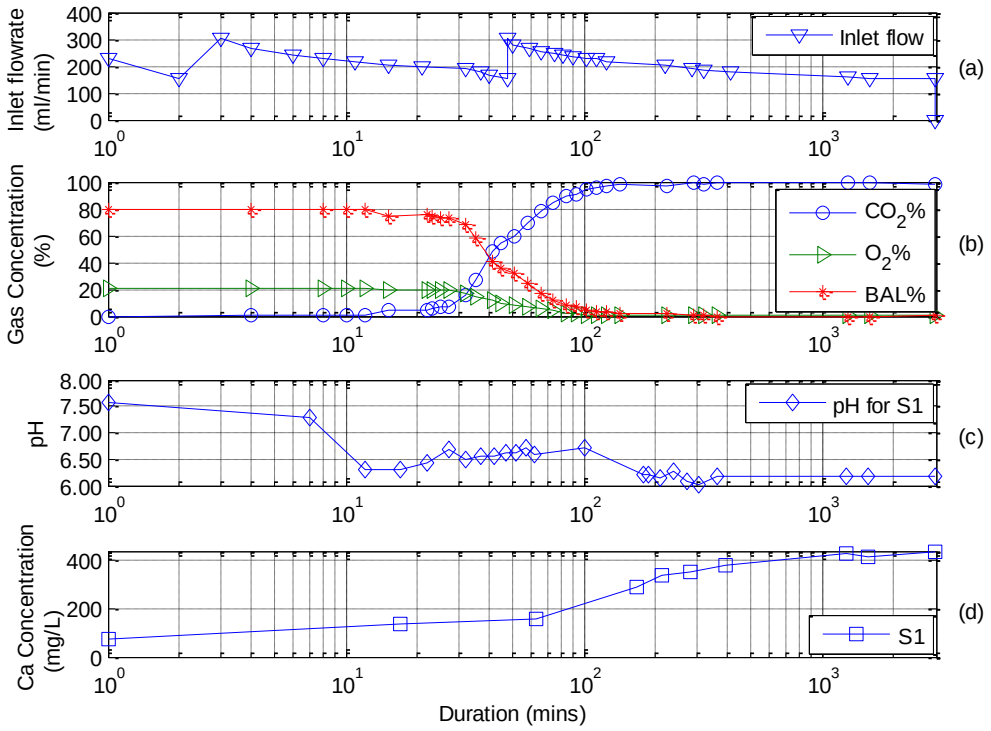

Fig. 5.18 Changes in the inlet flowrate (a), gas concentration in the head space (b), pH of pores water (c) and the exchangeable Ca^{2+} concentration (d) following CO_2 injection during Run 4, Trucal 5 under flooded conditions flowed by 100% CO_2. (The x-axis is logarithmic scale)

In summary, as described in section 5.1 and above, the injection of CO_2 into the limestone sand (Trucal 5) lowered the pH down to around 6.10. Because the limestone sand has strong buffering ability, after about two days of CO_2 injection, the pH was still above 6.10, which is higher than the pH of CO_2 saturated water at atmospheric conditions, 5.60 (Rowell, 1994b). Apart from the decrease in pH, the injected CO_2 caused continuous dissolution in the limestone sand and therefore increased the water alkalinity and the concentration of Ca and other major metals within the sample (such as Mg, Al, Fe, Cd, and As).

Once the CO_2 injection stopped, a slightly decrease in Ca^{2+} was noticed at the beginning and the value became stable for the following buffering

period. The response of Ca to CO_2 flux highlights that carbonate minerals are sensitive to CO_2 flux and could possibly be used as a parameter to monitor CO_2 leakage once the baseline is set.

5.2 Experiments on limestone sand Trucal 6

As explained in section 3.2.4, Run 5 and Run 6 (Table 3.5) were carried out with Trucal 6. The results with Trucal 6 are presented and discussed in the following sections.

5.2.1 Flowrate changes

5.2.1.1 Unsaturated conditions

Run 5 was carried out with Trucal 6 under unsaturated conditions. A decrease in the inlet flowrate was noticed, similar to Run 1-Run 4. The flowrate change and the calculated flowrate drop slope at each point were recorded and presented in Fig. 5.19. Similarly to Run 4, to minimise the interference with the column system for Run 5, the manual increase of the CO_2 inlet flowrate was kept at a minimum possible rate and frequency. Throughout the run, the inlet flowrate was increased twice as indicated in Fig. 5.19 (a).

It was observed that after the first manual increase in the flowrate, the inlet flowrate dropped from 300 ml/min to 188 ml/min within the following 55 minutes; after the second manual increase at 60 minutes, the flowrate dropped from 300 ml/min to 188 ml/min within the following 4,275 minutes (Fig. 5.19 (a)). The flowrate drop slope increased towards zero during the CO_2 injection. This indicates that the flowrate kept decreasing

during the run, but at a progressively slower rate (Fig. 5.19 (b)). A fluctuation in the flowrate was observed and a slight increase in the inlet flowrate was observed in Fig. 5.19 (a). This may be caused by the channelling formation, as explained in section 5.1.4, which may have changed the permeability of the sediments and further influenced the flowrate of the injected gas. A similar observation was noted by Hoefner and Fogler (1988). At t 4,355 minutes, the CO_2 injection was ceased. Overall, the CO_2 was injected into the system for about three days. The results are presented in the following sections.

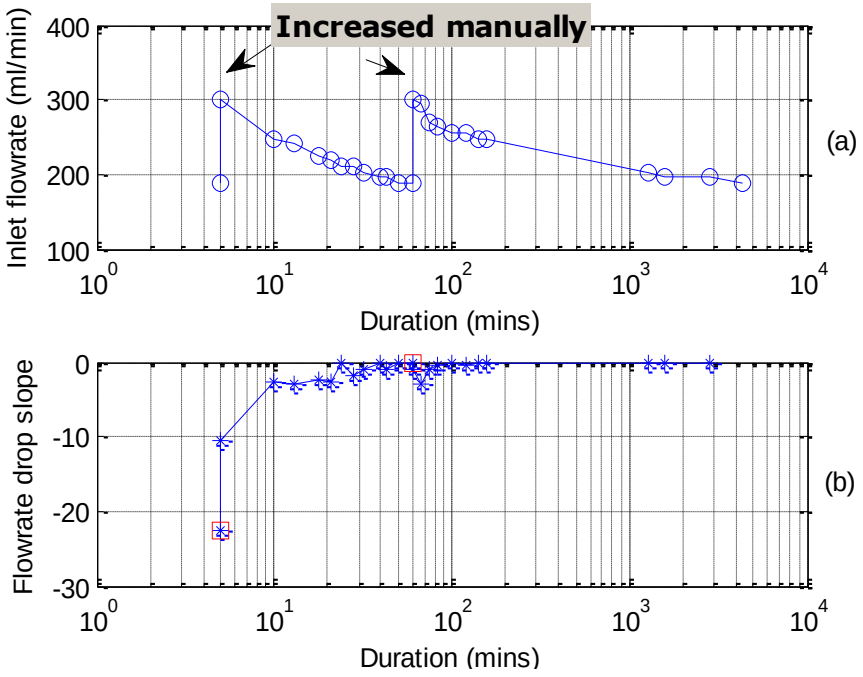

Fig. 5.19 Changes in the inlet flowrate and the flowrate drop slope for Run 5. (The x-axis is logarithmic scale)

5.2.1.2 Flooded conditions

Run 6 was carried out under flooded conditions. Similarly, the flowrate changes and the calculated flowrate drop slope at each point were recorded (Fig. 5.20 (a) and (b)). A continuous drop in the inlet flowrate

was observed with a slow dropping rate. Correspondingly, the inlet flowrate was manually increased once at the very beginning of the run, as indicated in Fig. 5.20. The flowrate decreased slowly from 300 ml/min to 146 ml/min during 8,804 minutes throughout the run, dropping to 157 ml/min in the first 1,735 minutes and nearly no change afterwards towards the end of the run. Fig. 5.20 (b) shows the flowrate drop slope and its increasing trend towards zero following the CO_2 injection. Similarly to the unsaturated conditions, an unstable change in the slope was observed at the beginning of the run, which may be caused by the channelling formation as explained before. After about 40 minutes, the drop slope in the flowrate was close to zero and stable for the following run. The CO_2 injection in Run 6 lasted for about six days.

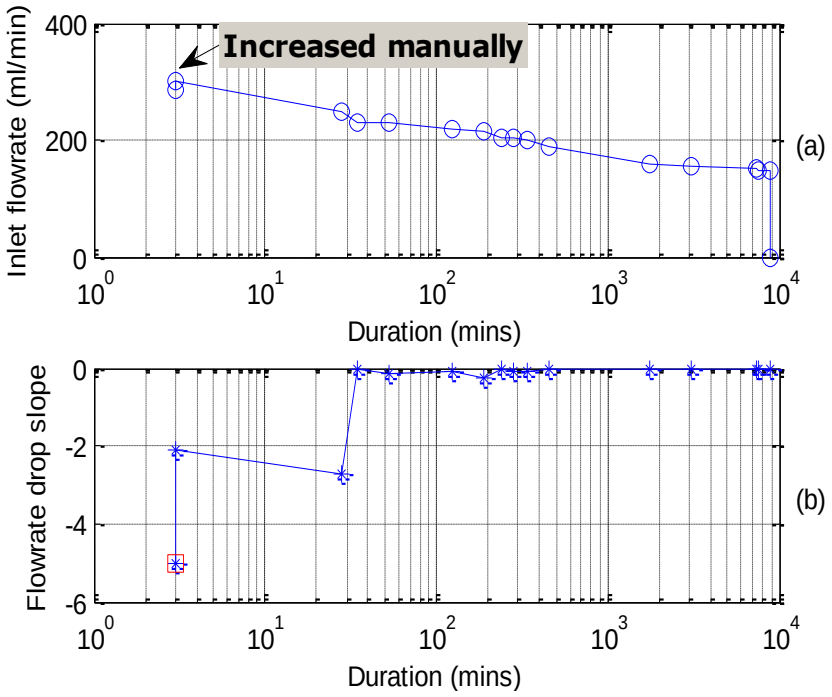

Fig. 5.20 Changes in the inlet flowrate and the flowrate drop slope for Run 6. (The x-axis is logarithmic scale)

5.2.2 pH changes

5.2.2.1 Flooded conditions

During Run 6, the water samples were collected from port S1, S3 and S5. The samples were used for both the pH measurement and ion concentration analysis to correlate with each other. The measured pH is presented as Fig. 5.21, with a ±0.01 standard error.

The initial pH (noted as pH at 0 minutes) in Run 6 was 7.07, 7.13 and 7.08 for S1, S3, and S5. Once the CO_2 was injected into the system, for S1, a slightly increase in the pH was noticed from 7.07 to 7.45 in the first 30 minutes, followed by a quick decrease from 7.45 to 7.01 from 30-45 minutes. Later, the pH was within a range of 6.94-7.13 from 50-230 minutes. From 230 to 400 minutes, another quick decrease in the pH was noticed from 6.94 to 6.31. After 400 minutes, no big changes in the pH were noticed, and the pH was within 6.17-6.29 until the end of the gas injection. When the CO_2 injection stopped at 8,807 minutes, the pH was 6.21. During the following 42 days buffering period the pH fluctuated within a range of 6.16-6.43, but no big increase in the pH was observed.

For S3, the pH started at 7.13. Similarly to S1, a slight increase in the pH was noticed once the CO_2 injected started, and the pH increased from 7.13 to 7.46 in the first 35 minutes. Later, a rapid pH decrease was observed from 7.46 to 7.21 in the following 15 minutes. From 50-108 minutes, the pH stabilised within the range of 7.18-7.29. From 108-260 minutes, a quick decrease in the pH was noticed, dropped from 7.29 to 6.47, and the pH was stable within 6.40-6.50 afterwards. At 1,745 minutes, the Rhizon sampler of S3 was damaged, and no more water was collected subsequently.

For S5, a similar pH trend was observed to that of S1 and S3 (Fig. 5.21). The initial pH for S5 was 7.08. For the first 35 minutes, the pH increased from 7.08 to 7.52, and later the pH decreased with a seesaw trend towards 6.30 until the end of the CO_2 injection. During the buffering period, the pH fluctuated between 6.22-6.48 and no big increase in the pH was observed. On 05/12/2011, which was the 12th day buffering, the water level decreased below the surface sediment (near S5 port). From this day, an increase of the pH of the collected water from S5 was observed. In the following 10 days (end of the run) buffering period, the pH continuously increased from 6.32 to 6.76.

As shown in Fig. 5.21, during the CO_2 injection, the first response in the pH was shown at S1 followed by S3 and S5. During the buffering period, there were variations in the pH between S1 and S5, which may be due to the decrease in the water level as explained above. No other differences were observed among the three ports.

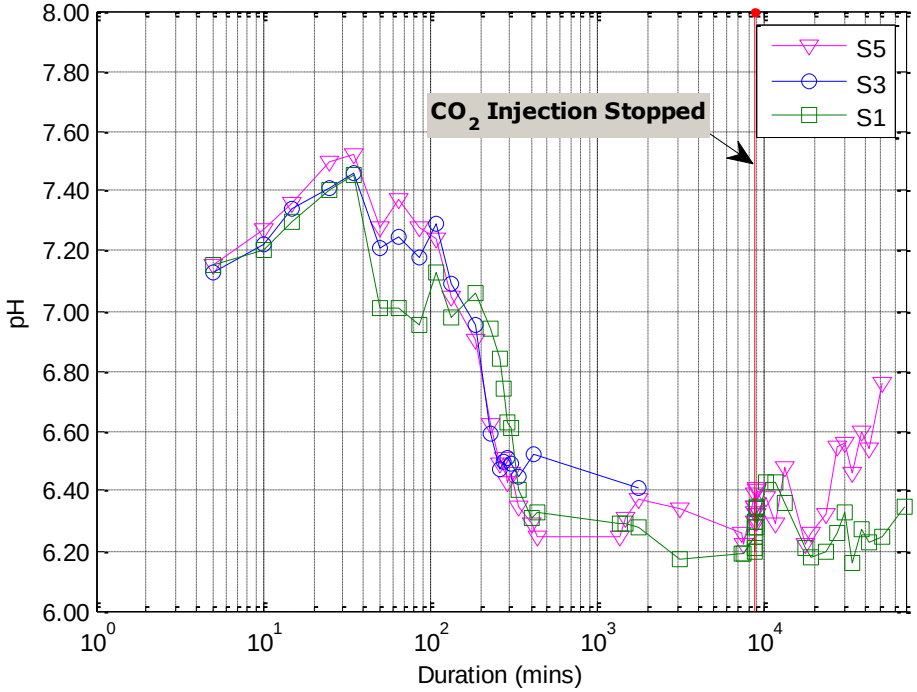

Fig. 5.21 pH changes of S1, S3, and S5 over time for Run 5.

As explained in section 5.1.2, the decrease in the pH was due to the reactions and equilibrium between CO_2, water, and the sediments. The slightly increase in the pH could be caused by the disturbance on the sediments by the injected gas, which enhanced the dissolution of limestone sand and further increased the alkalinity of the water (see section 5.1.2). Further results were analysed and compared to in the following sections explain the pH changes, such as changes in alkalinity, the gas concentration in the head-space and ion concentrations. Moreover, the changes in the pH of S5 after the 12^{th} buffering days showed that with less water, the pH rebounded back quicker than the pH under flooded conditions, as explained in section 5.1.2.

5.2.3 Gas concentration

5.2.3.1 Unsaturated conditions

The gas concentration within the headspace of the CO_2 column was assessed in Run 5, as presented in Fig. 5.22. BAL in the figure stands for the remaining gas in the head space except the CO_2 and O_2 and can be considered composed mostly of N_2. The accuracy of the gas measurement techniques was described in Table 3.6.

The initial concentration for the gas trapped in the headspace was CO_2% (0.00% vol), O_2% (19.20% vol) and BAL% (80.30% vol). Fig. 5.22 shows the gas concentration changes in the head space of the column system. CO_2 was detected after 40 minutes of flowing through the sediments (Fig. 5.22). A sharp increase in the CO_2 concentration was noticed afterwards. Within the following approximately two hours gas injection, the CO_2

concentration increased from 0.4% to 98.10%, with a decrease in the O_2 concentration from 19.40% to 0.10%. Later, the CO_2 concentration increased towards 99.9% slowly for the following injection. The CO_2 concentration reached its highest value, 99.9%, after about 3.5 hours of injection, with the O_2% decreased down to below the detection limit.

It is necessary to mention that, during Run 5, the gas discharge valve (V6 in Fig. 3.16) was accidently open during the first 30 minutes. This resulted in the injected gas releasing from the bottom valve, V6. Though there was a small percentage of the injected CO_2 gas flow through the sediments in the column, the changes in the concentration of the headspace would be expected to be small. Once the valve was properly closed, an increase in the CO_2 concentration was noticed, which was about 10 minutes after the problem was fixed. This event is to be considered in studying the CO_2 concentration trend for this specific run.

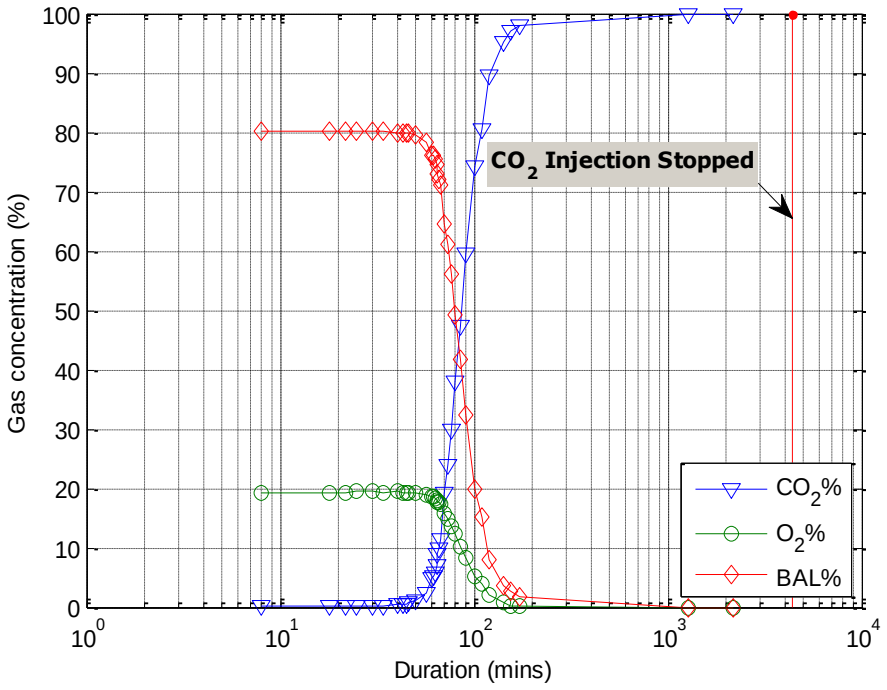

Fig. 5.22 Changes in the gas concentration of the head space inside the CO_2 column of Run 5.

5.2.3.2 Flooded conditions

The changes in the gas concentration were also measured following CO_2 injection for Run 6, and the results are presented in Fig. 5.23.

The initial concentration for the gas trapped in the headspace was CO_2% (0.04% vol), O_2% (19.20% vol) and BAL% (80.30% vol). About 1.10% CO_2 was detected after six minutes of flowing through the sediments and a sharp increase in the CO_2 concentration was noticed afterwards (Fig. 5.22). Within the following approximately two hours gas injection, the CO_2% increased from 0.04% to 97.60%, with a quick decrease in the O_2% from 19.00% to 0.40%. After two hours CO_2 injection, the increase rate in the CO_2% slowed down for the following injection. The CO_2 concentration reached to its highest value, 99.9%, after about 4 hours and 45 minutes CO_2 injection, with the O_2% decreased down to 0.0%. Similar to previous runs, Fig. 5.23 shows that even with a slow CO_2 injection inlet flowrate, a quick increase in the CO_2 concentration was noticed in Run 6, displacing the O_2 concentration and the remaining gas.

Compared with the N_2 column in Run 1-Run 4, where the injected N_2 gas came out of the column only after a few seconds, the delays in the detection of the CO_2 concentration could be caused by the reactions between the injected CO_2, the water and the sediments inside (see section 5.1.3). The differences between runs with Trucal 5 and Trucal 6 are highlighted and compared in Chapter 6.

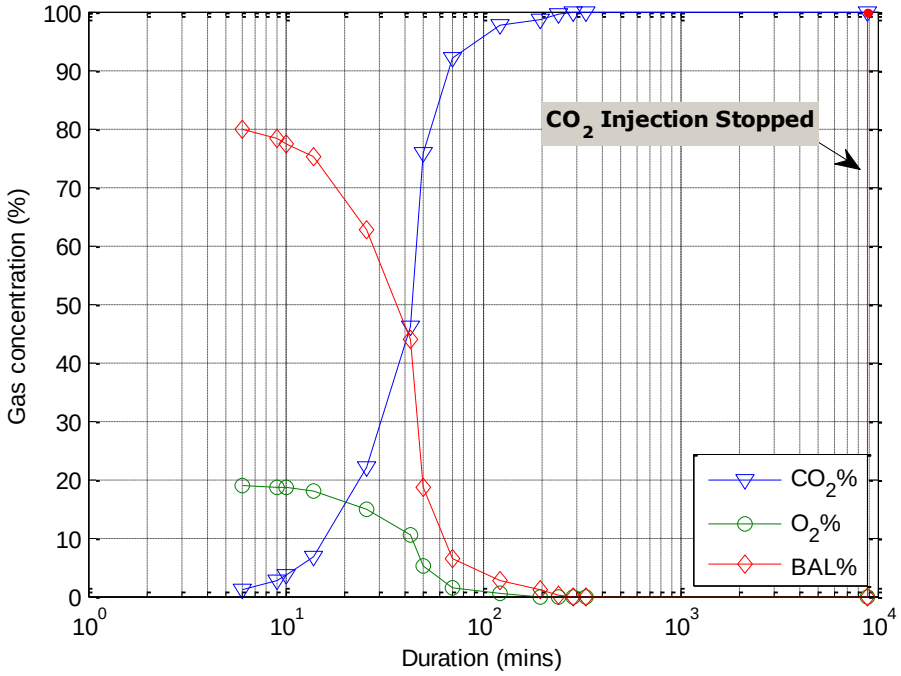

Fig. 5.23 Changes in the gas concentration of the head space inside the CO_2 column of Run 6.
Note: x-axis is logarithmic scale

5.2.4 Dome formation

Fig. 5.24 shows the top down view of Run 5 and the front view of Run 6 after the CO_2 injection. After the CO_2 injection, the sediments maintained the same depth as the pre-injection conditions, 55 cm. Unlike Trucal 5, no dome was noticed on the surface of the sediments at the end of the injection. It was noticed that with continuous injection of CO_2 into the column from the bottom, no gas was released from the top for a while and the gas was released later into the water as a plume. This phenomenon could be explained as that the injected CO_2 gas was trapped inside the column, accumulated in the sediments and eventually released outside when the pressure was high enough against the pressure caused by the water depth. During the injection, a channelling pathway was observed. However, the trapped CO_2 only uplifted the sediments slightly on the surface until the gas accumulated to a certain pressure and released

outside. When the trapped gas was released, the sediments settled down again.

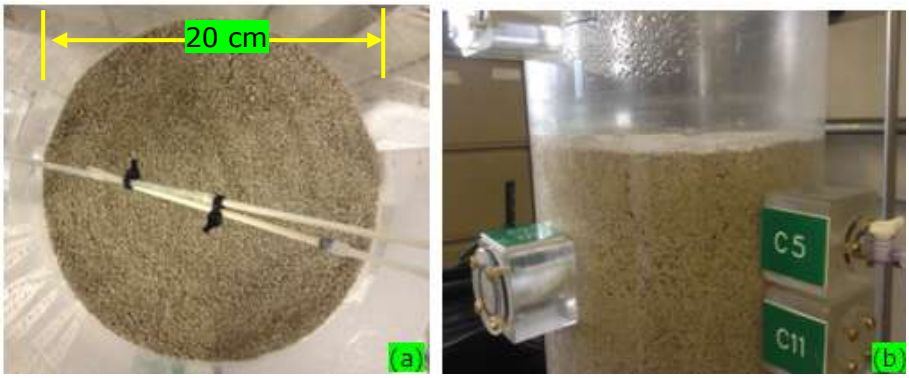

Fig. 5.24 Pictures for Run 5 and Run 6 after the CO_2 injection. (a) is a top down view for Run 5; and (b) is a front view of Run 6.

5.2.5 Exchangeable ion concentrations in the solution

5.2.5.1 Exchangeable-Ca

Fig. 5.25 presents the changes in the Ca^{2+} concentration of S1, S3 and S5 during Run 6. The results for S3 were incomplete because the Rhizon sampler was damaged after seven hours gas injection and no water could then be collected for the ICP/MS analysis. During the approximately six days of CO_2 injection, the samples were collected at the same time for all three ports, at 0 minutes, 15 minutes, 1.5 hrs, 4.5 hrs, 6.5 hrs, 24 hrs, 51 hrs, 126 hrs, 148 hrs following the CO_2 injection. Once the CO_2 injection stopped, the water samples were collected once a day at the beginning and less frequently for the following days to assess the buffering effects. The accuracy of the data presented in this section is the same as the previous measurement (see section 5.1.5).

The initial Ca^{2+} concentration for S1, S3 and S5 was 71.92 mg/L, 70.42 mg/L, and 66.22 mg/L, respectively. For S1, in the first 15 minutes, no big

difference in the Ca^{2+} concentration was observed compared with the initial conditions. For S1, from 15 minutes to 1.5 hrs, the first slightly increase in the Ca^{2+} was noticed from 65.84 mg/L to 90.37 mg/L. Later on, a sharp increase was observed during 1.5 hrs to 24 hrs, and the Ca^{2+} concentration increased about 290 mg/L from 90.37 mg/L. For the following five days gas injection, the Ca^{2+} concentration was within 380-400 mg/L (Fig. 5.25). Overall, after about six days of CO_2 injection, the Ca^{2+} concentration increased about 325 mg/L, with a peak value of 397.60 mg/L at the end of the gas injection. When the CO_2 injection stopped, the Ca^{2+} concentration was within a range of 373-403.80 mg/L. A similar trend was obtained for samples collected from S3 and S5. As stated above, after about six hours gas injection, no water could be collected from S3. Thus, only four samples were collected from S3 (Fig. 5.25).

A similar trend in the Ca^{2+} concentration of S1 was observed for S5 (Fig. 5.25). Overall, during the approximately six days of CO_2 injection, the Ca^{2+} concentration increased 320 mg/L from 66.22 mg/L. Once the CO_2 injection stopped the Ca^{2+} concentration decreased remaining within a range of 372-390 mg/L during the first ten days of the buffering. As described in Section 5.2.2, the water level decreased below the S5 port at the 10^{th} day buffering. After that, the Ca^{2+} concentration of S5 decreased continuously from 372.90 mg/L to 257.20 mg/L until the end of the buffering period (19 buffering days). Overall, for S1, S3 and S5, after about six days CO_2 injection, the Ca^{2+} concentration increased by an average of 469% compared with the initial conditions, 70 mg/L.

By comparing the pH values of each port in Fig. 5.25, a small but noticeable change among these ports was observed at the beginning of the run. After 10 minutes of CO_2 injection, the increase in Ca^{2+} started

first in port S1 and then followed by S5 and S3, which corresponded with the first pH changes in S1 (see Section 5.2.2). These changes indicated that the dissolution in S1 took place earlier than that in S5 and S3. After 100 minutes, the dissolution in S5 was higher than that in S1. This may be due to the increase in the CO_2 partial pressure within the head space, to which S5 is closer thus leading to quicker carbonate dissolution. With the exception of this, no other significant difference was observed from S1 and S5 during the gas injection process.

During the buffering period, the decrease in the Ca^{2+} concentration was higher in S5 than in S1. As explained in the previous section, the water at the level of S5 was insufficient to allow any sampling after 10 days of buffering assessment. After that, the Ca^{2+} concentration decreased quicker than that of S1. This change corresponded with the pH changes as in Fig. 5.21 and may be due to precipitation phenomena (as explained in Section 5.1.5).

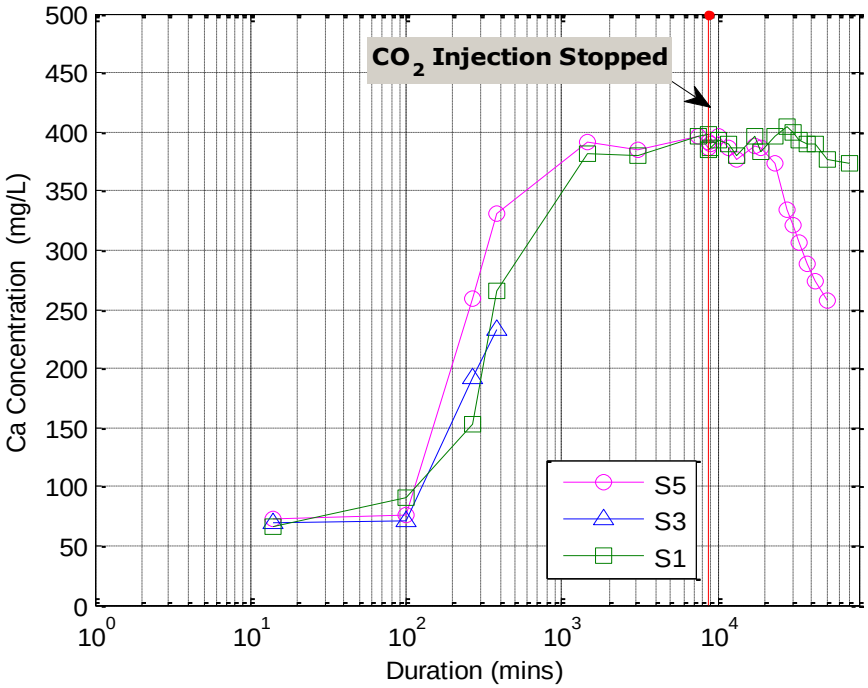

Fig. 5.25 Changes in the Ca^{2+} concentration of S1, S3 and S5 following the CO_2 injection of Run 6. (x-axis is logarithmic scale)

5.2.5.2 Other ion concentration

The concentration of other ions (Mg, Al, Fe, Pb, Cd, As and Hg) in the pore-water samples collected in S1, S3 and S5 during the run was also investigated. They are the major elements apart from $CaCO_3$ in Trucal 6 as described in Table 3.2. Sample collection was started before the CO_2 injection and the CO_2 injection was continued until 8,807 minutes. Even if the CO_2 injection stopped, water sample-collection was continued to assess the concentration changes during the following buffering period for a total of 16 samples until 69,318 minutes. A detailed description of the changes is presented in the following sections.

Changes in Mg concentration

A clear trend was observed in Mg concentration (Fig. 5.26). The initial concentration of Mg for all three ports were similar and around 14 mg/L. Once the CO_2 was injected into the system, a steady increase in Mg concentration was observed for S1. During the approximately six days CO_2 injection, the Mg concentration increased from 14 mg/L to 19 mg/L, reaching its peak value (19 mg/L) at the end of the injection (Fig. 5.26). During the buffering period, the dissolution of Mg continued with an oscillating trend towards the end of the run. Overall, during the approximately 42 days buffering period, Mg concentration increased about 1.07 mg/L from 19 mg/L. For S3, four samples were collected, and the changes in Mg concentration was similar to that of S1 (Fig. 5.26). For S5, a general increasing trend was also observed during the gas injection as that of S1. The Mg concentration reached its highest value of 18 mg/L when the CO_2 injection stopped. Similarly to S1, the dissolution of Mg

continued during the buffering period, and the Mg concentration increased about 1.57 mg/L from 18 mg/L.

Fig. 5.26 shows similar trends for all three ports, and no obvious differences were observed. After the CO_2 injection, the Mg concentration in S1, S3 and S5 increased by an average of 30% compared to the original conditions; while, after the approximately 42 days buffering period, overall the Mg concentration in S1, S3 and S5 increased by an average of 40% compared to the initial concentration, 14 mg/L.

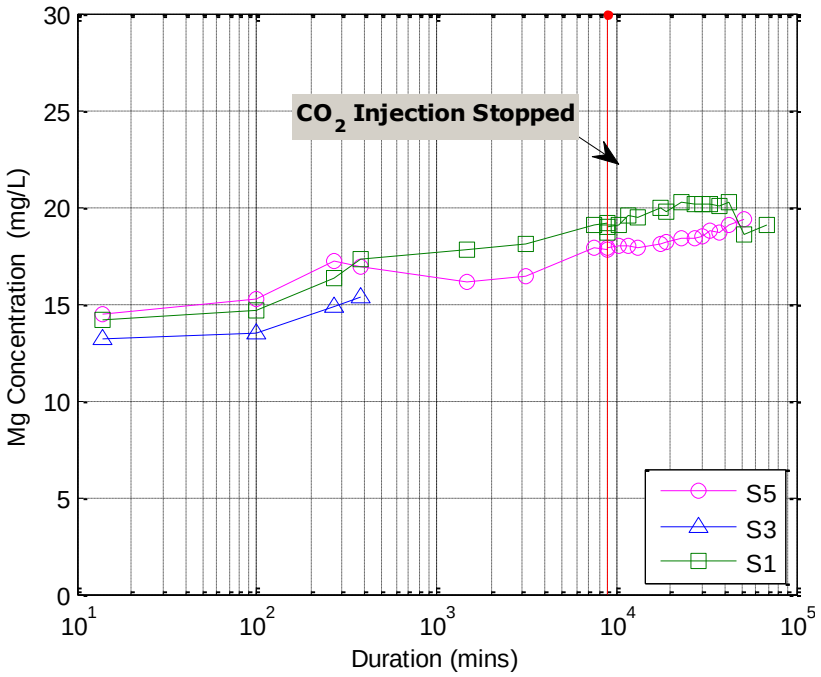

Fig. 5.26 Changes in Mg^{2+} concentration of S1, S3 and S5 following the CO_2 injection of Run 6. (The x-axis is logarithmic scale)

Changes in As concentration

There were changes in the concentration of other elements with a good consistency between all the three ports. A similar trend to the concentration of Ca was observed for As concentration. During the gas

injection, the concentration of As increased steadily at the beginning followed by a sharper rapid increase after 100 minutes. The concentration of As reached its peak value at the end of the CO_2 injection. After about six days of CO_2 injection, the concentration of As increased by an average of 149% compared with the original concentration of As, 0.24 µg/L. During the buffering period, a decreasing trend in the concentration of As was observed, and it decreased by an average of 20%.

No regular trends were observed in changes for other ions, which may be due to the low initial concentration of these elements. It is to be highlighted that the observed concentration of the increased element is still below safety limits for its biological impact as described in section 2.2.2.2. For example, the tolerance of As varies between different plants and damage to root membranes was observed when exposing to 10 mg/L As (Barrachina et al., 1995). The highest concentration of As for S1 and S5 were 0.69 µg/L and 0.64 µg/L, respectively. They are much lower than the harmful level.

5.2.6 Alkalinity

The changes of alkalinity were assessed for samples collected from the port S1 in Run 6, as presented in Fig. 5.27. The carbonate concentration was close to zero throughout the experiment. The alkalinity is therefore presented here as bicarbonate concentration, mg/L (ppm) as $CaCO_3$ equivalent.

The initial concentration for HCO_3^- was 180 mg/L as $CaCO_3$. During the first hour after the CO_2 injection, the concentration of HCO_3^- increased slowly from 180 to 216 mg/L. Another change in the concentration was

observed after the first hour, with a slow increase from 216 to 342 mg/L for the following 1.5 hrs and a sharp, continuous increase from 342 to 1,350 mg/L towards the end of the injection. When the CO_2 injection ceased, the alkalinity of S1 increased to 1,350 mg/L from 180 mg/L during the six days of CO_2 injection (Fig. 5.27). During the 42 days buffering period, the HCO_3^- concentration decreased a little bit and the HCO_3^- concentration was within a range of 1,110-1,317 mg/L. The results showed that the peak alkalinity concentration was correlated with the CO_2 injection, and the highest concentration was achieved at the time of the CO_2 injection stopped.

As explained in section 5.1.6, the changes in alkalinity resulted from the reactions and equilibrium among water, CO_2 and sediments. The injected CO_2 gas enhanced the dissolution of sediments within the column and influenced the alkalinity values.

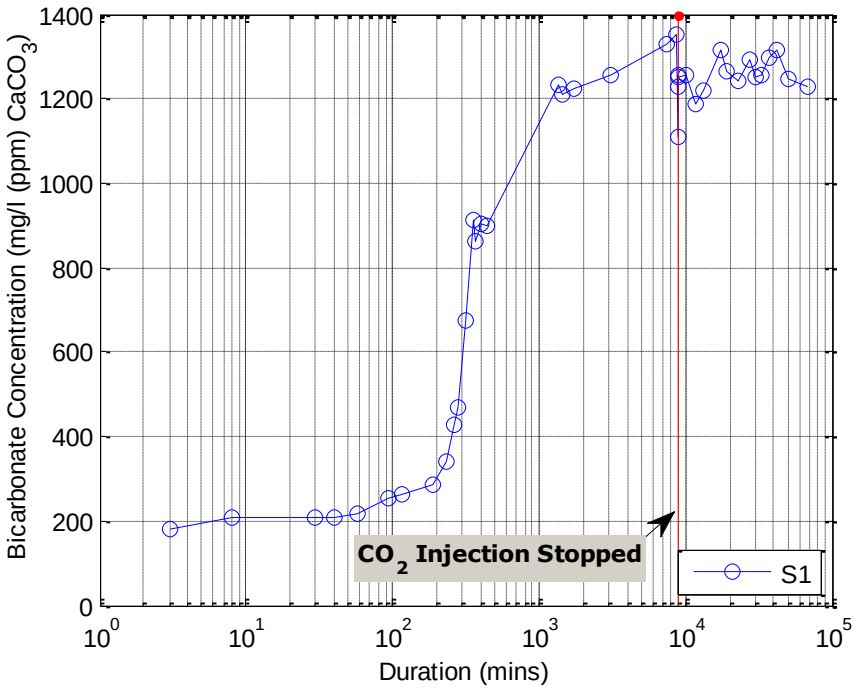

Fig. 5.27 Alkalinity changes (as bicarbonate concentration, mg/L as $CaCO_3$ equivalent) over time for samples collected from S1 during Run 6. (The x-axis is logarithmic scale)

5.2.7 Summary

Fig. 5.28 summarises the main parameters measured during Run 6, with Trucal 6 limestone sand under flooded conditions and CO_2 continuously injected.

Due to the injection of CO_2 (Fig. 5.28 (a)), a change in its concentration within the head space was recorded in Fig. 5.28 (b). CO_2 was detected after six minutes of flowing through the sediments, and later the CO_2 concentration increased steadily for the following 30 minutes followed by a sharp increase until the end of the CO_2 injection (Fig. 5.28 (b)). The CO_2 concentration reached its peak value, around 99%, after about 200 minutes. Fig. 5.28 (c) summarises the pH changes of S1 during the gas injection. An increase in the pH was noticed at the first 50 minutes after the CO_2 injection, and the pH stabilised around 7.00 during 50-200 minutes. The pH decreased quickly to 6.30 from 200 to 400 minutes. A further decrease in the pH (down to around 6.20) was noticed after two days of gas injection. The pH was then stable around 6.20 for the following four days of gas injection (Fig. 5.28 (c)). As explained in section 5.2, the decrease in the pH caused the dissolution of limestone, with an increase in the Ca^{2+} concentration (Fig. 5.28 (d)). The reactions between water-CO_2-sediments reached the equilibrium at pH 6.20 which was the lowest value recorded. As in the run with Trucal 5 the buffering potentiality of the limestone reduced the drop in pH to 6.20 instead of the 5.6 value of pure water in equilibrium with CO_2 at atmospheric pressure.

Apart from the decrease in the pH, the injected CO_2 caused continuous dissolution of limestone, increased water alkalinity and increased concentration of Ca and other major metals such as Mg and As. No regular

trends were observed for other trace elements. Once the CO_2 injection stopped, a slightly decreasing in Ca^{2+} concentration was noticed at first and was then stable for the following buffering period as in Trucal 5 experiments. This highlights that carbonate minerals are sensitive to CO_2 flux, being easily dissolved if exposed to CO_2 as in case of seepage. Due to this characteristic, anomalous high dissolution rates in carbonate minerals could be used as an indicator for CO_2 seepage.

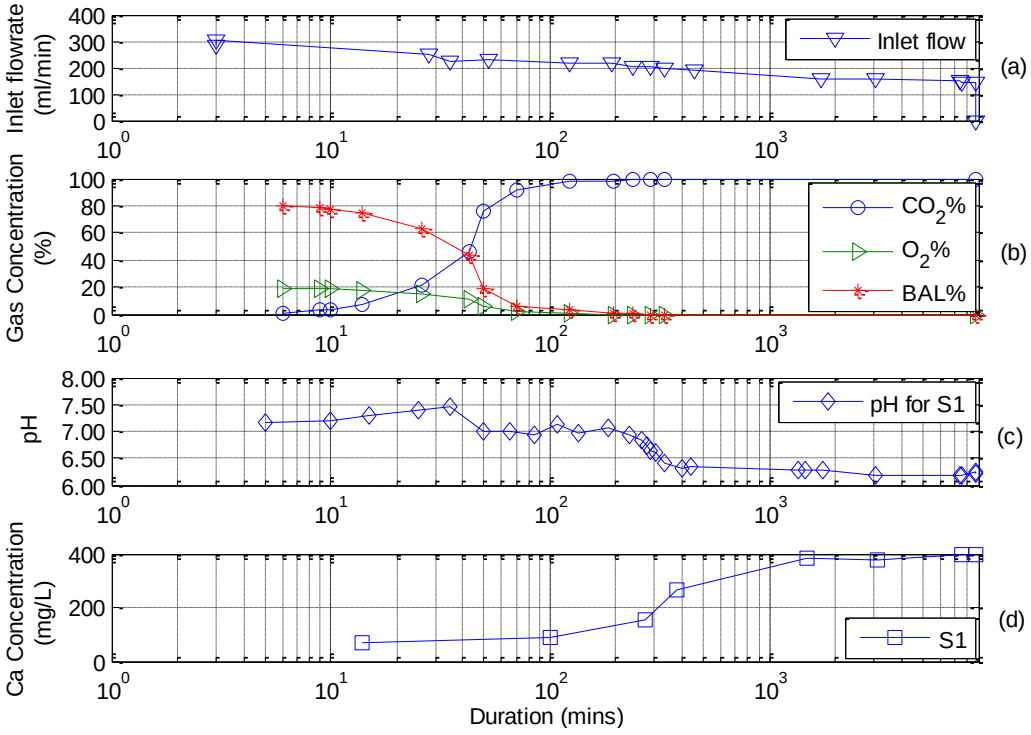

Fig. 5.28 Changes in the inlet flowrate (a), gas concentration in the head space (b), pH of pore water (c) and the exchangeable Ca^{2+} concentration (d) following CO_2 injection during Run 6, Trucal 6 under flooded conditions flowed by 100% CO_2.

5.3 Experiments on silica sand

As explained in section 3.2.4, Run 7 and Run 8 (Table 3.5) were carried out with silica sand to compare with the results with limestone sand. The comparison as below was carried out to assess the correlation between

sediments properties and its response to CO_2 release, variations in sediments chemical composition (carbonate vs. silica).

5.3.1 Flowrate changes

5.3.1.1 Unsaturated conditions

Run 7 was carried out with the silica sand under unsaturated conditions. A steady but slow decrease in the inlet flowrate was noticed, as presented in Fig. 5.29. As the flowrate did not decrease significantly following the CO_2 injection, the inlet flowrate was increased only once during Run 7 (as indicated in Fig. 5.29).

During the first day of the CO_2 injection, the inlet flowrate decreased from 300 ml/min to 158 ml/min within 1,470 minutes. The inlet flowrate was then increased manually to 300 ml/min, and the flowrate was stable around 300 ml/min for the following injection period. The gas injection lasted for two days. The changes in pH, the gas concentration within the head space and the ion concentration were investigated during as well as after the injection, as presented in the following sections.

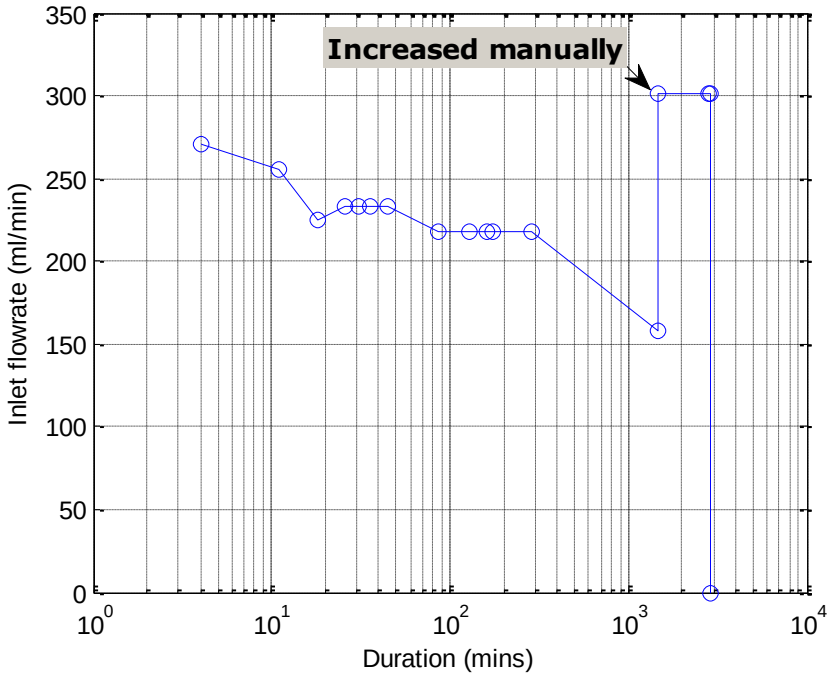

Fig. 5.29 Inlet flowrate changes over time- Run 7. The gas injected was ceased at 2,880 minutes. (The x-axis is logarithmic scale)

5.3.1.2 Flooded conditions

Run 8 was carried out under flooded conditions. Similarly to previous runs, a decrease in the inlet flowrate was noticed. The flowrate changes were recorded and presented as Fig. 5.30. During the run, the inlet flowrate was increased manually twice to 300 ml/min, as indicated in Fig. 5.30.

During the first 40 minutes of the CO_2 injection, the inlet flowrate decreased from 300 ml/min to 225 ml/min. The inlet flowrate was then increased manually to 300 ml/min. From 40-310 minutes, the flowrate dropped from 300 ml/min to 210 ml/min. The flowrate was manually increased to 300 ml/min again then. Until the CO_2 injection stopped, no further increase in the inlet flowrate was applied. At the end of the gas injection, the flowrate dropped to 218 ml/min during the two days gas injection. The whole gas injection process lasted for two days and five

hours. The changes in the pH, the gas concentration within the head space and the ion concentration were studied during the injection as well as after the injection. The results are presented in the following sections.

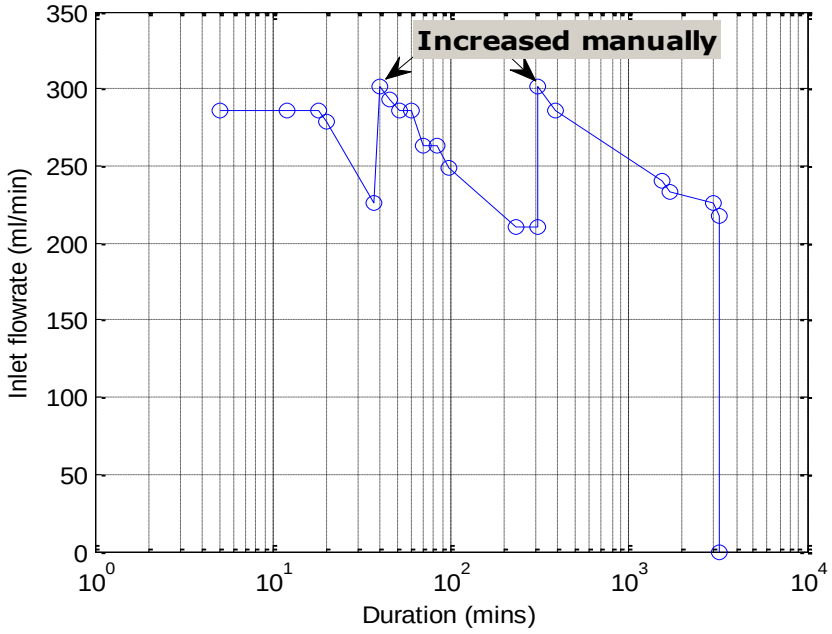

Fig. 5.30 Inlet flowrate changes over time- Run 8. The gas injection ceased at 3,185 minute. (The x-axis is logarithmic scale)

5.3.2 pH changes

5.3.2.1 Unsaturated conditions

During Run 7, the pH meter was left and sealed inside the columns (port S8, S10 and S11) to measure the pH constantly. The measured pH is presented in Fig. 5.31. All the data presented in Fig. 5.31 has a ±0.01 standard error.

Before the CO_2 was injected into the system, the initial pH for the sediments was around 7.40 for all the three ports, S8, S10 and S11. For S8, once the CO_2 was injected into the system, a sharp decrease in the pH was noticed. The pH decreased from 7.40 to 5.71 within 15 minutes. Later,

the pH was stable around 5.60 for the following injection period. When the CO_2 injection stopped, the pH of S8 was 5.57. Similar trend was also observed in S10 and S11, with a slightly delay in the pH drop compared with that of S8. For S10, the pH decreased from 7.45 to 5.89 after 40 minutes, while for S11, the pH decreased from 7.32 to 5.71 after 30 minutes. For the following CO_2 injection period, the pH of S11 was within a range of 5.60-5.77, while the pH of S10 was stable around 5.90. During the five days buffering period, no pH rebound was observed.

For the silica sand, due to its chemical composition (see Table 3.4), no significant weathering was expected during the gas injection (Blum et al., 1998; Romanak et al., 2012; Zheng et al., 2012). The main driving forces for the decrease in the pH during the CO_2 injection were the increase in the H^+ generated by the reactions between the injected CO_2 and water. The related reactions were presented in section 5.1.2.

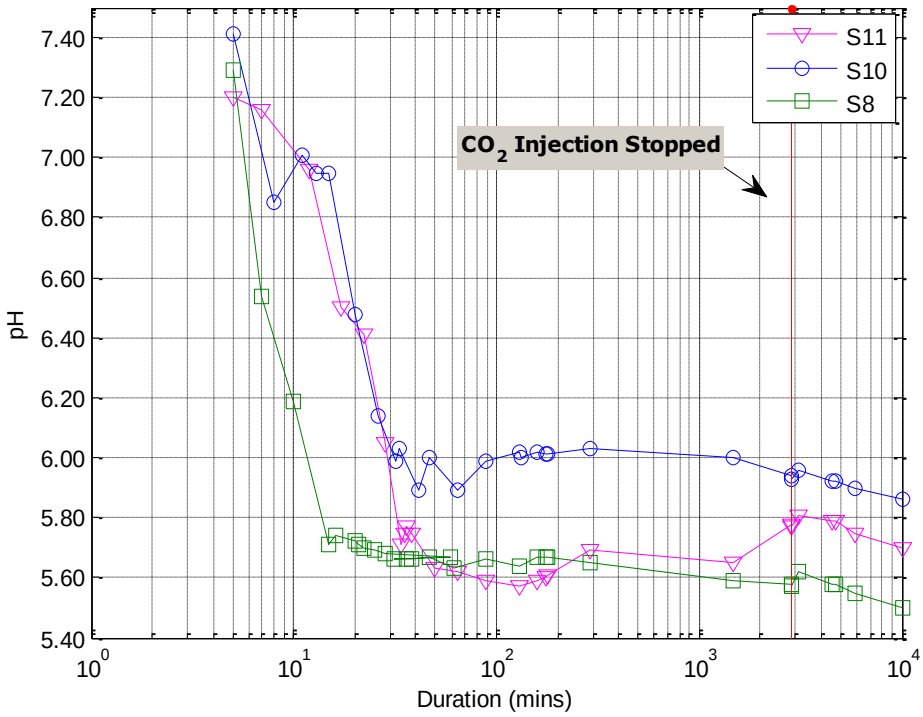

Fig. 5.31 pH changes of S8, S10, S11 over time for Run 7. Note: x-axis is logarithmic scale

5.3.2.2 Flooded conditions

During Run 8, the water samples were collected from S1, S3 and S5. The measured pH is presented as Fig. 5.32 with a ±0.01 standard error.

The initial pH for sediments in Run 8 was 7.23, 7.14 and 7.30 for S1, S3, and S5. For S1, a sharp decrease in the pH was noticed after five minutes gas injection decreasing from 7.23 to 5.83. Later, the pH decreased slowly towards 5.50 during the following CO_2 injection. There was a seesaw effect in pH of S1 for 100 minutes, which may be caused by the diffusion of H^+ within the column. The continuous injection of gas may disturb the water within the system causing the fluctuation in pH. For S3, a similar change in the pH was observed. The first rapid decrease in pH was over the first five minutes, with a decrease from 7.14 to 6.35. Later, the pH decreased with fluctuation towards 5.60 during the gas injection. When the CO_2 injection stopped after about three days, the pH decreased to 5.65. For S5, a continuous decrease was observed in the pH of the collected water sample. The pH firstly decreased from 7.30 to 6.06 within 25 minutes, and later it decreased towards 5.40 from 25-60 minutes. The pH was stable around 5.40 after 60 minutes. During the buffering periods, the pH for all three ports was slightly increased (0.4 units) with no significant changes. Comparing the pH increase (1.5 units) with limestone sand Trucal 5 after CO_2 injection stops, the small increase in pH with silica sand indicates its weak buffering ability.

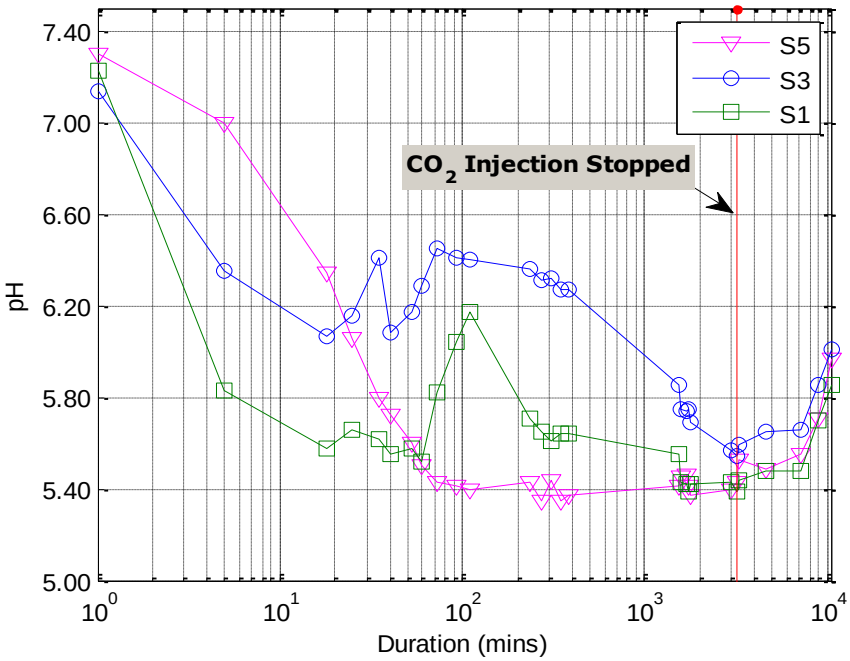

Fig. 5.32 pH changes of S1, S3, S5 over time for Run 8. Note: x-axis is logarithmic scale

5.3.3 Gas concentration

The gas concentration within the head space was recorded during Run 8 as presented in Fig. 5.33. The initial concentration for the gas trapped in the headspace was CO_2% (0.03%), O_2% (19.30%) and BAL% (80.50%). BAL in Fig. 5.33 stands for the remaining gas in the head space except the CO_2 and O_2 and can be considered composed mostly by N_2. The accuracy of each measurement by GA 2000 is presented in Table 3.6.

Fig. 5.33 shows that CO_2 is detected at 0.3% after five minutes of flowing through the sediments. A sharp increase in the CO_2 concentration was noticed afterwards. Within the following approximately two hours of gas injection, the CO_2 concentration increased from 0.3% to 97.90%, with a decreasing in the O_2 concentration from 19.20% to 0.20%. Later, the CO_2 concentration increased slowly towards the end of the injection, and

reached its highest value, 99.9%, after about four hours of CO_2 injection, with the O_2% decreased down to 0.0%.

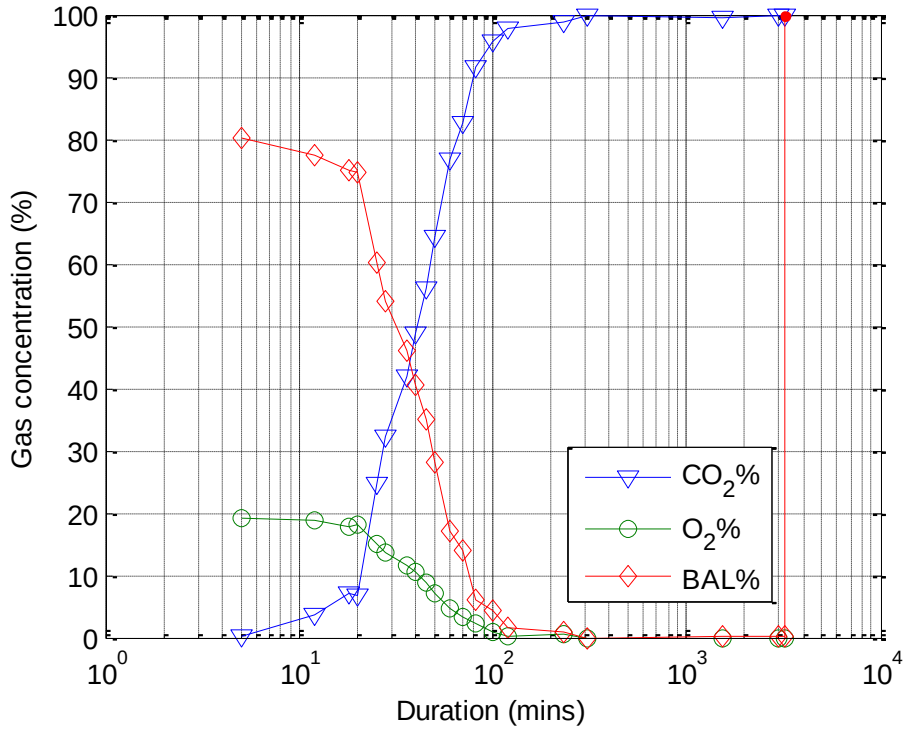

Fig. 5.33 The changes in the gas concentration of the head space inside the CO_2 column of Run 8.
Note: x-axis is logarithmic scale

5.3.4 Dome formation

As in Run 3 and Run 4, a dome was observed at the end of the CO_2 injection of Run 8. Fig. 5.34 shows the front view and the side view of the dome after the run. At the end of the run (about two days and five hours of CO_2 injection), the highest level of the dome was about 5.5 cm above the silica sand surface. During the run, channelling of the injected CO_2 gas was observed with some gas trapped between the sediments. The process and reasons for the formation of a dome in Run 8 are similar to Run 3 and Run 4 as explained in section 5.1.4.

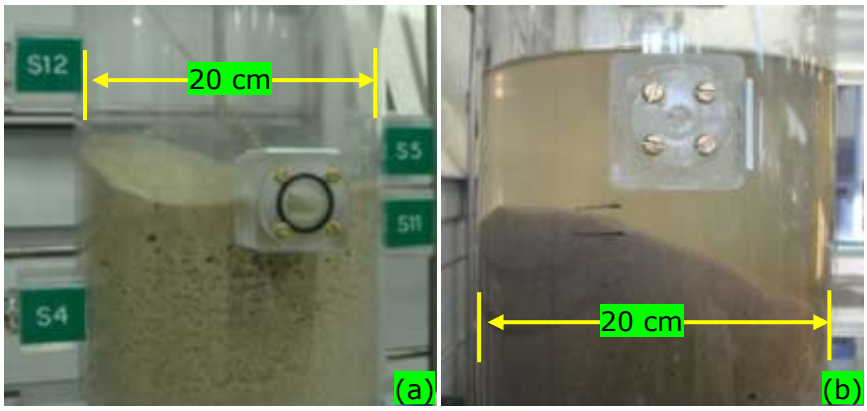

Fig. 5.34 Front view (a) and side view (b) of the dome formed of the CO_2 column after the gas injection- Run 8. Voids filled with gas are clearly visible inside the sediments on the left of the figure.

5.3.5 Exchangeable ion concentrations in the solution

The water samples were collected from ports S1, S3 and S5 and analysed by ICP/MS. During the run, the CO_2 injection was continued until 3,190 minutes. Water sample-collection was continued later to assess the concentration changes during the following buffering period. The major ion concentrations over time in the samples from Run 8 are presented in Appendix 8.

A general increase in all the major ions was observed but at different scales. By comparing the concentration at the end of the injection with the initial concentration, the ion concentrations increased 8% for Mg, 29% for Ca, 166% for Ti, 280% for Mn, 590% for Cr, 1,400% for Fe and 1,430% for Al. No big difference in the ion concentration was observed after the CO_2 injection stopped. A detailed description of the concentration of selected major elements is presented as follows.

5.3.5.1 Exchangeable-Al

Exchangeable-Al was assessed during the run and presented in Fig. 5.35. An increase in the concentration in all the three ports was noticed. At the end of the CO_2 injection, Al concentration in S1 was approximately 1,732% times higher than its initial concentration, while the concentration increased 1,403% and 1,155% compared to the initial conditions in S3 and S5 respectively (Fig. 5.35). The results indicated that the Al was mobilised and released from the sediments when CO_2 was present. Similar trends were shown in Fe and Ti concentration with a lower increase rate compared with Al.

Mobilisation of Al from sediments was also observed in Stage I experiment (section 4.4.1) and has been previously reported (Ardelan et al., 2009; Blake et al., 1999). As explained in section 4.4.1, when the CO_2 is injected into the system, H_2CO_3 is formed, which can further release H^+. The released H^+ in the solution reacted with the sediments and made the Al soluble. Based on the chemical composition of the silica sand as Table 3.4, the mobilised Al may come from an aluminium oxide, Al_2O_3.

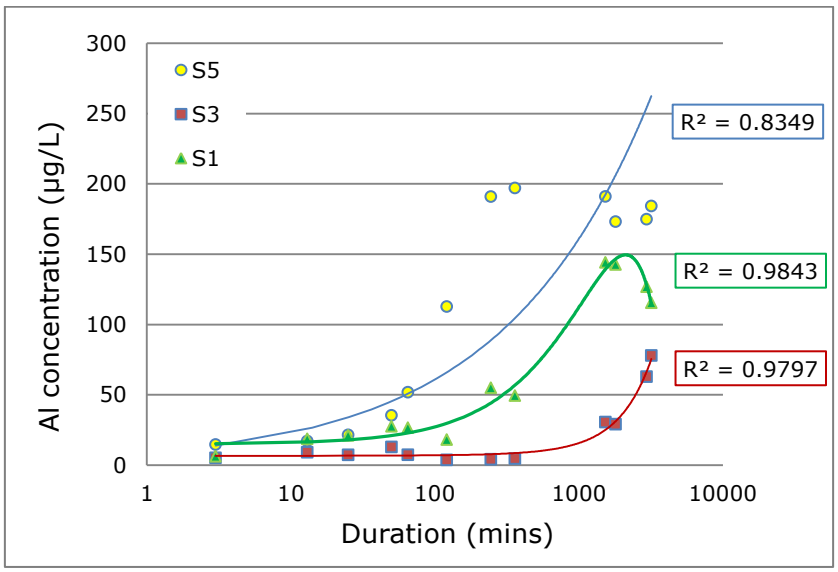

Fig. 5.35 Changes in exchangeable-Al of S1, S3 and S5 of Run 8.

5.3.5.2 Exchangeable-Mn

Exchangeable-Mn was assessed during the run and presented in Fig. 5.36. A steady and continuous increase in the concentration in all the three ports was observed. At the end of the CO_2 injection, Mn concentration in S1 was approximately 283% times higher than its initial conditions, while the concentration increased 313% and 244% times compared to the initial conditions in S3 and S5 respectively (Fig. 5.36). The results indicated that the Mn was mobilised and released from the sediments when CO_2 was present. After the CO_2 injection, the Mn concentration was also assessed. An increase in the Mn concentration was registered once the CO_2 injection stopped, which could be the reason for the slightly increase in the pH during the buffering period (Hem, 1978; Huang and Quist, 1983; Nogales et al., 1997). Based on the chemical composition of the sediment, the mobilisation of Mn came from the MnO_2 contained in the sediments. With less than 0.005% concentration in the sediments, the concentration of Mn in all three ports increased on an average of 280% compared with the initial conditions. This indicates and proves that Mn is more sensitive to acidity as previously reported by Blake and Goulding (2002).

Similar trends were shown in Mg concentration with smaller increase rate compared with Mn.

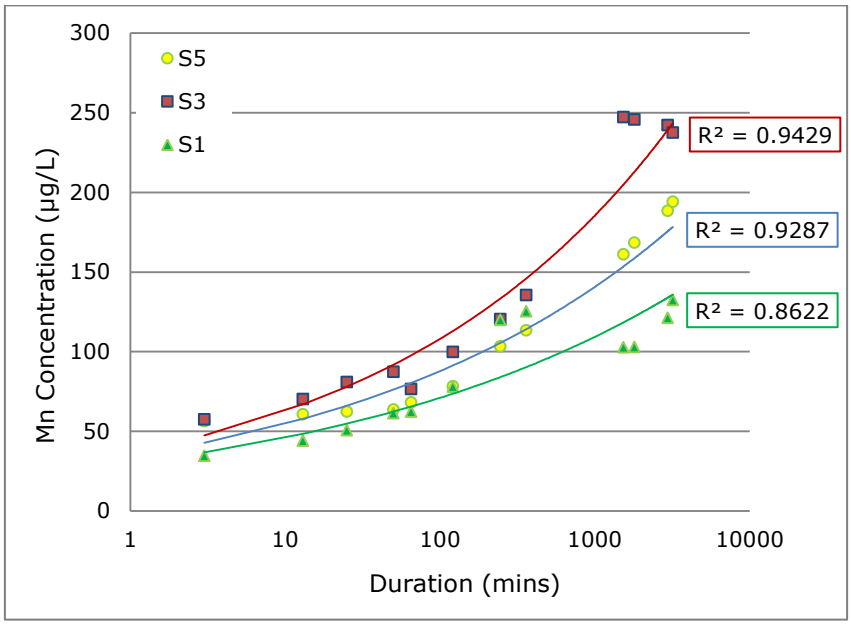

Fig. 5.36 Changes in exchangeable-Mn of S1, S3 and S5 Run 8. Note: The x-axis is logarithmic scale

5.3.5.3 Exchangeable-Cr

Fig. 5.37 presents the changes in the exchangeable-Cr concentration in S1, S3 and S5 following the CO_2 injection of Run 8. A general increasing trend was observed in the exchangeable-Cr for all three ports, S1, S3 and S5 (Fig. 5.37). At the end of the CO_2 injection, Cr concentration in S1 was approximately 465% higher than its initial conditions, while the concentration increased 849% and 456% in S3 and S5 respectively compared to the initial conditions (Fig. 5.35). The results indicated that the Cr was mobilised and released from the sediments when CO_2 was present. An overall increase in Cr concentration was also noticed in Stage I experiments.

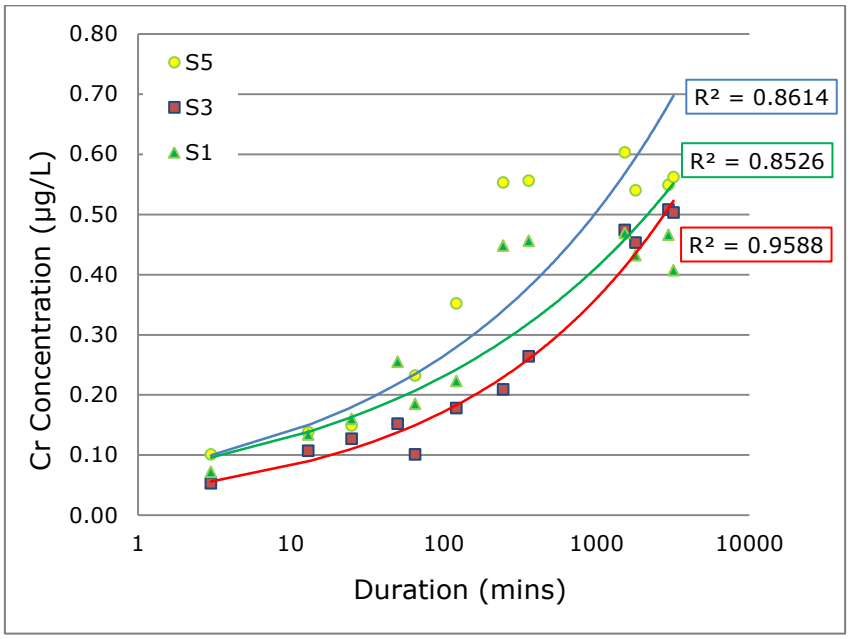

Fig. 5.37 Changes in exchangeable-Cr of S1, S3 and S5 of Run 8.
Note: The x-axis is logarithmic scale

5.3.6 Summary

Fig. 5.38 summarises the main parameters measured during Run 8, silica sand under flooded conditions with CO_2 continuously injected into the system.

Due to the constant injection of CO_2 into the system (Fig. 5.38 (a)), a change in the CO_2 concentration within the head space was noticed (Fig. 5.38 (b)). CO_2 was detected after six minutes of flowing through the sediments, and later the CO_2 concentration increased steadily for the next 15 minutes followed by a sharp increase afterwards until the end of the CO_2 injection (Fig. 5.38 (b)). The CO_2 concentration reached its peak value after about two hours of injection. Fig. 5.38 (c) summarises the pH changes of S1 during the gas injection. A quick drop in the pH was noticed first five minutes after the CO_2 injection, and the pH stabilised around

5.50-5.80 during the following injection. Correspondingly, the decrease in the pH caused sediment weathering, and subsequently the increase in the concentration of ions (see the selected data of Mn concentrations in (Fig. 5.38 (d)). As the sediments do not have strong buffering ability compared with Trucal 5 and Trucal 6, the pH reached its lowest value, around 5.50, which was close to the 5.60 value of pH of pure water in equilibrium with CO_2 at atmospheric conditions.

In conclusion, as described above and in section 5.3, the constant injected CO_2 brought down the pH quickly to around 5.50, causing an increase in almost all the major metal concentration contained in the sediments, for example Mg, Ti, Mn, Cr, Fe and Al (see section 5.3.5).

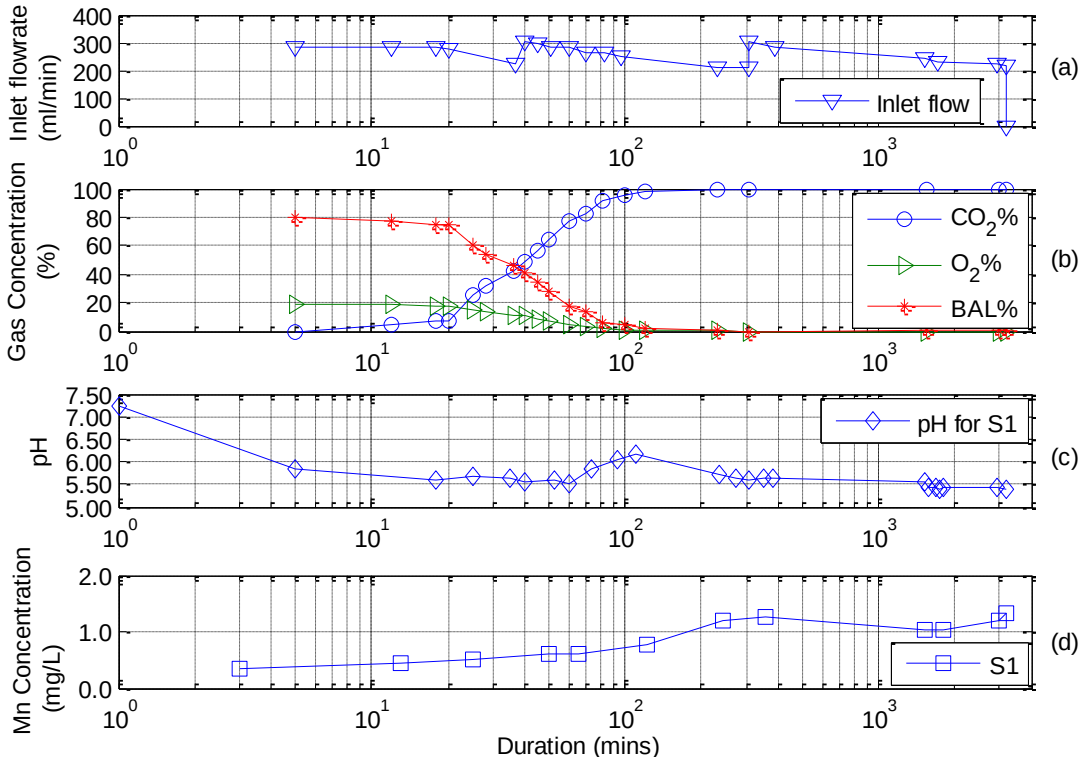

Fig. 5.38 Changes in the inlet flowrate (a), the gas concentration of the head space (b), pH of pore water (c) and the exchangeable Mn^{2+} concentration (d) following CO_2 injection during Run 8. (The x-axis is logarithmic scale)

Chapter 6 Interpretation of Stage II Results

Results from all runs from the Stage II experiments (Chapter 5) are compared in Chapter 6 to examine the correlation between sediment properties and their response to CO_2 release. The comparison focuses on the difference in the impact of CO_2 on limestone sand and silica sand samples (section 6.1). For the same type of sediments, unsaturated and flooded conditions are compared to assess the differences associated with various moisture contents (section 6.2). In addition, the differences in the impacts associated with particle size are compared in section 6.3.

6.1 Comparison of the impacts on carbonate and silica sand

6.1.1 Gas concentration changes

The CO_2% in the head space were compared using Trucal 5 and silica sand to assess the changes associated with different sediment types. Fig. 6.1 shows that the injected CO_2 flowed through the silica sand about three minutes faster than through Trucal 5, and the CO_2% increased quickly for both runs with a similar trend. By comparing every two adjacent points in Fig. 6.1, the increase rate at each point was calculated (Fig. 6.2). A clearly shift of the increase rate line was observed in Trucal 5 when compared with silica sand, which indicated that the increase in the CO_2 concentration was delayed in Run 4 (Trucal 5) in relation to that in Run 6 (silica sand). For the silica sand, the CO_2 concentration started to increase in the headspace at a low rate, about 0.5 (vol.) % min^{-1} during the first 10

minutes; while, for Trucal 5, the CO_2 concentration increased at a smaller rate, just over zero, during the first eight minutes.

For both runs, with moisture inside each column, the injected CO_2 first reacted with the water forming H_2CO_3, as explained in section 5.1, and then flowed through the sediments before being released at the surface of the column. Considering that both Trucal 5 and silica sand had a similar particle size, this cannot be addressed as the main cause of the observed differences; therefore the diverse chemical composition of the sediments should be advocated to explain such different behaviours of CO_2 movement. As explained in section 5.1, with Trucal 5, the injected CO_2 reacted and was partially absorbed into the sediments. This delayed its flow through the sediments and accumulation in the headspace. In a real scenario, mostly in calcareous sediments, the leaked CO_2 gas would react with the overlying soil causing stronger mineral weathering. It is also likely that less CO_2 will accumulate in the soil gas compared to silica sediments.

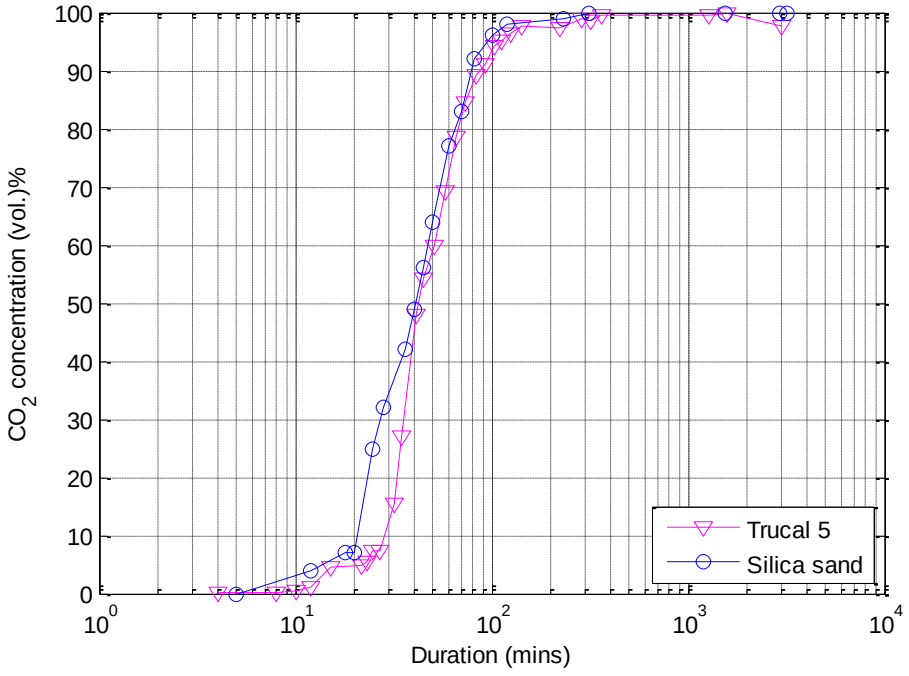

Fig. 6.1 A comparison in the gas concentration changes in the head space between the Trucal 5 (Run 4) and the silica sand (Run 8) under flooded conditions (The x-axis is logarithmic scale).

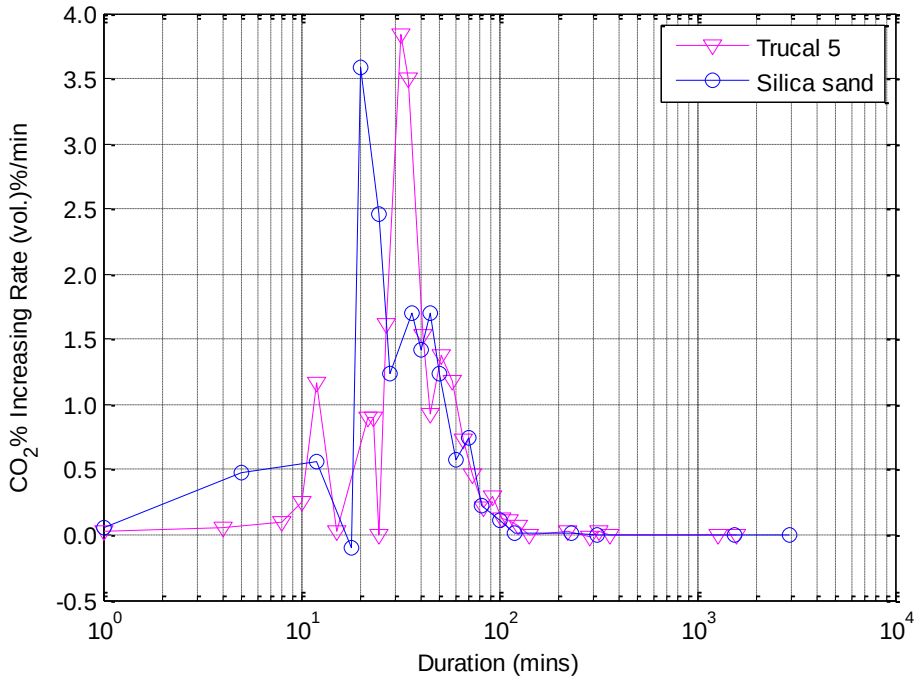

Fig. 6.2 A comparison in the CO_2% increasing rate over time between Trucal 5 and silica sand under flooded conditions.

6.1.2 pH changes

The pH changes associated with different sediment types were compared between Run 4 and Run 8 (Fig. 6.3). As shown in Fig. 6.3, with the constant injection of CO_2 into the system, the pH of the water sample for both the silica sand and Trucal 5 decreased quickly to its lowest values and stabilised during the following gas injection process. For the silica sand, with weak buffering abilities, the pH decreased quickly to about 5.80 in the first five minutes and was then around 5.50 afterwards with fluctuations; while, for Trucal 5, a decrease in the pH to about 6.30 was noticed between seven and ten minutes. The pH value then stabilised at around 6.10. After the CO_2 injection stopped, the pH rebounded slightly for Trucal 5 sample. No obvious change was observed for the silica sand after the CO_2 injection stopped.

Considering the two sediments have a similar particle size distribution and that the two runs were under the same conditions (see Table 3.5), the difference in the pH can be related to the variations in the chemical composition of the sediment. For the Trucal 5 sample, the sediments contained more than 98% calcium carbonate, which can further react with H^+ buffering the pH in the solution (see section 5.1). For the silica sand sample, there were limited amounts of carbonate minerals which can react with the H^+. Therefore, silica sand has a weak buffering capacity compared to the limestone sand (see section 5.3).

In summary, for both limestone sand and silica sand, the pH dropped quickly to its lowest point and stabilised around it after about ten minutes until the end of the CO_2 injection. It is evident from these results that pH is an excellent parameter to indicate the CO_2 intrusion into sediments. Moreover, with more carbonate minerals in the sediments, the decrease in the pH would be slower and smaller than that with the silica sand.

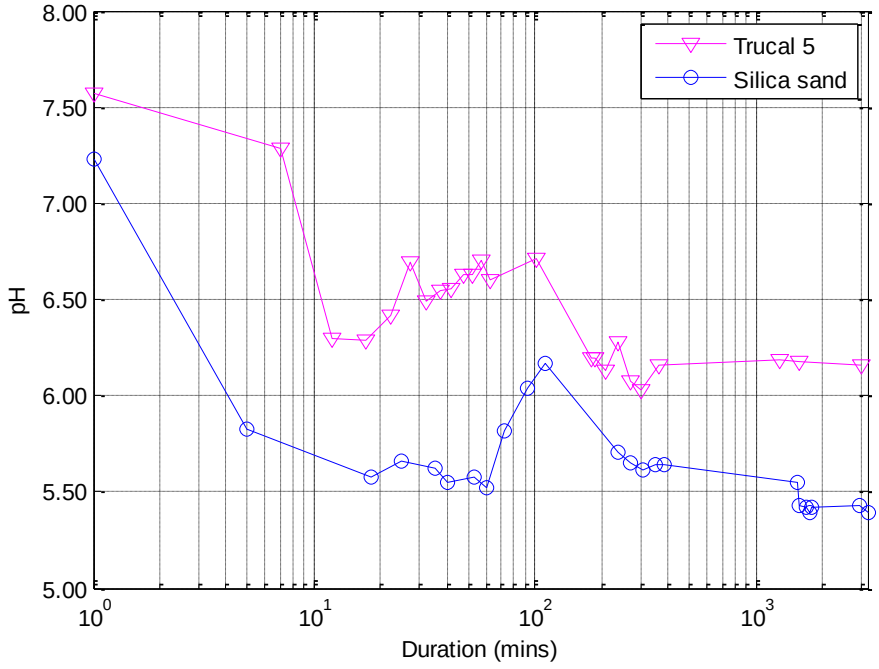

Fig. 6.3 A comparison in the pH changes of pore water between the Trucal 5 (Run 4) and the silica sand (Run 8) under flooded conditions. (The x-axis is logarithmic scale)

6.1.3 Ion concentration change

As presented in Chapter 5, the constant CO_2 injection increased the concentrations of some ions in the pore water from both the limestone sand Trucal 5 and the silica sand sediments. The concentrations of most of the major metals contained within the Trucal 5 were also increased. A general increase in all the major metals in the silica sediments was also observed.

6.2 Comparison of the impacts between different moisture levels in sediments

6.2.1 Gas concentration changes

A comparison in the CO_2 concentration changes in the head space between sediments with different moisture contents was carried out (Fig. 6.4). Fig. 6.4 (a) is the result of Trucal 6 sediments and Fig. 6.4 (b) is the results of the silica sand sediments. The results showed that there was a positive correlation between the impacts on the accumulating CO_2 concentration and different moisture contents. For both sediments, the graph showed that the CO_2 flowed through sediments quicker for the sediments under flooded conditions than that under unsaturated conditions. As explained in section 5.1.4, the free-flowing of injected gas was restricted by the presence of the solid matrix. The bubbles would partially be trapped between the limestone grains, and partially flow along the less resistant pathways. Furthermore, the accumulated gas trapped in the media would eventually form a connected path for the gas to pass through (Hoefner and Fogler, 1988; Oldenburg and Lewicki, 2005). Under flooded conditions, the voids between sediment particles were prefilled by water. This resulted

in fewer voids for the gas to fill. When the CO_2 was injected into the system, it had to overcome a higher hydrostatic pressure before starting to move through the sediments and bubbling into the headspace. In this way, the gas accumulated some pressure which should have facilitated the dislocation of particles with formation of wider channels where the gas can flow faster. Moreover, there was less head space in the columns with sediments under flooded conditions compared with that under unsaturated conditions for CO_2 to fill. These explain the quicker increase in the CO_2 concentration in the head space in the flooded system than the unsaturated system (Fig. 6.4).

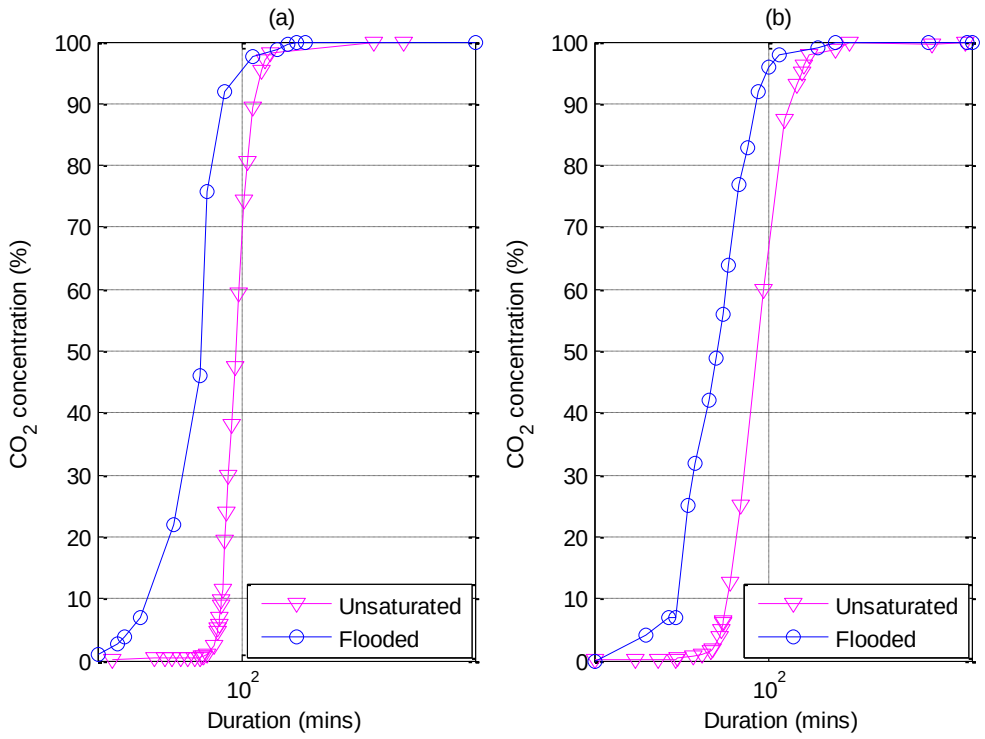

Fig. 6.4 A comparison in the CO_2 concentration changes in the head space under unsaturated conditions and flooded conditions, where (a) is for Trucal 6 (Run 5&6) and (b) is for silica sand (Run 7&8).

6.2.2 pH change

The pH changes in the sediments under different moisture conditions were compared (Fig. 6.5). As shown in Fig. 6.5, generally, for all samples, the pH decreased over time with the CO_2 injection. For Trucal 5, the decrease in the pH was noticed earlier in flooded conditions compared with unsaturated conditions. Similarly, the decrease in the pH was observed earlier in the runs in flooded conditions for both Trucal 6 and the silica sand. The decrease in the pH of the sediments under unsaturated conditions was delayed compared with that under flooded conditions. However, the changes in the pH under flooded conditions were quite unstable compared with that under unsaturated conditions. As explained in section 5.1.2, higher water content could influence the absorption of the injected CO_2 gas (Xu et al., 2005), which would lower the pH quicker than in unsaturated conditions. Higher water content would dilute the H^+ leading to the fluctuation in the pH.

In summary, the observed pH decrease was more rapid in sediment under flooded conditions. The pH changes in sediments under flooded conditions were quite unstable, which may be caused by uneven ion distribution in the solution or the gas disturbance in the system. There were differences between the sediments under different moisture content; however, no clear relationship can be established between the moisture content and pH change during the CO_2 injection.

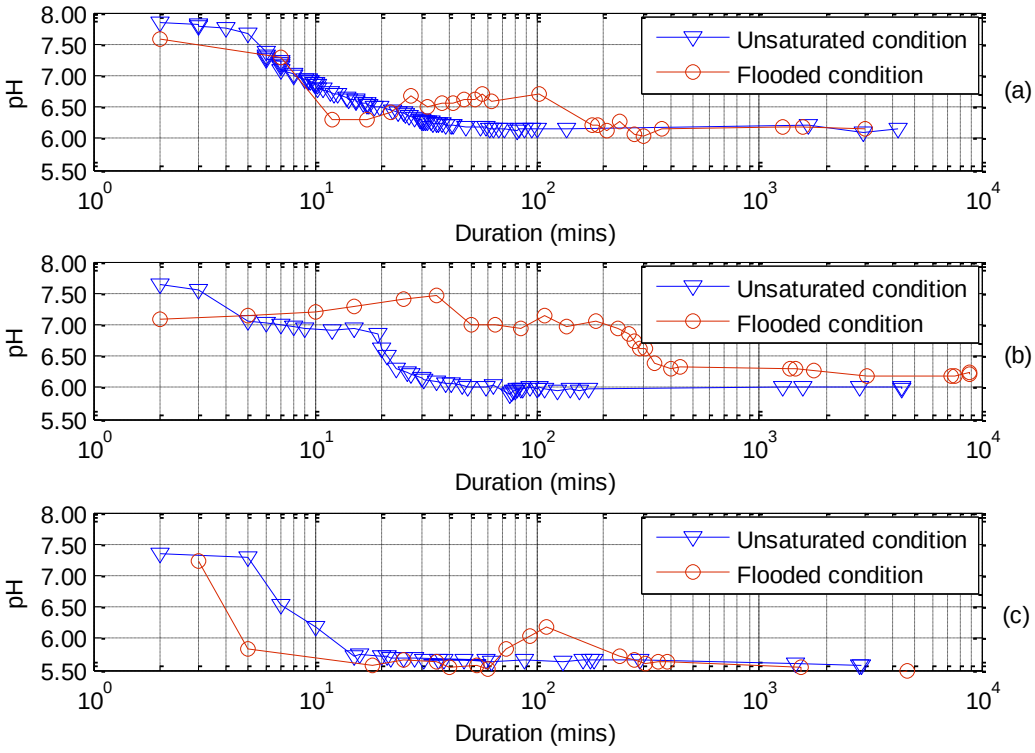

Fig. 6.5 A comparison in the pH changes of sediments under different water content. (a) is Trucal 5 under unsaturated (Run 2) or flooded conditions (Run 4); (b) is Trucal 6 under unsaturated (Run 5) or flooded conditions (Run 6); and (c) is silica sand under unsaturated (Run 7) or flooded conditions (Run 8).

6.3 Comparison of the influence of different particle sizes

6.3.1 Gas concentration change

The changes in the CO_2 concentration accumulating in the head space were compared between the Trucal 5 (Run 4) and Trucal 6 (Run 6) to assess the influence of particle sizes of sediments (Fig. 6.6). The results show that CO_2 flows through Trucal 6 quicker than through Trucal 5. After about six minutes, the CO_2 concentration in the head-space was 1.1% for Trucal 6 (Run 4), while it took 12 minutes for the CO_2 concentration to reach 1.0% for Trucal 5 (Run 6). Once CO_2 was detected, the CO_2% in the headspace increased sharply, displacing O_2 and the remaining gases in both columns.

Run 4 and Run 6 were both under flooded conditions. Trucal 5 and 6 have similar chemical composition (Table 3.2) and similar bulk density within the columns during the runs (Table 3.5). The only difference between the runs was the distribution of particle sizes of the sediments, Trucal 6 being coarser than Trucal 5 (see Table 3.2 and Table 3.3). As explained in section 5.1, the injected CO_2 would channel through the sediments flowing into the headspace. Because of the coarser limestone sand, the voids between the particles were bigger in Trucal 6 than that in Trucal 5. Consequently, Trucal 6 has a higher permeability and less resistant channelling pathways among the particles, causing the injected CO_2 gas to flow through Trucal 6 quicker than through Trucal 5. Further analysis was carried out to relate the particle size difference and the impacts on sediments it may cause, for example on pH change, dissolution of limestone sand and alkalinity changes.

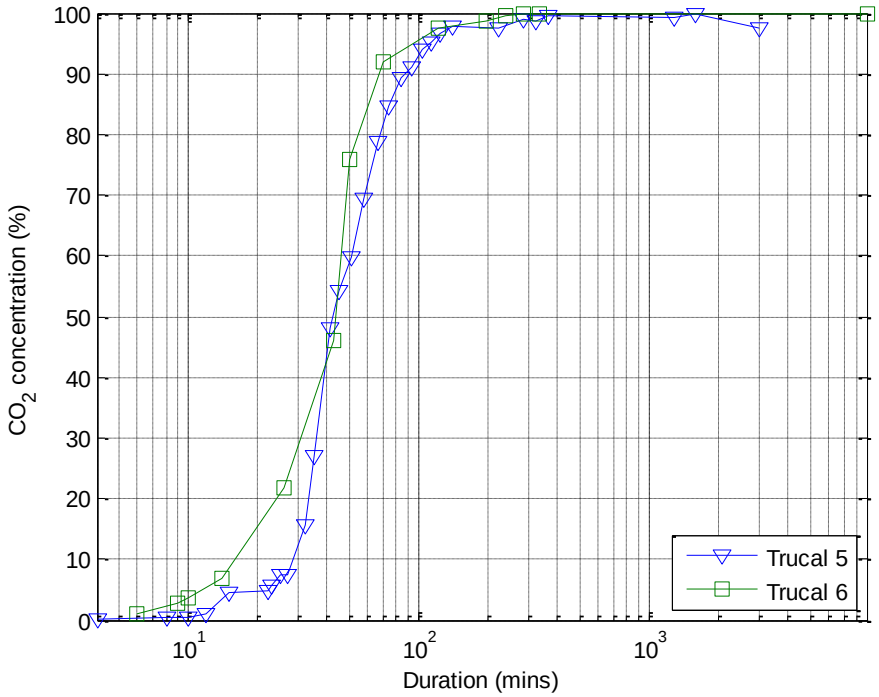

Fig. 6.6 A comparison in the CO_2 concentration changes in the head space between Trucal 5 (Run 4) and Trucal 6 under (Run 6) flooded conditions.

6.3.2 pH change

The pH changes in Trucal 5 and Trucal 6 were compared (Fig. 6.7). The pH decreased over time for both sediments (Fig. 6.7). For Trucal 5, a quick decrease in the pH was noticed in the first 10 minutes. Later the pH decreased and stabilised at about 6.20 after about 200 minutes of injection and was stable afterwards (Fig. 6.7). For Trucal 6, the pH increased during the first 30 minutes from 7.07 to 7.45, followed by a decrease. The pH decreased to 6.30 after about 400 minutes remaining within a range between 6.20 and 6.30 (Fig. 6.7). Fig. 6.7 indicated that the pH decrease in Trucal 6 was delayed in respect to that of Trucal 5.

As discussed in section 6.3.1, the coarser limestone sand, Trucal 6, resulted in the gas flowing through quicker than that in Trucal 5. This resulted in less CO_2 being trapped in the sediments, and caused less H^+ generated by the reaction between the CO_2 gas and water, which eventually lead to the delay in the pH change.

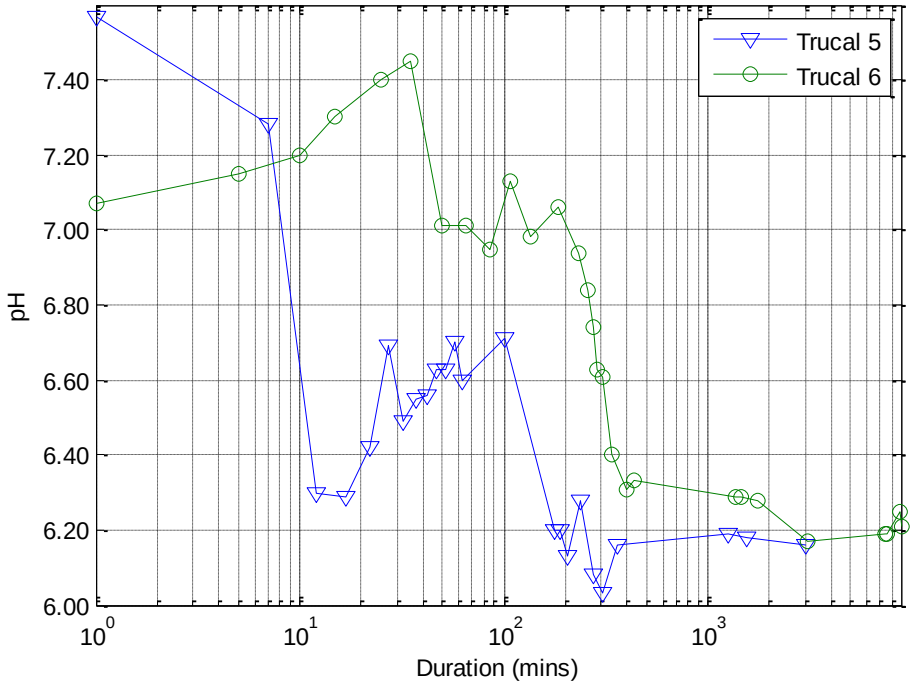

Fig. 6.7 A comparison in the pH changes of pore water between Trucal 5 (Run 4) and Trucal 6 (Run 6) under flooded conditions.

6.3.3 Dissolution of limestone sand

The changes in the Ca^{2+} concentration in the pore water of Trucal 5 and Trucal 6 were also assessed and compared, as presented in Fig. 6.8. In both the runs (Run 4 and Run 6) the sediments were under flooded conditions. Fig. 6.8 (a) shows the Ca concentration change over time for both runs, while Fig. 6.8 (b) presents the Ca concentration increasing rate over time for both runs, by comparing every two adjacent points in Fig. 6.8 (a).

The positive value in Fig. 6.8 (b) and the changes in the rate indicated that for both sediments the Ca^{2+} concentration kept increasing during the injection; this increase was faster at the beginning of the run, and slower towards the end. By comparing the two sediments, Fig. 6.8 (a) shows a clearly delay in the increase of the Ca^{2+} concentration in Trucal 6 compared with Trucal 5. For Trucal 5, once the CO_2 was injected into the system, a quick increase in the Ca^{2+} concentration was detected lasting until the end of the run; with Trucal 6, the dissolution of limestone sand did not start until 15 minutes after the CO_2 injection. After about 100 minutes, a quick increase was also observed with Trucal 6 (Fig. 6.8 (a)). Moreover, the highest Ca concentration increase rate of Trucal 5 was higher than that of Trucal 6 indicating that the dissolution of limestone sand Trucal 5 was higher than Trucal 6.

As described in Chapter 5, there were differences in the metal concentrations in pore water after the CO_2 injection. With Trucal 5, a mobilisation of metals was recorded for most of the major metals contained in the sample, for example Mg, Al, Fe, Cd, As; while, for Trucal 6, the increase in the metal concentration was only observed for Mg and As and with a slower rate of increase.

As explained in sections 6.3.1 and 6.3.2, the decrease in the pH was delayed in Trucal 6. Such delay resulted in the delayed increase in the Ca^{2+} concentration of Trucal 6 compared with Trucal 5. Moreover, for the coarser sand Trucal 6, the larger particle size generated a smaller active area compared with Trucal 5. Therefore, the sediments were less affected by the injected CO_2 resulting in the lower dissolution of limestone sand Trucal 6 compared with Trucal 5. Similar results were observed in other research (Shih et al., 2000; Zhang et al., 2007).

In conclusion, a correlation was observed between the particle size and the dissolution of limestone sand. With bigger particle size, a delay in the limestone sand dissolution would be expected and the dissolution rate is expected to be lower than that of the fine particles.

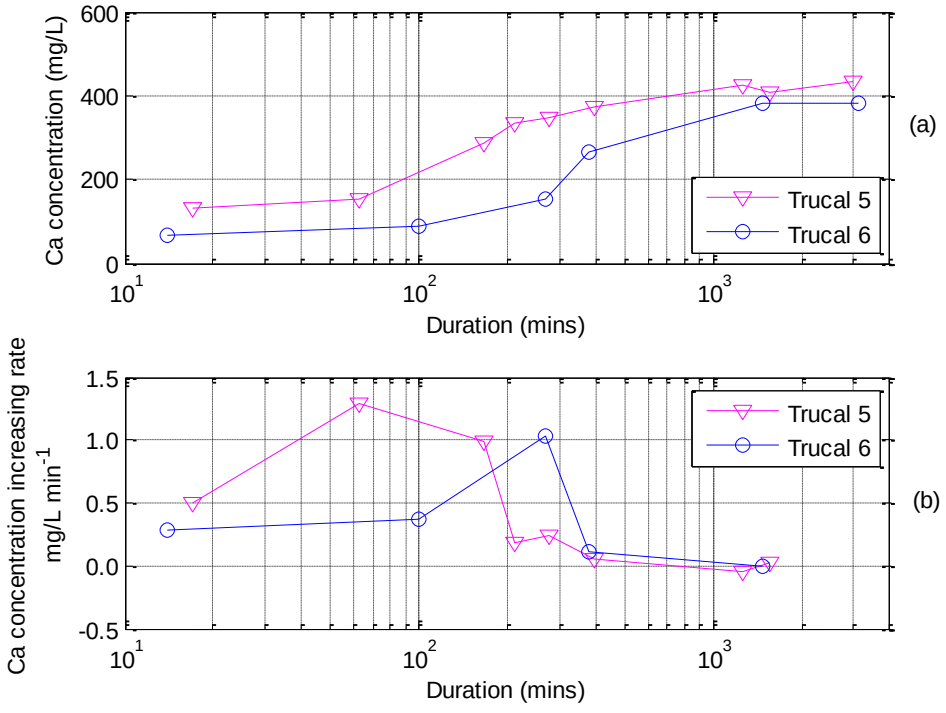

Fig. 6.8 A comparison in the exchangeable Ca concentration changes between Trucal 5 (Run 4) and Trucal 6 under (Run 6) flooded conditions. (a) is the concentration changes over time, and (b) is the Ca concentration increasing rate over time. Note: x-axis is logarithmic scale.

6.3.4 Alkalinity changes

Similarly, a comparison in the alkalinity changes was carried out between Trucal 5 (Run 4) and Trucal 6 (Run 6) under flooded conditions, and the results are presented as Fig. 6.9. A similar difference to the changes in the Ca^{2+} concentration was observed in the alkalinity changes between the two sediments. Fig. 6.9 indicated that the increase in the alkalinity concentration was delayed in Trucal 6 compared with Trucal 5, and the increasing rate in the alkalinity concentration was lower in Trucal 6. Similar explanation as the changes in the dissolution of limestone sand (see section 6.3.4) can be used here.

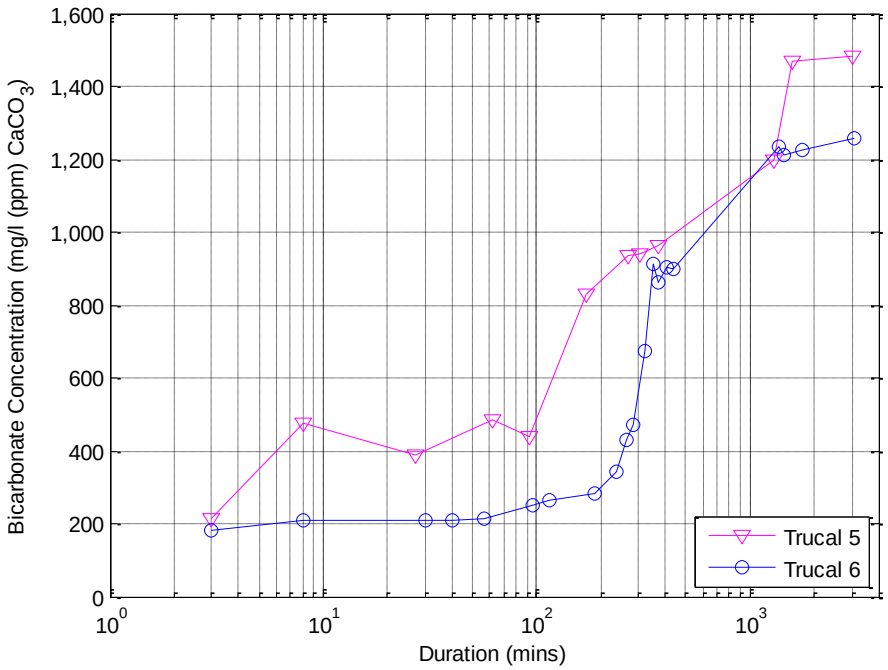

Fig. 6.9 A comparison in the alkalinity changes between Trucal 5 (Run 4) and Trucal 6 (Run 6) under flooded conditions. Note: x-axis is logarithmic scale.

In summary, as described in section 6.3, a correlation between the particle size and the differences of the impacts on sediments due to the elevated CO_2 concentration was observed. With bigger particle size, larger voids

existed among the particles, resulting in less CO_2 gas trapped in the sediments. Subsequently, a delayed decrease in the pH was noticed compared with the finer sediments. With coarser sand, the dissolution of limestone sand was slightly delayed and the dissolution rate was lower compared with the finer sediments. At the end of the CO_2 injection, higher mobilisation in the finer limestone sand was noticed compared with the coarser sand. As described in Chapter 5, a dome was formed at the end of the gas injection in the finer sand and no dome was noticed for the coarser sand.

6.4 Summary

By comparing impacts on sediments between limestone sand (Trucal 5 and 6) and silica sand, it was noticed that for both limestone sand and silica sand, the pH dropped quickly to its lowest point and stabilised around it after about ten minutes until the end of the CO_2 injection. It is evident from these results that pH is an excellent parameter to indicate the CO_2 intrusion into sediments. Moreover, with more carbonate minerals in the sediments, the decrease in the pH would be slower and smaller than that with the silica sand. The constant CO_2 injection increased the concentrations of some ions in the pore water from both the limestone sand Trucal 5 and the silica sand sediments. For the limestone sand sample, the Ca^{2+} concentration increased by 491% of the initial concentration due to the enhanced dissolution of $CaCO_3$. The concentrations of most of the major metals contained within the Trucal 5 were also increased. A general increase in all the major metals in the silica sediments was also observed.

For the same type of sediments, unsaturated conditions and flooded conditions are applied to assess the differences in the impacts of CO_2 associated with various moisture contents. The pH decrease was first observed in sediment under flooded conditions. The pH changes in sediments under flooded conditions were quite unstable, which may be caused by uneven ion distribution in the solution or the gas disturbance in the system. There were differences between the sediments under different moisture contents; however, no clear relationship can be established between the moisture content and pH change during the CO_2 injection.

As described in section 6.3, a correlation between the particle size and the differences of the impacts on sediments due to the elevated CO_2 concentration was observed. With bigger particle sizes, larger voids existed between the particles, resulting in less CO_2 gas trapped in the sediments. Subsequently, a delayed decrease in the pH was noticed compared with the finer sediments. With coarser sand, the dissolution of limestone sand was slightly delayed and the dissolution rate was lower compared with the finer sediments. At the end of the CO_2 injection, higher mobilisation in the finer limestone sand was noticed compared with the coarser sand.

Chapter 7 Conclusions and Future Work

This thesis examines the possible changes in soil chemistry resulting from potential CO_2/SO_2 leakage, which might be useful for identifying monitoring parameters if the leakage does happen, leading to the development of new approaches in detecting CO_2 leaks from CCS schemes. To achieve the aim and objectives, two types of laboratory experiments were carried out in this research: Stage I- Closed reactor experiments and Stage II- Flow through column system experiments (designed by the author). This chapter focuses on presenting conclusions from this research (section 7.2), and future work for further studies (section 7.3). Before presenting the main conclusions from this research, it is also necessary to consider limitations (section 7.1).

7.1 Limitations of this study

As a cost-effective approach, laboratory experiments were used in this research to achieve the research objectives (section 1.4). However, it has to be noted that this research has its limitations in terms of sediment types used, scale limitations of laboratory experiments, and column system design as discussed below.

In this research, the experiments were carried out with prepared homogeneous soil samples collected from the ASGARD field site (section 3.1.1) and well sorted mono-mineral sediments, Trucal 5 and Trucal 6 (limestone sand of different particle size) and silica sand (section 3.2.2). These types of sediments cannot represent completely the full complexity

of a natural system as explained in section 2.3.4. Firstly, soil mass in fields not only include soil materials used in this laboratory study but also soil gas, water, organic matter and microbes etc (Nikolaidis et al., 1994; Rowell, 1994b; Sass and Rai, 1987; Wu et al., 2010). Such differences could lead to discrepancies in the results between laboratory experiments and other field studies. For example, it was noticed that weathering rates determined in the laboratory experiments with pure minerals or for some whole soils are normally much higher (several orders of magnitude higher) than rates estimated from field studies (Stephens, 2002; van Grinsven and van Riemsdijk, 1992; Velbel, 1993). Besides, with the presence of organic matter the mobility of certain metals would differ when compared with the mono-mineral sediments used in this research (Nikolaidis et al., 1994; Sass and Rai, 1987; Wu et al., 2010). Therefore, results from the laboratory work cannot simply represent all the soils in the field except the specific soil related problem.

Secondly, the experiments in this research were carried out with highly idealised scenarios with no heterogeneity in the samples used, which are not representative of the real field. As explained in section 2.3.4, unlike the well prepared soil/sediments used in the laboratory reactors, soil heterogeneity and stratification phenomena exist in field, which play an important role in gas channel development (Semer et al., 1998). For example, if the overlying layers have lower permeability, the gas will be forced to spread horizontally until the layer of finer material is bypassed (Ji et al., 1993). CO_2 leakage along discrete sections relies on the nature of the media and the permeability of discontinuities, which would further influence the impacts on different soils/sediments by the leaked CO_2 (Gal et al., 2012; Ji et al., 1993). Therefore, the results from this research

cannot be simply scaled up without further investigation on the field conditions.

Regarding the scale limitations, the laboratory studies are carried out at a much smaller scale than the real field studies. Because of the small scale laboratory experiments, the injected CO_2 gas would be trapped inside the reactor and the ratio of CO_2/soil would be much higher than in the field (section 2.3.4), causing higher dissolution in the laboratory experiments (Patil et al., 2010). The results from this research are likely to be more representative of the soils/sediments surrounded by high levels of CO_2, such as the ones near a leaking injection well or along a fracture/fault.

Regarding the flow through column design, it was realised after the research that there was no measurement of the pressure difference across the sample during the experiments. This leads a lack of measurement of the permeability of the used sample, which is one of the limitations of the column design. Although the permeability measurement of samples used in the experiments can be accomplished by using other equipment (section 3.2.5.1), it would be easier if pressure gauges are added in the design and then the permeability could be calculated using these. Further improvements will be made for future research.

Overall, due to the limitations of this research, the data collected from this research should be treated with caution. Based on the sediments used in this research and the experimental design, the results from the laboratory work should be used to predict and compare with specific soil related problems instead of simply representing all the soils in the field. Because of the higher weathering rates and higher CO_2 concentration in the laboratory experiments, it is better to use the results from this research to represent the long term impacts on the specific related soils or to

demonstrate the conditions where the soils/sediments are surrounded by high levels of CO_2 (Lu et al., 2010). The research is believed to provide a step towards understanding the potential impacts of CO_2 seepage in soil, and potentially to be useful as a means of identifying indicators of the related problem when applied to full-scale designs, leading to the development of new approaches in detecting CO_2 leaks. The experimental apparatus (the continuous column system) newly designed by the author of this research was run successfully, providing an alternative way in respect to the majority of soil-column studies to study the issues of CO_2 seepage.

7.2 Conclusions

The impact of CO_2 emissions on soil properties is to drop the pH (section 4.3 and 5.1.8) which triggers metal mobilisation from soils (section 4.4 and section 5.1.8).

The conclusions in relation to the proposed objectives in section 1.4 are summarised as followings:

1). Incubation of ASGARD soils for three days at a high pressure and temperature in CO_2/SO_2 gas (100% CO_2 or CO_2/SO_2=99:1) did not cause significant changes in the soil mineralogical composition (section 4.1.3). This can be explained as the main phase quartz present in soils is not expected to change with CO_2 incubation (see section 4.1.3). Similarly, field studies at the ASGARD site showed no significant difference in mineralogical assemblages between gassed and non-gassed plots (West et al., 2009).

The 100% CO_2 incubation did not cause obvious change in pH (section 4.3.1), while a great reduction of pH was observed when the soil was incubated with 1% SO_2 and 99% CO_2 gas (section 4.3.2). However, pH was not measured until 3-4 days after the incubation was completed. Since H^+ could have been consumed by the soil mineral dissolution process during the buffering period, the measured change in pH may underestimate the true drop at the end of incubation. The measured pH cannot therefore be used to reflect the soil's instantaneous response to the addition of CO_2/SO_2 gas. The Stage II experiments (Chapters 5 & 6) involved measuring pH in real time to monitor changes in pH as the experiment progressed.

The pH drop induced by the exposure to CO_2 gas mobilised the metals from the soil causing an increase in several $CaCl_2$-exchangable metal concentrations in the soil solution following different increasing patterns (section 4.4). Al, Fe and Mn experienced the highest mobilisation from soils, followed by As, Cr, Cu and Pb. K and Mg showed the least increases. A slight decreasing trend was observed in Cd and Zn. Considering the temperature and pressure in field and the volume of emitted CO_2, heavy metal mobilisation to a toxic level is unlikely to happen for the investigated soils (section 4.4.1). With 1% SO_2, most $CaCl_2$-exchangable metals were highly mobilised from the soil and the concentration of certain metals exceeded the safety limits for plant growth, e.g. Ni, Al, Fe, Pb, Zn and Cu (section 4.4.2). Attention needs to be paid to the heavy metal mobilisation triggered by emissions of impure CO_2/SO_2 gas.

2). A laboratory apparatus (flow through column system) based on soil columns was designed by the author and used to assess the impact of

CO_2 on sediments and water in a controlled environment. Different runs (Table 3.5) were carried out with the system to assess the instantaneous response of different sediments following a short-term, small continuous release of CO_2.

These experimental results highlight the very fast drop in the pH of pore water to its lowest point for both carbonate and silica sand (section 5.1.2, 5.2.2 and 5.3.2) once CO_2 is added to the system. It is to be noted that even a small release of CO_2, as the one in the experiment which was less than 0.3 L/min, causes a drop in pH which is clearly detectable despite the buffering effect of the limestone used in the apparatus. The quick reaction to anomalous levels of CO_2 can play an important role for the prompt detection of CO_2 leakages from storage sites once the pH baseline is assessed. It is evident from these results that pH is an excellent parameter to indicate the CO_2 intrusion into sediments. In addition, the constant CO_2 injection increased most of the exchangeable ion concentrations in the pore water from both carbonate and silica sand (section 5.1.5, 5.2.5 and 5.3.5).

3). Some differences in responses were obtained between carbonate and silica sand (section 6.1). The results imply that with more carbonate minerals in the sediments, the decrease in the pH was slower and smaller than that with the silica sand (Fig. 6.3), as might be expected given the buffering capacity of carbonates. The mobilisation of ions from the carbonate sediments was mainly caused by the dissolution of carbonate minerals hosting such ions, while in the silica sand it was mainly from the metal oxides.

A correlation between the MC and the impacts of CO_2 was observed in the incubated ASGARD soils at unsaturated conditions of Stage I as

described in Chapter 4. The incubation process indicates that the more moisture within a soil sample, the more CO_2 was taken up by soil (section 4.2.1) and the higher the concentration of mobilised metal (section 4.4.1). With the constant CO_2 injection system, there were differences between the impacts on sediments under unsaturated conditions and flooded conditions; however, no clear relationship can be established between the MC and the impacts of the CO_2 intrusion (section 6.2).

A correlation between particle size and the differences of the impacts on sediments due to the CO_2 leakage was observed (section 4.4.3 and 6.3). With coarser sediments, a delayed decrease in the pH was noticed compared with the finer sediments following the CO_2 injection (Fig. 6.7). With coarser sand, the dissolution of limestone sand was slightly delayed and the dissolution rate was lower compared with the finer sediments (Fig. 6.8). At the end of the CO_2 injection, a higher mobilisation in the finer limestone sand was observed (section 6.3.3). The results from the batch experiments also indicate a higher mineral dissolution of the ground soils after the CO_2 incubation compared with the unground soil. This implies that particle size influences the response of the sediments to CO_2 exposure (section 4.4.3).

4). The recovery effects of different sediments following the CO_2 exposure were assessed and compared in Chapter 5 & 6.

Once the CO_2 injection stopped, a quick and steady recovery in the pH was observed with limestone sand under unsaturated conditions (Fig. 5.7); the pH recovery was observed only after the CO_2 injection stopped. No obvious increase in pH during the buffering period was observed for silica sand (section 5.3.2) and limestone sand under

flooded conditions (section 5.1.2.2). The results imply that carbonate sand has stronger buffering effects compared with silica sand, but flooded conditions could interfere with such buffering ability.

Once the CO_2 injection stopped, a slight decrease in Ca^{2+} concentration for limestone sand was observed for 6 days with an average drop of about 11% compared with the highest level when CO_2 injection stops, and the concentration was stable for the following 25 buffering days (Fig. 5.13). No big differences in the ion concentrations were observed for silica sand once the CO_2 injection stopped. The response of Ca to CO_2 exposure highlights that carbonate minerals are sensitive to CO_2 fluxes and could possibly be used as a parameter to monitor CO_2 leakage once the baseline is set.

7.3 Future work

Starting from these results, to follow up the research, further studies are suggested in the following ways.

Considering the more complex situation in the field, further experimentation in more complex settings should be carried out. As suggested by Prasad (1995) and Wren and Stephenson (1991), organic matter would influence the mobility of certain metals and it would also influence ion uptake by plants, for example Cr, As and Mn (Nikolaidis et al., 1994; Sass and Rai, 1987; Wu et al., 2010). It is therefore necessary to verify the influence of different amounts of organic matter in the soils exposed to CO_2 seepages. Besides, considering soil heterogeneity and stratification phenomena in the field, a more complex soil setting will be used for future work, e.g. packing different layers of soils/sediments. The

results with more complex soil settings will then be compared with that of natural analogues or storage sites and they could also be used to improve the development of reliable models.

During Stage II experiments, within the constraint of time, no impure gas (CO_2/SO_2 mixture) was investigated. As presented in section 2.2, the appearance of SO_2 in soil would likely lead to an even lower soil pH and further highly mobilised metal/metalloid concentrations compared with 100% CO_2 (Falkengren-Grerup et al., 1987; Likens and Bormann, 1974; Skiba, 1989; Tamm and Hallbäcken, 1988). As future work, further experiments with different sediments and various impurities in the gas (CO_2/SO_2) are suggested to assess the impact on the environment caused by such impurities.

At the beginning of this research, the Stage II experiment was designed to run at least one set of experiments with the soil from the ASGARD field. However, design and approval of the Stage II experiments took so long that no experiments were actually run with the soils from the ASGARD field. At this stage, no direct comparison could be made between Stage I and Stage II experiments. Stage I experiments are limited to providing indications for the Stage II experimental design. It is necessary to run the experiments with the same soils in Stage I to compare these two types of study to link them together, which will be carried out in the future.

This study provides useful information to help understanding the complex issue of the chemical effects of high-levels of CO_2 in top-layer soils. Some limitations are due to the relatively small-scale of the laboratory trials and to the simplified setting (i.e. use of mono-mineral sediments and sieved soil samples) as presented in section 7.1. The outcomes of the research highlight the following points:

- This experimental approach gathered chemical data helping the understanding of the geochemical processes involved in the CO_2-soil-water interaction. Combined with other studies of the impacts of CO_2 on the surrounding ecosystem (e.g. effects on groundwater chemistry, microbial community, and vegetation), this study enriches the knowledge of the potential impact of CO_2 leakage on the local environment, which is a key-issue in risk management of CCS projects.
- The observed instantaneous response to CO_2 leakage (mostly as pH drop) can be considered as a reliable indicator for the presence of CO_2 levels above the natural baseline in the field. These observations, when applied to the full-scale CO_2 storage sites will likely lead to the development of new methods in early detection of CO_2 leaks.
- These results can be generalised, considering the limitations stated above, to more complex scenarios under similar environmental conditions.
- The data collected on the chemical behaviour (e.g. dissolution rates, and alkalinity changes) of the CO_2-limestone-water system could be used to validate the mathematical modelling of CO_2 dissolution and reaction processes with limestone rocks and groundwater. Some of the results from the Stage II experiment have already been used in Dr. Mitchell's work to compare and correct his model (Mitchell, 2011).
- The newly designed experimental apparatus (the continuous column system) provides an alternative and innovative approach to the study of the chemical effects of CO_2 seepage in respect to the majority of soil-column experiments.

REFERENCES

ABICHOU, T., MAHIEU, K., CHANTON, J., ROMDHANE, M. & MANSOURI, I. 2011. Scaling methane oxidation: From laboratory incubation experiments to landfill cover field conditions. *Waste Management-Landfill Gas Emission and Mitigation,* 31**,** 978–986.

AIUPPA, A., FEDERICO, C., ALLARD, P., GURRIERI, S. & VALENZA, M. 2005. Trace metal modeling of groundwater-gas-rock inter-actions in a volcanic aquifer: Mount Vesuvius, Southern Italy. *Chemical Geology,* 216**,** 289-311.

AL-ABED, S.R, JEGADEESAN, G., PURANDARE, J. & ALLEN, D. 2007. Arsenic release from iron rich mineral processing waste: Influence of pH and redox potential. Chemosphere, 66**,** 775–782.

ALIANI, S., BORTOLUZZI, G., CARAMANNA, G. & RAFFA, F. 2010. Seawater dynamics and environmental settings after November 2002 gas eruption off Bottaro (Panarea, Aeolian Islands, Mediterranean Sea). *Continental Shelf Research,* 30**,** 1338-1348.

AMMARI, T. & MENGEL, K. 2006. Total soluble Fe in soil solutions of chemically different soils. *Geoderma,* 136**,** 876-885.

ANDREWS, J.A. 2001. Soil CO_2 dynamics, acidification, and chemical weathering in a temperate forest with experimental CO_2 enrichment. *Global Biogeochemical Cycles,* 15**,** 149-162.

ANNUZIATELLIS, A., CIOTOLI, G., PETTINELLI, E., BEAUBIEN, S.E., RUBIN, E.S., KEITH, D.W., GILBOY, C.F., WILSON, M., MORRIS, T., GALE, J. & THAMBIMUTHU, K. 2005. Geochemical and geophysical characterization of an active CO_2 gas vent near the village of Latera, Central Italy. *Greenhouse Gas Control Technologies 7.* Oxford: Elsevier Science Ltd.

ARAVIND, P. & PRASAD, M.N.V. 2005. Cadmium-Zinc interactions in a hydroponic system using Ceratophyllum demersum L.: Adaptive ecophysiology, biochemistry and molecular toxicology. *Brazilian Journal of Plant Physiology,* 17**,** 3-20.

ARDELAN, M.V. & STEINNES, E. 2010. Changes in mobility and solubility of the redox sensitive metals Fe, Mn and Co at the seawater-sediment interface following CO_2 seepage. *Biogeosciences,* 7**,** 569-583.

ARDELAN, M.V., STEINNES, E., LIERHAGEN, S. & LINDE, S.O. 2009. Effects of experimental CO_2 leakage on solubility and transport of seven trace metals in seawater and sediment. *Science of The Total Environment,* 407**,** 6255-6266.

ARRHENIUS, S. 1896. On the influence of carbonic acid in the air upon the temperature of the ground. *Philosophical Magazine and Journal of Science,* 41**,** 237-276.

ASTORRI, F., BEAUBIEN, S., CIOTOLI, G. & LOMBARDI, S. 2002. An assessment of gas emanation hazard using a geographic information system and geostatistics. *Health Physics,* 82**,** 8.

BACHU, S. 2008. CO_2 storage in geological media: Role, means, status and barriers to deployment. *Progress in Energy and Combustion Science,* 34**,** 254-273.

BARBER, S.A. 1995. *Soil nutrient bioavailability: A mechanistic approach,* New York, Chichester, Brisbane, Toronto and Singapore, John Wiley & Son, INC.

BARRACHINA, A.C., CARBONELL, F.B. & BENEYTO, J.M. 1995. Arsenic uptake, distribution, and accumulation in tomato plants: Effect of arsenite on plant growth and yield. *Journal of Plant Nutrition,* 18**,** 1237-1250.

BARTH, D.S., BENJAMIN, J.M., THOMAS, H.S., & KENNETH, W.B. 1989. Environmental Monitoring and Support Laboratory. *Soil Sampling Quality Assurance User's Guide. Second Edition.* Las Vegas: U.S. Environmental Protection Agency; NV. 89183-3478.

BEAUBIEN, S.E., CIOTOLI, G., COOMBS, P., DICTOR, M.C., KRÜGER, M., LOMBARDI, S., PEARCE, J.M. & WEST, J.M. 2008. The impact of a naturally occurring CO_2 gas vent on the shallow ecosystem and soil chemistry of a Mediterranean pasture (Latera, Italy). *International Journal of Greenhouse Gas Control,* 2**,** 373-387.

BEAUBIEN, S.E., LOMBARDI, S., CIOTOLI, G., ANNUZIATELLIS, A., HATZIYANNIS, G., METAXAS, A. & PEARCE, J.M. 2005. Potential hazards of CO_2 leakage in storage systems-Learning from natural systems. *In:* RUBIN, E. S., KEITH, D. W., GILBOY, C. F., WILSON, M., MORRIS, T., GALE, J. & THAMBIMUTHU, K. (eds.) *Greenhouse Gas Control Technologies 7.* Oxford: Elsevier Science Ltd.

BECKMAN COULTER INC., no date. *LS™ 200*. Available at: https://www.beckmancoulter.com/wsrportal/wsr/industrial/products/laser-diffraction-particle-size-analyzers/ls-200-series/index.htm (last accessed: 03/11/2012)

BECQUER, T., QUANTIN, C., SICOT, M. & BOUDOT, J.P. 2003. Chromium availability in ultramafic soils from New Caledonia. *Science of The Total Environment,* 301**,** 251-261.

BELZ, G.T. & AUCHTERLONIE, G.J. 1995. An investigation of the use of chromium, platinum and gold coating for scanning electron microscopy of casts of lymphoid tissues. *Micron,* 26**,** 141-144.

BENSON, S.M. 2005a. Lessons learned from industrial and natural analogs for health, safety and environmental risk assessment for geologic storage of carbon dioxide. *Carbon Dioxide Capture for Storage in Deep Geologic Formations.* Amsterdam: Elsevier Science.

BENSON, S.M. 2005b. Overview of geologic storage of CO_2. *In:* SASS, B., MONZYK, B., RICCI, S., GUPTA, A., HINDIN, B. & GUPTA, N. (eds.) *Impact of SOx and NOx in Flue Gas on CO_2 Seperation, Compression, and Pipeline Transmission.* London: Elsevier.

BENSON, S.M., APPS, J., HEPPLE, R., LIPPMANN, M., TSANG, C.F., LEWIS, C., GALE, J. & KAYA, Y. 2003. Health, safety andenvironmental risk assessment for geologic storage of carbon dixide: Lessons learned from industrial and natural analogues. *Greenhouse Gas Control Technologies - 6th International Conference.* Oxford: Pergamon.

BENSON, S.M. & SURLES, T. 2006. Carbon dioxide capture and storage: An overview with emphasis on capture and storage in deep geological formations. *Proceedings of the IEEE,* 94**,** 1795-1805.

BERG, A. & BANWART, S.A. 2000. Carbon dioxide mediated dissolution of Ca-feldspar: implications for silicate weathering. *Chemical Geology,* 163**,** 25-42.

BERGKVIST, B.O. 1987. Leaching of metals from forest soils as influenced by tree species and management. *Forest Ecology and Management*, 22**,** 29-56.

BERTHE, G., SAVOYE, S., WITTEBROODT, C. & MICHELOT, J.L. 2011. Changes in containment properties of claystone caprocks induced by dissolved CO_2 seepage. *Energy Procedia,* 4**,** 5314-5319.

BEUSELINCK, L., GOVERS, G., POESEN, J., DEGRAER, G. & FROYEN, L. 1998. Grain-size analysis by laser diffractometry: Comparison with the sieve-pepette method. *Catena,* 32**,** 193-208.

BILLETT, M.F., PARKERJERVIS, F., FITZPATRICK, E.A. & CRESSER, M.S. 1990. Forest soil chemical-changes between 1949/50 and 1987. *Journal of Soil Science,* 41**,** 133-145.

BINI, C. & BRESOLIN F. 1998. Soil acidification by acid rain in forest ecosystems: A case study in northern Italy. *Science of the Total Environment,* 222**,** 1-15.

BINLEY, A., HENRYPOULTER, S. & SHAW, B. 1996. Examination of solute transport in an undisturbed soil column using electrical resistance tomography. *Water Resources Research,* 32**,** 763-769.

BLAKE, L. & GOULDING, K.W.T. 2002. Effects of atmospheric deposition, soil pH and acidification on heavy metal contents in soils and vegetation of semi-natural ecosystems at Rothamsted Experimental Station, UK. *Plant and Soil,* 240**,** 235-251.

BLAKE, L., GOULDING, K.W.T., MOTT, C.J.B. & JOHNSTON, A.E. 1999. Changes in soil chemistry accompanying acidification over more than 100 years under woodland and grass at Rothamsted Experimental Station, UK. *European Journal of Soil Science,* 50**,** 401-412.

BLAKE, L., GOULDING, K.W.T., MOTT, C.J.B. & POULTON, P.R. 2000. Temporal changes in chemical properties of air-dried stored soils and their interpretation for long-term experiments. *European Journal of Soil Science,* 51**,** 345-353.

BLUM, J.D., GAZIS, C.A., JACOBSON, A.D. & CHAMBERLAIN, C.P. 1998. Carbonate versus silicate weathering in the Raikhot watershed within the High Himalayan Crystalline Series. *Geology* 26**,** 411-414.

BOOJAR, M.M.A. & GOODARZI, F. 2007. The copper tolerance strategies and the role of antioxidative enzymes in three plant species grown on copper mine. *Chemosphere,* 67**,** 2138-2147.

BOUILLON, P.-A., HENNES, S. & MAHIEUX, C. 2009. ECO_2: Post-combustion or Oxyfuel-A comparison between coal power plants with integrated CO_2 capture. *Energy Procedia,* 1**,** 4015-4022.

BRADL, H.B. 2004. Adsorption of heavy metal ions on soils and soils constituents. *Journal of Colloid and Interface Science,* 277**,** 1-18.

BSI (BRITISH STANDARD INSTITUTION). 1990. Clause 5: Determination of permeability by the constant-head method. In: *Methods of test for soils for civil engineering purposes. Compressibility, permeability and durability tests.* BS 1377-5:1990, pp 11-15.

BUCHER, A.S. & SCHENK, M.K. 2000. Toxicity level for phytoavailable zinc in compost-peat substrates. *Scientia Horticulturae,* 83**,** 339-352.

BUTNOR, J.R., JOHNSEN, K.H. & MAIER, C.A. 2005. Soil properties differently influence estimates of soil CO_2 efflux from three chamber-based measurement systems. *Biogeochemistry,* 73**,** 283-301.

CALEVRO, F., CAMPANI, S., FILIPPI, C., BATISTONI, R., DERI, P., BUCCI, S., RAGGHIANTI, M. & MANCINO, G. 1999. Bioassays for testing effects of Al, Cr and Cd using development in the amphibian Pleurodeles waltl and regeneration in the planarian Dugesia etrusca. *Aquatic Ecosystem Health and Management,* 2**,** 281-288.

CAMARDA, M., GURRIERI, S. & VALENZA, M. 2009. Effects of soil gas permeability and recirculation flux on soil CO_2 flux measurements performed using a closed dynamic accumulation chamber. *Chemical Geology,* 265**,** 387-393.

CARAMANNA, G., WEI, Y., MAROTO-VALER, M.M., NATHANAIL, P. & STEVEN, M. 2012. Design and use of a laboratory rig for the study of the chemical-physical effects on aquatic environments of potential seepage from CO_2 storage sites. *Greenhouse Gases: Science and Technology,* 2**,** 136-143.

CARAMANNA, G., WEI, Y., MAROTO-VALER, M. M., NATHANAIL, P. & STEVEN, M. 2013. Laboratory experiments and field study for the detection and monitoring of potential seepage from CO_2 storage sites. *Applied Geochemistry,* 30**,** 105-113

CARBONELL-BARRACHINA, A.A., JUGSUJINDA, A., BURLO, F., DELAUNE, R.D. & PATRICK, W.H. 2000. Arsenic chemistry in municipal sewage sludge as affected by redox potential and pH. *Water Research,* 34**,** 216-224.

CATLETT, K.M., HEIL, D.M., LINDSAY, W.L. & EBINGER, M.H. 2002. Soil chemical properties controlling zinc(2+) activity in 18 colorado soils. *Soil Science Society of America Journal,* 66**,** 1182-1189.

CELIA, M.A., BACHU, S., NORDBOTTEN, J.M., GASDA, S.E. & DAHLE, H.K. 2005. Quantitative estimation of CO_2 leakage from geological

storage: Analytical model, numerical modeal, and data needs. *Greenhouse Gas Control Technologies, 7***,** 663-671.

CHEN, A., ZHAO, Z.W., JIA, X., LONG, S., HUO, G. & CHEN, X. 2009. Alkaline leaching Zn and its concomitant metals from refractory hemimorphite zinc oxide ore. *Hydrometallurgy,* 97**,** 228-232.

CHEN, J., ZHANG, D. D., WANG, S., XIAO, T. & HUANG, R. 2004. Factors controlling tufa deposition in natural waters at waterfall sites. *Sedimentary Geology,* 166**,** 353-366.

CHOU, L., GARRELS, R.M. & WOLLAST, R. 1989. Comparative study of the kinetics and mechanisms of dissolution of carbonate minerals. *Chemical Geology,* 78**,** 269-282.

CLOW, D.W. & MAST, M.A. 2010. Mechanisms for chemostatic behavior in catchments: Implications for CO_2 consumption by mineral weathering. *Chemical Geology,* 269**,** 40-51.

COGBILL, C.V. & LIKENS, G.E. 1974. Acid precipitation in the northeastern United States. *Water Resource Research,* 10**,** 1133

COOK, A.C., HAINSWORTH, L.J., SOREY, M.L., EVANS, W.C. & SOUTHON, J.R. 2001. Radiocarbon studies of plant leaves and tree rings from Mammoth Mountain, CA: A long-term record of magmatic CO_2 release. *Chemical Geology,* 177**,** 117-131.

COYNE, M.S. & THOMPSON, J.A. 2006. Surface chemistry of soil. *Fundamental Soil Science.* United States: Thomson Delmar Learning.

CRASWELL, E.T. & WARING, S.A. 1972. Effect of grinding on the decomposition of soil organic matter--I. The mineralization of organic nitrogen in relation to soil type. *Soil Biology and Biochemistry,* 4**,** 427-433.

CROWDER, A. 1991. Acidification, metals and macrophytes. *Environmental Pollution*, 71**,** 171-203.

CUNNINGHAM, J. 2010. *The effect of below ground carbon dioxide emissions on the recovery of plants and soil.* MSc Dissertation thesis, University of Nottingham.

DAMEN, K., FAAIJ, A. & TURKENBURG, W. 2003. Health, safety and environmental risks of underground CO_2 sequestration: Overview of mechanisms and current knowledge. *Climatic Change (reprinted in 2006),* 74**,** 289-318.

DARCY, H. 1856. Les Fontaines Publiques de la Ville de Dijon. Paris: Victor Dalmont.

DAS, D.B. & MIRZAEI, M. 2013. Experimental measurement of dynamic effect in capillary pressure relationship for two-phase flow in weakly layered porous media. *AIChE Journal*, 59(5)**,** 1723–1734. DOI: 10.1002/aic.13925.

DAS, D.B., MIRZAEI, M. & WIDDOWS N. 2006. Non-uniqueness in capillary pressure–saturation–relative permeability relationships for two-phase flow in porous media: Interplay between intensity and distribution of random micro-heterogeneities. *Chemical Engineering Science,* 61**,** 6786–6803.

DAUPHAS, N., POURMAND, A. & TENG, F.Z. 2009. Routine isotopic analysis of iron by HR-MC-ICPMS: How precise and how accurate? *Chemical Geology,* 267**,** 175-184.

DAVIES, F.T., PURYEAR, J.D., NEWTON, R.J., EGILLA, J.N. & SARAIVA GROSSI, J.A. 2002. Mycorrhizal fungi increase chromium uptake by sunflower plants: influence on tissue mineral concentration, growth, and gas exchange. *Journal of Plant Nutrition,* 25**,** 2389-2407.

DAVIS, B.L., JENKINS, R., MCCARTHY, G.J., SMITH, D.K. & WONG-NG, W. Specimen preparation in X-ray diffraction. In: V. E. BUHRKE, R. JENKINS, D. K. SMITH eds. *Preparation of specimens for X-ray fluorescence and X-ray diffraction analysis.* John Wiley & Sons, Inc. 1998, pp.141-143.

DE MATOS, A.T., FONTES, M.P.F., DA COSTA, L.M. & MARTINEZ, M.A. 2011. Mobility of heavy metals as related to soil chemical and moneralogical characteristics of Brazilian soils. *Environmental Pollution,* 111**,** 429-435.

DE WIT, H.A., MULDER, J., NYGAARD, P.H. & AAMLID, D. 2001. Testing the aluminium toxicity hypothesis: A field manipulation experiment in mature spruce forest in Norway. *Water Air and Soil Pollution,* 130**,** 995-1000.

DELHAIZE, E. & RYAN, P.R. 1995. Aluminum toxicity and tolerance in plants. *Plant Physiology,* 107**,** 315-321.

DICKENS, G.R., KÖLLING, M., SMITH, D.C. & SCHNIEDERS, L. 2007. Rhizon Sampling of Pore Waters on Scientific Drilling Expeditions: An Example from the IODP Expedition 302, Arctic Coring Expedition (ACEX). *Scientific Drilling*, 4**,** 22-25.

DOOLEY, J.J., TRABUCCHI, C. & PATTON, L. 2010. Design considerations for financing a national trust to advance the deployment of geologic CO_2 storage and motivate best practices. *International Journal of Greenhouse Gas Control,* 4**,** 381-387.

DREYBRODT, W. 1999. Chemical kinetics, speleothem growth and climate. *Boreas,* 28**,** 347-356.

EDWARDS, H.G.M., VILLAR, S.E.J., JEHLICKA, J. & MUNSHI, T. 2005. FT-Raman spectroscopic study of calcium-rich and magnesium-rich carbonate minerals. *Spectrochimica Acta Part A: Molecular and Biomolecular Spectroscopy,* 61**,** 2273-2280.

EGIARTE, G., CAMPS ARBESTAIN, M., RUÍZ-ROMERA, E. & PINTO, M. 2006. Study of the chemistry of an acid soil column and of the corresponding leachates after the addition of an anaerobic municipal sludge. *Chemosphere,* 65**,** 2456-2467.

EKENE, B. 2011. The impact of controlled injection of soil carbon dioxide (CO_2) concentration on the growth and development of wheat (triticum aestivum L.) and soil chemical properties. MSc Dissertation thesis, University of Nottingham.

ERMAKOV, I.V., KOPTSIK, S.V., KOPTSIK, G.N. & LOFTS, S. 2007. Transport and accumulation of heavy metals in undisturbed soil columns. *Global Nest Journal,* 9**,** 187-194.

ESPA, S., CARAMANNA, G. & BOUCHÉ, V. 2010. Field study and laboratory experiments of bubble plumes in shallow seas as analogues of sub-seabed CO_2 leakages. *Applied Geochemistry,* 25**,** 696-704.

FALKENGREN-GRERUP U. & ERIKSSON, H. 1990. Changes in soil, vegetation and forest yield between 1947 and 1988 in beech and oak sites of southern Sweden. *Forest Ecology and Management,* 38**,** 37–53.

FALKENGREN-GRERUP, U., LINNERMARK, N. & TYLER, G. 1987. Changes in acidity and cation pools of south Swedish soils between 1949 and 1985. *Chemosphere,* 16**,** 2239-2248

FANG, W.-C. & KAO, C.H. 2000. Enhanced peroxidase activity in rice leaves in response to excess iron, copper and zinc. *Plant Science,* 158**,** 71-76.

FARRAR, C.D., SOREY, M.L., EVANS, W.C., HOWLE, J.F., KERR, B.D., KENNEDY, B.M., KING, C.Y. & SOUTHON, J.R. 1995. Forest-killing diffuse CO_2 emission at Mammoth Mountain as a sign of magmatic unrest. *Nature,* 376**,** 675-678.

FAURIA, K.E. & REMPEL, A.W. 2011. Gas invasion into water-saturated, unconsolidated porous media: Implications for gas hydrate reservoirs. *Earth and Planetary Science Letters,* 312**,** 188–193

FENG, M.-H., SHAN, X.-Q., ZHANG, S. & WEN, B. 2005. A comparison of the rhizosphere-based method with DTPA, EDTA, $CaCl_2$, and $NaNO_3$ extraction methods for prediction of bioavailability of metals in soil to barley. *Environmental Pollution,* 137**,** 231-240.

FETTER, C.W. Hydraulic conductivity of earth materials. In: *Applied Hydrogeology* (3rd edition). the University of Michigan: Prentice Hall. 1994, pp 93-103.

FORD, J. 2006. The geological of the ASGARD site, Sutton Bonington. Nottingham, British Geological Survey: 40.

FORTIN, D. & LANGLEY, S. 2005. Formation and occurrence of biogenic iron-rich minerals. *Earth-Science Reviews,* 72**,** 1-19.

FREDD, C.N. & FOGLER, H.S. 1998. Influence od transport and reaction on wormhole formation in porous media. *AIChE Journal,* 44**,** 1933-1949.

FREDERICK, R.T. & THOMPSON, L.M. 1993. *Soils and soil fertility* New York, Oxford University Press.

FREETH, S.J. & REX, D.C. 2000. Constraints on the age of Lake Nyos, Cameroon. *Journal of Volcanology and Geothermal Research,* 97**,** 261-269.

FROST, R.R. & GRIFFIN, R.A. 1977. Effect of pH on adsorption of arsenic and selenium from landfill leachate by clay minerals. *Soil Science Society of American Journal,* 41**,** 53-57.

FU, Q., LU, P., KONISHI, H., DILMORE, R., XU, H., SEYFRIED, W. & ZHU, C. 2009. Coupled alkali-feldspar dissolution and secondary mineral precipitation in batch system: 1. New experiments at 200°C and 300 bars. *Chemical Geology,* 258**,** 125-135.

FULLER, W.H., KORTE, N.E., NIEBLA, E.E. & ALESII, B.A. 1976. Contribution of the soil to the migration of certain common and trace metals. *Soil Science,* 122**,** 223–235.

GAL, F., BRACH, M., BRAIBANT, G., BÉNY, C. & MICHEL K. 2012. What can be learned from natural analogue studies in view of CO_2 leakage issues in Carbon Capture and Storage applications? Geochemical case study of Sainte-Marguerite area (French Massif Central). *International Journal of Greenhouse Gas Control*, 10**,** 470–485.

GAL, F., MICHEL, B., GILLES, B., FRÉDÉRIC, J. & KARINE, M. 2011. CO_2 escapes in the Laacher See region, East Eifel, Germany: Application of natural analogue onshore and offshore geochemical monitoring. *International Journal of Greenhouse Gas Control,* 5**,** 1099-1118.

GALE, J. & DAVISON, J. 2004. Transmission of CO_2-safety and economic considerations. *Energy,* 29**,** 1319-1328.

GALLOWAY, J.N., THORNTON, J.D., NORTON, S.A., VOLCHOK, H.L. & MCLEAN, R.A.N. 1982. Trace metals in atmospheric deposition: A review and assessment. *Atmospheric Environment,* 16**,** 1677-1700.

GARCIA, S. 2010. *Experimental and simulation studies of iron oxides for geochemical fixation of CO_2-SO_2 gas mixtures.* PhD Thesis, University of Nottingham.

GARFIELD, E. 1985. Acid rain. Part 1. What is it and what does it do?: Current comments. *Essays of an information scienctist*, 8**,** 77-86. Available at: http://www.garfield.library.upenn.edu/essays/v8p077y1985.pdf (last accessed: 21/11/2012)

GAUS, I. 2010. Role and impact of CO_2-rock interactions during CO_2 storage in sedimentary rocks. *International Journal of Greenhouse Gas Control,* 4**,** 73-89.

GERLACH, R.W., DOBB, D.E., RAAB, G.A. & NOCERINO, J.M. 2002. Gy sampling theory in environmental studies. 1. Assessing soil splitting protocols. *Journal of Chemometrics,* 16**,** 321-328.

GERLACH, T.M., DOUKAS, M.P., MCGEE, K.A. & KESSLER, R. 2001. Soil efflux and total emission rates of magmatic CO_2 at the Horseshoe Lake tree kill, Mammoth Mountain, California, 1995-1999. *Chemical Geology,* 177**,** 101-116.

GESSA, C.E., MIMMO, T., DEIANA, S. & MARZADORI, C. 2005. Effect of aluminium and pH on the mobility of phosphate through a soil-root interface model. *Plant and Soil,* 272**,** 301-311.

GIDDA, T., CANN, D., STIVER, W.H., ZYTNER & R.G. 2006. Airflow dispersion in unsaturated soil. *Journal of Contaminant Hydrology,* 82**,** 118–132.

GIGGENBACH, W. F. 1990. Water and gas chemistry of Lake Nyos and its bearing on the eruptive process. *Journal of Volcanology and Geothermal Research,* 42**,** 337-362.

GIGGENBACH, W.F., SANO, Y. & SCHMINCKE, H.U. 1991. CO_2-rich gases from Lakes Nyos and Monoun, Cameroon; Laacher See, Germany; Dieng, Indonesia, and Mt. Gambier, Australia-variations on a common theme. *Journal of Volcanology and Geothermal Research,* 45**,** 311-323.

GOLUBEV, S.V., POKROVSKY, O.S. & SCHOTT, J. 2005. Experimental determination of the effect of dissolved CO_2 on the dissolution kinetics of Mg and Ca silicates at 25^{o}C. *Chemical Geology,* 217**,** 227-238.

GOULDING, K.W.T., BAILEY, N.J., BRADBURY, N.J., HARGREAVES, P., HOWE, M., MURPHY, D.V., POULTON, P.R. & WILLISON, T.W. 1998. Nitrogen deposition and its contribution to nitrogen cycling and associated soil processes. *New Phytologist,* 139**,** 49-58.

GREEN, T.R., TANIGUCHI, M., KOOI, H., GURDAK, J.J., ALLEN, D.M., HISCOCK, K.M., TREIDEL, H. & AURELI, A. 2011. Beneath the surface of global change: Impacts of climate change on groundwater. *Journal of Hydrology,* 405**,** 532-560.

GUPTA, R.K., DEN ELSHOUT, S.V. & ABROL, I.P. 1987. Effect of pH on zinc adsorption-precipitation reactions in an alkali soil. *Soil Science,* 143**,** 198-204.

HA-DUONG, M. & KEITH, D. 2003. Carbon storage: the economic efficiency of storing CO_2 in leaky reservoirs. *Clean Technologies Environmental Policy,* 5**,** 181–189.

HAMAMOTO, S., TOKIDA, T., MIYAZAKI, T. & MIZOGUCHI, M. 2008. Dense gas flow in volcanic ash soil: Effect of pore structure on density-driven flow. *Soil Science Society of America Journal,* 72**,** 480-486.

HARTER, R.D. 1983. Effect of soil pH on adsorption of lead, copper, zinc, and nickel. *Soil Science Society of American Journal,* 47**,** 47-51.

HARVEY, L. 2007. Dangerous anthropogenic interference, dangerous climatic change, and harmful climatic change: Non-trivial distinctions with significant policy implications. *Climatic Change,* 82**,** 1-25.

HARVEY, O.R., QAFOKU, N.P., CANTRELL, K.J., LEE, G., AMONETTE, J.E. & BROWN, C.F. 2013. Geochemical implications of gas leakage associated with geologic CO_2 storage - A qualitative review. *Environmental Science and Technology,* 47**,** 23-36.

HASZELDINE, R.S., QUINN, O., ENGLAND, G., WILKINSON, M., SHIPTON, Z.K., EVANS, J.P., HEATH, J., CROSSEY, L., BALLENTINE, C.J. & GRAHAM, C.M. 2005. Natural geochemical analogues for carbon dioxide storage in deep geological porous reservoirs, a United Kingdom perspective. *Oil and Gas Science and Technology,* 60**,** 33-49.

HEIRI, O., LOTTER, A.F. & LEMCKE, G. 2001. Loss on ignition as a method for estimating organic and carbonate content in sediments: Reproducibility and comparability of results. *Journal of Paleolimnology,* 25**,** 101-110.

HEM, J.D. 1978. Redox processes at surfaces of manganese oxide and their effects on aqueous metal ions. *Chemical Geology,* 21**,** 199-218.

HENRIKSEN, A. & WRIGHT, R.F. 1977. Concentrations of heavy metals in small norwegian lakes. *Water Research,* 12**,** 101-112.

HEPPLE, R.P. 2005. Human health and ecological effects of carbon dioxide exposure. *Carbon Dioxide Capture for Storage in Deep Geologic Formations.* Amsterdam: Elsevier Science.

HESSE, P.R. 1971a. Iron, aluminium and manganese. *A textbook of soil chemical analysis.* London: John Murry Ltd.

HESSE, P.R. 1971b. Total (elemental) analysis and some trace elements. *A textbook of soil chemical analysis.* London: John Murry Ltd.

HILL, D.P. & PREJEAN, S. 2005. Magmatic unrest beneath Mammoth Mountain, California. *Journal of Volcanology and Geothermal Research,* 146**,** 257-283.

HILLIER, S. 2000. Accurate quantitative analysis of clay and other minerals in sandstones by XRD: comparison of a rietveld and a reference intensity ratio (RIR) method and the importance of sample preparation. *Clay Minerals,* 35**,** 291-302.

HO, T.-Y., CHIEN, C.-T., WANG, B.-N. & SIRIRAKS, A. 2010. Determination of trace metals in seawater by an automated flow injection ion chromatograph pretreatment system with ICPMS. *Talanta,* 82**,** 1478-1484.

HODSON, M.E. & LANGAN, S.J. 1999. A long-term soil leaching column experiment investigating the effect of variable sulphate loads on soil solution and soil drainage chemistry. *Environmental Pollution,* 104**,** 11-19.

HOEFNER, M.L. & FOGLER, H.S. 1988. Pore evolution and channel formation during flow and reaction porous media. *AIChE Journal,* 34**,** 45-54.

HOFMANN, D.J., BUTLER, J.H. & TANS, P.P. 2009. A new look at atmospheric carbon dioxide. *Atmospheric Environment,* 43**,** 2084-2086.

HOLLOWAY, S., PEARCE, J.M., HARDS, V.L., OHSUMI, T. & GALE, J. 2007. Natural emissions of CO_2 from the geosphere and their bearing on the geological storage of carbon dioxide. *Energy,* 32**,** 1194-1201.

HOLLOWAY, S., PEARCE, J.M., OHSUMI, T. & HARDS, V.L. 2005. A review of natural CO_2 occurrences and their relevance to CO_2 storage. British Geological Survey External Report, CR/05/104, 117.

HONG, C., JIA, Y., YANG, X., HE, Z. & STOFFELLA, P. 2008. Assessing lead thresholds for phytotoxicity and potential dietary toxicity in selected vegetable crops. *Bulletin of Environmental Contamination and Toxicology,* 80**,** 356-361.

HRACHOVÁ, J., MADEJOVÁ, J., BILLIK, P., KOMADEL, P. & FAJNOR, V.S. 2007. Dry grinding of Ca and octadecyltrimethylammonium montmorillonite. *Journal of Colloid and Interface Science,* 316**,** 589-595.

HUANG, C.P. & QUIST, G.C. 1983. The dissulution of a manganese ore in dilute aqueous solution. *Environment International,* 9**,** 379-389.

IDE, S.T., FRIEDMANN, S.J. & HERZOG, H.J. 2006. CO_2 leakage through existing wells: Current technology and regulatory basis. *8th International Conference on Greenhouse Gas Control Technologies.* Trondheim, Norway.

IEA. 2008. World energy outlook 2008. *Global energy trends to 2030.* Paris: International Energy Agency, OECD.

IPCC. 2005a. Carbon dioxide capture and storage. *In:* IPCC (ed.) *Special Report on CO_2 Capture and Storage.* Bert Metz, Ogunlade Davidson, Heleen de Coninck, Manuela Loos, Leo Meyer ed. United Kingdom and New York: Intergovermental Pannel on Climate Change.

IPCC. 2005b. Technical Summary on Carbon dioxide capture and storage. *In:* IPCC (ed.) *Special Report on CO_2 Capture and Storage.* Edward Rubin, Leo Meyer, Heleen de Coninck ed. United Kingdom and New York: Intergovermental Pannel on Climate Change.

IRHA, N., STEINNES, E., KIRSO, U. & PETERSELL, V. 2009. Mobility of Cd, Pb, Cu, and Cr in some Estonian soil types. *Estonian Journal of Earth Sciences,* 58**,** 209-214.

JAFFE, P.R., WANG, S., GALE, J. & KAYA, Y. 2003. Potential effect of CO_2 releases from deep reservoirs on the quality of fresh-water aquifers. *Greenhouse Gas Control Technologies - 6th International Conference.* Oxford: Pergamon.

JAIN, A.K. & JUANES, R. 2009. Preferential mode of gas invasion in sediments: grain-scale mechanistic model of coupled multiphase fluid flow and sediment mechanics. *Journal of Geophysical Research: Solid Earth (1978–2012),* 114 (B8).

JI, W., DAHMANI, A., AHLFELD, D.P., LIN, J.D., & HILL III, E. 1993. Laboratory Study of Air Sparging: Air Flow Visualization. *Groundwater Monitoring & Remediation,* 13**,** 115–126.

JIA, Y., TANG, S., WANG, R., JU, X., DING, Y., TU, S. & SMITH, D.L. 2010. Effects of elevated CO_2 on growth, photosynthesis, elemental composition, antioxidant level, and phytochelatin concentration in Lolium mutiforum and Lolium perenne under Cd stress. *Journal of Hazardous Materials,* 180**,** 384-394.

JOHNSON, A.H., ANDERSN, S.B. & SICCAMA, T.G. 1994. Acid rain and soils of the Adirondacks. I. Changes in pH and available calcium, 1930–1984. *Canadian Journal of Forest Research*, 24**,** 39-45.

JOHNSON, N.M., LIKENS, G.E., FELLER, M.C., & DRISCOLL, C.T. 1984. Acid Rain and Soil Chemistry. *Science*, 225**,** 1424-1425.

JOHNSON, P.C., JOHNSON, R.L., NEAVILLE, C., HANSEN, E.E., STEARNS, S.M. & DORTCH, I.J. 1997. An Assessment of Conventional In Situ Air Sparging Pilot Tests. *Ground Water,* 35**,** 765–774.

JOHNSON, R.L., JOHNSON, P.C., MCWHORTER, D.B., HINCHEE, R.E. & GOODMAN, I. 1993. An overview of in situ air sparging. *Ground Water Monitoring Review,* Fall**,** 127–135.

JONES, G. 1994. Global warming, sea level change and the impact on estuaries. *Marine Pollution Bulletin,* 28**,** 7-14.

JÖNSSON, U., ROSENGREN, U., THELIN, G. & NIHLGARD, B. 2003. Acidification-induced chemical changes in coniferous forest soils in southern Sweden 1988–1999. *Environmental Pollution,* 123**,** 75–83.

JOSSI, M., FROMIN, N., TARNAWSKI, S., KOHLER, F., GILLET, F., ARAGNO, M. & HAMELIN, J. 2006. How elevated pCO_2 modifies total and metabolically active bacterial communities in the rhizosphere of two perennial grasses grown under field conditions. *FEMS Microbiology Ecology,* 55**,** 339-350.

KAMANN, P.J., RITZI, R.W., DOMINIC, D.F. & CONRAD, C.M. 2007. Porosity and permeability in sediment mixtures. *Ground Water,* 45**,** 429-438.

KANNAN, R. 2009. Uncertainties in key low carbon power generation technologies - Implication for UK decarbonisation targets. *Applied Energy,* 86**,** 1873-1886.

KARBERG, N.J., PREGITZER, K.S., KING, J.S., FRIEND, A.L. & WOOD, J.R. 2005. Soil carbon dioxide partial pressure and dissolved inorganic carbonate chemistry under elevated carbon dioxide and ozone. *Oecologia,* 142**,** 296-306.

KASAI, E., MIMURA, H., SUGIYAMA, K., SAITO, F., AKIBA, K. & WASEDA, Y. 1994. Mechano-chemical changes in natural and synthetic zeolites by dry grinding using a planetary ball mill. *Advanced Powder Technology,* 5**,** 189-203.

KECK, C.M. & MULLER, R.H. 2008. Size analysis of submicron particles by laser diffractometry—90% of the published measurements are false. *International Journal of Pharmaceutics,* 355**,** 150-163.

KEMP, P.H. 1971. Chemistry of natural water-II Alkalinity. *Water Research,* 5**,** 413-420.

KHARAKA, Y.K., COLE, D.R., THORDSEN, J.J., KAKOUROS, E. & NANCE, H.S. 2006. Gas-water-rock interactions in sedimentary basins: CO_2 sequestration in the Frio Formation, Texas, USA. *Journal of Geochemical Exploration,* 89**,** 183-186.

KHARAKA, Y.K., THORDSEN, J.J., HOVORKA, S.D., NANCE, H.S., COLE, D.R., PHELPS, T.J. & KNAUSS, K.G. 2009. Potential environmental issues of CO_2 storage in deep saline aquifers: Geochemical results from the Frio-I Brine Pilot test, Texas, USA. *Applied Geochemistry,* 24**,** 1106-1112.

KHARAKA, Y.K., THORDSEN, J.J., KAKOUROS, E., AMBATS, G., HERKELRATH, W.N., BEERS, S.R., BIRKHOLZER, J.T., APPS, J.A., SPYCHER, N.F., ZHENG, L., TRAUTZ, R.C., RAUCH, H.W. & GULLICKSON, K.S. 2010. Changes in the chemistry of shallow groundwater related to the 2008 injection of CO_2 at the ZERT field site, Bozeman, Montana. *Environmental Earth Science,* 60**,** 273–284.

KING, S.O., MACH, C.E. & BREZONIK, P.L. 1992. Changes in trace metal concentrations in lake water and biota during experimental acidification of Little Rock Lake, Wisconsin, USA. *Environmental Pollution,* 78**,** 9-18.

KLUTE, A. 1990. *Methods of soil analysis. Part 1 Physical and mineralogical methods,* Madison, Wisconsin USA, American Society of Agronomy, Inc; Soil Science of America, Inc.

KOCHIAN, L.V. 1995. Cellular mechanism of aluminum toxicity and resistance in plants. *Annual Review of Plant Physiology and Plant Molecular Biology,* 46**,** 237-260.

KOORNNEEF, J., RAMÍREZ, A., TURKENBURG, W. & FAAIJ, A. 2012. The environmental impact and risk assessment of CO_2 capture, transport and storage – An evaluation of the knowledge base. *Progress in Energy and Combustion Science,* 38**,** 62-86.

KOORNNEEF, J., SPRUIJT, M., MOLAG, M., RAMIREZ, A., FAAIJ, A. & TURKENBURG, W. 2009. Uncertainties in risk assessment of CO_2 pipelines. *Energy Procedia,* 1**,** 1587-1594.

KRUGER, M., JONES, D., FRERICHS, J., OPPERMANN, B.I., WEST, J., COOMBS, P., GREEN, K., BARLOW, T., LISTER, R., SHAW, R., STRUTT, M. & MOLLER, I. 2011. Effects of elevated CO_2 concentrations on the vegetation and microbial populations at a terrestrial CO_2 vent at Laacher See, Germany. *International Journal of Greenhouse Gas Control,* 5**,** 1093-1098.

KRUGER, M., WEST, J., FRERICHS, J., OPPERMANN, B., DICTOR, M.-C., JOULIAND, C., JONES, D., COOMBS, P., GREEN, K., PEARCE, J., MAY, F. & MOLLER, I. 2009. Ecosystem effects of elevated CO_2 concentrations on microbial populations at a terrestrial CO_2 vent at Laacher See, Germany. *Energy Procedia,* 1**,** 1933-1939.

KUBOVA, J., MATUS, P., BUJDOS, M. & MEDVED, J. 2005. Influence of acid mining activity on release of aluminium to the environment. *Analytica Chimica Acta,* 547**,** 119-125.

KUSAKABE, M., TANYILEKE, G.Z., MCCORD, S.A. & SCHLADOW, S.G. 2000. Recent pH and CO_2 profiles at Lakes Nyos and Monoun, Cameroon: Implications for the degassing strategy and its numerical simulation. *Journal of Volcanology and Geothermal Research,* 97**,** 241-260.

LAKKARAJU, V.R., ZHOU, X., APPLE, M.E., CUNNINGHAM, A., DOBECK, L.M., GULLICKSON, K. & SPANGLER, L.H. 2010. Studying the vegetation response to simulated leakage of sequestered CO_2 using spectral vegetation indices. *Ecological Informatics,* 5**,** 379-389.

LASPINA, N.V., GROPPA, M.D., TOMARO, M.L. & BENAVIDES, M.P. 2005. Nitric oxide protects sunflower leaves against Cd-induced oxidative stress. *Plant Science,* 169**,** 323-330.

LEE, E.H., PAUSCH, R.C., ROWLAND, R.A., MULCHI, C.L. & RUDORFF, B.F.T. 1997. Responses of field-grown soybean (cv. Essex) to elevated SO_2 under two atmospheric CO_2 concentrations. *Environmental and Experimental Botany,* 37**,** 85-93.

LEE, J.-S., KIM, D.-K., LEE, J.-P., PARK, S.-C., KOH, J.-H., CHO, H.-S. & KIM, S.-W. 2002. Effects of SO_2 and NO on growth of Chlorella sp. KR-1. *Bioresource Technology,* 82**,** 1-4.

LERMAN, A. & STUMM, W. 1989. CO_2 storage and alkalinity trends in lakes. *Water Research,* 23**,** 139-146.

LEWICKI, J., BIRKHOLZER, J. & TSANG, C.-F. 2007a. Natural and industrial analogues for leakage of CO_2 from storage reservoirs: identification of features, events, and processes and lessons learned. *Environmental Geology,* 52**,** 457-467.

LEWICKI, J.L., OLDENBURG, C.M., DOBECK, L. & SPANGLER, L. 2007b. Surface CO_2 leakage during two shallow subsurface CO_2 releases. *Geophysical Research Letters,* 34.

LI, H., YAN, J. & ANHEDEN, M. 2009. Impurity impacts on the purification process in oxy-fuel combustion based CO_2 capture and storage system. *Applied Energy,* 86**,** 202-213.

LI, Q., CHEN, L.-S., JIANG, H.-X., TANG, N., YANG, L.-T., LIN, Z.-H., LI, Y. & YANG, G.-H. 2010. Effects of manganese-excess on CO_2 assimilation, ribulose-1,5-bisphosphate carboxylase/oxygenase, carbohydrates and photosynthetic electron transport of leaves, and antioxidant systems of leaves and roots in Citrus grandis seedlings. *BMC Plant Biology,* 10**,** 42.

LIDON, F.C. 2002. Rice plant structural changes by addition of excess manganese. *Journal of Plant Nutrition,* 25**,** 287-296.

LIKENS, G.E. & BORMANN, F.H. 1974. Acid rain: a serious regional environmental problem. *Science,* 184**,** 1176-1179.

LIKENS, G.E., DRISCOLL, C.T. & BUSO, D.C. 1996. Long-term effects of acid rain: response and recovery of a forest ecosystem. *Science,* 272**,** 244–246.

LIN, Y.H. 2010. Effects of aluminum on root growth and absorption of nutrients by two pineapple cultivars [Ananas comosus (L.) Merr.]. *African Journal of Biotechnology,* 9**,** 4034-4041.

LITTLE, M. & JACKSON, R. 2010. Potential impacts of leakage from deep CO_2 geosequestration on overlying freshwater aquifers. *Environmental Science and Technology,* 44**,** 9225–9232.

LU, J., PARTIN, J., HOVORKA, S. & WONG, C. 2010. Potential risks to freshwater resources as a result of leakage from CO_2 geological storage: A batch-reaction experiment. *Environmental Earth Sciences,* 60**,** 335-348.

LUDWIG, W., AMIOTTE-SUCHET, P. & PROBST, J.L. 1999. Enhanced chemical weathering of rocks during the last glacial maximum: A sink for atmospheric CO_2? *Chemical Geology,* 159**,** 147-161.

MACPHERSON, G.L., ROBERTS, J.A., BLAIR, J.M., TOWNSEND, M.A., FOWLE, D.A. & BEISNER, K.R. 2008. Increasing in shallow goundwater CO_2 and limestone weathering, Konza Prairie, USA. *Geochimica et Cosmochimica Acta,* 72**,** 5581-5599.

MADEJÓN, P., RAMÍREZ-BENÍTEZ, J.E., CORRALES, I., BARCELÓ, J. & POSCHENRIEDER, C. 2009. Copper-induced oxidative damage and enhanced antioxidant defenses in the root apex of maize cultivars differing in Cu tolerance. *Environmental and Experimental Botany,* 67**,** 415-420.

MADLAND, M.V., FINSNES, A., ALKAFADGI, A., RISNES, R. & AUSTAD, T. 2006. The influence of CO_2 gas and carbonate water on the mechanical stability of chalk. *Journal of Petroleum Science and Engineering,* 51**,** 149-168.

MAJERUS, V., BERTIN, P. & LUTTS, S. 2007. Effects of iron toxicity on osmotic potential, osmolytes and polyamines concentrations in the African rice (Oryza glaberrima Steud.). *Plant Science,* 173**,** 96-105.

MANNINGS, S. & SMITH, S. 1996. Effect of acid deposition on soil acidification and metal mobilisation. *Environmental Geochemistry,* 11**,** 139-143.

MARIN, A.R., PEZESHKI, S.R., MASSCHELEN, P.H. & CHOI, H.S. 1993. Effect of dimethylarsenic acid (DMAA) on growth, tissue arsenic, and photosynthesis of rice plants. *Journal of Plant Nutrition,* 16**,** 865-880.

MAROTO-VALER, M.M., FAUTH, D.J., KUCHTA, M.E., ZHANG, Y. & ANDERSON, J.M. 2005. Activation of magnesium rich minerals as carbonation feedstock materials for CO_2 sequestration. *Fuel Processing Technology,* 86**,** 1627-1645.

MARSCHNER, H. 1995. Functions of mineral nutrients: Micronutrient. *Mineral nutrition of higher plants, second edition.* London: Academic Press.

MARULANDA, C., CULLIGAN, P.J. & GERMAINE, J.T. 2000. Centrifuge modeling of air sparging-a study of air flow through saturated porous media. *Journal of Hazardous Materials*, 72**,** 179–215.

MASSCHELEYN, P.H., DELAUNE, R.D. & PATRICK, W.H. 1991. Effect of redox potential and pH on arsenic speciation and solubility in a contaminated soil. *Environmental Science & Technology,* 25**,** 1414-1419.

MATTUCK, R. & NIKOLAIDIS, N.P. 1996. Chromium mobility in freshwater wetlands. *Journal of Contaminant Hydrology,* 23**,** 213-232.

MAYER, R. 1998. Soil acidification and cycling of metal elements: cause-effect relationships with regard to forestry practices and climatic changes. *Agriculture Ecosystems & Environment,* 67**,** 145-152.

MCGECHAN, M.B. & LEWIS, D.R. 2002. SW—Soil and Water: Transport of Particulate and Colloid-sorbed Contaminants through Soil, Part 1: General Principles. *Biosystems Engineering*, 83**,** 255–273.

MCGINNIS, D.F., SCHMIDT, M., DELSONTRO, T., THEMANN, S., ROVELLI, L., REITZ, A. & LINKE, P. 2011. Discovery of a natural CO_2 seep in the German North Sea: Implications for shallow dissolved gas and seep detection. *J. Geophys. Res.,* 116**,** C03013.

MCGRATH, A.E., UPSON, G.L. & CALDWELL, M.D. 2007. Evaluation and mitigation of landfill gas impacts on cadmium leaching from native soils. *Ground Water Monitoring & Remediation,* 27**,** 99-109.

MERRY, R.H., TILLER, K.G. & ALSTON, A.M. 1986. The effects of contamination of soil with copper, lead, and arsenic on the growth and composition of plants. I. Effects of season, genotype, soil temperature, and fertilizers. *Plant and Soil,* 91**,** 115-128.

MILLER, D.E. & WATMOUGH, S.A. 2009. Soil acidification and foliar nutrient status of Ontario's deciduous forest in 1986 and 2005. *Environmental Pollution,* 157**,** 664-672.

MIRBAGHERI, S.A. 2004. Modeling contaminant transport in soil column and ground water pollution control. *International Journal of Environmental Science and Technology,* 1**,** 149-158.

MITCHELL, M. 2011. *Mathematical modelling of carbon dioxide dissolution and reaction processes.* PhD Thesis, University of Nottingham.

MOL, G., VRIEND, S.P & VAN GAANS, P.F.M 2003. Feldspar weathering as the key to understanding soil acidification monitoring data; a study of acid sandy soils in the Netherlands. *Chemical Geology,* 202**,** 417–441.

MORTATTI, J. & PROBST, J.-L. 2003. Silicate rock weathering and atmospheric/soil CO_2 uptake in the Amazon basin estimated from

river water geochemistry: Seasonal and spatial variations. *Chemical Geology,* 197**,** 177-196.

NATIONAL FOOD AUTHORITY. 1993. Australian Food Standards Code: March, 1993. Australian Goverment Public Service, Canberra.

NAY, S.M., MATTSON, K.G. & BORMANN, B.T. 1994. Biases of chamber methods for measuring soil CO_2 efflux demonstrated with a laboratory apparatus. *Ecology,* 75**,** 2460-2463.

NIKOLAIDIS, N.P., ROBBINS, G.A., SCHERER, M., MCANINCH, B., BINKHORST, G., ASIKAINEN, J. & SUIB, S.L. 1994. Vertical distribution and partitioning of chromium in a glaciof luvial aquifer. *Ground Water Monitoring & Remediation,* 14**,** 150-159.

NIST (National Institute of Standards & Technology). 2009. Trace Elements in Water, Standard Reference Material 1643e. Produced by Stephen A. Wise & Robert L. Watters, Jr.. Available at: https://www-s.nist.gov/srmors/certificates/1643E.pdf?CFID=2509239&CFTOKEN=7973d96d10ac6788-AA8E5548-EF57-B5F4-2C40D3499770F1A2&jsessionid=f0305b8699150354478a4c612c554e52f397 (last accessed: 27/03/2013)

NOGALES, R., GALLARDO-LARA, F., BENITEZ, E., SOTO, J., HERVAS, D. & POLO, A. 1997. Metal extractability and availability in a soil after heavy application of either nickel or lead in different forms. *Water, Air, and Soil Pollution,* 94**,** 33-44.

NOGUES, J.P., COURT, B., DOBOSSY, M., NORDBOTTEN, J.M. & CELIA, M.A. 2012. A methodology to estimate maximum probable leakage along old wells in a geological sequestration operation. *International Journal of Greenhouse Gas Control,* 7**,** 39-47.

NOIRIEL, C., GOUZE, P. & BERNARD, D. 2004. Investigation of porosity and permeability effects from microstructure changes during limestone dissolution. *Geophysical Research Letters,* 31**,** L24603.

NOIRIEL, C., LUQUOT, L., MADÉ, B., RAIMBAULT, L., GOUZE, P. & VAN DER LEE, J. 2009. Changes in reactive surface area during limestone dissolution: An experimental and modelling study. *Chemical Geology,* 265**,** 160-170.

NOVOZAMSKY, I., LEXMOND, T.M. & HOUBA, V.J.G. 1993. A single extraction procedure of soil for evaluation of uptake of some heavy metals by plants. *International Journal of Environmental Analytical Chemistry,* 51**,** 47-58.

NRC (National Research Council (U.S.)). Committee on Biologic Effects of Atmospheric Pollutants. 1974. Chromium. National Academy of Sciences. pp. 155. ISBN 978-0-309-02217-0.

OLDENBURG, C.M., BRYANT, S.L. & NICOT, J.-P. 2009. Certification framework based on effective trapping for geologic carbon sequestration. *International Journal of Greenhouse Gas Control,* 3**,** 444-457.

OLDENBURG, C.M. & LEWICKI, J.L. 2005. Leakage and seepage of CO_2 from geological storage sites into surface water. *Environmental Geology,* 50**,** 691-705.

PACALA, S. & SOCOLOW, R. 2004. Stabilization wedges: Solving the climate problem for the next 50 years with current technologies. *Science,* 305**,** 968-972.

PAGE, A.L. 1982a. Arsenic. *In:* PAGE, A. L. (ed.) *Methods of soil analysis. Pt. 2, Chemical and microbiological properties.* 2 Edition ed. Madison, Wisconsi USA: American Society of Agronomy, Inc.; Soil Science Sciety of American, Inc.

PAGE, A.L. 1982b. Lead. *In:* PAGE, A. L. (ed.) *Methods of soil analysis. Pt. 2, Chemical and microbiological properties.* 2 Edition ed. Madison, Wisconsi USA: American Society of Agronomy, Inc.; Soil Science Sciety of American, Inc.

PALANDRI, J.L. & KHARAKA, Y.K. 2005. Ferric iron-bearing sediments as a mineral trap for CO_2 sequestration: Iron reduction using sulfur-bearing waste gas. *Chemical Geology,* 217**,** 351-364.

PALINTEST. 2012. *Complete Soil Management Kit.* Available at: http://www.palintest.com/media/uploads/117.pdf (last accessed: 27/12/2012)

PARNELL JR, R.A. & BURKE, K.J. 1990. Impacts of acid emissions from Nevado del Ruiz volcano, Colombia, on selected terrestrial and aquatic ecosystems. *Journal of Volcanology and Geothermal Research,* 42**,** 69-88.

PASCHKE, M.W., VALDECANTOS, A. & REDENTE, E.F. 2005. Manganese toxicity thresholds for restoration grass species. *Environmental Pollution,* 135**,** 313-322.

PATIL, R.H., COLLS, J.J. & STEVEN, M.D. 2010. Effects of CO_2 gas as leaks from geological storage sites on agro-ecosystems. *Energy,* 35**,** 4587-4591.

PATIL, R.H. 2012. Impacts of carbon dioxide gas leaks from geological storage sites on soil ecology and above-ground vegetation, Diversity of Ecosystems, Mahamane Ali (Ed.), ISBN: 978-953-51-0572-5, InTech, Available from: http://www.intechopen.com/books/diversity-of-ecosystems/impacts-of-carbon-dioxide-gas-leaks-from-geological-storage-sites-on-soil-ecology-and-terrestrial-ec (last accessed: 21/11/2012)

PATRA, M., BHOWMIK, N., BANDOPADHYAY, B. & SHARMA, A. 2004. Comparison of mercury, lead and arsenic with respect to genotoxic effects on plant systems and the development of genetic tolerance. *Environmental and Experimental Botany,* 52**,** 199-223.

PEARSON, P.N. & PALMER, M.R. 2000. Atmospheric carbon dioxide concentrations over the past 60 million years. *Nature,* 406**,** 695-699.

PECHARSKY, V.K. & ZAVALIJ, P.Y. 2009. *Fundamentals of powder diffraction and structural characterization of materials,* New York, Springer Science & Business Media.

PEDERSON, J., KARLSTROM, K., SHARP, W. & MCINTOSH, W. 2002. Differential incision of the Grand Canyon related to Quaternary faulting-Constraints from U-series and Ar/Ar dating. *Geology,* 30**,** 739-742.

PEREIRA, L.B., MAZZANTI, C.M.D.A., GONCALVES, J.F., CARGNELUTTI, D., TABALDI, L.A., BECKER, A.G., CALGAROTO, N.S., FARIAS, J.G., BATTISTI, V., BOHRER, D., NICOLOSO, F.T., MORSCH, V.M. & SCHETINGER, M.R.C. 2010. Aluminum-induced oxidative stress in cucumber. *Plant Physiology and Biochemistry,* 48**,** 683-689.

PETIT, J.R., JOUZEL, J., RAYNAUD, D., BARKOV, N.I., BARNOLA, J.M., BASILE, I., BENDER, M., CHAPPELLAZ, J., DAVIS, M., DELAYGUE, G., DELMOTTE, M., KOTLYAKOV, V.M., LEGRAND, M., LIPENKOV, V.Y., LORIUS, C., PEPIN, L., RITZ, C., SALTZMAN, E. & STIEVENARD, M. 1999. Climate and atmospheric history of the past 420,000 years from the Vostok ice core, Antarctica. *Nature,* 399**,** 429-436.

PIERCE, M.L., & MOORE, C.B. 1980. Adsorption of arsenite and arsenate on amorphous iron hydroxide from dilute aqueous solutions. *Environmental Science & Technology,* 14**,** 214-216.

PIPITONE, G. & BOLLAND, O. 2009a. Modeling of oxy-combustion flue gas desulfurization by seawater absorption. *Environmental Progress & Sustainable Energy,* 28**,** 20-29.

PIPITONE, G. & BOLLAND, O. 2009b. Power generation with CO_2 capture: Technology for CO_2 purification. *International Journal of Greenhouse Gas Control,* 3**,** 528-534.

PIRES, J.C.M., MARTINS, F.G., ALVIM-FERRAZ, M.C.M. & SIMÕES, M. 2011. Recent developments on carbon capture and storage: An overview. *Chemical Engineering Research and Design,* 89**,** 1446-1460.

POKROVSKY, O.S., GOLUBEV, S.V. & SCHOTT, J. 2005. Dissolution kinetics of calcite, dolomite and magnesite at 25°C and 0 to 50 atm pCO_2. *Chemical Geology,* 217**,** 239-255.

POKROVSKY, O.S., GOLUBEV, S.V., SCHOTT, J. & CASTILLO, A. 2009. Calcite, dolomite and magnesite dissolution kinetics in aqueous solutions at acid to circumneutral pH, 25 to 150 °C and 1 to 55 atm pCO_2: New constraints on CO_2 sequestration in sedimentary basins. *Chemical Geology,* 265**,** 20-32.

POSCHENRIEDER, C., GUNS, B., CORRALES, I. & BARCEL, J. 2008. A glance into aluminum toxicity and resistance in plants. *Science of The Total Environment,* 400**,** 356-368.

PRASAD, M.N.V. 1995. Cadmium toxicity and tolerance in vascular plants. *Environmental and Experimental Botany,* 35**,** 525-545.

PUEYO, M., LOPEZ-SANCHEZ, J.F. & RAURET, G. 2004. Assessment of $CaCl_2$, $NaNO_3$ and NH_4NO_3 extraction procedures for the study of Cd, Cu, Pb and Zn extractability in contaminated soils. *Analytica Chimica Acta,* 504**,** 217-226.

QIN, W.-Q., LI, W.-Z., LAN, Z.-Y. & QIU, G.-Z. 2007. Simulated small-scale pilot plant heap leaching of low-grade oxide zinc ore with integrated selective extraction of zinc. *Minerals Engineering,* 20**,** 694-700.

RADOSZ, M., HU, X., KRUTKRAMELIS, K. & SHEN, Y. 2008. Flue-gas carbon capture on carbonaceous sorbents: Toward a low-cost multifunctional carbon filter for "green" energy producers. *Industrial & Engineering Chemistry Research,* 47**,** 3783-3794.

RAYMOND, P.A. & COLE, J.J. 2003. Increase in the export of alkalinity from north America's largest river. *Science,* 301**,** 88-91.

REHKÄMPER, M., SCHÖNBÄCHLER, M. & STIRLING, C.H. 2007. Multiple collector ICP-MS: introduction to instrumentation, measurement techniques and analytical capabilities. *Geostandards Newsletter,* 25**,** 23-40.

RICE, K.C. & HERMAN, J.S. 2012. Acidification of Earth: An assessment across mechanisms and scales. *Applied Geochemistry*, 27**,** 1-14.

ROBERTS, J.J., WOOD, R.A. & HASZELDINE, R.S. 2011. Assessing the health risks of natural CO_2 seeps in Italy. *PANS,* 108**,** 16545-16548.

ROBINSON, B.W. & NICKEL, E.H. 1983. The SEM examination of geologucal samples with a semiconductor backscattered-electron detector: Discussion. *American Mineralogist,* 68**,** 840-842.

ROGIE, J.D., KERRICK, D.M., SOREY, M.L., CHIODINI, G. & GALLOWAY, D.L. 2001. Dynamics of carbon dioxide emission at Mammoth Mountain, California. *Earth and Planetary Science Letters,* 188**,** 535-541.

ROMANAK, K.D., SMYTH, R.C., YANG, C., HOVORKA, S.D., REARICK, M. & LU, J. 2012. Sensitivity of groundwater systems to CO_2: Application of a site-specific analysis of carbonate monitoring parameters at the SACROC CO_2-enhanced oil field. *International Journal of Greenhouse Gas Control,* 6**,** 142-152.

RÖMKENS, P.F.A.M., BOUWMAN, L.A. & BOON, G.T. 1999. Effect of plant growth on copper solubility and speciation in soil solution samples. *Environmental Pollution,* 106**,** 315-321.

ROSS, S.M. 1994. Retention, transportation and mobility of toxic metals in soils. *Toxic metals in Soil-Plant Systems*. (ed. S.M. Ross), 27-62. Wiley, London.

ROWELL, D.L. 1994a. Soil acidity and alkalinity. *Soil Science : Methods and Applications.* Harlow, Essex; New York: Longman Scientific & Technical; Wiley.

ROWELL, D.L. 1994b. *Soil Science : Methods and Applications,* Harlow, Essex; New York, Longman Scientific & Technical; Wiley.

RUSSELL, E.W. 1973. The effect of soil acidity and alkalinity on plant growth. *Soil condition and plant growth.* London and New York: LONGMAN.

SAHAN, Y., BASOGLU, F. & GUCER, S. 2007. ICP-MS analysis of a series of metals (namely: Mg, Cr, Co, Ni, Fe, Cu, Zn, Sn, Cd and Pb) in black and green olive samples from Bursa, Turkey. *Food Chemistry,* 105**,** 395-399.

SANDATLAS. 2012. *Limestone*. Available at: http://www.sandatlas.org/2012/10/limestone/ (last accessed: 27/03/2013)

SARKAR, D., ANDRA, S.S., SAMINATHAN, S.K.M. & DATTA, R. 2008. Chelant-aided enhancement of lead mobilization in residential soils. *Environmental Pollution,* 156**,** 1139-1148.

SASS, B., MONZYK, B., RICCI, S., GUPTA, A., HINDIN, B. & GUPTA, N. 2005. Chapter 17 - Impact of SO_x and NO_x in flue gas on CO_2 separation, compression and pipeline transmission. *Carbon Dioxide Capture and Storage in Deep Geological Formation.* Amsterdam: Elsevier Science.

SASS, B.M. & RAI, D. 1987. Solubility of amorphous chromium(III)-iron(III) hydroxide solid solutions. *Inorganic Chemistry,* 26**,** 2228-2232.

ŠČANČAR, J., MILAČIČ, R. & HORVAT, M. 2000. Comparison of various digestion and extraction procedures in analysis of heavy metals in sediments. *Water, Air, and Soil Pollution,* 118**,** 87-99.

SCHUMACHER, B.A., SHINES, K.C., BURTON, J.V., PAPP, M.L. & BLUME, L.J. 1990. A Comparison of Soil Sample Homogenization Techniques. United States. *Soil Science Society of America Journal,* 54**,** 1187-1190

SCHMOGER, M.E.V., OVEN, M. & GRILL, E. 2000. Detoxification of arsenic by phytochelatins in plants. *Plant Physiology,* 122**,** 793-801.

SEEBERG-ELVERFELDT, J., SCHLÜTER, M., FESEKER, T. & KÖLLING, M. 2005. Rhizon sampling of porewaters near the sediment-water interface of aquatic systems. *Limnology and Oceanography: Methods,* 3**,** 361-371.

SEEVAM, P.N., RACE, J.M. & DOWNIE, M.J. 2007. Carbon dioxide pioelines for sequestration in the UK: An engineering gas analysis. *Journal of Pipeline Engineering,* 6**,** 133-146.

SEMER, R., ADAMS, J.A. & REDDY, K.R. 1998. An experimental investigation of air flow patterns in saturated soils during air sparging. *Geotechnical and Geological Engineering,* 16**,** 59–75.

SHIH, S.-M., LIN, J.-P. & SHIAU, G.-Y. 2000. Dissolution rates of limestones of different sources. *Journal of Hazardous Materials,* 79**,** 159-171.

SHORT, M.B., BAYGENTS, J.C. & GOLDSTEIN, R.E. 2005. Stalactite growth as a free-boundary problem. *Physics of Fluids,* 17**,** 083101.

SIMON, F.O. & ROLLINSON, C.L. 1976. Chromium in rocks and minerals from the southern California batholith. *Chemical Geology,* 17**,** 73-88.

SIMS, R.E.H., SCHOCK, R.N., ADEGBULULGBS, A., FENHANN, J., KONSTANTINAVICIUTE, I., MOOMAW, W., NIMIR, H.B., SCHLAMADINGER, B., TORRES-MARTINEZ, J., TURNER, C., UCHIYAMA, Y., VUORI, S.J.V., WAMUKONYA, N. & ZHANG, X. 2007. Energy supply *In:* METZ, B., DAVIDSON, O. R., BOSCH, P. R., DAVE, R. & MEYER, L. A. (eds.) *Climate change 2007: mitigation of climate change. Contribution of working group III to the fourth assessment report of the Intergovernmental Panel on Climate Change.* Cambridge, United Kindom and New York, NY, USA: IPCC.

SKIBA, U., CRESSER, M.S., DERWENT, R.G. & FUTTY, D.W. 1989. Peat acidification in Scotland. *Nature,* 337**,** 68-69.

SKJELKVALE, B.L., STODDARD, J.L. & ANDERSEN, T. 2001. Trends in surface water acidification in Europe and North America (1989–1998). *Water Air Soil Pollution*, 130**,** 787–792.

SMEDLEY, P.L. & KINNIBURGH, D.G. 2002. A review of the source, behavious and distribution of arsenic in natural waters. *Applied Geochemistry,* 17**,** 517-568.

SMITH, E., NAIDU, R. & ALSTON, A.M. 1998. Arsenic in the soil environment. A review. *Advances in Agronomy,* 64**,** 149-195.

SMITH, K.L., COLLS, J.J., STEVEN, M.D. 2005. A facility to investigate effects of elevated soil gas concentration on vegetation. *Water, Air and Soil Pollution,* 161**,** 75-96

SMITH, K.L., STEVEN, M.D. & COLLS, J.J. 2007. The ASGARD facility. *Resource document for UKCCSC 2007*.

SMITH, S.A., SORENSEN, J.A., STEADMAN, E.N. & HARJU, J.A. 2009. Acid gas injection and monitoring at the Zama oil field in Alberta, Canada: A case study in demonstration-scale carbon dioxide sequestration. *Energy Procedia,* 1**,** 1981-1988.

SMYTH, R.C., HOVORKA, S.D., KATHERINE, J.L., ROMANAK, D., PARTIN, J.W., WONG, C. & YANG, C. 2009. Assessing risk to fresh water resources from long term CO_2 injection–laboratory and field studies. *Energy Procedia,* 1**,** 1957-1964.

SOREY, M.L., FARRAR, C.D., GERLACH, T.M., MCGEE, K.A., EVANS, W.C., COLVARD, E.M., HILL, D.P., BAILEY, R.A., ROGIE, J.D., HENDLEY II, J.M., & STAUFFER, P.H. 1996. Invisible CO_2 gas killing trees at Mammoth Mountain, California. U.S. Geological Survey- Reducing the risk from volcano hazards.

SPANGLER, L.H., DOBECK, L.M., REPASKY, K.S., NEHRIR, A.R., HUMPHRIES, S.D., BARR, J.L., KEITH, C.J., SHAW, J.A., ROUSE, J.H., CUNNINGHAM, A.B., BENSON, S.M., OLDENBURG, C.M., LEWICKI, J.L., WELLS, A.W., DIEHL, J.R., STRAZISAR, B.R., FESSENDEN, J.E., RAHN, T.A., AMONETTE, J.E., BARR, J.L., PICKLES, W.L., JACOBSON, J.D., SILVER, E.A., MALE, E.J., RAUCH, H.W., GULLICKSON, K.S., TRAUTZ, R., KHARAKA, Y., BIRKHOLZER, J. & WIELOPOLSKI, L. 2010. A shallow subsurface controlled release facility in Bozeman, Montana, USA, for testing near surface CO_2 detection techniques and transport models. *Environmental Earth Sciences,* 60.

SPOSITO, G. 1994. Temperature effects. *Chemical equilibria and kinectics in soils.* New York Oxford: Oxford University Press.

SRODON, J., DRITS, V. A., MCCARTY, D.K., HSIEH, J.C.C. & EBERL, D.D. 2001. Quantitative X-ray diffraction analysis of clay-bearing rocks from random preparations. *Clays and Clay Minerals,* 49**,** 514-528.

ST. LOUIS, M.E. & HESS, J.J. 2008. Climate change: Impacts on and implications for global health. *American Journal of Preventive Medicine,* 35**,** 527-538.

STEENEVELDT, R., BERGER, B. & TORP, T.A. 2006. CO_2 capture and storage: Closing the knowing-doing gap. *Chemical Engineering Research and Design,* 84**,** 739-763.

STENHOUSE, M., ARTHUR, R. & ZHOU, W. 2009. Assessing environmental impacts from geological CO_2 storage. *Energy Procedia,* 1**,** 1895-1902.

STEPHENS, J.C. 2002. *Response of soil mineral weathering to elevated carbon dioxide.* PhD thesis. California Institute of Technology. Available at: http://www.clarku.edu/faculty/jstephens/documents/Stephens_Full_Thesis.pdf (last accessed: 12/11/2012)

STEPHENS, J.C. & HERING, J.G. 2002. Comparative characterization of volcanic ash soils exposed to decade-long elevated carbon dioxide concentrations at Mammoth Mountain, California. *Chemical Geology,* 186**,** 301-313.

STEPHENS, J.C. & HERING, J.G. 2004. Factors affecting the dissolution kinetics of volcanic ash soils: Dependencies on pH, CO_2, and oxalate. *Applied Geochemistry,* 19**,** 1217-1232.

STEVENS, C.J., DISE, N.B. & GOWING D.J. 2009. Regional trends in soil acidification and exchangeable metal concentrations in relation to acid deposition rates. *Environmental Pollution,* 157**,** 313-319.

STEVENS, S.H., PEARCE, J.M. & RIGG, A.A.J. Natural analogs for geologic storage of CO_2: An integrated global research program. First National Conference on Carbon Sequestration, 2001 Washington, D.C., USA. U.S. Department of Energy, National Energy Technology Laboratory.

STRAZISAR, B.R., WELLS, A.W., DIEHL, J.R., HAMMACK, R.W. & VELOSKI, G.A. 2009. Near-surface monitoring for the ZERT shallow CO_2 injection project. *International Journal of Greenhouse Gas Control,* 3**,** 736-744.

TAMM, C.O. & HALLBÄCKEN, L. 1988. Changes in soil acidity in two forest areas with different acid deposition: 1920s to 1980s. *Ambio,* 17**,** 56-61

TAN, K.H. 2009a. Inorganic soil constituents. *Environmental Soil Science, Third Edition.* Boca Raton, London, New York: CRC Press.

TAUB, D.R., MILLER, B. & ALLEN, H. 2008. Effects of elevated CO_2 on the protein concentration of food crops: A meta-analysis. *Global Change Biology,* 14**,** 565-575.

TIAN, S., FAN, Q., XU, Y., WANG, Y. & JIANG, A. 2001. Evaluation of the use of high CO_2 concentrations and cold storage to control of Monilinia fructicola on sweet cherries. *Postharvest Biology and Technology,* 22**,** 53-60.

TOFTEGAARD, M.B., BRIX, J., JENSEN, P.A., GLARBORG, P. & JENSEN, A.D. 2010. Oxy-fuel combustion of solid fuels. *Progress in Energy and Combustion Science,* 36**,** 581-625.

TORP, T.A. & GALE, J. Demonstrating storage of CO_2 in geological reservoirs: The Sleipner and SACS projects. 6th International Conference on Greenhouse Gas Control Technologies, Oct 01-04 2002 Kyoto, Japan. Pergamon-Elsevier Science Ltd, 1361-1369.

TUBIELLO, F.N., SOUSSANA, J.F. & HOWDEN, S.M. 2007. Crop and pasture response to climate change. *Proceedings of the National Academy of Sciences of the United States of America,* 104**,** 19686-19690.

TURNER, M.A. & RUST, R.H. 1971. Effects of chromium on growth and mineral nutrition of soybeans. *Soil Science Society of America meeting,* 35**,** 755-758.

TYLER, L.D. & MCBRIDE, M.B. 1982. Mobility and extractability of cadmium, copper, nickel, and zinc in organic and mineral soil columns. *Soil Science,* 134**,** 198-204.

USEPA (UNITED STATES ENVIRONMENTAL PROTECTION AGENCY). 1990. *Title IV: Acid Deposition Control, Overview - The Clean Air Act Amendments of 1990.* Public Law 101–549, 104, The United States Statutes at Large (Stat.) 2399. Available at: http://www.epa.gov/oar/caa/caaa_overview.html#titleIV (last accessed: 12/03/2013)

USEPA (UNITED STATES ENVIRONMENTAL PROTECTION AGENCY). 1995. Acid Rain Program. Available at: http://www.epa.gov/airmarkets/progsregs/arp/ (last accessed: 12/03/2013)

USEPA (UNITED STATES ENVIRONMENTAL PROTECTION AGENCY). 2012. *Acid rain in new England: a brief history.* Available at:

http://www.epa.gov/region1/eco/acidrain/history.html (last accessed: 21/11/2012)

VAN DER ZWAAN, B. & SMEKENS, K. 2009. CO_2 capture and storage with leakage in an energy-climate model. *Environmental Modeling & Assessment,* 14**,** 135-148.

VAN GESTEL, C.A.M. 2008. Physico-chemical and biological parameters determine metal bioavailability in soils. *Science of the Total Environment,* 406**,** 385-395.

VAN GRINSVEN, J.J.M. & VAN RIEMSDIJK, W.H. 1992. Evaluation of batch and column techniques to measure weathering rates in soils. *Geoderma*, 52**,** 41-57.

VELBEL, M.A. 1993. Constancy of silicate-mineral weathering-rate ratios between natural and experimental weathering: implications for hydrologic control of differences in absolute rates. *Chemical Geology,* 105**,** 89-99.

VESTRENG, V., NTZIACHRISTOS, L., SEMB, A., REIS, S., ISAKSEN, I.S.A. & TARRASON, L. 2009. Evolution of NO_x emissions in Europe with focus on road transport control measures. *Atmospheric Chemistry and Physics,* 9**,** 1503–1520.

VOLTATTORNI, N., CARAMANNA, G., CINTI, D., GALLI, G., PIZZINO, L. & QUATTROCCHI, F. Study of natural CO_2 emissions in different Italian geological scenarios: A refinement of natural hazard and risk assessment. *In:* LOMBARDI, S., ALTUNINA, L. K. & BEAUBIEN, S. E., eds. Advances in the Geological Storage of Carbon Dioxide NATO Science Series, 2006 Berlin. Springer Publishing, 75-190.

VOLTATTORNI, N., SCIARRA, A., CARAMANNA, G., CINTI, D., PIZZINO, L. & QUATTROCCHI, F. 2009. Gas geochemistry of natural analogues for the studies of geological CO_2 sequestration. *Applied Geochemistry,* 24**,** 1339-1346.

WANG, T.-H., LI, M.-H. & TENG, S.-P. 2009. Bridging the gap between batch and column experiments: A case study of Cs adsorption on granite. *Journal of Hazardous Materials,* 161**,** 409-415.

WASEDA, Y., MATSUBARA, E. & SHINODA, K. 2011. *X-ray diffraction crystallography,* Verlag, Berlin, and Heidelberg, Springer.

WERNBERG, T., RUSSELL, B.D., MOORE, P.J., LING, S.D., SMALE, D.A., CAMPBELL, A., COLEMAN, M.A., STEINBERG, P.D., KENDRICK, G.A. & CONNELL, S.D. 2011. Impacts of climate change in a global hotspot for temperate marine biodiversity and ocean warming. *Journal of Experimental Marine Biology and Ecology,* 400**,** 7-16.

WEI, Y., MARATO-VALERA, M., STEVEN, M.D. 2011. Environmental consequences of potential leaks of CO2 in soil. *Energy Procedia,* 4**,** 3224-3230.

WEST, J.M., PEARCE, J.M., COOMBS, P., FORD, J.R., SCHEIB, C., COLLS, J.J., SMITH, K.L. & STEVEN, M.D. 2009. The impact of controlled

injection of CO_2 on the soil ecosystem and chemistry of an English lowland pasture. *Energy Procedia,* 1**,** 1863-1870.

WIDEN, B. & LINDROTH, A. 2003. A calibration system for soil carbon dioxide efflux measurement chambers: Description and application. *Soil Science Society of America Journal,* 67**,** 327-334.

WIERENGA, P.J. & VAN GENUCHTEN, M.T. 1989. Solute transport through small and large unsaturated soil columns. *Ground Water,* 27**,** 35-42.

WILKINSON, M., GILFILLAN, S.M.V., HASZELDINE, R.S. & BALLENTINE, C.J. 2008. Plumbing the depths-testing natural tracers of subsurface CO_2 origin and leakage, Utah, USA. *In:* GROBE, M., PASHIN, J. C. & DODGE, R. L. (eds.) *Carbon Dioxide Sequestration in Geological Media-State of the Science.* American Association of Petroleum Geologists Studies

WILSON, E. & GERARD, D. 2007. *Carbon Capture and Sequestration: Integrating Technology, Monitoring, Regulation.*, Blackwell Publishing, Ames, IA (United States).

WILSON, E.J., FRIEDMANN, S.J. & POLLAK, M.F. 2007. Research for deployment: incorporating risk, regulation, and liability for carbon capture and sequestration. *Environmental Science & Technology,* 41**,** 5945-5952.

WOJTOWICZ, J.A. 2001. The carbonate system in swimming pool water. *Journal of the Swimming Pool and Spa Industry,* 4**,** 54-59.

WONG, P.Z., KOPLIK, J. & TOMANIC, J.P. 1984. Conductivity and permeability of rocks. *Physical Review B,* 30**,** 6606-6614.

WREN, C.D. & STEPHENSON, G.L. 1991. The effect of acidification on the accumulation and toxicity of metals to freshwater invertebrates. *Environmental Pollution,* 71**,** 205-241.

WU, C., LUO, Y. & ZHANG, L. 2010. Variability of copper availability in paddy fields in relation to selected soil properties in southeast China. *Geoderma,* 156**,** 200-206.

WU, Y. & HENDERSHOT, W.H. 2010. The effect of calcium and pH on nickel accumulation in and rhizotoxicity to pea (Pisum sativum L.) root-empirical relationships and modeling. *Environmental Pollution,* 158**,** 1850-1856.

XIONG, Z.T. 1998. Lead uptake and effects on seed germination and plant growth in a Pb hyperaccumulator *Brassica pekinensis* Rupr. *Bulletin of Environmental Contamination and Toxicology,* 60**,** 285-291.

XU, J., DAI, S., HAN, X., SUN, S. & ZHANG, P. 2006. Leaching of copper from an industrial cludge applied on a soil column. *Bulletin of Environmental Contamination and Toxicology,* 76**,** 663-670.

XU, X., SONG, C., MILLER, B. G. & SCARONI, A. W. 2005. Influence of moisture on CO_2 separation from gas mixture by a nanoporous adsorbent based on polyethylenimine-modified molecular sieve

MCM-41. *Industrial & Engineering Chemistry Research,* 44**,** 8113-8119.

YANAGI, M., WATANABE, Y. & SAIKI, H. 1995. CO_2 fixation by *Chlorella* sp. HA-1 and its utilization. *Energy Conversion and Management,* 36**,** 713-716.

YANG, J.Y., YANG, X.E., HE, Z.L., LI, T.Q., SHENTU, J.L. & STOFFELLA, P.J. 2006a. Effects of pH, organic acids, and inorganic ions on lead desorption from soils. *Environmental Pollution,* 143**,** 9-15.

YANG, Q.W., LAN, C.Y., WANG, H.B., ZHUANG, P. & SHU, W.S. 2006b. Cadmium in soil-rice system and health risk associated with the use of untreated mining wastewater for irrigation in Lechang, China. *Agricultural Water Management,* 84**,** 147-152.

YILDIZ, N. 2005. Response of tomato and corn plants to increasing Cd levels in nutrient culture. *Pakistan Journal of Botany,* 37**,** 593-599.

ZACHOS, J., PAGANI, M., SLOAN, L., THOMAS, E. & BILLUPS, K. 2001. Trends, rhythms, and aberrations in global climate 65 Ma to present. *Science,* 292**,** 686-693.

ZENG, F., CHEN, S., MIAO, Y., WU, F. & ZHANG, G. 2008. Changes of organic acid exudation and rhizosphere pH in rice plants under chromium stress. *Environmental Pollution,* 155**,** 284-289.

ZHANG, B., WANG, X.-Q., LI, X., NI, Y.-Q. & LI, H.-Y. 2010. Aluminum uptake and disease resistance in *Nicotiana rustica* leaves. *Ecotoxicology and Environmental Safety,* 73**,** 655-663.

ZHANG, R., HU, S., ZHANG, X. & YU, W. 2007. Dissolution kinetics of dolomite in water at elevated temperatures. *Aquatic Geochemistry,* 13**,** 309-338.

ZHENG, L., APPS, J.A., SPYCHER, N., BIRKHOLZER, J.T., KHARAKA, Y.K., THORDSEN, J., BEERS, S.R., HERKELRATH, W.N., KAKOUROS, E. & TRAUTZ, R.C. 2012. Geochemical modeling of changes in shallow groundwater chemistry observed during the MSU-ZERT CO_2 injection experiment. *International Journal of Greenhouse Gas Control,* 7**,** 202-217.

ZHOU, X., APPLE, M.E., DOBECK, L.M., CUNNINGHAM, A.B. & SPANGLER, L.H. 2013. Observed response of soil O_2 concentration to leaked CO_2 from an engineered CO_2 leakage experiment. *International Journal of Greenhouse Gas Control,* 16**,** 116-128.

APPENDIX

Appendix 1 Homogenisation test for prepared sample in StageI

Table A.1 Particle size distribution for five random subsamples

No.	Clay (0-3.9 μm) (wt%)	Silt (3.9-63 μm) (wt%)	Sand (63-2000 μm) (wt%)
1	7.95%	20.95%	71.10%
2	7.64%	19.86%	72.50%
3	8.23%	21.37%	70.40%
4	7.71%	20.19%	72.10%
5	7.64%	21.26%	71.10%
Average	7.83%	20.73%	71.44%
Standard Deviation	0.26%	0.67%	0.85%
The intralaboratory precision goals	2.0%	3.0%	3.0%

Table A.2 Loss on ignition MC, OC and CC for five random subsamples

No.	MC (%)	OC (%)	CC (%)
1	1.41%	0.54%	0.12%
2	1.42%	0.54%	0.12%
3	0.93%	0.48%	0.09%
4	1.42%	0.55%	0.10%
5	1.25%	0.52%	0.10%
Average	1.29%	0.53%	0.11%
Standard Deviation	0.21%	0.03%	0.01%

Table A.3 pH for five random subsamples

No.	pH
1	5.68
2	5.63
3	5.65
4	5.76
5	5.61
Average	5.67

Appendix 2 A recent run of water samples showing typical certified reference comparisons and also the LOD for selected elements. By ICPMS equipment model XSeriesII

Sample	Na (mg/L)	Mg (mg/L)	K (mg/L)	Ca (mg/L)	Al (µg/L)	Ti (µg/L)	V (µg/L)	Cr (µg/L)	Mn (µg/L)	Fe (µg/L)
Blank a	0	0	0	0	0	0	0	0	0	0
Std 20 ppb	0.023	0.021	0.022	0.072	20.78	0.007	20.72	20.73	20.19	20.57
Std 40 ppb	0.043	0.042	0.046	0.148	41.27	0.016	40.53	40.65	40.13	40.24
Std 100 ppb	0.109	0.106	0.117	0.39	98.31	0.007	100.6	100.5	100.4	101
Std 10 ppm	10.25	10.11	10.49	10.1	1.274	0.028	0.014	0.064	0.3	0.005
Std 20 ppm	20.2	20.28	20.59	20.13	3.623	0.104	0.015	0.081	0.603	0.008
Std 30 ppm	29.94	30.01	29.35	30.14	2.276	0.135	0.025	0.096	0.876	0.011
Washout	0.007	0.003	-0.009	-0.014	0.029	-0.001	0.002	0.012	-0.008	0.001
Washout	0.003	0.002	-0.006	-0.015	-0.204	-0.003	0	0.005	-0.01	0
Oper Balnk_1	-0.002	0	-0.007	-0.016	-0.092	0.002	0	0.002	-0.003	0.027
Oper Blank_2	-0.004	-0.001	-0.006	-0.018	-0.178	-0.004	0	-0.004	-0.013	-0.017
Oper Balnk_3	-0.005	-0.001	-0.005	-0.018	-0.183	0.001	-0.003	0.001	-0.013	-0.028
Oper Blank_4	-0.005	-0.001	-0.003	-0.017	-0.067	-0.006	-0.002	0	-0.011	-0.047
Oper Balnk_5	-0.005	-0.001	-0.001	-0.017	-0.185	0.006	0.001	0.006	-0.015	-0.03
Oper Blank_6	-0.005	-0.001	-0.001	-0.018	-0.165	-0.004	0.001	0.005	-0.014	-0.055
Oper Balnk_7	-0.005	-0.001	0	-0.018	-0.218	-0.004	0	0.006	-0.014	-0.038
Oper Blank_8	0	0	-0.005	-0.013	-0.046	-0.001	0.004	0.001	-0.011	-0.033
Oper Balnk_9	-0.003	-0.001	-0.004	-0.018	-0.054	0.004	0.001	0.005	-0.01	-0.061
Oper Blank_10	-0.004	-0.001	-0.003	-0.017	-0.132	-0.006	-0.001	-0.006	-0.011	-0.041
Limit of detection (LOD)	0.005	0.001	0.007	0.005	0.188	0.013	0.006	0.012	0.010	0.074
Limit of quantification (LOQ)	0.017	0.004	0.023	0.016	0.626	0.043	0.019	0.041	0.034	0.246
CRM_NIST 1643E-1	19.99	7.829	2.031	31.1	138.3	0.071	36.56	19.64	36.73	93.57
CRM_NIST 1643E-2	19.99	7.865	2.032	31.27	138.4	0.07	36.31	19.61	36.88	93.48
Average measured value	19.99	7.847	2.0315	31.185	138.35	0.0705	36.435	19.625	36.805	93.525
Accredited value (NIST)	20.23	7.841	1.984	31.5	138.33	None	36.93	19.9	38.02	95.7
% recovery	99	100	102	99	100		99	99	97	98

Co (µg/L)	Ni (µg/L)	Se (µg/L)	Rb (µg/L)	Sr (µg/L)	Mo (µg/L)	Cd (µg/L)	Cs (µg/L)	Cu (µg/L)	Zn (µg/L)	As (µg/L)	Ba (µg/L)	Pb (µg/L)	U (µg/L)
0	0	0	0	0	0	0	0	0	0	0	0	0	0
20.56	20.66	20.29	20.07	19.9	20.77	20.03	20.28	21.26	20.55	20.47	20.13	20.18	20.6
40.37	40.62	39.72	39.93	39.62	40.41	39.79	40.21	41.98	40.12	40.75	39.82	39.77	40.83
101	101.1	100.3	100.3	100.1	100.1	99.77	100	104.3	100.5	100.8	99.77	100.2	98.81
0.005	0.032	0.081	0.351	0.258	0.328	0.002	0.017	0.084	0.07	0.04	0.033	0.034	0.009
0.008	0.054	0.043	0.577	0.496	0.1	0.002	0.01	0.315	0.589	0.044	0.062	0.063	0.004
0.011	0.095	0.053	0.87	0.744	0.06	0.002	0.012	0.21	0.554	0.025	0.064	0.087	0.002
0.001	-0.034	0.002	0	-0.006	0.017	0.001	0.001	-0.014	-0.222	-0.046	0.001	0	0.001
0	-0.033	0.011	-0.001	-0.007	0.015	0.002	0.001	-0.013	-0.236	0.011	0.002	0.001	0.001
-0.001	0.033	0.005	0	-0.005	0.01	0.002	0.001	0.026	0.211	0.025	-0.003	0	0
-0.001	-0.038	0.006	0.001	-0.008	0.007	0	0.001	-0.027	-0.294	-0.023	-0.005	-0.001	0
-0.001	-0.034	-0.004	-0.001	-0.007	0.006	0	0.001	-0.025	-0.29	-0.014	0.002	-0.001	0
-0.001	-0.04	0.016	0	-0.006	0.004	0	0	-0.028	-0.275	-0.01	-0.005	-0.002	0
0	-0.043	0.01	-0.002	-0.007	0.004	0.002	0	-0.029	-0.297	-0.039	-0.004	-0.001	0
0	-0.043	0.004	-0.004	-0.009	0.004	0	0.001	-0.026	-0.3	-0.022	-0.006	-0.002	0
0	-0.041	0.026	-0.003	-0.008	0.002	0	0.001	-0.033	-0.321	-0.027	-0.006	-0.002	0
0.001	-0.046	0.012	-0.001	0.012	0.055	0.001	0	-0.038	-0.284	-0.012	0.032	-0.001	0
0	-0.045	0.003	-0.002	0	0.024	0	0	-0.041	-0.331	-0.018	0.002	-0.003	-0.001
0	-0.041	0.002	-0.003	-0.004	0.021	0	0.001	-0.029	-0.266	0.036	-0.002	-0.002	-0.001
0.002	0.013	0.025	0.005	0.019	0.049	0.003	0.002	0.016	0.099	0.070	0.034	0.003	0.001
0.007	0.043	0.084	0.016	0.063	0.163	0.008	0.005	0.054	0.330	0.233	0.115	0.008	0.004
24.99	57.11	10.08	13.7	314.7	120	5.971	0.002	21.18	67.61	53.23	521.3	17.71	0.002
25.03	56.7	10.27	13.69	313.9	120	6.074	0.002	21.15	66.95	52.95	524.6	17.88	0.001
25.01	56.905	10.175	13.695	314.3	120	6.0225	0.002	21.165	67.28	53.09	522.95	17.795	0.0015
26.4	60.89	11.68	13.8	315.2	118.5	6.408	None	22.2	76.5	58.98	531	19.15	None
95	93	87	99	100	101	94		95	88	90	98	93	

Appendix 3 Procedure for sediments packing in Stage II

To pack sediments into each column identically, a standard procedure was planned as follows:

- Samples were collected from the packed sediments and placed into a big flat 1 m x 1 m container.
- The samples were well mixed with a spade to overcome any possible gradation and layering of the sediments inside the shipping bag during the transport.
- The same amount of sediments was collected from each bag and weighted. These samples were labelled as sample 1 and sample 2.
- Sample 1 was poured inside the N_2 column, and its height inside the column was noted.
- The same procedure was used to fill the CO_2 column by using sample 2.
- The heights of the sediments inside the two columns were matched to be the same.
- The valves V12 and V6 (Fig. 3.16) were opened to inject the same amount of water from the bottom of each column into the mixing chamber.
- The samples were left absorbing the water for 24 hrs.
- The excess water was released through the discharge points, V12 and V6 (Fig. 3.16).
- Seal the column with the top lid and tight the bolts using a spanner. Tight the bolts again after 5 min.
- Let the sediments settle for at least an hour before starting the gas injection.

Appendix 4 Intrinsic permeability test for Trucal 5 and Trucal 6

Table A.4 General information of the rig and the packed sand

PARAMETERS	VALUE	UNIT
Packed sand density	1,448	kg/m^2
Internal diameter of the permeameter cell (r)	0.08	m
Difference between the corresponding gland point (y)	6.9	cm
Temperature correction factor for the viscosity of water to standardize the permeability to 20 °C (Rt)	1.0922	n/a
Dynamic viscosity of water (μ)	0.001002	kg/(m·s)
Density of water (ρ)	1,000	kg/m^2
acceleration due to gravity (g)	9.8	m/s^2

Table A.5 Collected data during each Run of Trucal 5

RUNS	TIMES, t (s)	VOL, Q (ml)	DIFFERENCE BETWEEN THE TWO MANOMETER LEVELS, h (cm)
Run 1	26.64	100	2.9
	54.34	200	
	81.30	300	
	107.54	400	
	134.20	500	
Run 2	26.00	100	3.6
	52.66	200	
	79.43	300	
	105.06	400	
Run 3	21.12	100	5.1
	43.03	200	
	63.83	300	
	85.71	400	

Table A.6 Collected data during each Run of Trucal 6

RUNS	TIMES, t (s)	VOL, Q (ml)	DIFFERENCE BETWEEN THE TWO MANOMETER LEVELS, h (cm)
Run 1	5.97	100	5.5
	11.13	200	
	16.29	300	
	21.99	400	
Run 2	10.22	100	3.0
	19.99	200	
	30.2	300	
	40.83	400	
	50.89	500	
Run 3	16.89	100	2.3
	33.13	200	
	49.34	300	
	67.06	400	
	84.48	500	

Appendix 5 Procedure for determination of Phenolphthalein Alkalinity (PA) and Total Alkalinity (TA)

Determination of PA:

- Remove the cap of the 5 mL vessel in the test kit; raise and fill the vessel with the water sample collected from the column ports by Rhizon samplers.
- Add 1 drop of Phenolphthalein indicator through the cap port, and mix carefully swirling the vessel in tight circles.
- If the solution remains colourless, record the PA as zero, and proceed with the determination of TA (see below).
- If the solution is pink or red, process the next step.
- Take the titration syringe from the kit and push plunger completely into the syringe. Insert the tip into HI 3811-0 solution and pull plunger out until the lower edge of the plunger seal is on the 0 mL mark of the syringe (this means that 1 mL of solution is inside the syringe which has a reverse scale).
- Place syringe tip into the cap port of the plastic vessel and slowly add the titration solution dropwise, swirling to mix after each drop. Continue adding titration solution until the solution in the plastic vessel turns colourless.
- Read the millilitres of titration solution from the syringe scale, and multiply by 300 to obtain mg/L (ppm) $CaCO_3$.

Determination of TA:

- Remove the cap of the 5 mL vessel in the test kit; fill the vessel with the water sample collected from the column ports by Rhizon samplers.

- Add 1 drop of Bromophenol blue indicator through the cap port and mix carefully. If the solution is yellow, then it is acidic and an acidity test must be carried out. If the solution is green or blue, then process the next step (in this research, the solution is blue; therefore, the following procedure is processed).
- Take the titration syringe and push plunger completely into the syringe. Insert the tip into HI 3811-0 solution and pull the plunger out until the lower edge of the plunger seal is on the 0 mL mark of the syringe.
- Place the syringe tip into the cap port of the plastic vessel and slowly add the titration solution dropwise, and swirling to mix after each drop. Continue add titration solution until the solution in the plastic vessel turns yellow.

Read the millilitres of titration solution from the syringe scale, and multiply by 300 to obtain mg/L (ppm) $CaCO_3$.

Appendix 6 Changes in exchangeable-Ca over time during Run 4

PORTS	DURATION (minutes)	Ca (mg/L)
S1	0	73.67
	17	132.10
	63	155.10
	167	288.90
	212	333.60
	277	345.50
	392	373.10
	1262	424.70
	1562	409.60
	2982	435.20
	5582	400.80
	8795	380.40
	11677	377.80
	17262	371.30
	25792	397.20
	30187	387.10
	41917	387.10
	47717	363.10
S3	0	74.15
	17	74.43
	63	104.60
	167	148.00
	212	165.30
	277	159.30
	392	229.90
	1262	323.50
	1562	346.40
	2982	398.00
	5582	369.70
	8795	354.20
	11677	361.40
	17262	347.90
	25792	377.20
	30187	347.50
	41917	352.40
	47717	345.30
S5	0	75.95
	17	78.43
	63	157.50
	167	261.00
	212	295.50
	277	330.10
	392	358.50
	1262	401.00
	1562	392.10
	2982	408.50
	5582	380.70
	8795	362.00
	11677	357.70
	17262	356.10
	25792	377.50
C1	0	81.39
	17	76.06
	63	71.18
	167	67.89
	212	69.41
	277	68.04
	392	68.40
	1262	68.77
	1562	71.66
	2982	69.91
	5582	91.26
	8795	78.94
	11677	76.10
	17262	77.07
	25792	79.23
	30187	76.95
	41917	76.35
	47717	77.02
C5	0	84.23
	17	75.75
	63	79.78
	167	77.39
	212	75.20
	277	78.94
	392	78.10
	1262	72.31
	1562	66.92
	2982	73.02
	5582	66.03
	8795	68.40
	11677	76.07
	17262	71.66
	25792	69.91
	30187	67.32
	41917	71.02
	47717	68.53

Note: The row with green background highlights the time of CO_2 injection stopped.

***Appendix 7 C*hanges in exchangeable-Ca in port S3 and C3 over time during Run 3**

PORTS	*DURATION (minutes)*	*Ca (mg/L)*
S3	0	75.9
	10	83.05
	45	81.67
	70	89.67
	100	99.3
	1440	321.9
	1720	325.2
	2770	334.3
	3190	339.8
	4170	343.5
	4390	339.1
	5550	343.4
	5770	345.3
	5890	342.9
	7360	342.2
	9860	339.9
	11580	341.9

PORTS	*DURATION (minutes)*	*Ca (mg/L)*
C3	1	91.26
	110	78.94
	2770	76.1
	3190	77.07
	5544	79.23
	5770	76.95
	7360	76.35
	9860	77.02
	11580	79.78
	12705	84.23

Note: The row with green background highlights the time of CO_2 injection stopped.

Appendix 8 Major ion concentrations of the water sample collected from S1, S3 and S5 over time during Run 8

PORT	DURATION (minutes)	CONCENTRATION Al (µg/L)	Fe (µg/L)	Mg (mg/L)	Ti (µg/L)	Cr (µg/L)	Mn (µg/L)
S1	0	6.30	5.15	17.83	0.17	0.07	34.60
	13	18.70	6.35	18.27	0.25	0.13	44.09
	25	21.18	4.73	18.43	0.13	0.16	50.68
	50	27.61	6.64	18.57	0.14	0.26	61.34
	65	26.65	8.03	17.35	0.09	0.19	62.32
	121	18.20	5.16	19.10	0.15	0.22	78.01
	245	55.03	10.89	19.22	0.21	0.45	119.90
	360	49.47	10.82	19.05	0.18	0.46	125.30
	1530	144.20	18.60	18.72	0.16	0.47	102.70
	1800	142.70	27.20	18.23	0.19	0.43	102.90
	2955	126.90	13.17	18.86	0.15	0.47	121.20
	3190	115.50	12.53	19.12	0.11	0.41	132.40
	4635	110.20	12.64	19.33	0.12	0.40	150.40
	7140	124.80	14.83	19.12	0.11	0.38	163.30
	10445	103.70	14.83	18.92	0.17	0.36	177.50

PORT	DURATION (minutes)	ION CONCENTRATION Al (µg/L)	Fe (µg/L)	Mg (mg/L)	Ti (µg/L)	Cr (µg/L)	Mn (µg/L)
S3	0	5.19	2.02	17.08	0.08	0.05	57.47
	13	9.16	3.03	17.58	0.18	0.11	70.22
	25	7.33	3.00	17.40	0.12	0.13	80.90
	50	12.93	3.80	17.71	0.09	0.15	87.34
	65	7.40	3.15	17.20	0.12	0.10	76.55
	121	3.76	1.44	17.80	0.14	0.18	99.81
	245	4.20	2.02	17.99	0.15	0.21	120.40
	360	4.71	2.31	18.76	0.18	0.26	135.50
	1530	30.64	10.51	19.74	0.32	0.47	247.20
	1800	29.13	9.59	19.34	0.23	0.45	245.70
	2955	62.94	13.22	18.84	0.33	0.51	242.20
	3190	77.98	23.11	18.63	0.34	0.50	237.50
	4635	84.40	19.59	19.40	0.32	0.54	261.80
	7140	74.95	16.35	19.56	0.32	0.46	277.50
	10445	64.58	13.33	19.73	0.19	0.45	296.20

PORT	DURATION (minutes)	ION CONCENTRATION Al (µg/L)	Fe (µg/L)	Mg (mg/L)	Ti (µg/L)	Cr (µg/L)	Mn (µg/L)
S5	0	14.68	1.58	17.22	0.13	0.10	56.38
	13	17.15	5.64	17.25	0.25	0.14	60.69
	25	21.54	3.13	17.23	0.11	0.15	62.38
	50	35.44	5.45	16.96	0.19	0.15	63.68
	65	51.87	9.28	17.40	0.27	0.23	68.12
	121	112.80	23.29	17.47	0.52	0.35	78.28
	245	191.00	33.67	17.63	0.59	0.55	103.30
	360	197.10	36.69	17.66	0.65	0.56	113.40
	1530	191.10	31.97	18.07	0.67	0.60	161.10
	1800	173.20	23.49	18.28	0.38	0.54	168.40
	2955	174.90	24.27	18.23	0.41	0.55	188.40
	3190	184.30	49.09	18.61	0.43	0.56	194.10

4635	140.70	16.81	18.67	0.31	0.47	206.60
7140	127.50	15.64	18.50	0.26	0.43	217.40
10445	155.70	49.73	18.86	0.39	0.53	234.90

Note: The green background highlights the time of CO_2 injection stopped.